Advanced modelling and technico-economic optimization of operation strategies of electrochemical storage systems accounting for cycling constraints

Alberto Vazquez Rodriguez

PSL UNIVERSITÉ PARIS

THÈSE DE DOCTORAT

DE L'UNIVERSITÉ PSL

Préparée à Mines Paris - PSL

Modélisation avancée des systèmes de stockage électrochimique de l'énergie en vue de la maitrise du vieillissement/remplacement et de l'optimisation technico-économique des stratégies de sollicitation.

Advanced modelling and techno-economic optimization of operation strategies of electrochemical storage systems accounting for cycling constraints.

Soutenue par

Alberto Erick VAZQUEZ RODRIGUEZ

Le 07 décembre 2023

École doctorale n°621

Ingénierie des Systèmes, Matériaux, Mécanique, Energétique

Spécialité

Energétique et procédés

Composition du jury :

Milos PANTOS Professor, Université de Ljubljana	*Président*
Philippe POGGI Professeur des Universités, Université de Corse Pascal Paoli	*Rapporteur*
Delphine RIU Professeure des Universités, Université Grenoble Alpes	*Rapportrice*
Stefano BRACCO Associate Professor, Université de Gênes	*Examinateur*
Theodoros KALOGIANNIS PhD, Senior Expert, Vrije Universiteit Brussel	*Examinateur*
Andrea MICHIORRI HDR, Chargé de Recherche, Mines Paris - PSL	*Examinateur*
Georges KARINIOTAKIS HDR, Directeur de Recherche, Mines Paris - PSL	*Directeur de thèse*

MINES PARIS | PSL

To my dear and loving parents,
Mauricia Rodriguez Salinas and Alfredo Vazquez Rodriguez.
To you both, I owe everything.

To Camille Bouvet,
together we withstood the journey.
The sky is clear, let us sit under the linden and enjoy the fresh air.

Acknowledgements

First, I want to thank Georges Kariniotakis, François-Pascal Neirac, and Andrea Michiorri for accepting me in the Ph.D. program and for accompanying me through the years. Thanks for the patience and believing that we could reach the finish line. Your reassurance, insights and support allowed me to continue and were invaluable to me. Thanks to the team at PERSEE and the other Ph.D. candidates (by now all doctors) that I met along the way. Our interactions were seldom, but I appreciated each one of them as the conversations were always engaging and enriching.

I want to thank also Anicet Blanc because, even if our professional paths separated quickly, it is because you believed and fought for me that my second adventure in France started and keeps going strong. Your guidance, humor and goodwill during my internship and the beginning of my Ph.D. journey were vital and I will forever be grateful.

Thanks to the friends and all the support I had through the years at SPIE. Thanks to Sara for being like a sister, thanks Robin & Phillipe for helping to endure the sometimes dullness of the grind. Thanks to the colleagues and persons I've had the pleasure to work with at the now defunct SPIE Aix Photovoltaic Department : Fabien, Eric, Phillipe, Julien, Patrick, Arthur, Ambre, Djimmy, Alexandre, Thomas, Remi, Nicolas, Luciana, and Pierre. The service is gone, but the work we did remains.

To all the friends I've made along the way : Mika, Nico, Momo, Thibault (Tibi-tibi), Elodie, Hugo (Hougo), Mathias, Seb, Camille, Stephanie, Michel, JB, Chloé. The shared adventures helped me grow and discover this country. To you not only I must thank, but also apologize for my chronic disappearances. Here is looking at you, and to new adventures.

And Camille, to you not only I am grateful, but also in debt for your support and companionship. You had to endure through the years the sleepless nights, the incoherent ramblings, the constant monologues of self-doubt and incertitude. The personal sacrifices I made were never only personal as you had to endure them as well. I can only write here a thank you, but I hope my actions from now-on forward repay little by little this debt. We started building something great together, let's keep at it.

At last, I want to thank my parents Alfredo and Mauricia. You taught me everything that is important in life, to be resilient, to persevere and to be a good person. I hope I can carry these leanings through my ongoing and future life. This is not only for me, but for you.

Table des matières

Acronyms and abbreviations

AFM	Atomic Force Microscope
ANN	Artificial Neural Networks
AO ZNI	Call for tenders for the Non-Interconected Zones published by the Energy Regulation Commision
ARIMA	Autoregressive Integrated Moving Average
BESS	Battery Energy Storage System
BMS	Battery Management System
BoL	Beginning-of-Life
CRE	French Energy Regulation Commission
DNF	Doyle-Fuller-Newman
DoD	Depth of Discharge
DSM	Demand-Side Management
DSO	Distributed System Operator
EC	Ethylene Carbonate
ECM	Equivalent Circuits Models
EESS	Electrical Energy Storage System
EIM	Electrochemical Impedance Models
EIS	Electrochemical Impedance Spectroscopy
EM	Electrochemical Models
EMF	Electro-Magnetic Force
EMS	Energy Management System
EoL	End-of-Life
EoS	End-of-Service
ESS	Energy Storage System
EU	European Union
EV	Electric Vehicle
FEM	Finite Element Method
GDS	Generale Du Solaire
GUI	Graphical User Interface

HEV Hybrid Electric Vehicles
HMI Human-Machine Interface
HV High Voltage

IEC International Electrotechnical Commission
IEEE Institute of Electrical and Electronics Engineers
IRENA International Renewable Energy Agency

KF Kalman Filter

LCOE Levelized Cost Of Energy
LFP Lithium Iron Phosphate
LiB Li-ion battery
LiBESS Lithium-ion Battery Energy Storage System
LMO Lithium Manganese Oxide
LP Linear Problem
LTO Lithium Titanate
LV Low Voltage

MAPE Mean Absolute Percentage Error
MILP Mixed Integer Linear Problem
MINLP Mixed Integer Non-Linear Problem
ML Machine Learning
MWp Megawatt Peak Capacity

NBA Network Battery Aggregator
NCA Lithium Nickel Cobalt Aluminium Oxide
NCM Lithium Nickel Cobalt Manganese Oxide
NLP Non-Linear Problem
NMC Nickel Manganese Cobalt
NN Neural Network

OCV Open Circuit Voltage

PCC Point of Common Coupling
PCS Power Conversion System
PLC Programmable Logic Controller
PMS Power Management System
PNNL Pacific Northwest National Laboratory
PoC Proof-of-concept
PPA Power Purchase Agreement
PSH Pumped Storage Hydropower
PSoC Partial State-of-Charge Cycling

PV	Photovoltaic
R&D	Research & Development
RES	Renewable Energy Sources
RMSE	Root Mean Squared Error
ROI	Return On Investment
RT-EMS	Real-Time EMS
RUL	Remaining Useful Life
SCADA	Supervisory Control and Data Acquisition
SEI	Solid Electrolyte Interface
SEM	Scanning Electron Microscopy
SNL	Sandia National Laboratory
SoC	State Of Charge
SoH	State Of Health
SSM	Supply-Side Management
TSO	Transmission System Operator
VPP	Virtual Power Plants
vRES	Variable Renewable Energy System
ZNI	Non-Interconnected Zones

List of Symbols

Physics Constants and Values

θ	Optimization vector.
I_k	DC battery current at time k.
T	Temperature in °C
V_k	Battery terminal voltage at time k.
z_k	State of charge at time k.

Battery physical values & Characteristics

η	Charge/discharge efficiency parameter.
ν_T	Self-discharge thermal coefficient.
ξ	Internal resistance.
C	Storage Capacity in Ampere-hours Ah.
E	Stored energy in Wh.
I	Current in Amperes (A).
SoC	State of charge.
V_{OC}	Open Circuit Voltage.

Superscripts and subscripts

amb	Ambient or surrounding environment.
d	Degradation source, where $d = P,\ I,\ T$.
int	Internal.

Nomenclatures for the Optimisation Framework

λ^j	Convection heat exchange coefficient.
B	Storage/Battery resource, the aggregation of all batteries j.
C_p^j	Thermal capacity.
c_k	Cost associated with each energy source k.
E_0^j	Initial energy capacity.
G	Electrical grid.
j	Unique battery identifier.
k	Energy resource, where $k = G,\ S,\ S*, B,\ j$.
L_i	Local load.
$P_i^{k_0 \to k_1}$	Power from resource k_0 to k_1, where $\{k_0, k_1\} \in k$.
P_i^k	Power output from the energy resource k.
P_{max}^k	Maximal power output from the energy resource k.

P_{min}^{k}	Minimal power output from the energy resource k.
$P_{i,in}^{S}$	Solar power available.
R_{int}^{j}	Internal resistance.
S	Solar resource.
$S*$	Unexploited solar resource.
T_{i}^{j}	Internal temperature.
T_{air}	Ambient air temperature.

Table des figures

Liste des tableaux

Chapitre 1

Introduction

Résumé en français

Ce chapitre présente l'importance et le rôle que les systèmes de stockage ont dans un système électrique. Particulièrement, ce chapitre met en lumière comment les systèmes de stockage basés sur des technologies Li-ion (LiBESS) répondent favorablement aux besoins pour incrémenter le taux d'énergies renouvelables dans le mix énergétique, ainsi que proportionner des services système (e.g. régulation de la tension ou la fréquence).

L'état de l'art concernant les LiBESS, les principes chimiques, et les différentes approches de modélisation est présenté. Une attention particulière est donnée aux différentes modèles physiques et numériques existantes pour estimer la température interne, l'état de charge et l'état de santé vis-à-vis leur importance pour la modélisation des LiBESS. Sur ces trois paramètres, une série des défis et problématiques existantes à résoudre afin d'étendre leur déploiement à une échelle industrielle sont listés.

La structure de la thèse pour répondre à ces défis est ensuite exposé brièvement par chapitre : le deuxième chapitre présente le développement d'un démonstrateur et le scenario industriel cible de la thèse, le troisième chapitre le développement des modèles des paramètres clés pour les LiBESS, et le quatrième chapitre présente leur application dans des environnement d'optimisation.

1.1 Context

Electrical energy demand has seen an almost continuous increase since 1985, rising on average by 2.2% annually since 2009. In this period, the part of Renewable Energy Sources (RES) of the total electricity generation has followed the trend worldwide reaching up to

11.7%, a share that has more than doubled in the last 10 years. This increase has replaced primarily coal and oil-generated electricity [1]. With the global effort to reduce greenhouse emissions, consolidated via the Paris Agreement in 2015 and followed up by the European Renewable Energy Directives, the proportion of RES in the energy mix is only bound to increase. An example of this trend is that the objective for the European Union (EU) in 2030 was initially set to 32% the share of RES, but it has already been increased to 45% [2, 3].

This increase in RES brings with it an inherent increase in intermittency. Wind and solar, both Variable Renewable Energy System (vRES), are the two most prominent intermittent energy sources today. They are expected to provide 52% of the total electricity generation by 2050 [4]. This increase in vRES share is however not without its drawbacks, as it adds stress and complexity to electrical grid operation and management.

For Distributed System Operator (DSO) and Transmission System Operator (TSO), the actors responsible for maintaining the balance between consumption and demand, the share of vRES has to be continuously kept in check. Too much vRES can endanger the safety and operation of the grid and, because of that, limits on their share on the grid are sometimes applied. If the vRES share limit is reached, any exceeding vRES power plants are disconnected to ensure the stability of the system. [5].

To go beyond the initial limit, DSOs and TSOs need to make use of auxiliary mechanisms to maintain the stability of the grid. These are known as ancillary services, and although the exact services included within this category can vary from one classification source to another, here we can distinguish the following : frequency and voltage control, transmission security, economic dispatch, trading enforcement, and black-start capability. Frequency and voltage control ensure that the characteristics of the electrical signal maintain a nominal operation. Transmission security assures that the grid can withstand the power transfer from point A to point B. Economic dispatch minimizes the total cost of electricity production, trading enforcement creates the framework for power trades between producers and consumers and, at last, black-start assures that in case of critical failure, the electrical grid can be restored [6]. DSOs/TSOs have at their disposal tools to provide ancillary services such as active/reactive power injection, power scheduling, time-shifting, and dispatching to mention a few. These tools require either additional energy sources or some kind of power control systems, and they represent part of the costs associated with running an electrical grid [6, 4].

At higher shares of vRES penetration, the grid managers need to compensate for the intermittency by reinforcing or upgrading the ancillary services in place. Although

the costs vary per study on the matter, a consensus is found in that strong financial investment is needed at vRES penetration above 50%. The grid inertia, capacity reserves, and total capacity requirements must be evaluated constantly as the variable energy share increases [7].

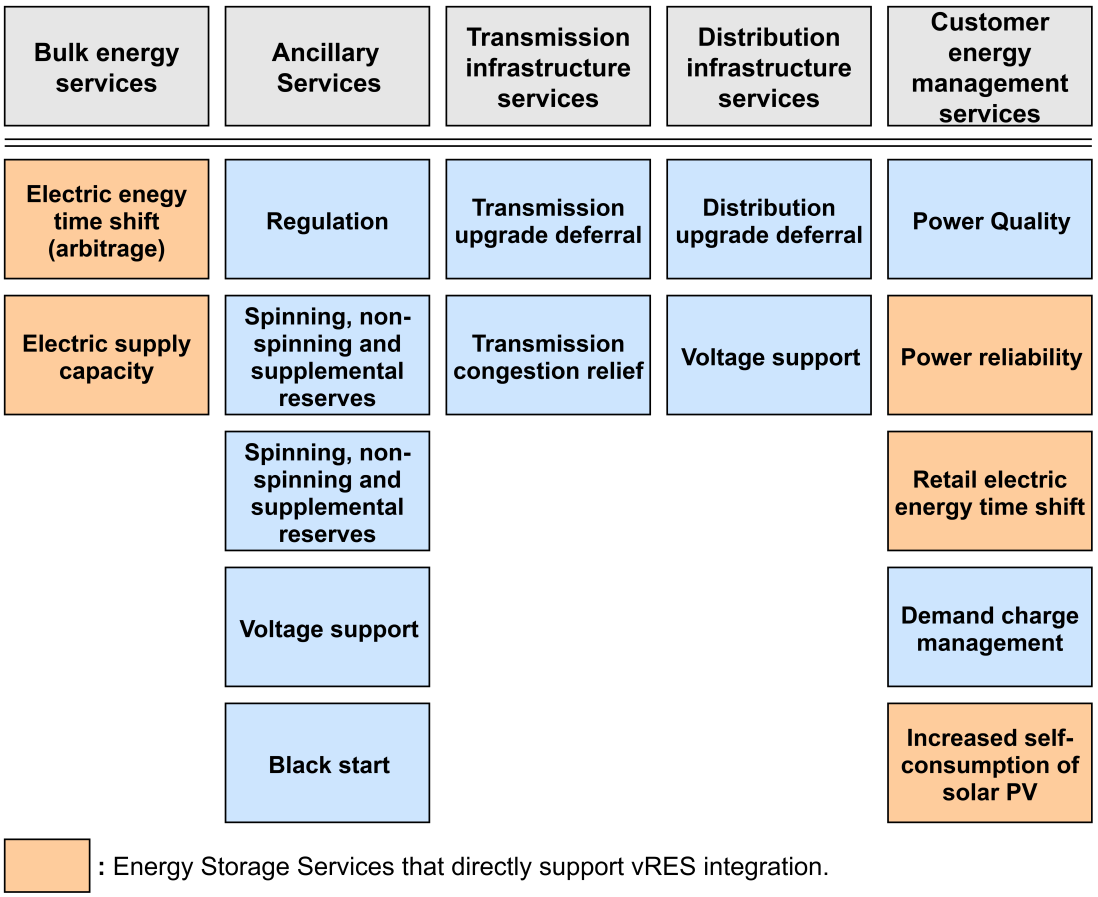

FIGURE 1.1 – Services and usages BESS can provide. Source : [4].

In figure 1.1 we can appreciate the areas in which vRES integration has an impact (red boxes) on energetic systems and requires some mitigation. Energy Storage System (ESS) can provide a solution for them, and in addition, they can offer a lot more services as well. From the 5 ancillary services mentioned before, only trading enforcement services (based purely upon metering and metering control) do not have a direct benefit from it. It is possible however to imagine (albeit unrealistically) that grids with ESS could become auto-sufficient and could avoid the need for any trading at all.

1.1.1 vRES intermittency mitigation

The vRES presence in a grid requires better performance from the ramping, load-following, capacity regulation, and reliability systems deployed [8]. The techniques used

to mitigate the intermittency change depending on the vRES and the size of the concerned grid. For large-scale grids, mitigation can be grouped into three families : Supply-Side Management (SSM) and Demand-Side Management (DSM), and Energy Storage System (ESS) based. In SSM, vRES aggregation can form Virtual Power Plants (VPP) that greatly reduce the intermittency for wind and solar (figure 1.2). Wind and solar forecasting help DSOs/TSOs to smooth the intermittency in a short-scale timeframe as well, either via additional generation units or in the case of wind farms, using the variable speed capabilities to increase power output temporarily [9, 10]. Both forecasting and VPP can also be used together, allowing for participation in energy and reserve markets [11].

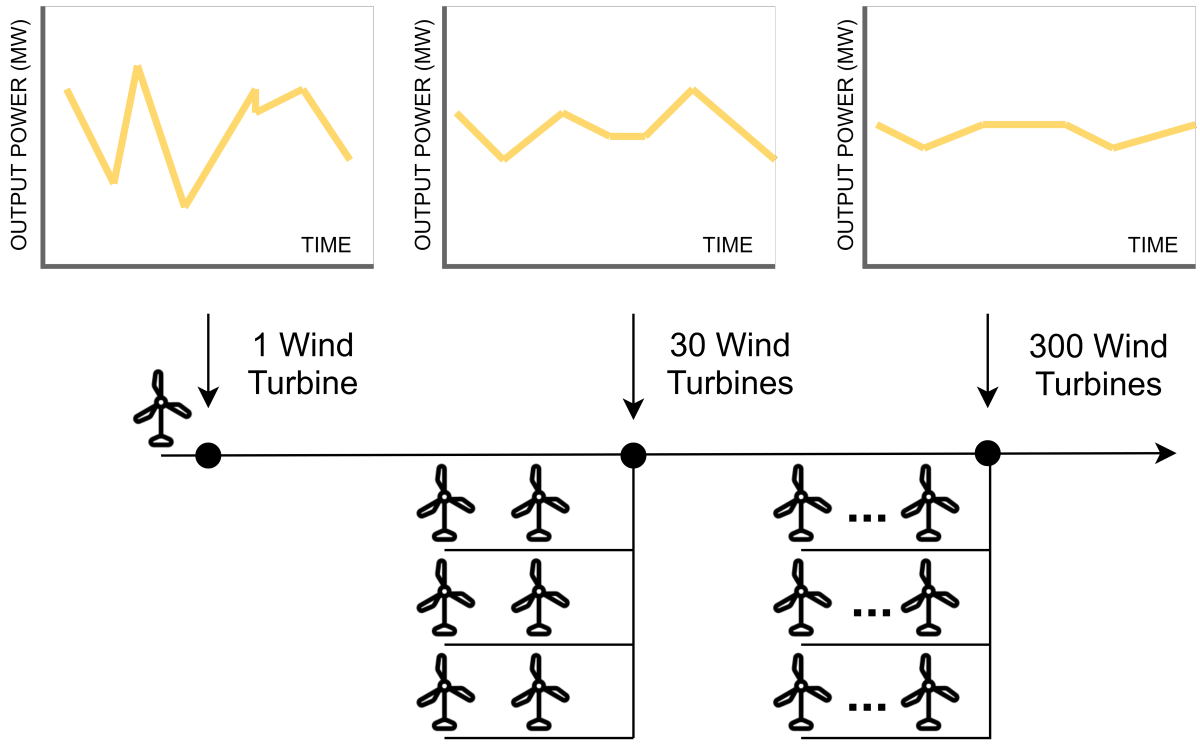

FIGURE 1.2 – Wind generation aggregation example. As the number of wind turbines considered increases (left to right), the power injection to the grid (yellow line) seen at the PCC has less intermittence and variance. Adapted from : [9].

Under DSM we can find energy reduction programs and load management programs. The former is self-explanatory, and the latter aims to change the load patterns in the grid to increase the general efficiency. Load management programs can use either direct control of loads such as thermal load activation for wind intermittency mitigation[12] for example, or financial incentives to shift the population consumption habits [9].

At last, ESS-based intermittency mitigation techniques can be applied on both the production and demand sides. ESS can act as an energy buffer unit (EBU) in power production equipment and smooth the output thanks to ramp-rate control, power mo-

ving average control, and/or low pass filter algorithms[13]. Control algorithms can also be designed to not smooth a single generator output, but the whole vRES power plant instead [14, 15]. On the demand side, BESS can help mitigate vRES intermittency through charge control. EV controlled charging [16, 17, 18], and discharge control with V2G technologies in the future [19] can offer vRES mitigation.

In the case of microgrids, Naeem and Hassan [20] broadly classified the vRES mitigation techniques in the 6 following families.

1. **Complementary RES.** By using a secondary RES, it is possible to counteract the missing power due to the original vRES. Wind power production tends to be stronger when the sun is out, potentially taking the production need previously given by solar power plants [21].
2. **Energy Cooperation.** By communicating and creating electrical links between zones, it is possible to request or give power to neighbouring regions that either have complementary energy sources or have an energy need. This exchange, which is later regularized, is the basic principle of how interconnected electricity markets operate.
3. **Energy Storage Systems.** The intermittency can be fully mitigated via this method. By storing any vRES surplus and using the storage in case of production deficit, the variability of the energy source is solved. These kinds of solutions will however be limited by the characteristics and dimensions of the storage.
4. **Demand Response (DR) Management.** It is possible to mitigate over- and under-production by controlling the loads in the system. Instead of storing the energy in a system with the purpose of later restoring it, if a process can be time-shifted without major consequences, it can then absorb the power fluctuations in the grid.
5. **Dispatchable Generators (or Production Response Management).** On the other spectrum of the last classification, intermittency can be counteracted via controllable energy generators in the grid. Classically this is done via diesel generators on large-scale grids, but they represent a higher cost compared to DR given that additional production systems must be kept in place.
6. **Hybrid Techniques.** This can be understood as a combination of two or more of the categories mentioned before. They require strong coordination between all the actors in the grid and are better adapted to small and local systems.

These categories identified for microgrids require a communication infrastructure between the elements to truly control the intermittency. It is also possible to categorize them as before : SSM includes family #1,#2, and #4. DSM with #5, and ESS-based for both

supply and demand in #3. Of the three, ESSs are widely popular as they can offer solutions adapted to many scenarios other than pure intermittency mitigation.

1.1.2 Electrical Energy Storage Systems for vRES Production Systems

Energy storage can be mechanical (pumped storage, flywheel), electrical (capacitors), thermal (molten salts), chemical (hydrogen, methane), and/or electrochemical (batteries). All these allow the storage of electrical energy, but the implementation and application of each are different. For example, mechanical methods require a strong financial investment and infrastructure, and chemical storage is better suited for cases when the energy does not need to be restored in electrical form [8].

As the power and capacities available for each kind of energy storage is different, some are inherently more adequate for vRES production systems. Figure 1.3 summarizes the standard power and energy ranges of different ESS technologies, as well as the common usage in an electrical grid. As it can be seen, electrochemical storage technologies have a wider range of applications compared to other kinds. They scale well in terms of power and in energy, and they are capable of providing different services for up to several hours. The domains at which electrochemical Energy Storage System (ESS) are proficient are uninterrupted power supply, power quality, and transmission and distribution support [22].

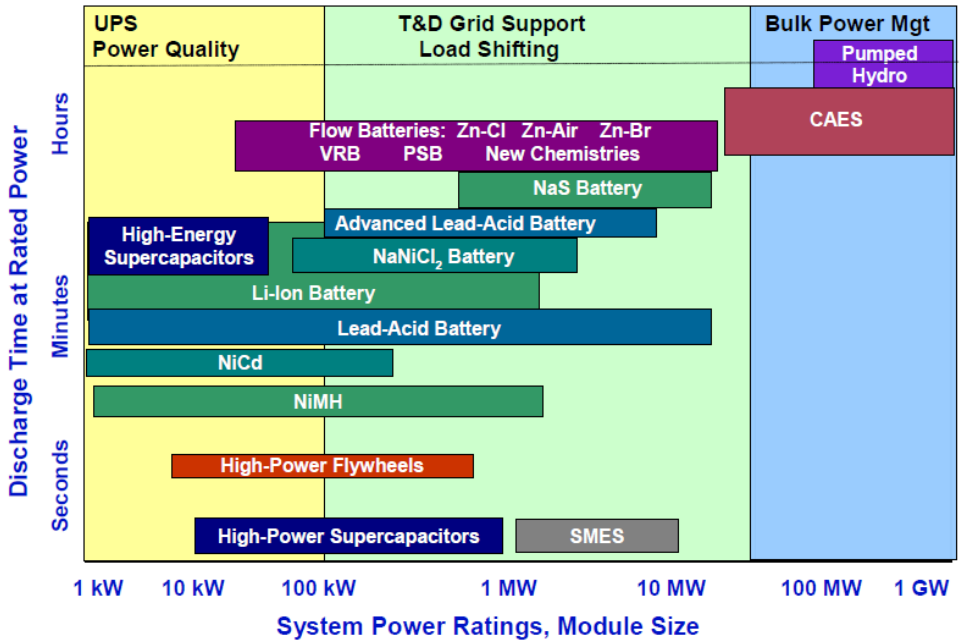

FIGURE 1.3 – Energy Storage System comparison given the rated power and expected discharge duration. Source : [23].

The continuous advances in electrochemical storage technology is part of the reason

why it is so versatile. As Lithium-ion Battery Energy Storage System (LiBESS) become more reliable and inexpensive, the applications for which they started to become cost-efficient increased accordingly. The electrical grid is one of these markets that benefit from the advancements in battery technologies. As mentioned before, the applications go from ancillary services, which help to ensure the nominal operation of the grid via voltage/frequency support, up to grid recovery or black-out mitigation [24]. Although historically storage deployment was primarily pumped storage hydropower (PSH), the speed and more convenient economics of batteries promoted their expansion as most grid applications do not benefit as much from the large energy storage capacity of PSH [25]. Battery energy density, efficiency, and lifespan have continued to improve, and modern Battery Energy Storage System (BESS) can reach up to 15 years of service. The price for BESS has also seen a continuous decrease in recent years, and it is expected for it to continue [22, 26].

1.1.2.1 BESS for Transmission and Distribution System Support

For the worldwide effort of reducing greenhouse emissions, the evolution and diversity of battery solutions have been beneficial. The apparition of LiFePO (LFP) battery cells in 1997 extended the lithium technology presence into the previously almost lead-exclusive market of electrochemical batteries for utility energy storage [27, 28], as well into newer domains such as the EV market. These grid-related applications can be seen in table 1.1, and the specific needs from the BESS vary strongly in responsiveness and needed capacity. E.g., Frequency regulation services need a fast and high-power response but not necessarily for long periods of time. In contrast, peak shaving requirements of power and capacity from the BESS are more balanced. Currently, around 50% of the deployed electrochemical power capacity is used for frequency regulation, followed in second place by electric supply reserve capacity with 10% and with less than 5% used in renewables firming [4]. By 2030, a conservative estimation positions the stationary battery storage capacity to 100 GWh, with almost half of it for behind-the-meter applications and the other half for utility services [29].

The future success of the deployment of BESS, especially LiBESS will be also contingent on the cost evolution, regulatory frameworks, and technological advancements that facilitate their integration and improve their operation capabilities [8, 29]. In addition, the control systems for industrial deployment face also challenges. The dynamic beha-

Services Provided by BESS	**Description**
Demand Side Management	ESS could increase or reduce the electric load at a node in the network.
Energy Arbitrage	Market optimisation can be done by storing energy when rates are low and selling at high demand moments.
Fast Response Frequency Regulation	Active power injection or withdrawal that responds to the deviations from the nominal frequency in the grid.
Voltage Support	Reactive power injection or withdrawal that responds to the deviations from the nominal frequency in the grid.
Microgrids	Small-scale grid in which local energy sources are present (e.g., BESS) to control both power production and consumption.
Renewable Firming	Increase the capacity and reduce variability in the energy and power output for vRES.
Transmission System Deferral	BESS can provide power closer to the load reducing the transmission network to use.
Off-Grid Systems	Small-scale system in which all the energy sources are local and limited. These local sources must guarantee the electrical grid.

TABLE 1.1 – Examples of services that can be provided by a BESS. Adapted from [4, 30].

viour of the BESS has to be considered, and precise model development and integration in such control systems needs to adapt to its evolving behaviour and the industrial site requirements [31].

Frequency and Voltage Regulation In this usage, the BESS follows a droop control. That is, the output power of the BESS responds to any deviation from the nominal frequency F_{nom} in the electrical grid. They usually take the form of a function $P(F)$ with a deadband around the nominal frequency. For voltage regulation the BESS can also have a droop control mechanism applied. In this case, the system injects reactive power depending on the deviation from the grid nominal voltage $P(U)$.

Although voltage regulation is expected from most production sites, frequency regulation is subject to a stricter framework. As it needs power generation, a regulatory and remuneration framework is generally proposed. In these, BESS bid their availability and regulation ability for a pre-determined period [32].

Energy Arbitrage A potential use for BESS is in the spot energy market. BESS allow to optimize the production to better use the price variations in the electrical grid. Never-

theless, this usage for BESS is still not economically feasible as electricity prices are too low in average. In a future where storage is more affordable the usage of BESS in this market could grow [32].

Demand-side management In these BESS applications we can find peak-shaving and load smoothing. Peak-shaving uses the storage to provide the power that exceeds the standard power of a point in the grid. Load smoothing does not focus on the peak power requested, but on reducing the variability of consumption. These two services, which can also be behind-the-meter solutions, help to avoid network congestion, transmission losses, increase power quality in general, and help mitigate vRES intermittency as mentioned before [32, 4].

vRES Capacity Increase & Firming The capacity factor of an energy source is the ratio of the output energy to the maximal theoretical output (1.1). A 1 kW diesel generator power plant that produces 12 kWh in one day given a down-time of twelve hours would have a capacity factor of 50%. In the case of individual solar and wind power plants, their capacity factors are classically estimated to be between 12%-15% and 20%-40% [33]. This low value in conjunction with high variability represent a problem to the grid managers as they need to guarantee the capacity production from the whole grid, and thus volatility of electricity is to be expected with large vRES penetration [34].

$$\text{Capacity Factor} = \frac{\text{Output Energy}}{\text{Max. Power} * \text{Time Window}} \tag{1.1}$$

To tackle the first problem and increase the capacity factor, the vRES power plants can do one of two things : have a secondary energy source to increase the total energy output or reduce the power rating from the power plant. The first solution represents higher financial investment, whilst the second promotes curtailment and by consequence a longer time before positive ROI. A middle ground between these two is the utilization of an energy storage. By using an ESS, the investment needed is reduced and energy is not wasted due to curtailment. Figure 1.4 shows an example of the three scenarios for a 100 kWc solar plant that is required to attain a 20% capacity factor. In a) the central is coupled with a complementary generator(often gas generators), in b) the rating was set to a lower limit, and in c) a storage was added to absorb the exceeding power. As it can be appreciated, the power rating from the complementary generator in a) would need to be at least 50% of the installed PV capacity to have the site work at its maximal kVA rating

the longest possible [1]. For the case with the reduced kVA rating alone, around 40% of the solar potential would need to be wasted. At last, in c) by using a storage and limiting the kVA rating it is possible to attain the capacity factor without PV power waste and a smaller power rating for the storage. In addition, the storage does not need to be next to the vRES source as dispersed ESS can be used for this [35].

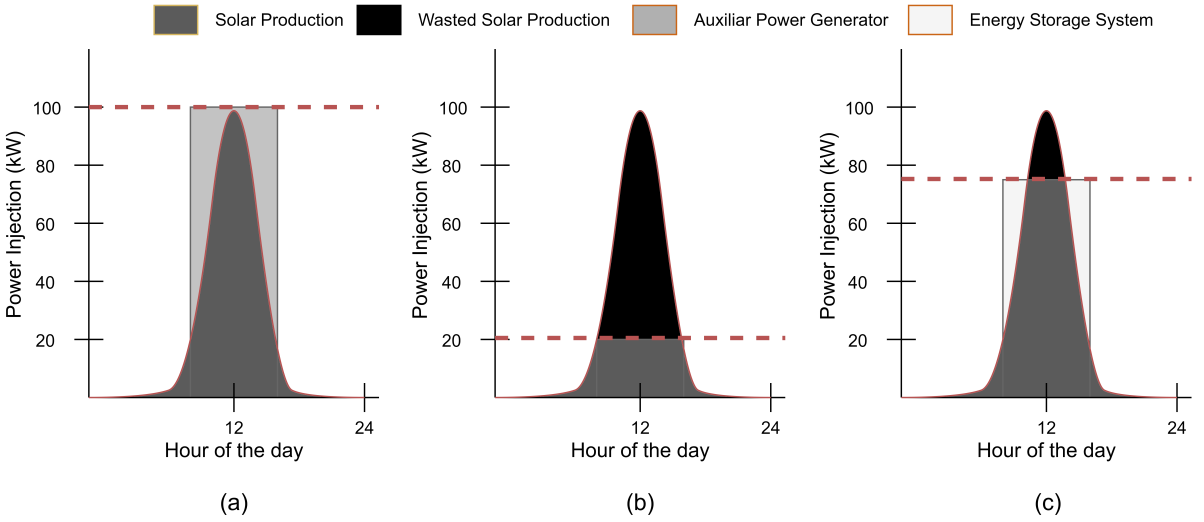

FIGURE 1.4 – Three scenarios for a PV power plant with a capacity factor of 20%. The dotted line represents the nominal power as considered by the grid operator.

Once the capacity factor is set or known for the vRES, the spotlight is given then to its intermittency. Tackling this problem and reducing the variability is known as *capacity firming*, and what is expected from a firmed capacity is the ability to respect power setpoints for a predetermined amount of time. Just as before, this can be achieved through the same three methods of auxiliary generators, curtailment, and ESS to compensate the over- and under-fluctuations. In previous works, the capacity firming scenario has seen the application of stochastic and deterministic strategies which aim to propose a solution to the PV uncertainty [36, 37, 38], but not enough attention has been given to the behaviour of the BESS when use for this application.

As vRES capacity firming needs a stronger financial commitment, their implementation has to be supported by the energy market. Capacity firming allows vRES to be more adept to current corporate Power Purchase Agreement (PPA), but the high cost of using BESS for this purpose in new power plants remains a barrier [39]. For this reasons, financial frameworks of vRES capacity firming must be proposed using day-ahead markets that remunerate capacity, either by bidding mechanisms or a by beneficial payment

1. A lower rating could be used to attain a capacity factor of 20%, but the operation of the secondary generator would need to be longer. A transformer is also less efficient at low load factors.

schemes [40]. In 2018, only 7 utility-scale hybrid power plants were classified for renewable firming in the U.S. representing 5% of the installed U.S. capacity [41]. Worldwide, BESS for vRES firming represented only 3% of the storage capacity but, as renewable integration is expected to increase and battery costs expected to decrease, it is estimated that by 2030 the BESS for capacity firming will represent around 13% of the total storage capacity worldwide with 24-57 GWh [4].

Microgrids A microgrid will be considered as any small-sized electrical grid composed of local loads and generators with or without [2] access to the utility grid. A residential microgrid for instance will be composed of at least a set of local loads (house demand), a set of electric generators (classically residential solar plants in rooftops), and a control system. This last element is a key component as it will coordinate the generators and the load to satisfy the needs of the microgrid or, if having a PCC, the needs of the utility.

By adding battery energy storage systems to these infrastructures, the benefits for the microgrid are wide and varied : higher resiliency, better flexibility, an ability to opt-in to improved energy price rate structures by the DSO, and even provide certain grid services [30]. BESS provide for the microgrids a way to manage the local production and demand, and shift energy to where it has more economic sense. As Li-ion BESS price continues to decrease, the penetration of BESS will continue to rise in future years for micro-grid uses.

1.2 Motivation and Challenges

The deployment of large-scale Lithium-ion Battery Energy Storage System (LiBESS) for energy production systems is a relatively new affair. Previously, many of these tasks were reserved to lead-based batteries but the limitations this technology had in energy density and electrical characteristics restricted their usage [27]. Nowadays most of the ancillary services provided by the Transmission System Operator (TSO) and Distributed System Operator (DSO) can be provided by LiBESS, including the services related to the increasing penetration of vRES. As these often involve Partial State-of-Charge Cycling (PSoC) cycling and a fast response requirement, lithium-ion based solutions presented themselves as a solution to the stress vRES bring to the grid [4].

In insular and small-sized electrical grids, the penetration of vRES is a more present concern than in continental sized grids. In the French islands for example, the maximal

2. Off-grid sites are considered a type of microgrid.

share of vRES was historically set to 30% to ensure grid safety [5]. As it is easier to attain a higher share of vRES in the electrical mix on these scenarios, the risks and costs of intermittency have to be explicitly taken into account by TSO/DSOs to ensure the safety of the grid. Reserve requirements often need to be larger, and the vRES lower capacity factor implies a larger cost for the grid operator [7]. To mitigate this, one of the tools DSOs have is imposing capacity firming requirements to new vRES electric power plants.

In 2015, the French Energy Regulation Commission (CRE) launched a call for tenders for new PV power plants in their Non-Interconnected Zones (ZNI) referenced in this work as AO ZNI 2015. In this call for projects, the proposed remuneration scheme and operational constraints formed a PV capacity firming framework which encourages the use of LiBESS to reduce the inherent intermittency from the vRES and increase the capacity from the sited for the DSO [42]. With a similar second call for tenders launched in 2018, this gives a total PV capacity firmed plant population of more than 100 MWc and 50 MWh of accumulated power injection and storage in these territories [43].

With an expected service life of 20 years for these power plants, the PV developers and constructors must anticipate the financial and technical challenges the sites will experience in their lifetime. To have long and short-term control on the performance of these site, the new problems developers need to face can be summarized in two : PV Forecasting, and BESS modelling with optimal usage. The focus in this work will be given to the second one, the BESS modelling and optimization.

As the use of high capacity LiBESS for energy production systems is recent, and even more for PV capacity firming scenarios, the specific behaviour the LiBESS has under this use is unknown. Li-ion BESSs are heavily influenced by the operational temperature, and the consequences it has on both longevity and performance is important. In addition, the State Of Charge (SoC) and State Of Health (SoH) have to be estimated and monitored in real time to ensure the battery management.

SPIE, the industrial partner of this thesis, is an international multi-technical electricity enterprise. It proposes and develops embedded solutions for diverse industries, including for PV power plants. As part of a partnership with GDS, a pure PV developer, SPIE faced the need in 2017 to start development on an Energy Management System (EMS) and Power Management System (PMS) to answer the control needs of future PV capacity firming sites that follow the AOCREZNI 2015. And within these developments, the need for precise LiBESS models to estimate the previously mentioned parameters was reaffirmed.

The challenges to address the LiBESS modelling constraints are primarily data scar-

city and low computational resources. Models and solutions would need to be precognized for situations without laboratory-grade data and the inability to perform recurrent characterization tests after deployment. The specific charge/discharge pattern from a PV capacity firming use case can also impact the system in unexpected ways, and long-term feedback of this is unavailable. The models themselves also need to be PV industry-focused, and run on modest hardware in isolated sites. As consequence, computationally inexpensive and reliable solutions are preferred.

Industrial Technical Gaps. To develop and deploy the control system for PV power plants under the AOZNI 2015 capacity firming framework, it is necessary to develop an Energy Management System (EMS) and an Power Management System (PMS). The following industrial challenges and knowledge gaps are faced in this process :

- **(IG1)** Model the BESS in a way that is easy to deploy in industrial sites and allows a correct control of the installation.
- **(IG2)** Develop algorithms that optimize the financial performance given the intermittency of the solar production and the storage.

1.3 State of the art

This section provides an overview of Li-ion battery chemistry and a review of the current paradigms applied for LiBESS modelling. The objectives of these are to provide a theoretical background to contextualize the need of LiBESS-specific models, and to identify **research gaps** existing in the literature that fail to address the challenges of LiBESS integration in industrial PV capacity scenarios.

Additional information on these subjects will be provided later in each corresponding chapter.

1.3.1 Lithium-based BESS chemistry

Since the discovery of the voltaic pile in the 1800s by Alessandro Volta, battery technology has been a prolific field of research. Primary (non-rechargeable) and secondary (rechargeable) batteries have been subject to a plethora of physical and chemical configurations to attain better and longer-lasting cells. The modern dry alkaline battery cell was first patented in 1947, with wet alkaline cells mass produced since 1889. For the secondary batteries, the technological path followed lead-acid based cells (1854), nickel-based cells (1897), and more recently (1965) lithium-based technologies amongst others [44].

Although lead batteries have been historically the preferred choice for stationary energy storage due to its low cost, ease of operation, and relative safety, lithium technologies have progressed since their apparition (see table 1.2 for a technological timeline) and have become a suitable replacements.

Year	**Chemistry**	**Wh/kg**	**Wh/L**
1978	Li//TiS2	130	280
1981	Li//LiAlCl4-SO2	63	208
1983	Li//NbSe3	95	250
1987	LiAl//polyaniline	-	180
1987	Li//MoS2	52	140
1989	Li//V2O5	10	40
1989	LiAl//polypyrolle	-	180
1989	Li//Li0.3MnO2	50	140
1990	LiVOx	200	300
1991	C//LiCoO2	150-190	184-240
1993	C/LiMn2O4	100	180
1997	LiFePO	90-160	220

TABLE 1.2 – Technological evolution of Lithium based battery cells. Adapted from [45, 46, 28].

The basic principle of any electrochemical cell is the oxidation (1.2) and reduction (1.3) reactions that occur at the electrodes. In these two, either an electron is given to a material (reduction), or an electron is taken from it (oxidation). The two reactions together form a redox cell (1.4) for which its electrical open circuit potential and energy capacity is dependent on the materials used and their physical structure [47]. The exact composition of these electrodes, as well as the electrolyte through which the elements travel in the cell, are what define a specific cell against another.

$$\mathrm{xLi} + \mathrm{ne} \iff \mathrm{bB} \tag{1.2}$$

$$\mathrm{cC} - \mathrm{ne} \iff \mathrm{dD} \tag{1.3}$$

$$\mathrm{aA} + \mathrm{cC} \iff \mathrm{bB} + \mathrm{dD} \tag{1.4}$$

Lithium, the most electropositive [3] element in nature, belongs to the set of materials which offer attractive characteristics for battery manufacturing. Although not existent in its pure form, its extraction can be done from different ores. The specific energy of Li metal is 3860 $\mathrm{mAhg^{-1}}$, and it presents a standard redox potential of −3.04 V. In addition, it is a

3. Tendency to donate electrons, the contrary to electronegativity [48].

Technology		OCV	Energy Density
Lithium Iodine	$Li/LiI/I_2$	2.8 V	100-200 Wh kg^2
Lithium Bromine Trifluoride	Li/BrF_3	5 V	2680 Wh kg^{-1}
Lithium Thionyl-Chloride	$Li//SOCl_2$	3.6 V	N/A
Lithium Sulfur Dioxide	$Li\text{-}SO_2$	2.95 V	280 Wh kg^-1
Lithium Manganese Oxide	$Li\text{-}MnO_2$	3.3 V	150-250 Wh kg^-1

TABLE 1.3 – Non-exhaustive list of Primary Lithium Cells technologies

light metal (6.941 g mol^{-1} and density of 0.51 g cm^{-3}) which increases its attractiveness for embedded and portable applications.

As stated before, lithium-based batteries can be regrouped into primary and secondary. The former (see table 1.3) are the most energy dense having an average density of 250 Wh kg^{-1}, while the latter exhibit a weaker energy density with the advantage of rechargeable. The difference between these two battery types depends on the lithium form and, more fundamentally, the kind of process taking place.

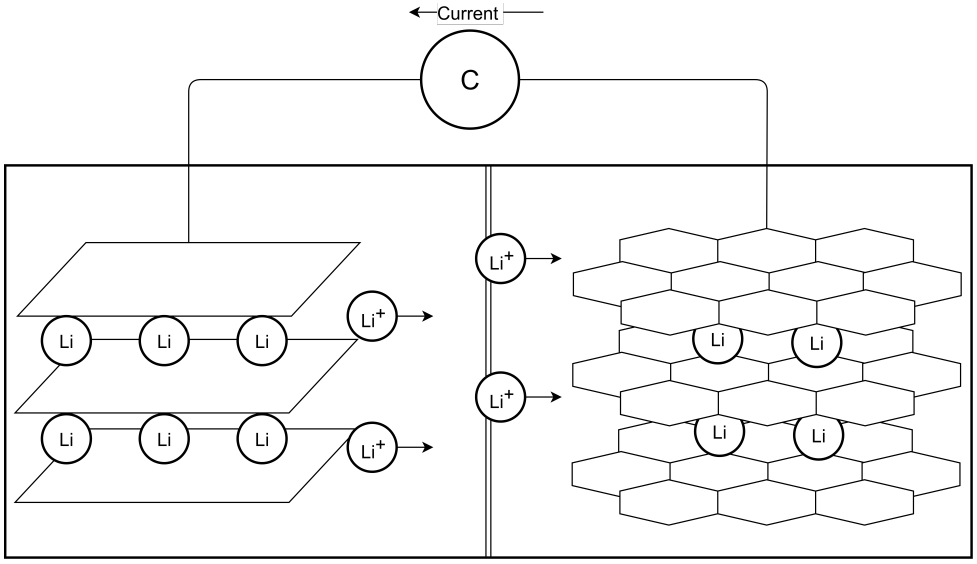

FIGURE 1.5 – Lithium intercalation in the negative pole of the Li-ion cell.

In primary batteries, lithium is present as a metal anode and is sent to the cathode in the discharge process. Secondary lithium batteries are instead based on the notion of lithium ions intercalation (see fig 1.5) in the cathode. Although lithium metal can be present in rechargeable batteries to supply the ions, most use two lithium compounds as electrodes and pure Li metal is not present [47]. Secondary battery cells that use lithium compounds are known as Li-ion battery (LiB), name that will also be adopted in this work to reference this kind of battery technology. An example of a LiB chemistry is a $LiCoO_2//C$ cell in which the anode is composed of graphite, and for which its cell reactions are seen in (1.5) - (1.7). Table 1.4 summarizes this and other modern graphite li-ion

Type	Cathode	Cell voltage (V)	Energy Density (Wh kg^{-1}
LCO	$LiCoO_2$	3.7-3.9	140
LNO	$LiNiO_2$	3.6	150
NCA	$LiNi_{0.8}Co_{0.15}Al_{0.05}O_2$	3.65	130
NMC	$LiNi_xCo_yCo_{1-x-y}O_2$	3.8-4.0	170
LMO	$LiMn_2O_4$	4.0	120
LNM	$LiNi_{1/2}Mn_{3/2}O_4$	4.8	140

TABLE 1.4 – Graphite-based li-ion cells. Source : [47].

batteries with their relevant electrical characteristics. Nowadays, the commercially available lithium technologies vary primarily between Lithium Nickel Cobalt Manganese Oxide (NCM),Lithium Nickel Cobalt Aluminium Oxide (NCA), Lithium Iron Phosphate (LFP), Lithium Titanate (LTO), Lithium Manganese Oxide (LMO) and Lithium Titanate (LTO) to mention a few [49, 27]

$$xLi^+ + xe^- + 6\,C \rightleftharpoons Li_xC_6 \tag{1.5}$$

$$LiCoO_2 \rightleftharpoons Li_{1-x} + xLi^+ + xe^- \tag{1.6}$$

$$LiCoO_2 + 6\,C \rightleftharpoons Li_{1-x}CoO_2 + LixC_6 \tag{1.7}$$

In the realm of rechargeable battery technologies, other non-lithium-based solutions exist but Li-ion cells present more advantageous behaviours like low self-discharging rates, higher specific energy, and no memory effect. The Li-ion battery (LiB) technology is however not free of a set of drawbacks. Over-discharge and over-charge of LiB cells can permanently damage the electrodes, and because of this systems that control each cell voltage and operation are needed [46]. This control system, referred to as Battery Management System (BMS), guarantees the continuous operation and helps to extend the useful life of the batteries. The following section 1.3.1.1 will offer a short review of the issues LiB batteries can face due to operation in standard and extreme situations, as well as the challenges they represent.

1.3.1.1 Li-ion battery issues and challenges

The three main situations which can impact a LiB performance and expected life are the over-discharge, the over-charge, and the operation under extreme temperatures. The different reactions occurring can be generalized into the dissolution of the electrode, the generation of flammable/reactive elements inside the cell, and/or the creation of a Solid Electrolyte Interface (SEI) [50]. For this last one, although its apparition on the

anode is normal at the early stages of the LiB life, its unchecked growth is a concern due to performance and capacity losses. SEI immobilizes part of the available lithium generating these losses.

The SEI formation process due to cycling can be seen in figure 1.6, and it can be a risk-factor for critical failure. The presence of the SEI increases the stress of the cell and can be at the origin of a malfunction. As the cycles go, the charge/discharge process makes the SEI layer grow and dendrites can appear. If the dendrites become large enough, a short-circuit can happen. This in turn creates a heat source that starts an exothermic chain reaction in neighbouring cells if it reaches a threshold temperature. This uncontrollable reaction is known as a thermal runaway and, although it can be generated by external factors too, the SEI is recognized as a key factor that can trigger it [31, 51].

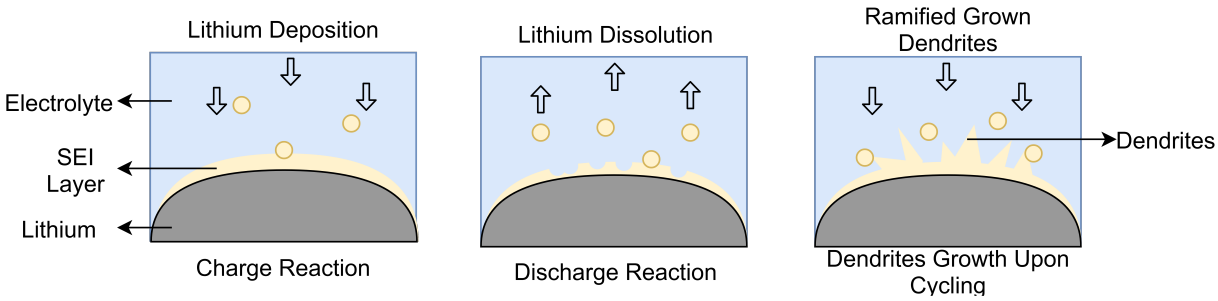

FIGURE 1.6 – SEI dendrite formation process. Adapted from : [47].

Battery over-discharge When discharging the batteries, it is possible to reach voltages at which undesirable reactions start to appear. The electrodes can start to dissolve into the electrolyte which reduces both the available exchange surface and available solvent. In $LIPF_6$ cells, this reduction of material is observed at potentials below 1.5 V vs Li/Li^+. The capacity and life of batteries suffering from these phenomena decreases as consequence.

A second phenomenon that can occur if the voltage reaches low levels is the oxidation of the current collectors. Copper oxidizes (1.8) at low voltages and then can redeposit at the electrodes. This increases the internal resistance of the cell and can additionally generate copper dendrites [52].

$$Cu \longrightarrow Cu^+ + e^- \tag{1.8}$$

Battery over-charge Capacity degradation due to high voltage (over-charge) in LiB cells can be considered to be issued from the next phenomena : lithium deposition at the anode, electrolyte oxidation at the cathode, oxygen evolution, and increase in self-discharge. Lithium deposition occurs as the available ions react and solidify (reaction in

(1.9)) instead of intercalating with the electrodes.

$$Li^+ + e^- \longrightarrow Li(s) \tag{1.9}$$

For electrolyte oxidation, this process is highly dependent on the electrolyte itself used inside the cell. Reported decomposition voltages with common electrolytes in commercial LiB cell batteries is around 4.5 V. Similar to the case of over-discharge, the loss in electrolyte impacts the capacity, efficiency, and also generates secondary products that can impose a safety risk. Oxygen is one of these by-products, and its accumulation can react with lithium aggressively. Self-discharge has also been linked to electrolyte oxidation, generating as well some irreversible capacity loss given that lithium is used in part of the by-products[52].

Operation outside standard conditions : High and low temperatures. LiBs are very susceptible to operation outside a definite range of temperatures. The effects of operating temperature involve the three main parameters for the batteries : capacity/power fade, self-discharge, and the risk of thermal runaway. For all three, it is possible to distinguish the related effects coming from low and high temperatures.

For high temperature, capacity and power were reported to decrease significantly upon cycling when temperatures are above 50 °C for any LiB. Storage of unused LiBs at high temperatures also reported an impact on both parameters. Self-discharge also increases at high temperature storage due to some SEI elements dissolving in the electrolyte and increasing conductivity. Lastly, thermal runaway is promoted by operation in hot conditions too. After reaching a critical temperature, an uncontrollable chain reaction can take place : at 85 °C, the SEI decomposes exothermically which continues to rise the temperature. As the temperature continues to rise, other films can form and decompose, the electrolyte might vaporize and combust, and/or separators could fuse creating short-circuits in an exothermic feedback [53, 54].

Regarding the operation under cold temperatures (<0 °C), this impacts the LiB by promoting SEI formation primarily. This reduces the capacity due to the active material loss and increases the internal resistance. The risk of SEI dendrites formation rises as well and thus the risk of a short circuit[55, 53]. This critical failure scenario can generate a thermal runaway too.

1.3.2 LiBESS Modelling

The modelling of Lithium-ion Battery Energy Storage System (LiBESS) is an ongoing field of research. As mentioned before, the proliferation and variety of Li-ion technologies pushes for a reliable understanding of the different processes and degradations the battery cell suffers due to its usage. A precise estimation of power and energy capacity loss due to SEI growths or other parasitic phenomena not only allows pre-emptive actions to reduce downtime in time-critical systems, but also gives the opportunity to enhance the control systems built around a LiBESS such as an EMS/PMS.

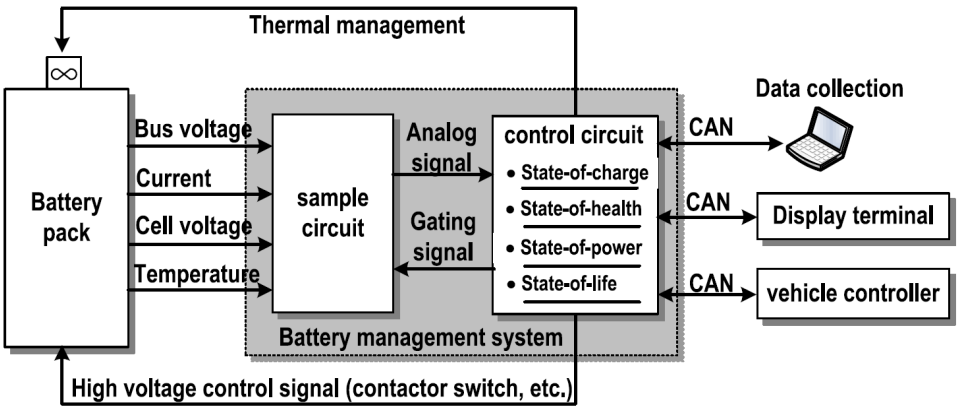

FIGURE 1.7 – Schematic of the elements in a BESS and interactions by the BMS. Source : [56].

As seen in section 1.3.1, LiBESS are particularly sensible to thermal-related degradation. Operation in certain ranges of temperature impacts the power output, capacity, self-discharge rate and probability of a thermal leakage [53, 50]. To reduce the occurrence of these phenomena, Battery Management Systems (BMS) are implemented to monitor the battery, estimate the State Of Charge (SoC), the State Of Health (SoH), and avoid undesirable BESS operation [57].

Different BMS approaches and levels exist and are used depending on the application. Either at cell, module or system level, new electrical and control architectures are constantly being proposed to improve BESS performance and accuracy [58, 59, 60, 61]. The general architecture of a BMS can be seen in figure 1.7, and the functions of a BMS can be listed as follows :

- State estimation
- System control
- Error management
- Thermal Management
- Measurements and monitoring
- Communication

From this list we can easily distinguish between functions that are hardware related and those dependent on software. The error management protocols, safety of individual or array of cells, switch control systems, and voltage and temperature sensors are mostly hardware subjects of research in BMS development [59, 60]. The software side, composed primarily in state estimation, is however more related to cell battery modelling research.

On battery modelling, the approaches available follow two branches in general : either a physics-based model or a mathematical model. Whilst the former focuses in the representation of the chemical and physical phenomena, the latter focuses on parameter estimation given previous collected data. This distinction creates a difference in the expected computational load and therefore limits their implementation to specific scenarios.

Physical Modelling One of the most complete physical representations of battery cells are the thermo-chemo-electro-mechanical models. As the name implies, these family of models regroup and relate all the physical phenomena and processes that occur when charging and discharging the cell (see table 1.5). A multi-physics solution that takes in account these reactions and models each phenomenon not only demands high processing power, but it also requires material modelling parameters that are usually difficult to obtain [51].

Process	Common Physical Modelling Paradigm
Intercalation reaction	Butler-Volmer equation.
Electronic conduction	Ohm's Law.
Diffusion in active particles	Mass balance equations.
Swelling/Stress	Virtual Power models (Continuum mechanics).
Phase segregation	Sharp interface modelling (Cahn-Hilliard theory).
Electron Migration	Electroneutrality (Maxwell equations)
Electrolysis	Faraday's Law
Ionic diffusion in the electrolyte	Mass balance equations
Ionization reaction	Reaction rates in mass balance equations.
SEI formation	SEI formation models

TABLE 1.5 – List of processes that occur in Li-ion battery cells. Adapted from : [51].

Another existent physical approach to the modelling problem is the Doyle-Fuller-Newman (DNF) li-ion battery model. In this implementation, the Ohm's law equation is applied to the electrodes to link the potentials with the intercalation current density, i.e. the current from the electrolytic medium entering the electrode. Fick's law is then used to describe the ion-concentration and diffusion at the electrolyte, and at last the Butler-Volmer equation describes the intercalation current density given the different potentials

and an equilibrium or open-circuit voltage [62, 63].

Multiple implementations of the DNF li-ion model have been reported in the literature, most with the focus of finding reliable and efficient simplifications to the nonlinear partial differential equations (PDE). Xia et al. [63] used a spatial and temporal discretization to convert the DNF model into a set of coupled nonlinear algebraic equations to simplify and speed up the calculations. Kehs et al. [64] utilized Legendre polynomials and Galerkin projections as the solutions to the equations, and Forman et al. [65] approximated the diffusion expression analytically to have a simpler system. This list of works, although not exhaustive, shows the predominance and importance of the model and how any implementation in real time applications is still a challenge [31, 51, 63, 66, 67].

Another common approach to physical modelling of li-ion cells is the abstraction of its properties into equivalent circuits. Here the cell behaviour is approximated by electric linear elements, allowing for simpler and faster approximations of the battery state. The trade-off of this advantage is the loss of insight into the physical phenomena that occurs in operation. The appendix B includes a summary of different equivalent circuit models of a battery cell, and figure 1.8 shows three og the most simple cell equivalences.

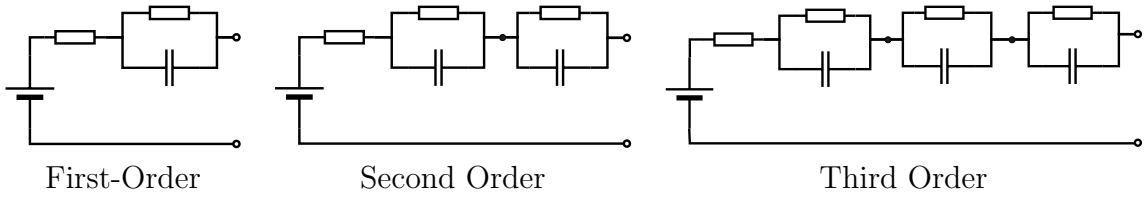

FIGURE 1.8 – RC equivalent circuits of a battery cell

Thermoelectric models, i.e., models that explicitly take into account the cell temperature and heat generation, can also be implemented with equivalent circuits. Panday et al. (2015) proposed a temperature-dependent SoC equation for a second-order RC equivalent circuit [68], while in other works the effect is considered to create a general average OCV-SOC relation [31, 69]. This approach is however underused, and literature is scarce.

Mathematical Modelling and Parameter adjustment As mentioned before, complete physical models, although effective, are often computational heavy processes and thus ill-suited to implement in devices with time-critical activities, low processing power or limited energy availability. In contrast, data-driven mathematical models have proven to be responsive and to provide high accuracy(<3% error) for state estimation [47, 70].

Within this rubric, another distinction can be done depending on the level of abstraction the model has. A purely data-driven model is the most abstract (figure 1.9) and

it fits a general function to a set of data so it can have a similar behaviour, not being important the understanding of the underlying mechanisms as they are "hidden" in the fitting. For example, Guo et al. (2015) modelled the capacity fade by using a Bayesian approach where only some physic variables were used to improve the results [71].

The parameters that data-driven mathematical models estimate are often the State Of Charge (SoC) and State Of Health (SoH). These two parameters are indicative of the general state of the storage system and, although useful for management purposes, do not offer explicit physical or chemical information. Hu et al. (2014) used k-nearest neighbour regression to estimate the capacity of the storage [72], and other authors have used extreme machine learning and neural networks to create models based only in the state of the system [73, 74].

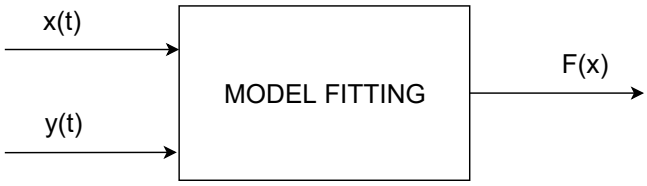

FIGURE 1.9 – General Operation of a Mathematical Model

For less abstract approaches, a mix between physical and a data-driven modelling are also available solutions. While the systems dynamics are described usually by simple physical models, the parameters are obtained generally through data-fitting techniques. One common implementation of these techniques are equivalent circuits and Kalman/Particle Filters for parameter estimation [69, 70, 75].

1.3.2.1 LiBESS Thermal modelling

Historically, thermal characterization of Li-ion battery (LiB) has been primarily based on single and pack cells. The simplified single 1D cell thermal model is commonly based on the energy balance equation. Seen in equation (1.10), this foresees a uniform temperature in the cell and stipulates that the energy generated within the cell is equal to the heat stored and the heat exchanged with the ambient temperature [76]. This model, although simple, requires the temperature dependence of the open voltage circuit. It is also unable to represent the effect of temperature in the electrochemical reactions, which limits the insights we can obtain from it [77].

$$Q = I(V_{oc} - V) - T\frac{\mathrm{d}V_{oc}}{\mathrm{d}T} = h(T - T_a) + mC_p\frac{\mathrm{d}T}{\mathrm{d}t} \tag{1.10}$$

Three dimensional models of this approach have also been proposed. Damay et al.

used a thermal network that distinguishes each of the axis in a cell pack, and Chen et al. proposed a 3D model for a layered cell [78, 77]. These approaches, use simplification methods in which variables are combined to reduce the computational effort they take. More detailed modelling of the thermal component often use Finite Element Method (FEM) coupled with the electrochemical and transport phenomena occurring within the cell [79].

Besides charge/discharge temperature modelling, thermal models for runaway scenarios have also been proposed. Although similar in principle to (1.10), in this scenario the heat sources become more abundant. Tran et al. did a review on the different heat sources and modelling approaches occurring in the phenomena, and explicitly considered 6 different sources of heat. Amongst them, the most predominant heat generation source for a thermal runaway is the appearance of an internal short circuit (ISC). This itself has been modelled with good results in NCA 1865 cells, and even the case of short circuit induced by nail penetration has been investigated for thermal runaway [80]. Spotniz and Franklin also explored the kinetic reactions of LiB under abusive conditions, focusing more in the chemical and kinetic reactions taking place [81].

A very important thing to mention from the previous mentioned models is that to develop and validate the proposed equations, a series of experimental measurements have been done in laboratory or near-laboratory conditions. Li-ion cells were subject to adiabatic and isothermal tests in [76], an experimental setup with an insulation and a cooling system was built for the same purpose in [78], and in [77] the temperature, surface temperature, and voltage were studied under constant ambient temperature at different discharge rates.

All these tests done on the systems diverge strongly from what can done or obtained from whole BESS that are deployed in industrial sites. As commercialized BESS have proprietary LiB and BMS technologies, the kind of cell that is used is not always common information. Even for the case in which the cell type is known, the physical characteristics of the cell pack and the power requested from each pack at any given time remain hidden from the final user. As systems are fully integrated, battery pack temperature measurements become limited and inadvisable as they could mean some form of alteration to the structure of the BESS and void the associated warranty as consequence.

Research Gaps. Given the previous works on LiB thermal modelling, it is possible to observe that environments and measurements are from laboratory-controlled experiments. Models based on industrial environments where measurements are unavailable or scarce is not widely treated. The following research gap can be identified from this :

— **(RG1)** In cases where the LiBESS is in operation and data is scarce, suitable methods and models to estimate the thermal behaviour is unclear. This without even taking into account that BESS architectures and operation can change depending on the manufacturer and the sophistication of the BMS.

1.3.2.2 LiBESS State-of-Charge Modelling

The State Of Charge (SoC) is one of the most important parameters any BMS has to estimate. Defined as the current capacity of the system compared to the current maximal capacity (1.11), this is a crucial indicator for the end-user and the associated control system. An incorrect SoC can waste energy storage potential by stopping charge or discharge too soon even while energy remains available, or at worse it can permanently damage the system by allowing an over-discharge that generates secondary reactions as seen before.

$$\mathrm{SoC} = \frac{E_t}{E_{\max,t}} \tag{1.11}$$

Because the key role it has in battery management decisions, a lot of interest has been given to the SoC estimation methods. For a single LiB cell, these can be broadly classified into looking-up based, ampere-hour integral methods, model-based estimation, and data-driven. In the case of battery pack SoC estimation the techniques used are either to estimate each cell, use the worst performing cell as reference, or assuming the system behaviour as a single cell. By using screening processes to ensure that batteries have similar physical behaviours before the pack construction, and by bias corrections methods, the difficulties of battery pack estimation due to cell differences are reduced [56].

Look-up based methods These methods are based entirely on a direct relationship between a physical measurement and the SoC. This measurement can be the internal resistance, the impedance, the Electro-Magnetic Force (EMF) or the OCV. The simplest of these is the OCV-SoC relation as seen in figure 1.10. The SoC is determined depending on the OCV measurement at the cell terminals after some relaxation time. Using an EMF-SoC look-up is similar to it, but it also needs to have a more extensive look-up database to represent the different discharge currents it can have [82]. Resistance and impedance

look up tables, although have reported errors lower than 2%, are more complex as require complex charge/discharge cycles [83, 84].

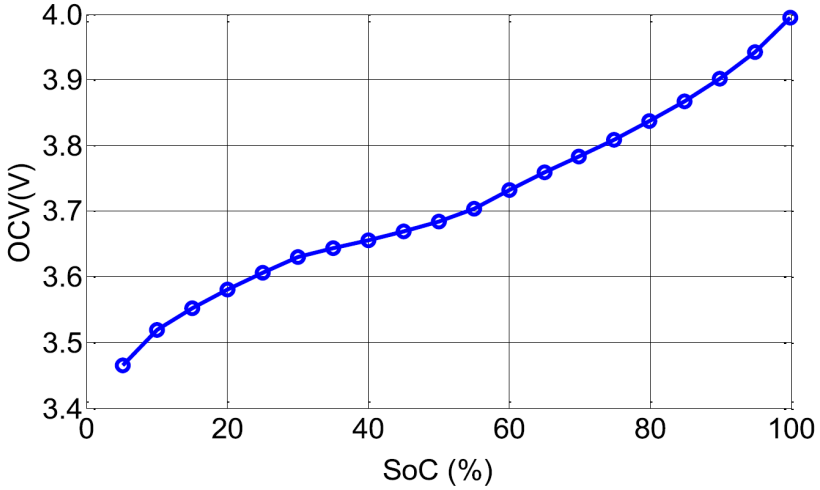

FIGURE 1.10 – OCV-SoC relation for a Li-ion Polymer Battery cell. Source : [56].

The major inconvenient of this method lays in the need for the LiB to be in a static or non-operational state. Look-up tables (except EMF) require static conditions and are incompatible with any real-world application [85].

Ampere-hour Integral Methods Also referenced as coulomb counting, this is one of the most used methods in SoC estimation. Based on equation (1.12), it estimates the SoC by measuring the current in and out of the system and integrating it over time. The most basic version here presented consists only of an efficiency coefficient η and the nominal capacity C_{nom} [85].

$$\mathrm{SoC}(t) = \mathrm{SoC}_0(t_0) - \frac{\eta}{C_{nom}} \int_{t_0}^{t} I(t)\,\mathrm{d}t \tag{1.12}$$

The inconvenience this method presents is however that it inherently has a cumulative error that can be important if recurrent calibrations are not done. The precision of the measurement devices can slow down the error growth, but it cannot eliminate it completely, and in addition the initial $\mathrm{SoC}_0(t_0)$ measurement has to be accurate to avoid carrying over an error from the beginning [85, 56]. By improving the initial SoC_0, it has been reported that is possible to limit the error below 4% [86].

More advanced versions of this method have also been reported. Panday et al. incorporated an SoC model that uses this approach for the SoC and includes a thermal component to improve the estimation [68]. Feng et al. used a modified version of it to calculate the State-Of-Discharge (SoD) via a current and temperature dependent efficiency

parameters, showing good results for cells when compared to the manufacturer data [87].

Model Based Methods This category includes any model that aims to predict the SoC by using an intermediary model that simulates the behaviour and state of the cell. It is possible to distinguish three classes : Electrochemical Models (EM), Equivalent Circuits Models (ECM), and Electrochemical Impedance Models (EIM).

For electrochemical models, these are based on the 1D charge/discharge behaviour as described by Newman-Fuller-Doyle. This model, based on the kinetics and chemical reactions within the electrolytes and anodes, is able to express the current density and potentials found in the cell. The set of equations in this model are able to predict the cell potential and power under different discharge conditions [62]. Simplifications that go from order reduction up to a single-particle approach reduce the computational effort they require, but even after that they remain complex for wide-spread application in BMS [56].

Different implementations of Equivalent Circuits Models (ECM) circuits have also been reported in the literature. These include first-order RC models for LiNMC cells, and first-order RC with hysteresis for $LiFePO_4$ technologies. In both of these the parameter fitting process was done through a multi-swarm particle optimization [88]. Cheng et al (2016) used a third-order RC model to approach the behaviour of LiNMC/graphite cells, showing a reduction in root mean-squared errors (RMSE) when compared to second (-6.25%) or first-order (-87.5%) RC equivalent circuit for the terminal voltage [69]. For these examples, to estimate the SoC it was also required the use of either look-up tables or coulomb integrators in addition to the ECM. The complexity and effort in ECM is localised primarily in determining the values for the electrical elements to reproduce the dynamics of the system [89, 68].

In what concerns EIM, they are an advanced version of Ethylene Carbonate (EC) models as they incorporate additional elements in the circuit. These supplementary elements (Warburg, constant phase, ZARC, etc.) are determined using Electrochemical Impedance Spectroscopy (EIS), and have been found to show SoC errors of less than 1%. The high computational efficiency of these methods is also an advantage [85, 56]. However, due to the need of doing EIS on the batteries, these methods are ill-adapted for embedded solutions as in EVs [90].

An important element in this family of methods is the usage of different techniques to increase the precision and robustness of the state estimation in the models. Any model-based method follows the general process seen in figure 1.11, and the choice of state estimation technique is key. Barillas et al. [70] did a comparison of four algorithms when

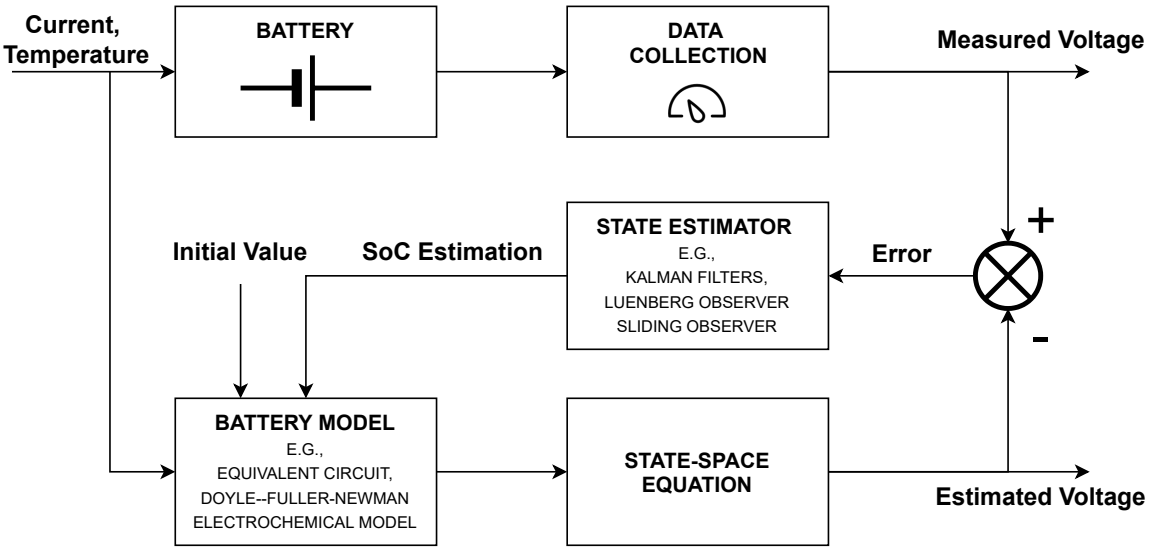

FIGURE 1.11 – Example of the process followed in model-based methods. Adapted from : [56].

applied with an EC model and, although the SoC precision was similar, a trade-off between computational time and results was obvious. Sigma-point filter methods had the best results, but it was more computationally expensive, while a Luenberg observer was the fastest but with a larger error (See appendix A for details on the methods).

Data-driven Estimation Methods Methods in this class have the particularity of being primarily based on input-output data and are also referenced as black-box models or learning algorithms. The underlying behaviour and equations do not have any real physical connection with the battery cells, and thus are unable to give insights or other information other than the one used for creating the model. The advantage of this is that little knowledge of the system and mechanics is needed, and thus any uncertainty is implicitly managed by the model [56].

The techniques here include are Neural Network (NN) Methods, Deep Learning (DL) Methods, Support Vector Machines (SVM), Fuzzy Logic Methods, and Genetic Algorithms Methods to mention a few. The average error found in these methods was found to be less than 6%, which is relatively high compared to other SoC estimation methods. Deep learning reduces the error to <2%, but it is computationally more expensive. They all are however adept for embedded systems and offer independent models that can be applied in many cases. The main drawback is that they require a large amount of training data to be effective and are sensitive to the quality of the data [90]. Appendix A offers more details on the inner workings of these methods.

Research Gaps : We can distinguish the following gaps in research within the majority of the SoC estimation research :

— **(RG2)** Model-based methods for whole BESS are not commonly developed and validated. Focus is mostly given to individual cells or battery packs at most which ignore or do not include a BMS that modifies the behaviour.

— **(RG3)** Although data-driven models are adapted for large-scale and complex BESS, their usage is limited as they need to be first deployed. In the development phase of new projects, data is not available and the applicability of these models is limited as consequence.

1.3.2.3 LiBESS State-of-Health Modelling

The State Of Health (SoH) is defined as the current maximal capacity C_t relative to the nominal capacity C_{nom} maximal current and is normally expressed as a percentage. Related terms are the Capacity Loss C_{loss} and the Remaining Useful Life (RUL). This last one indicates the remaining time the BESS can operate before reaching its End-of-Life (EoL), i.e., the SoH at which the system is considered to no be able to provide its original service. EoL is normally defined by the manufacturer to be between 70%-80% of capacity retention (SoH= 0.7).

$$\text{SoH} = \frac{C_t}{C_n} \tag{1.13}$$

$$C_{\text{loss}} = 1 - \text{SoH} \tag{1.14}$$

$$\text{RUL} = t(SoH = SoH_{EoL}) - t \tag{1.15}$$

To model this parameter, just as with the case of SoC estimation, multiple approaches and techniques exist. Berecibar et al. in a critical review of SoH estimation proposed two general classifications for methods aimed at real-life applications. The first, named experimental techniques, revolves around direct measurements or models based on measurements. The second classification, adaptive models, includes numerical methods with parameter estimation techniques that are coupled with EC models [91].

Experimental techniques In this category, it is possible to further divide into two families : direct measurements and models based on measurements [91]. Direct measurements methods to estimate the SoH are :

— Internal Resistance : By using Ohm's law (1.16) it is possible to monitor the internal resistance of a battery. These methods need to apply different discharge currents to determine the SoH, which naturally increases with aging [91, 92]

$$R_{\text{int}} = \frac{\Delta U}{\Delta I} \tag{1.16}$$

— Impedance Measurements : Similar to the last method, the impedance of the battery can indicate the health of the system. The impedance, obtained through EIS, is however an element of a more general EC model which tends to have a higher accuracy [92].

For the case of SoH models based on measurements, they differ in that they feed the measurements to models which afterwards estimate the SoH. They include the following techniques :

— Data maps
— Probabilistic methods
— Coulomb counting
— Support Vector Algorithms
— Parity Relations
— Failure Detection
— Sample Entropy
— Big Data
— Destructive methods

For the majority of these, charge/discharge and internal resistance measurements are used to determine the degradation from the battery. They however still need vast information on the behaviour of new and old batteries. It is impossible to approximate the degradation without generating such a dataset beforehand, and only physical models used for failure detection and prediction could avoid using such datasets. In all cases, the more accurate estimations of the SoH from a cell are obtained through destructive methods, e.g., Scanning Electron Microscopy (SEM), Atomic Force Microscope (AFM), and Raman spectroscopy. However, the permanent damage to the cell eliminates its usefulness in any real-life application [91].

In the reported literature, these techniques have an average error of 6%, with the internal resistance methods having the worst performance (min. error of 5%, max. error of 20%). Amongst those with better results are big data methods and impedance, having higher accuracy with a lower variability. The other techniques such as Support Vector Algorithms have shown good results on RUL prediction, but with the caveat of the results being only for small batteries so far [93, 94].

Adaptative models In this category, we can find the following techniques :

— Autoregressive Integrated Moving Average (ARIMA)
— Kalman Filters (Standard, Extended, Unscented, Dual Extended)
— Observers
— Fuzzy Logic
— Artificial Neural Networks
— Least Squares.

All these methods have shown in general a good performance to estimate the SoH compared to measurements-based methods. Figure 1.12 from [91] shows an average max. error of 10%, and an average error of less than 5%. In these, it is important to mention that Kalman filters are more common in real-life applications due to the low computational effort they require. ANN and fuzzy logic have seen an increased interest recently and have shown promising results too. Bai et al. used a neural network with a dual extended Kalman filter to predict capacity retention in cells, converging rapidly and having a Mean Absolute Percentage Error (MAPE) error of less than 3.5% in long term predictions [95]. Similarly, He et al. used a similar approach to create RUL probability distributions [96].

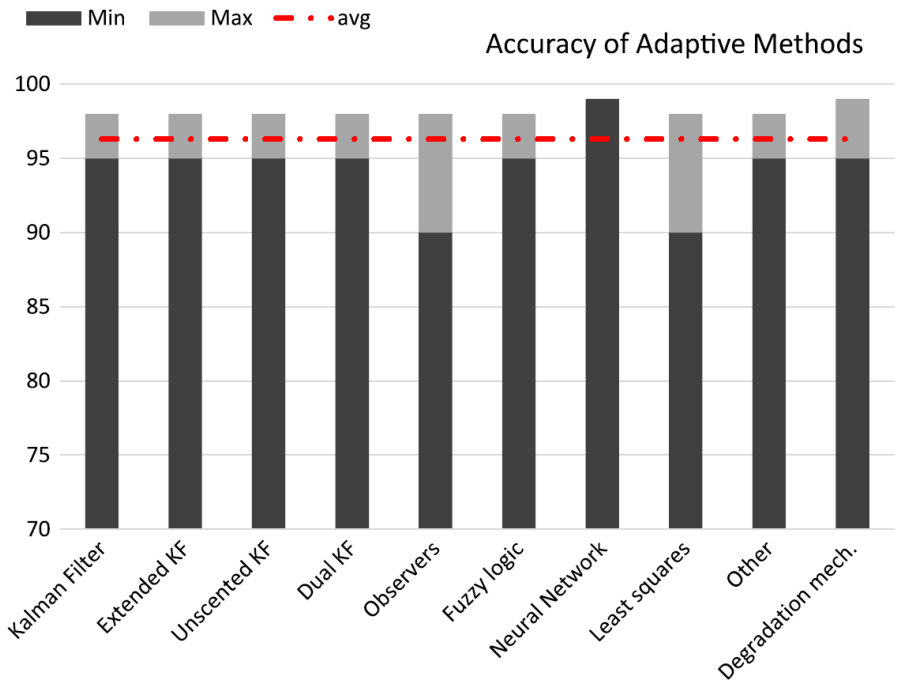

FIGURE 1.12 – Min., max., and average errors found per type of adaptive method in SoH modelling. Source : [91]

Research Gaps. As in the case of SoC modelling, the State-of-Health estimation algorithms are diverse and use techniques that are not always adapted to all BMS. The next research gaps are noted :

- **(RG4)** The experimental results reported in the literature focus primarily on battery cells, and not integrated LiBESS on the operation. Degradation databases for LiBESS under specific use scenarios are not available either.
- **(RG5)** The applicability of the SoH models on large-scale systems is not widely treated. Maintenance operations (battery pack replacements) and operation in real conditions are rarely considered. SoH models can include SoC estimation, but temperature dependence is left aside.

1.4 Objectives and Methodology

The analysis of the previous state of art and the detected research gaps shows that there is a lack of information about the actual behaviour modelling of BESS in industrial conditions. LiBESS models are a current subject of research, but they do not address the issues faced in data-scarce scenarios or all-in-one models (SoC, SoH, and Temperature). Consequently, there is little understanding of the impact that the thermal modelling component can have on SoC/SoH estimation in short and long-term industrial applications. The objectives of the thesis address the identified gaps and provide insights on the behaviour of LiBESS operating under an industrial PV capacity firming framework, all backed by real industrial data. The objectives are as follows :

1. Develop and validate a thermal model applicable for industrial LiBESS. The model will allow us to estimate the intra-day operational temperature using generic data available in industrial sites, while also having an easy interoperability with the SoC and SoH models deployed in the control systems. (**IG1**,**RG1**).
2. Propose a State-of-Charge and State-of-Health LiBESS model adequate for parameterization and deployment in industrial hybrid PV plants under capacity frameworks. By including the thermal component in the SoC/SoH estimation, the consequences of the power profiles requested to the LiBESS can be previewed. (**RG2**, **RG4**, **RG5**)
3. Study the impact the LiBESS models have in hybrid projects. Through the development of optimization frameworks that determine the optimal operation of the LiBESS, we aim to evaluate the performance and financial results of industrial sites depending on the LiBESS model used. (**IG2**, **RG3**, **RG5**)

However, to successfully achieve these goals a prior milestone must be completed. As the models are to be based and applied on industrial sites, it is necessary to develop and deploy the sites beforehand. This resulted in an important phase to build the experimental sites. Once the sites were fully deployed, the methodology followed was divided into the 4 steps seen in figure 1.13.

First the PV-BESS hybrid plants operating under a PV capacity firming framework were used to recover the measurements issued from the different equipment on site. Afterwards, the LiBESS parameters of interest were modelled with the collected data. These are specifically the temperature, the SoC, and the SoH for a LiBESS. The models were validated afterward.

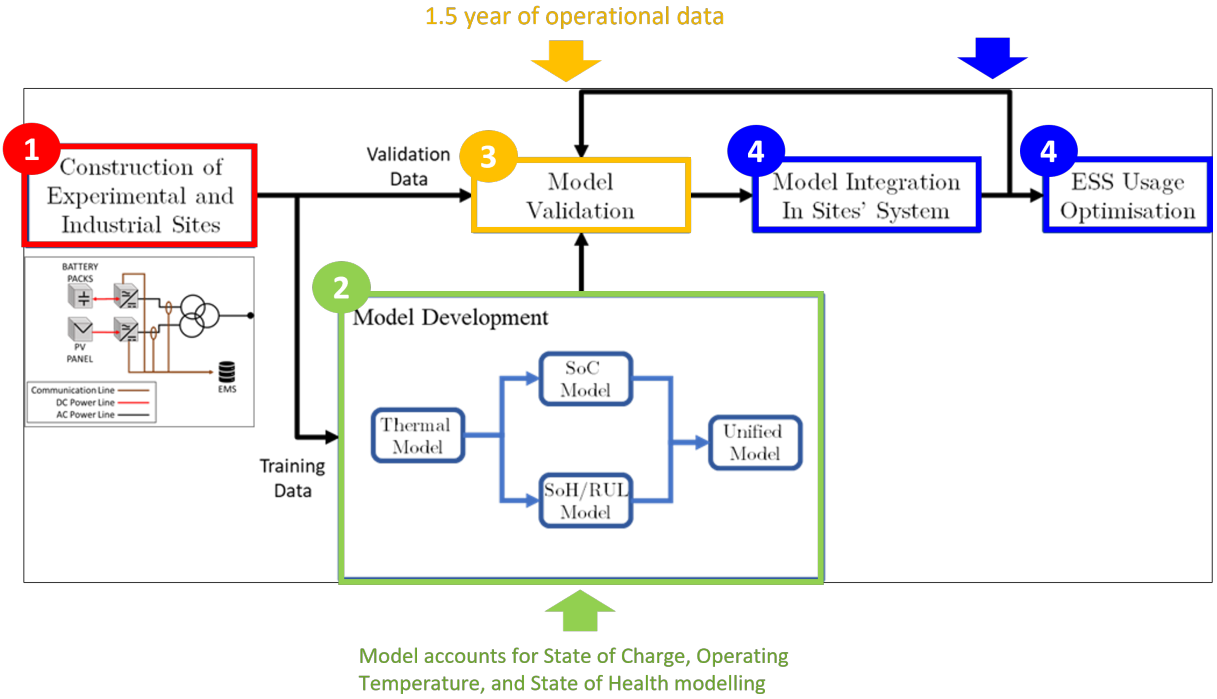

FIGURE 1.13 – Methodology followed in this thesis : 1- Data collection setup construction and data gathering, 2- Model training, 3- Model validation, 4-Model integration in operational systems and optimization.

The validated models aim to imitate the real behaviour the batteries exhibit, as well as reduce the operational errors that are a consequence of the deviations from the characteristics published by the manufacturer. At last, they were integrated into the control system on the sites and/or applied to the optimization frameworks used for project development. In this work, the two use cases for which the LiBESS models are applied are two : the PV capacity firming framework that the data collection sites follow, and a battery aggregation scenario for a small-sized grid. In both, energy availability and expected

revenues are considered as a result of the optimal short-term scheduling process given the LiBESS models. This is to showcase the importance of integrating advanced BESS models in the control systems and the project development phase of new vRES projects.

1.5 Structure of the thesis

This first chapter presents the subject of LiBESS modelling, as well as their importance to increase RES penetration in the electrical grid. Research and industrial gaps are identified for LiBESS modelling, and the methodology to try and tackle these subjects is presented.

The latter chapters in this thesis will follow the process followed to develop, validate, and put into application the LIBESS modelling in the aforementioned usages. The order and subjects treated per chapter are :

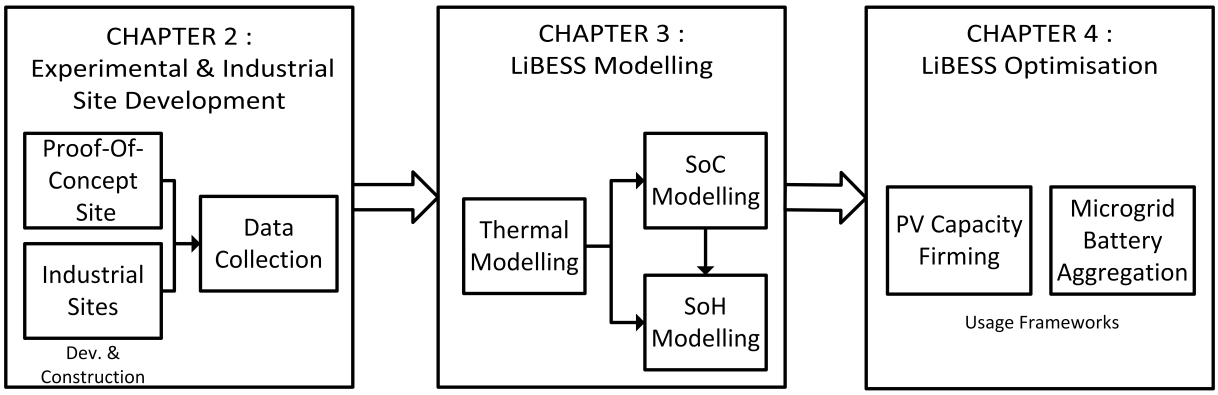

FIGURE 1.14 – Structure of the chapters

— **Chapter 2.** This chapter follows the development and construction of one experimental and four industrial PV+LiBESS capacity firming production sites under the scope of the thesis. The sites were built as data collection and model validation setups for large-scale LiBESS models developed under common industrial constraints. An overview of the sites is presented, including the specific operational constraints the sites were designed to follow. A description of the Power Management System (PMS) and Energy Management System (EMS) built, as well as the post-deployment feedback of both is expanded to shine light upon the place and importance the BESS model has in such systems. In this chapter, an overview of existing BESS characterization protocols is done as well. The focus is here given to system-wide parameters of battery systems and not at the battery cell level. Within this scope, the parameters are classified into two categories, power-related and energy (or battery) related.

The protocols were applied in the experimental site, and the results are presented for each LiBESS to establish the difference between the manufacturer published characteristics and the real behaviour.

— **Chapter 3.** LiBESS models are presented and developed to better predict and estimate the system state when operated under a PV capacity firming framework. The models developed are a thermal model to predict operational temperature, a State Of Charge (SoC) model, and a State Of Health (SoH) model. The two last ones include a thermal dependence that is often ignored. All the models are trained and validated using the real operational data from the sites shown in chapter 2, and are subject to the data scarcity this implies. The results and errors found by the models are then presented.

— **Chapter 4.** After validating the LiBESS models, the two optimization frameworks previously mentioned are developed while incorporating the battery models. The optimal schedule and operation of the two use-cases scenarios were evaluated under different models that are based either on the BESS datasheet published by the manufacturer, or the LiBESS model parameters found in chapter 3. The change in expected revenue and Levelized Cost Of Energy (LCOE) is evaluated for several PV weather scenarios to observe the sensibility and impact that the improved battery model, trained with real operational data, has on the day-ahead planning of BESS resources. This on both the base scenario of PV capacity firming, and the extension application of battery aggregation.

At last, a conclusion of the thesis is provided. This is accompanied by a general analysis of the results, contributions, and perspectives for LiBESS models for industrial PV production sites.

Chapitre 2

Experimental and Industrial Data Collection Sites

Résumé en français

Ce chapitre décrit le développement et déploiement de cinq centrales hybrides photovoltaïques (PV) avec des systèmes de stockage d'énergie par batteries de type Li-ion (LiBESS). Ces centrales, conçues pour répondre aux contraintes et exigences de la Commission de Régulation de l'Énergie (CRE) pour les zones non-interconnectes en France, ont aussi l'objectif de permettre la collecte des données sur les performances et comportement des LiBESS sous les diverses contraintes opérationnelles. Ces données seront utilisées lors du développement et validation des modèles des LiBESS dans les chapitres suivants.

Une revue des premiers phénomènes observés liées à la présence des LiBESS et des mesures correctives mises en place pour atténuer ces phénomènes est présenté. Des différentes techniques de caractérisation des LiBESS sont aussi explorés, et leur pertinence dans un contexte de centrales hybrides PV-LiBESS en opération est évalué. Cela car ces techniques et protocoles sont généralement prévus pour des conditions de laboratoire ou usine et ils ne sont pas conçus pour des environnements en production.

En résumé, ce chapitre établit les bases pour une compréhension approfondie des performances des LiBESS et des systèmes hybrides PV-LiBESS dans des conditions réelles d'exploitation. Les données obtenues, ainsi que la divergence entre les caractéristiques d'usine et les réelles constatés sur site, sont essentielles pour le développement et la valorisation de modèles de performance et d'optimisation des BESS.

2.1 Introduction

As seen in the precedent chapter 1, Lithium-based storage solutions are continuously growing into more diverse applications due to their more advantageous characteristics. With this wider range of applications, the kind of charge/discharge profile the Battery Energy Storage System (BESS) experiences becomes more diverse and the exact behaviour of the storage in both short- and long-term becomes more uncertain. To optimise the duration and performance of the BESS, the deployed EMS and PMS, systems in control of the BESS, would require knowing the effects the specific power profiles have in the storage. And to achieve this, a precise and specific BESS model would need to be available.

In the last chapter, a series of works where referenced to show the diversity of approaches available when modelling a Li-ion battery (LiB) cell behaviour. Although some models show better results in terms of accuracy than others, little has been said about their application on industrial sites.

In the literature focused on BESS physical modelling, real-life applications are constrained to research in battery technologies and architectures to improve the cell characteristics. The dynamics of such cells are commonly verified using specialized techniques as Electrochemical Impedance Spectroscopy (EIS), which can give insight into the physical and chemical mechanism in play [51, 31]. In contrast, mathematical methods coupled with simple physical models do not require specialized measurement techniques or equipment when deployed and as consequence they have been reported more prominently for time-critical applications [97, 98, 70].

Up to this day, the primary focus of models intended for use in embedded systems lies in the correct prediction of the SoC and/or Remaining Useful Life (RUL) of the storage, with a special interest in the cell behaviour when adapted to hybrid electric vehicles (HEV). Montaru et Pelissier (2009) used chronopotentiometry [1] coupled with an impedance-based battery model to estimate the SoC, being their model validated by using a typical HEV current profile [99]. Castano et al. (2015) used the new European driving cycle to simulate the usage in a real time application [97], and Barillas et al. (2015) similarly used load profiles of transportation machines to validate their comparison of state estimation algorithms [70], and Neural Network (NN) modelling coupled with Kalman filter was used by He et Al (2014) to validate the SOC accuracy in real life electric

1. Characterization technique in which the voltage response is observed when a current profile is imposed.

vehicles [73]. In addition to the mentioned, multiple works have been reported with either Electric Vehicle (EV) or HEV's driving cycles as the source for the validation sets when proposing SOH, RUL or SOC estimation methods [100, 101, 102, 74, 103, 88, 69, 66, 104, 105].

From the mentioned literature, it is obvious that the application of all these battery models has been mostly neglected for its use in hybrid Photovoltaic (PV) centrals where their expected behaviour can be more variable. Weishar and Bessler (2017) used lifetime prediction for a stationary photovoltaic battery system, but their approach was focused on li-ion LFP/graphite technology, using parameters and SEI growth's behaviour specific to the kind of cell [67]. In addition, the system by Weishar had 5 kW_p in power with a 1 Wh/W_p ratio which constraints the range of relevance. It is here that the subject and development of a general-purpose li-ion model adapted to the behaviour of large PV power plants (> 100 kW_p) becomes pertinent. The development of this model, intended for use in industrial power plants, needs in-situ data of the storage control and behaviour. A full-scale experimental site can provide the data for this purpose.

Furthermore, a real hybrid PV testing site (in comparison to a laboratory experimental setup) implies a set of constraints in terms of amount and resolution of data that can be acquired. This "forces", so to speak, to find solutions and models that behave as expected in similar conditions. In the reported literature, the vast majority of models and testing done to battery cells use data collection setups and control signals with a frequency superior to 1 Hz, and little to no attention is given to the importance of this resolution to the model results. Du et al. (2014) used a sampling interval of 20 seconds for an intensive machine learning approach, and resolutions of 1 minute have also been used for lifetime prediction [74, 67], but in most cases the sampling rate of the measurements is not specified.

It is this tunnel vision in the data frequency and specific HEV validation sets that generates an opportunity to explore these fields when applied to solar installations.

2.2 Objective and chapter structure

In this chapter, the development of an experimental and 4 industrial hybrid PV-BESS power plants is presented. The sites were developed to respect a specific PV Capacity Firming framework as published by the French Energy Regulation Commission (CRE) to accomplish two things : serve as a Proof-of-concept (PoC) to demonstrate the control system is in agreement with the framework requirements, and as a data-collection setup

to capture the behaviour the BESS exhibit under the system constraints.

The construction of the sites is considered a vital methodological element for this thesis. Thanks to the hybrid PV-BESS power plants, the available industrial data-points for model development increased substantially. Given the aim is to develop and validate models for industrial applications with constraints linked to those environments, this was a necessary first as systems of the same kind were uncommon at the time. From the five resulting operating hybrid power plants, four are 100% property of the industrial client GDS, but they provide their data to SPIE and this thesis as part of the partnership during the maintenance service period until 2023.

The different objectives and contributions set at the study-phase and deployment of the newer centrals were :

— Produce a real-scenario PV-BESS control system in which to incorporate different BESS models to measure the impact on real-time operation and financial results.
— Provide BESS datasets that reflect their behaviour under a vRES capacity firming framework and that are constrained to typical measurement devices in industrial sites.
— Industrialize the developed PV+BESS control system.
— Provide operational sites in which to test the effectiveness of future BESS models.

An understanding of the different ways BESS are characterized is also vital before and after the sites are deployed. They allow to evaluate the BESS and have reference values to observe their evolution. As consequence, a review of different historical characterization techniques and frameworks for Li-based BESS will be done too. The purpose of this review on characterization are :

— Offer a base knowledge of protocols for BESS characterization in laboratory and industrial conditions.
— Showcase the pertinence and limits such protocols have on industrial operational BESS via deviation analysis from the manufacturer published data.

Results of the characterization procedures will not cover the BESS from the industrial sites. The financial and operational constraints from such sites prohibited the execution of the tests and as consequence that specific data from those sites is not available.

In summary, the structure of the chapter is as follows : Sections 2.3-2.4 presents a technical review of the two different kind of sites and the EMS deployed in them. This includes a review of the first observed phenomena on the different sites, as well as the corrections put in place to mitigate such phenomena. At last, in section 2.5 the LiBESS characterization protocols will be treated. The limitations and advantages they

offer in a hybrid PV+BESS context will be discussed, as well as the constraints they could impose to the power plant owner and operator. Applications of these protocols in the experimental hybrid LiB-PV plant will then mentioned and compared to the manufacturer initial specification for the BESS.

2.3 Hybrid LiB-PV Plant Development : Experimental site development

In this section we present the development and construction of a hybrid PV+BESS site owned and managed by SPIE, the industrial partner of this thesis. This site was developed to showcase the proficiency of SPIE to develop and operate Energy Management System (EMS)/Power Management System (PMS) dedicated to Variable Renewable Energy System (vRES) and hybrid systems. Built in spring 2018 and located near Port-de-Bouc in France, the plant was also built as an experimental site in which to test new control algorithms and equipment before their adoption and deployment on industrial sites. The first mode of operation deployed in this site was a control system developed in-house that follows a capacity firming framework.

2.3.0.1 Technical specifications

At the site location, the global irradiation on a horizontal plane is 4530 $Wh/m^2/day$ [2]. The photovoltaic installation is composed of two solar rooftops :

- Installed PV Power : 22.68 kW_c
  - 52 modules facing north, i.e., 14.04 kW_c
  - 32 modules facing south, i.e., 8.64 kW_c

and the associated inverters were two Sunny Tripower without transformer from the brand SMA. Table 2.1 shows their key electrical characteristics.

Each of the rooftops are not bound to a specific inverter, and in each inverter one MPPT was used for the northern orientation and the other one for the southern rooftop. The inverter *SMA 10000TL* has 8.64 kW_p facing south and 4.86 kW_c facing north, which gives a ratio DC/AC of 1.35. For the second inverter, the south/north distribution is 5.4 kW_p and 3.78 kW_p. This gives a DC/AC ratio of 1.15. Figure 2.1 shows the solar panels distribution for the site.

2. Data obtained from PVGIS © European Communities, 2001-2012

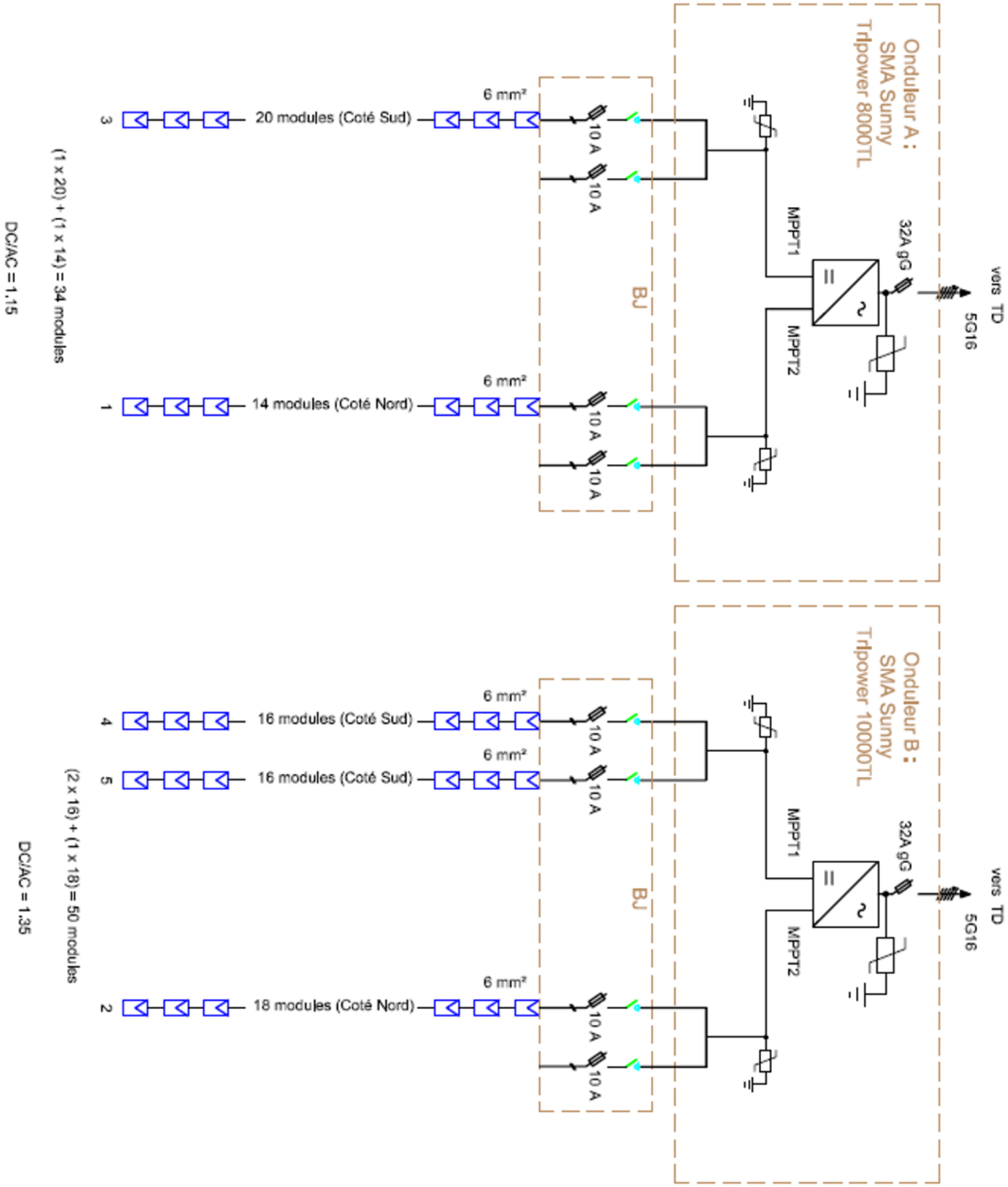

FIGURE 2.1 – Inverter's electrical Scheme DC/AC

	Inverter Model	
	8000TL	**10000TL**
Max. generator power	13500W$_p$	
Max input voltage	1000V	
MPP Voltage Range	330 to 800V / 580V	370 to 800V / 580V
MPP Inputs	2	2
Rated Power	8000W	10000W
Max. AC apparent power	8000VA	10000VA
AC voltage range	160 to 280V	
Max. Output Current	11.6A	14.5A
Max. Efficiency	98%	98%

TABLE 2.1 – Technical specifications of the solar inverters.

Li-ion Storage System : Battery and Inverter The site has 19.5 kWh in storage capacity. This is divided in three LG RESU6.5 [3] subsystems of 6.5 kWh which incorporate an internal BMS. The main function of the BMS in these batteries is to avoid operation outside the limits imposed by the manufacturer. These limits, as well as other technical characteristics, are summarised in table 2.2.

Factory-issued battery characteristics	
Nominal Voltage	51.8 V
Operating Voltage	42 to 58.8 V
Nominal Capacity	126 Ah
Nominal Energy	6.5 kWh
Weight	52 kg.
Standard Power	2.2 kW
Maximum Power	4.2 kW
Maximum Current	100 A (42 V)
Charge/Discharge Current	37.8 A
Faradic Charge Efficiency (24°)	99%
Round-Trip Efficiency	95%
Cooling	Natural Convection
Operating Temperature	-10 to 45°
Optimal Temperature	15 to 30°

TABLE 2.2 – Technical Specifications of Battery Pack RESU6.5

As can be seen from the single-line diagram of the site in Figure 2.2, each battery pack is coupled with a single-phase inverter SMA Sunny Island 4.4M [4] to globally create

3. Model : R48126P3S
4. Model : SI4.4M-12

a three-phase system. The most relevant technical specification of these inverters are seen in table 2.3

AC Side		**DC Side**	
Rated Power	3300W	Rated Voltage	48V
Voltage Range	202V to 253V	Voltage Range	41V to 60V
Frequency Range	45 to 65 Hz	Rated Charging Current	63A
Rated Current	14.5A	Rated Discharging Current	75A
Total Harmonic Distortion	<5%	Maximum Charging Current	75A
Displacement Power Factor cosϕ	-1 to 1	Capacity Range	50 to 10000Ah

TABLE 2.3 – Technical Specifications of Sunny Island 4.4M-12

From these characteristics a set of complementary limits can be derived for the system. One example is the decrease in charge/discharge AC power from the inverter if it's near its lower threshold in voltage.At 44V or lower, the DC current would exceed the rated 75A if the rated power of 3.3kW is requested. It is also obvious that, even though the maximum power the storage system can give is 4.2 kW, this value is never reached given the inverter limits. In any use-case scenario, the BMS embedded in the RESU6.5 battery packs communicates directly with the inverter using the protocol CAN2.0B over an Ethernet interface, and it is due to this communication that the different safety constraints are respected.

Control and Data-collection equipment In addition to the equipment for power generation, control and surveillance devices were added. To manage the connection and disconnection from the energy grid, a *Schneider* motorized protection relay was integrated with a PLC to manage any analog or discrete Input/Output.

Measurement devices were also installed to monitor the electric grid and the weather conditions. The equipment is :

- 4 Grid power Monitors Enerium 50 (Class 0,5s) which measure :
  - I, Current at each phase.
  - V, voltage at each phase.
  - F, Frequency of the grid.
  - P, Active Power at each phase.

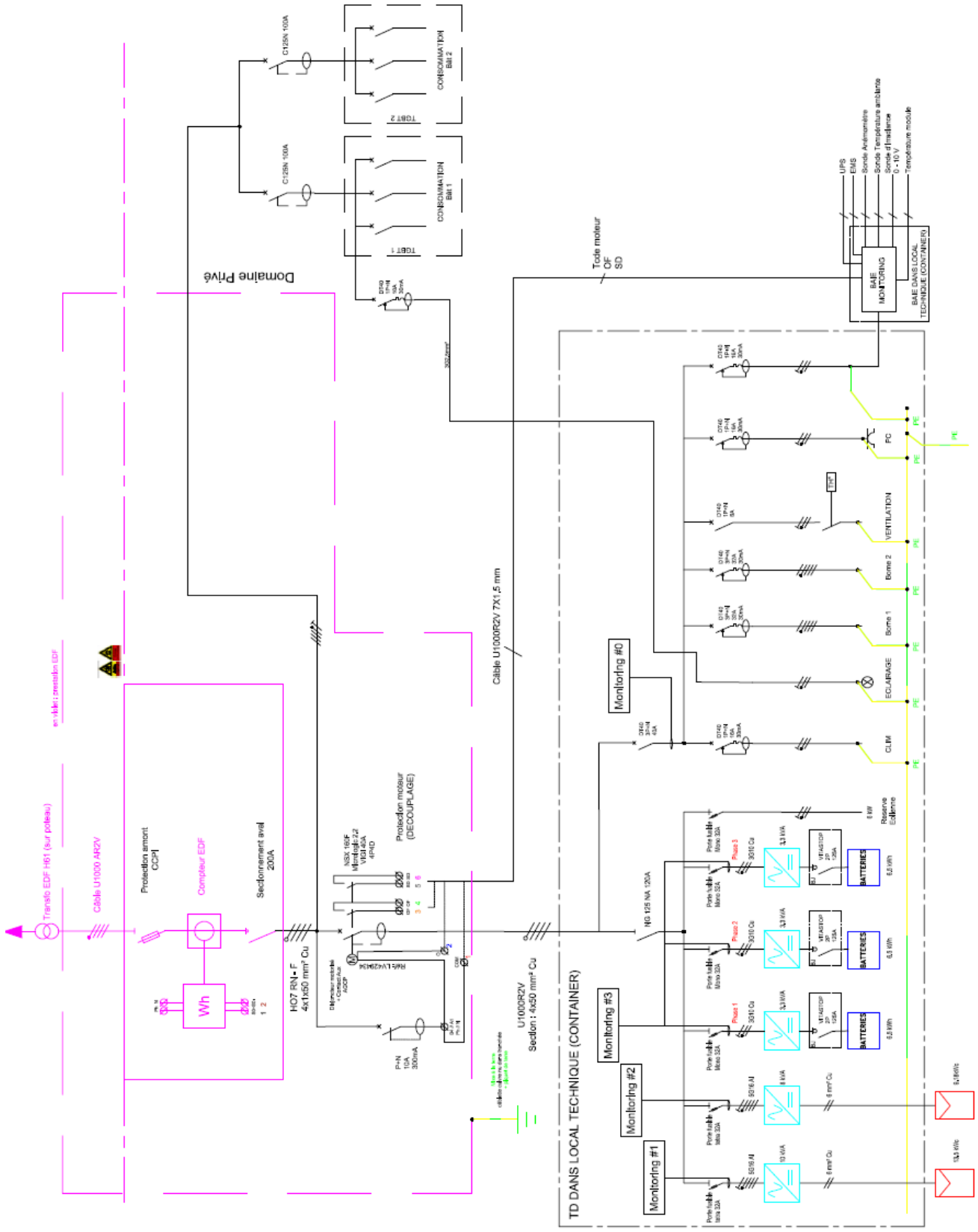

FIGURE 2.2 – Single-line electric schema of the experimental hybrid PV-BESS built by SPIE.

  - Q, Reactive Power at each phase.
  - S, Apparent Power at each phase
- 4 Weather sensors :
  - 2 * Irradiance Sensor (Meteocontrol SI-12-TC, 0...10V, ±0.3%)
  - Temperature Sensor PT1000 (Meteocontrol, 0...10V, <1%)

These devices offer a higher refresh rate (1 second) than the inverters, which is important when diagnosing the electric grid current state and when controlling the power injection. The power monitors offer in addition the option to observe the total harmonic distortion in current, voltage and power, but these values are not of interest in this work as inverters are required to produce a very small amount of harmonics.

2.3.0.2 Energy Management System

Even though the technical conception, deployment of the physical equipment and construction of the site required a strong time investment, the most time-consuming activity was the development of an Energy Management System able to collect, process and control the different processes happening at the site. This system was built around a proprietary Supervisory Control and Data Acquisition (SCADA) framework *Ignition*, which is an OPC-UA server with drivers for compatible controllers, Modbus Devices and other OPC-UA servers that allow the supervision of the central. The storage of the different variables (known as tags inside the system) is managed by the SCADA too. For data logging, this is done too through the SCADA and stored in an SQL database.

The internal programming for all the algorithms were done using the implemented scripting language Jython (java implementation of Python). This scripting environment has the simple syntax of a normal Python (2.5+) kernel, but it has the disadvantage of not being compatible with most libraries that exist for the standard distribution. To extend the capabilities of the system, it is is also a possible to develop complete modules for the system in Java via the Maven framework. This option, although more programming-intensive, unlocks the ample existing libraries for Java and, when necessary, can help to solve the bootlenecks found in Jython.

Algorithm The EMS created for the site serves the double functionality of being an experimental setup for data collection and strategy testing, as well as making available a customizable system that can be adapted to the grid operator requirements. The experimental site exposed in this section was designed to respect the constraints for hybrid PV power plants in the island of Corsica following the AO CRE ZNI 2015.

The most important element of these constraints is the existence of day-ahead planning for the power injection. To generate the schedule, the central follows a relative straight-forward procedure :

1. Recover photovoltaic production forecasts from an external provider.
2. Subtract from the PV forecast production the energy to be stored in the batteries.
3. Ensure the respect of the constraints imposed to the day-ahead planning by the grid manager.
4. Send the day-ahead production plan to the grid manager.
5. Generate a SoC prediction for the energy storage system given the production plan.

It is noteworthy that the procedure needs, to effectively reduce the energy to be stored in the batteries from the PV production forecast, a battery model that considers both the performance and its own behaviour when charging or discharging at any given power and SoC.

Graphical User Interface (GUI) The primary functionality of the GUI developed is the visualization in real-time of the state and power injection of the site. The PV production and injection/withdrawal from the electrical grid are shown (fig. 2.3) amongst other performance indicators of the site. A secondary screen, seen in 2.4, shows the grid injection for a day with a time-resolution of 1 minute.

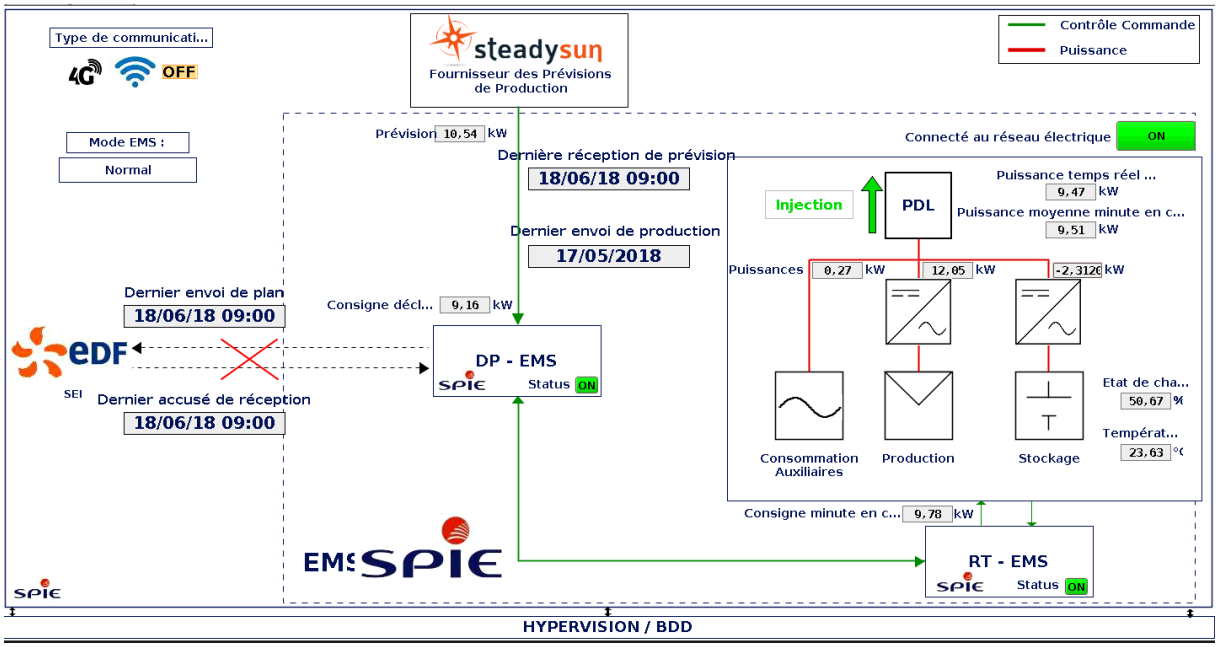

FIGURE 2.3 – Home screen of the developed GUI

From figure 2.4 it is possible to quickly assess the behaviour and performance of the Energy Management System. The blue line represents the photovoltaic production as it

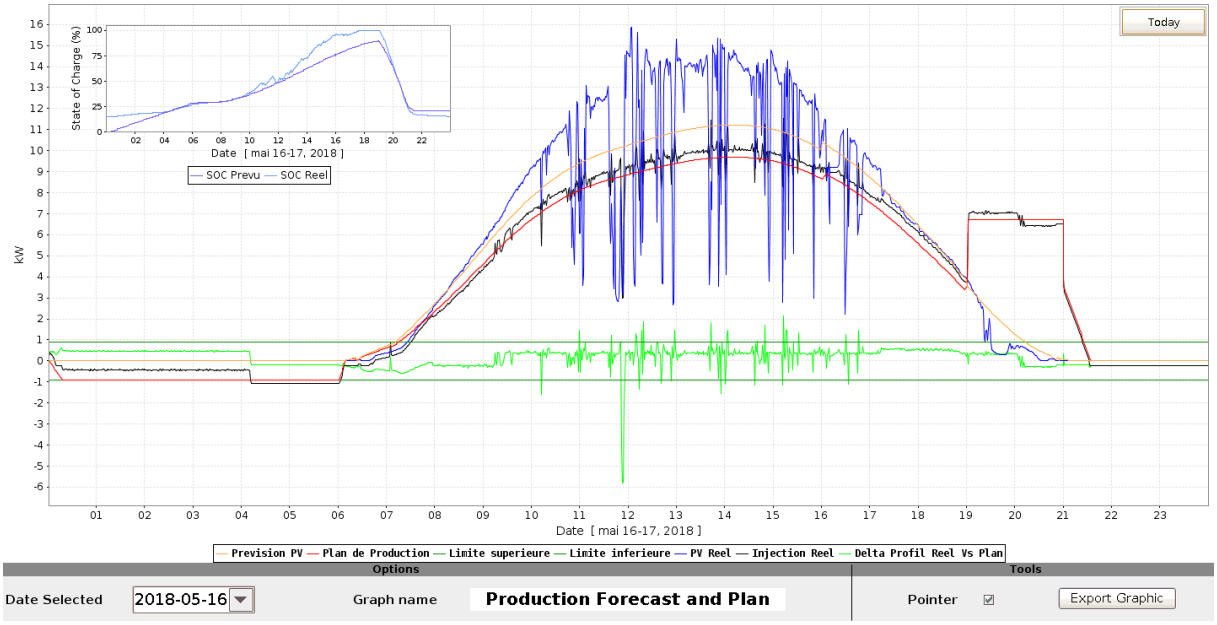

FIGURE 2.4 – Injection Curve with a timestep of 1 min.

was generated by the inverters, while the black line represents the net injection to the grid. As it can be seen, for this particular day the photovoltaic production was very erratic but the regulation done reduced considerably these variations and managed to stay most of the time within a 5% margin of the scheduled power. This regulation is done first by changing the setpoint of the battery inverters , and then by limiting the power from the PV inverters when the power from the storage is unable to counterbalance any PV excess.

Communication Even though the li-ion batteries communicate only with its corresponding inverter via an exclusive channel, a complementary network in Modbus TCP/IP (using ethernet interfaces) was set in place. This network regroups the photovoltaic inverters, the charger/inverters, and all the monitoring equipment installed at the site. This network, as shown in figure 2.5, connects all the data sources with a server that stores the data and serves as the connection to the external world.

Inverter communication As mentioned, there are two different kinds of inverter in the site : a photovoltaic inverter (coupled with solar panels) and a battery inverter. The former, having the three electrical phases as output, makes available information for each phase in AC (I,V,P,Q) as well as information belonging to each MPP input (V, I, P). The latter offers the same AC information but only for the one phase it is connected.

Each battery inverter is also the interface from which the battery storage system state and configuration is recovered. The ongoing *voltage*,*current*, *SOC* and *SOH* of each li-ion

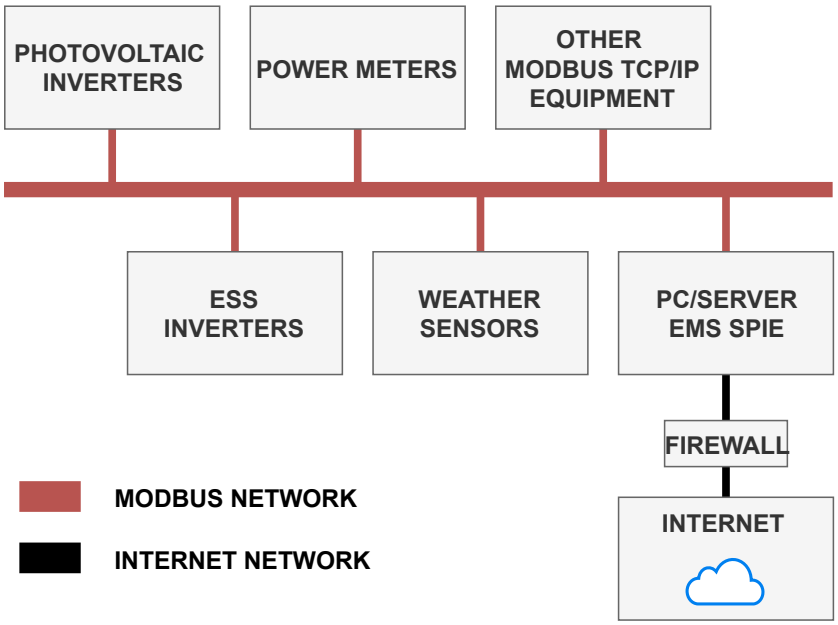

FIGURE 2.5 – Communications Network Topology for the pilot site.

battery pack are recovered via this equipment, and some operation limits can also be modified through it (e.g., SOC lower limit to allow discharge).

Furthermore, both kinds of inverters are able to control the power they inject to the electrical grid. The *active* and *reactive* can be set either directly in terms of power (kW or kVAr) or by setting a cosϕ. The preferred control method used in the site presented here is the first one, which is by specifying the wished output power value.

Being the inverters not preconceived for laboratory testing, there are limitations in the refresh rate of the values as well as the response time when giving setpoints. The values from the equipment can be read every ~8 seconds, while the setpoints can be updated with an interval of around 2 seconds. There is also a delay of ~1 kW/s for the inverter to reach the requested power as reported by the manufacturer [106].

Data resolution The refresh rate is mostly delimited by the equipment it comes from. The power meters and the datalogger have the highest refresh rate as the values are updated each second, while the inverters update themselves at a slower rate. The SCADA, at peak performance, can register data with a 50ms difference between registers. In theory this means that the maximal resolution possible for a recorded signal is 50ms., nonetheless the equipment found in most photovoltaic centrals do not need to continuously record data that fast and datalogging is usually capped at 1 Hz.

2.4 Industrial PV Capacity Firming Sites

In addition to the experimental testing site described in section 2.3, data from four additional hybrid photovoltaic sites was made available thanks to an industrial partnership with Generale Du Solaire (GDS). The four solar projects, awarded with a special power purchase agreement (PPA) due to being built under the AO CRE ZNI 2015 framework, were equipped with a SCADA system developed by SPIE and based on the software developed for the experimental site.

The control system put in place not only aims to respect the specific requirements the grid manager imposed to these kinds of projects, but it also allows the recovery of critical data from the equipment on site. The programming and deployment of this supervision system, although not really within the scope of the research, were a vital part of the project. The collected data from these sites could be used in the future to not only to develop and refine battery models as in this work, but to develop system-wide modelling of hybrid centrals.

2.4.1 Sites Description

The additional four hybrid PV-Storage power plants are located in the island of Corsica in the Mediterranean sea. They represent some of the winners of the 2015 call for tenders by the CRE for PV solar installations for the non-interconnected zones of France (AO CRE ZNI 2015), i.e., the French islands for which there is no electrical connection with continental France. The sites, when answering to this call for tenders, must adhere to several grid requirements in both operation and production planning. In exchange, they are offered an advantageous energy purchase price.

The different sites are divided in two industrial rooftop solar plants, one ground solar plant, and one hangar rooftop solar plant. Each site is composed of a solar production system that ranges between 0.8 and 1.8 MWp in installed photovoltaic power, and a Li-Ion battery energy storage system (LiBESS) with a capacity that ranges between 1.2 and 2.6 MWh. The storage systems were implanted in proximity to the PCC, and Table 2.4 summarizes the power and energy characteristics of the sites.

These industrial sites are expected to be operational for a duration of 20 years. Because of this, the battery sizing and the different ratios between the storage capacity and the installed power (kWh/kWc) falls within a range of 1.35 and 1.43. The over-capacity of the storage helps the site to better withstand the aging without compromising the performance of the site. These ratios are significantly higher than the ratio in the experimental hybrid

	Site #01	Site #02	Site #03	Site #04
Installed PV Power	1497 kWp	1820 kWp	1499 kWp	892 kWp
Installed Storage Power	1560 kW	2030 kW	1610 kW	980 kW
Installed Storage Capacity	2028 kWh	2610 kWh	2088 kWh	1218 kWh

TABLE 2.4 – Installed Power and Storage per site in the Corsica island.

site (0.86 Wh/Wc) as the site does not need to adhere to the longevity constraint. The sizing of the storage was chosen to allow a continuous discharge for 2 hours (at around 0.5C) with a full charge. The maximum peak charge or discharge power from the LiBESS at any given moment is limited to 0.8C (or full discharge in 1.2 hours).

2.4.1.1 AO CRE ZNI 2015 Grid Requirements

Although not explicitly described in the call for tenders [42], the framework answers the need of a reliable electrical grid in vulnerable systems such as islands. Thanks to the presence of energy storage systems linked to the photovoltaic fields, the power plants are no longer considered as variable energy sources by the grid manager. This lack of classification as variable comes with its own benefits and constraints : The site will not be disconnected in case of an energy surplus in the grid (which has important financial ramifications), but it must announce its power production with some anticipation to the grid manager. The respect of those announcements is then used to decide the compensation for the energy injected to the grid.

A summary of the requirements requested to all the sites within the framework can be divided in three sections :

- Storage capacity requirements :
  - Minimal capacity ratio : 0.5 Wh/Wc
- Engagement requirements :
  - Day-ahead power injection engagements with 3 intra-day adjustments. Day-ahead at 16 :00, and same-day before 04 :00, 10 :00 and 14 :00
  - Resolution of the power injection engagement is 1 minute (1440 values per day)
  - Power injection engagement limit values [5] :
    - Maximal value admitted :
      - 70% of installed PV power.

5. Relative to the installed PV power in kWp.

- Minimal value admitted outside 19 :00-21 :00 :
  - -5% of installed PV power.
- Minimal value admitted between 19 :00-21 :00 :
  - 20% of installed PV power.
- Min/Max change between consecutive engagement values :
  - [-0.3%,0.6%] from 00 :00 to 10 :00.
  - [-0.3%,0.3%] from 10 :00 to 14 :00 .
  - [-0.6%,0.3%] from 14 :00 to 19 :00 and from 21 :00 to 24 :00.
  - [-100%,100%] from 19 :00 to 21 :00.

- Operation requirements :
  - Power injection control at a scale of 1 minute.
  - Deviation from the engaged power of 5%[5] is allowed before penalties apply.
  - Output power must stay within the limits imposed by the utility grid :
    - 75%[5] for injection.
    - -10%[5] for withdrawal.

These engagement and operation requirements can be seen visually in Figure 2.6. Regarding the capacity requirement of 0.5 Wh/Wp, this requisite is a natural consequence of the minimal engagement between 19 :00 and 21 :00 being least 20% of the installed PV peak power for a two-hour period. The storage has to be at least 0.4 Wh/Wp to be able to respect that constraint at the beginning of the power plant operation.

2.4.1.2 Electrical Configuration

The power plant distributes energy to the grid in High Voltage (HV), however both the photovoltaic and battery systems are composed of the Low Voltage (LV) production elements (battery cells and PV panels) and an associated LV inverter (400-480V). A LV-HV transformer is present in each site to accommodate this grid requirement.

Noteworthy is the lack of DC link between the BESS and the PV panels. Because of this, each system can behave and act independently from the production of the other given that the power from the grid is always available. In two of the sites located in the Corsica island, the PV and LiBESS share the LV-HV transformer but the winding is different. The power exchange between the systems is done as consequence in high voltage and behind the power plant meter. This can be seen in 2.7.

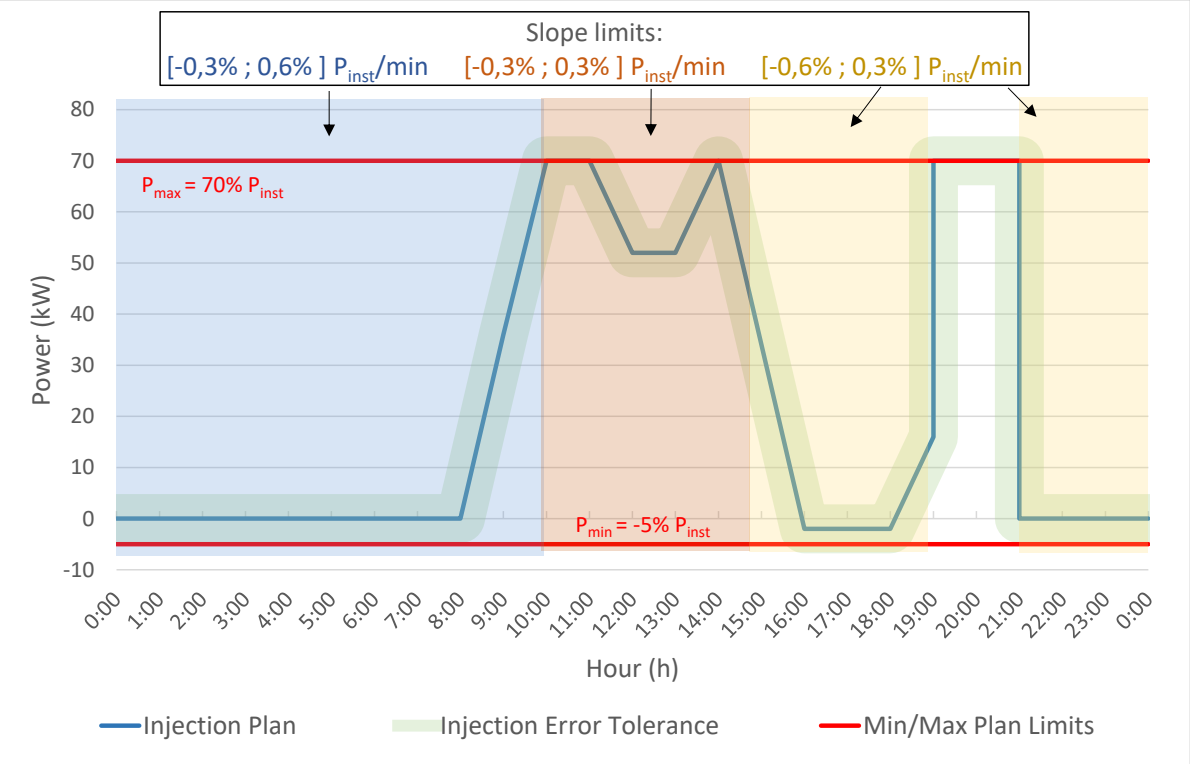

FIGURE 2.6 – Engagement and operational constraints imposed at the call for tender CRE-ZNI 2015.

2.4.1.3 Energy Compensation Scheme

The way the energy pricing works for these hybrid centrals is what allows investors to install BESS. All the energy produced and injected to the grid in this PV capacity firming framework is bought by the grid manager at two different prices per kWh. The base rate, which applies to most of the day, is defined by the power plant owner at the moment of answering the call for tenders for each hybrid plant [6]. The second rate applies only for the production that takes place at peak hours (between 19 :00 and 21 :00), and it is the same base rate with an added bonus of 200€/MWh. This price structure can be seen here below :

$$€/kWh = \begin{cases} \text{Tariff} & t < 19:00 \text{ or } t > 21:00 \\ \text{Tariff} + 0.2€/kWh & 19:00 \geq t \leq 21:00 \end{cases}$$

The average base price proposed by all the investors at the call for tenders for this kind of projects for the French islands was of 204.3€/MWh in 2015 [107], and in 2019 this price decreased to 107.3€/MWh for those with PV capacity firming capabilities. For reference,

6. The base tariff for each site is confidential.

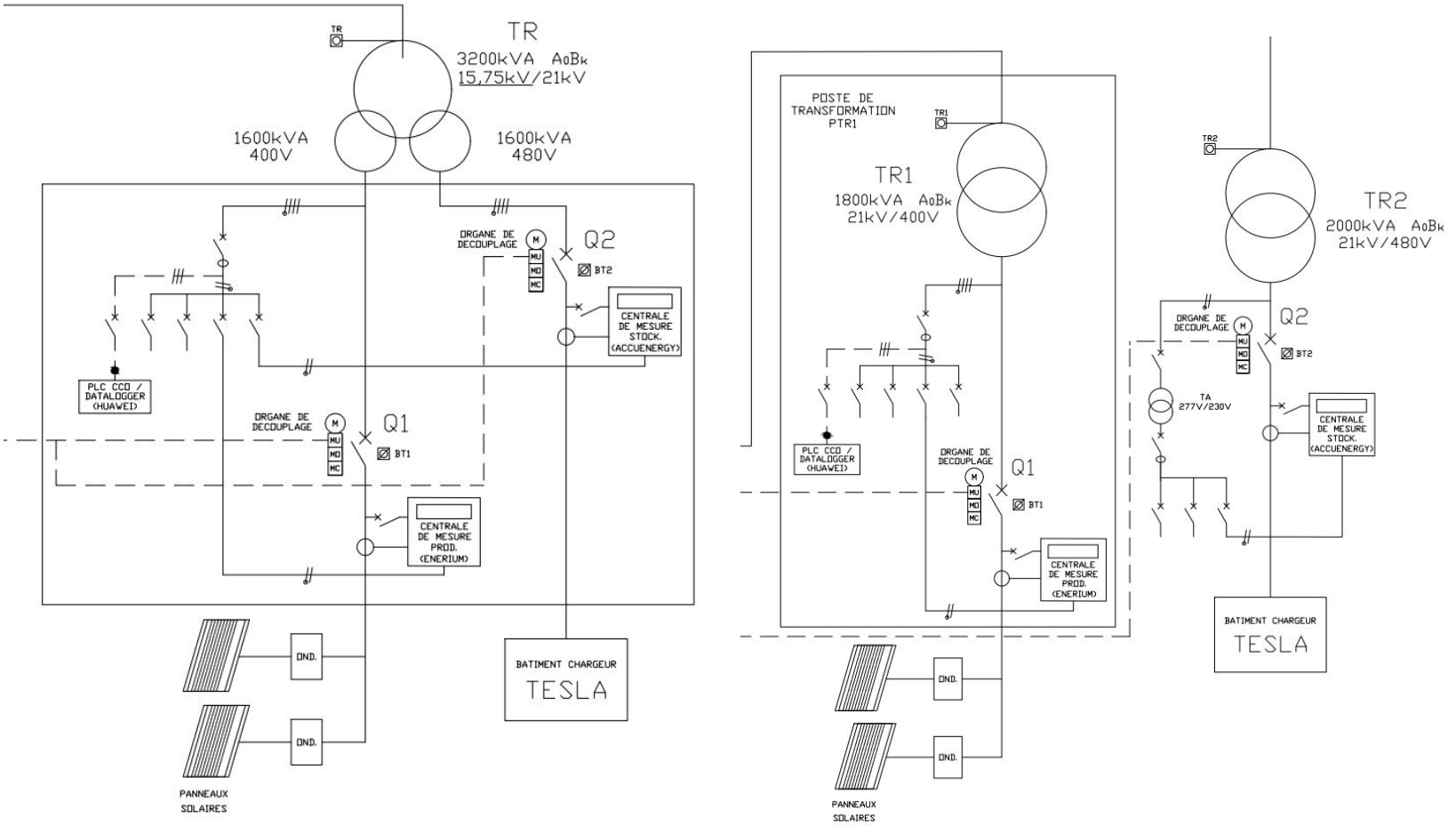

(a) (b)

FIGURE 2.7 – Electrical Configuration of the Storage and Production Subsystems for sites with a single transformer (left), and those with a transformer per subsystem (right).

the base-price for pure PV power plants in the same period had an average proposed price of 93.8€/MWh [43].

$$\text{Remuneration} = \frac{Price}{60} * (\text{Production} - \text{Penalty}) \tag{2.1}$$

Given the site standard MWh price c_G, the remuneration is calculated per minute using equation (2.1), where the penalty is function of the installed PV power P_{kWp}, the power engagement P_i^E, and the average grid injection P_i^G for the minute i. This penalty function has two different regimes :

— In case of over-production, i.e., $P_i^G \geq 1.05 * P_i^E$:

$$\text{Penalty} = P_i^G \tag{2.2}$$

— In case of under-production, i.e., $P_i^G \leq 0.95 * P_i^E$:

$$\text{Penalty} = \frac{P_i^{G2}}{P_{kWp}} - \left(\frac{1}{10} + 2\frac{P_i^E}{P_{kWp}}\right) * P_i^G + \left(P_i^E - \frac{5 * P_{kWp}}{100}\right) * \left(\frac{15}{100} + \frac{P_i^E}{P_{kWp}}\right) \tag{2.3}$$

The resulting penalty from equations (2.2),(2.3) can be considered as an equivalent power in kW that has to be subtracted from the real injection, just as in the equation (2.1). The behaviour of this penalty can be easily observed in Figure 2.8 for a 1 kWp hybrid PV plant. In this figure, the lower right shows the quadratic penalty in case of under-production, and the upper left the linear penalty in case of overproduction.

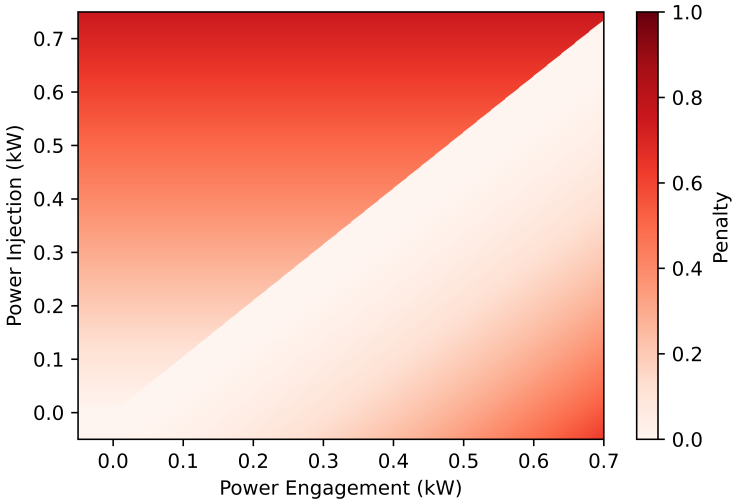

FIGURE 2.8 – Equivalent penalty power for a given power engagement(x-axis) and a given grid injection (y-axis). Darker color means a higher penalty.

Another particularity is that, regardless of the number of penalties incurred during a day, the net compensation for a day must be either zero or positive, i.e. :

$$\sum_{i=1}^{1440} \text{Remuneration}(i) - \sum_{i=1}^{1440} \text{Penalty}(i) \geq 0 \tag{2.4}$$

For completeness, it is also worth mentioning the third way to obtain penalties in the AO CRE ZNI framework of 2015. As stated before, this framework relies on day-ahead production engagements from the power plants. Failure to respect the engagement, or having day-ahead engagements that don't respect the constraints explained in section 2.4.1.1 will result on a day with a net energy production of zero. This scenario, although it is very important to avoid and is taken in account by the SCADA on site, will be mostly ignored as it has no direct link with the real-time operation of the hybrid power plants.

2.4.1.4 BESS and operational data collection

The resolution for the different datapoints on the Corsica hybrid power plants depends on the importance of the measure itself. Although the recording of the points only occurs when a change in value is detected, the maximum rate at which the data is saved is not equal amongst the measurements. Most non-essential measures, like the ambient temperature, are being recorded at best at a rate of 1 point each 10 seconds. In the case of essential indicators, measurements are done at a maximum rate of 1 point per second [7]. By having a higher save rate in power measurement for example, the quality of financial results and forecasting increases as it allows to have a more reliable minute power average.

The four sites treated in this section share the same manufacturers and measurement equipment. Here below there is a non-exhaustive list of the measurements that are being recorded for each kind of subsystem.

- Photovoltaic System :
  - Active Power.
  - Reactive Power.
- Li-ion Energy Storage System :
  - Active Power.
  - Reactive Power.
  - Available Discharge Energy.
  - Available Charge Energy.

7. The system is not invulnerable to data loss. If the instantaneous load for the database is too high, some values won't be recorded

    - Full Charge Energy.
- Power Meters :
    - Active Power (in High Voltage).
    - Reactive Power (in High Voltage).
- Weather sensors :
    - Irradiation.
    - Ambient temperature.
    - External Surface Temperature of Battery Cabinet.

All data is stored in a SQL database located at the local server of each site. Backups of the databases are done once each month on a remote site, and all stored data is directly available locally through the SCADA system and the HMI in place. Data exports can be done at any resolution greater than the recording rate, and the values are weighted averages in intervals between recordings are not uniform.

Data Export for Battery Modelling All the sites were provided with custom code to export the BESS battery related data. Given the lack of transparency by the manufacturer regarding the batteries DC measurements (e.g., voltage, temperature, and DC current), only the macro-scale reported values by the embedded BMS are available. These data exports are meant to be used to develop the battery model for the sites in future chapters, and are composed by :

- AC Output Power.
- State of Charge.
- Available Discharge Energy at Inverter Nominal Power.
- Full charge energy.
- Total Exported Energy.
- Ambient Temperature.
- Cabinet surface temperature where the battery racks are located.

All the measurements mentioned before are published by the BMS except for the temperature measurements. These are obtained through external sensors. For the battery temperature, as it is forbidden to install third party equipment inside of the battery cabinets, the sensor was placed on the exterior surface (Figure 2.9) to try and record the thermal behaviour. Putting a sensor inside the battery cabinets where the racks of battery are installed would void the warranty and was thus prohibited by the equipment owner.

FIGURE 2.9 – Example of the temperature sensors installed outside the battery cabinets.

2.4.2 Post-Deployment Feedback

Two of the sites started their operation in March 2020, and the other two followed by November 2020 [8]. The Figure2.10 shows one of the first results from one of the hybrid centrals in operation. The SCADA screen capture shows the standard behaviour from the hybrid PV in the capacity firming framework, in which the average grid injection per minute (black line) follows the power engagement done to the grid manager (red line) with some deviations. The left top curve within this figure represents the expected and real SoC of the storage system through the day. In the figure it is also possible to appreciate some of the constraints imposed in the engagements, such as the allowed rate of change between in engagement between 18 :00 and 19 :00, or the strong power engagement between 19 :00 and 21 :00 to take advantage of the remuneration bonus.

As it was explained in section 2.3.0.2, to determine the wished instantaneous power from the different components in the power plant, several indicators and measurements published by the different equipment are used. For the EMS deployed in the Corsica sites, the first iteration relied mainly in one indicator : the state of charge as reported by the battery controller [9]. The algorithm that was followed can be seen in figure 2.11 and can

8. The start of service was delayed by the Covid-19 pandemic.
9. An explicit SoC indicator is not given but calculated with a published remaining energy indicator and a maximal energy capacity from the BMS

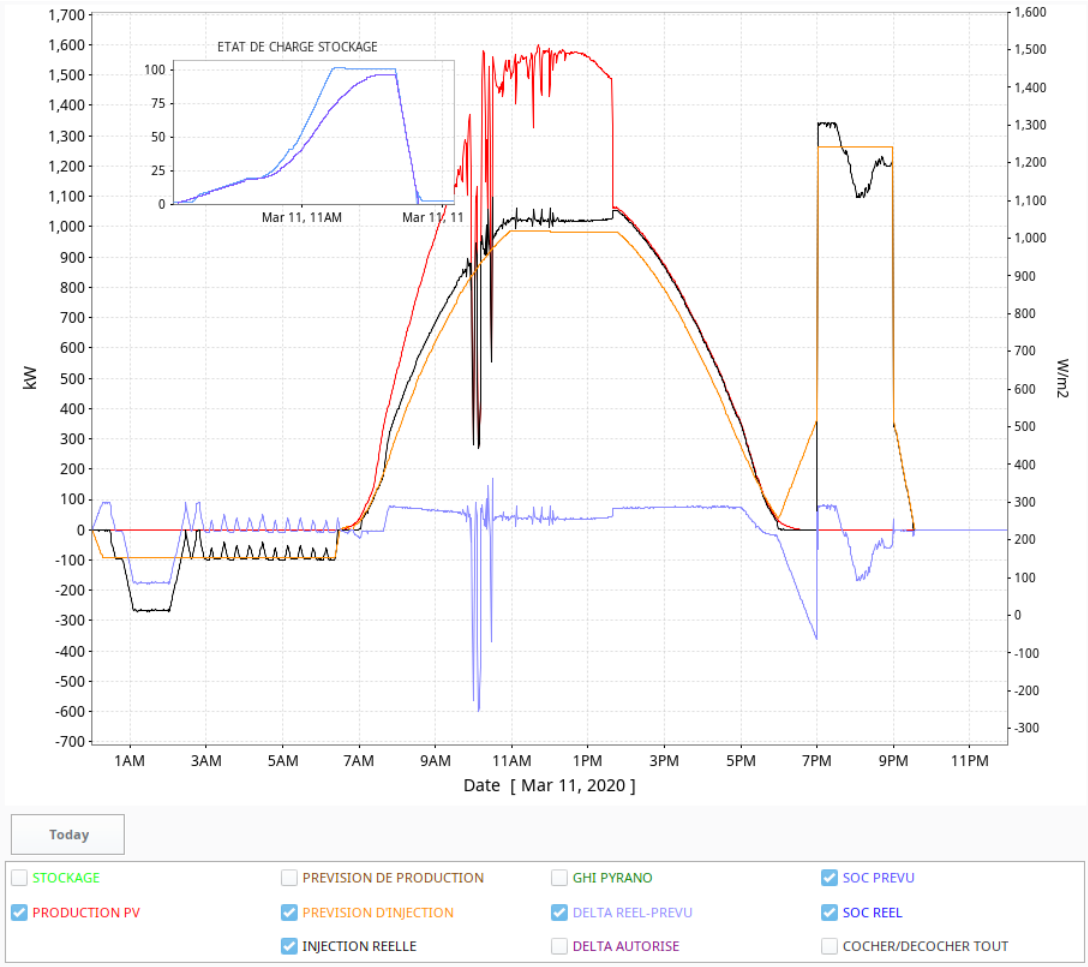

FIGURE 2.10 – Typical behaviour of one of the four hybrid centrals. This image shows some erratic behaviour due to differences in the battery model used for prediction and the real system in place.

be summarized as follows :

For each minute the SoC of the battery is lower than the expected value, reduce the amount of power to inject to the grid by an increasing percentage of the PV field power rating. When the batteries are more charged than expected, increase the power to inject to the grid.

The algorithm just presented here, although can alleviate deviations due to erroneous photovoltaic production forecast, showed some aberrant behaviour. The two most prominent behaviours were an excess in energy withdrawal from the grid in the mornings and a damping-like effect at peak hours. Both are caused by different deficits in the real-time management system as it is unable to correctly compensate the presence of an imperfect BESS model incorporated in the EMS. Details of these observations will be discussed below.

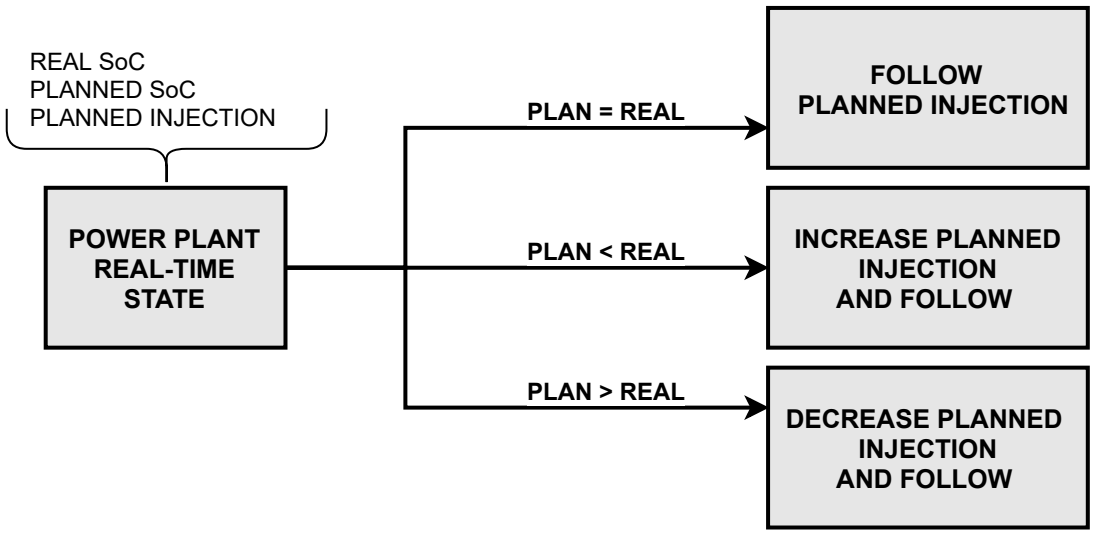

FIGURE 2.11 – Discrete logic used to determine the change in the current setpoint. It is dependant on the expected and the real SoC of the BESS.

2.4.2.1 Excess Energy Withdrawal Before Dawn

In the mornings the charging orders given to the battery controller increase substantially (observable in figure 2.12). This is a problem because the grid manager established limits to the allowed power withdrawal that are not respected in this scenario.

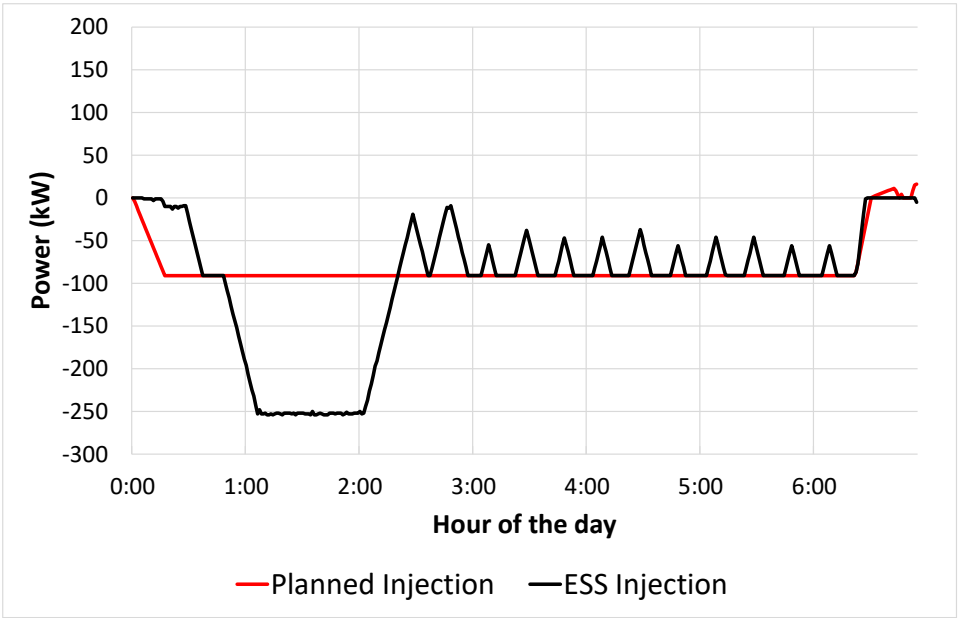

FIGURE 2.12 – Example of early morning behaviour of the ESS integrated at the industrial PV capacity firming sites.

Origin During this phenomenon, the state of charge reported by the battery controller stops being updated for an undetermined time. The lack of feedback regarding the charged energy in the storage creates the illusion that the power order is not enough, and thus the charging order is increased to compensate. As the battery values become live again, the sudden increase in state of charge due to overly aggressive charging is compensated now by reducing the charging power. The smaller oscillations seen later are a response of the system charging faster than expected, decreasing the requested power. This continues until a point in which the SoC is less than expected and the charging power is increased.

Possible consequences A stable low charge/discharge power creates less stress to the battery cells and can extend the battery life expectancy. Given that the higher charging power in the morning is not necessary, this situation can be translated into unnecessary degradation for the energy storage system [108].

Solution implemented A complete override of the algorithm to choose the power of the current minute was done. The algorithm seen in Figure 2.11 is no longer used in the mornings, and only the initial scheduled power order for the minutes is used. This solution avoids the over-charge, but it generates a deviation from the expected SoC and the real observed value.
Further updates to the BESS model could also replace the deployed solution. If the expected SoC was correctly predicted from the beginning, there would not be need to change the requested power.

2.4.2.2 Damping Behaviour in Peak Hours

At the start of peak hours (19 :00 - 21 :00), the battery has more energy than the forecasted when generating the day-ahead schedule. Because of this, a higher injection order is given until the SoC decreases below the expected to use the extra stored energy. Once the SoC decreases below the expected value, the power is then reduced. This power reduction surpasses the allowed margin of error, generating- penalties to the remuneration of the day and another increase in power injection to compensate.

Origin The damping phenomena is due to differences between the battery model used to generate the day-ahead prediction and the real battery system. The high discharge power has a lower efficiency, and the state of charge decreases faster than what the control system expects. This continues until the point in which the SoC is lower than the reference value.

At this point a continuous decrease in power takes place but as efficiency is still lower than expected, the state of charge continues to decrease. The power request from the BESS has to significantly lower to compensate the deviation.

Possible consequences The effects on the battery due to the damping are not considered as important given that the main degradation comes from the high discharge power and not the variation it presents in this period of time. The phenomena however can influence the penalty the hybrid plant suffers as the injection falls outside the allowed deviation of 5%.

Solution implemented A second override of the algorithm is applied during the peak hours. The battery controller publishes a value of for the remaining discharge energy, and this value isused to calculate the power injection order instead of using the expected and real SoC.

In both of these aberrant behaviours, a precise battery model could be used to solve the issues. If 100% confidence existed in the battery model, there would not be need to check the SoC as reported by the battery controller. The power injection for peak hours could be calculated while taking into account the change in performance, creating better day-ahead schedules.

2.4.2.3 Revised RT-EMS algorithm

Following the modifications described in the last section, the implemented algorithm followed by the EMS for real-time operation (RT-EMS) can be seen in figure 2.13. This algorithm, just as the one before, is based only in instantaneous observable data from the sites without any direct or indirect data look-up in the historical database.
The three different operation situations for the algorithm are as follow :

— Before 6 a.m. or after 9 p.m. :
  The scheduled charging power is used without modification.
— After 6 a.m. and before 7 p.m. :
  The algorithm that compares the planned and real SoC is used.
— Between 7 p.m. and 9 p.m. :
  The energy available as published by the battery controller is used to determine the power.

By following this more static set of rules, the aberrant behaviour was mostly corrected (see figure 2.14). Both the oscillatory behaviour at peak hours and the overuse of the grid

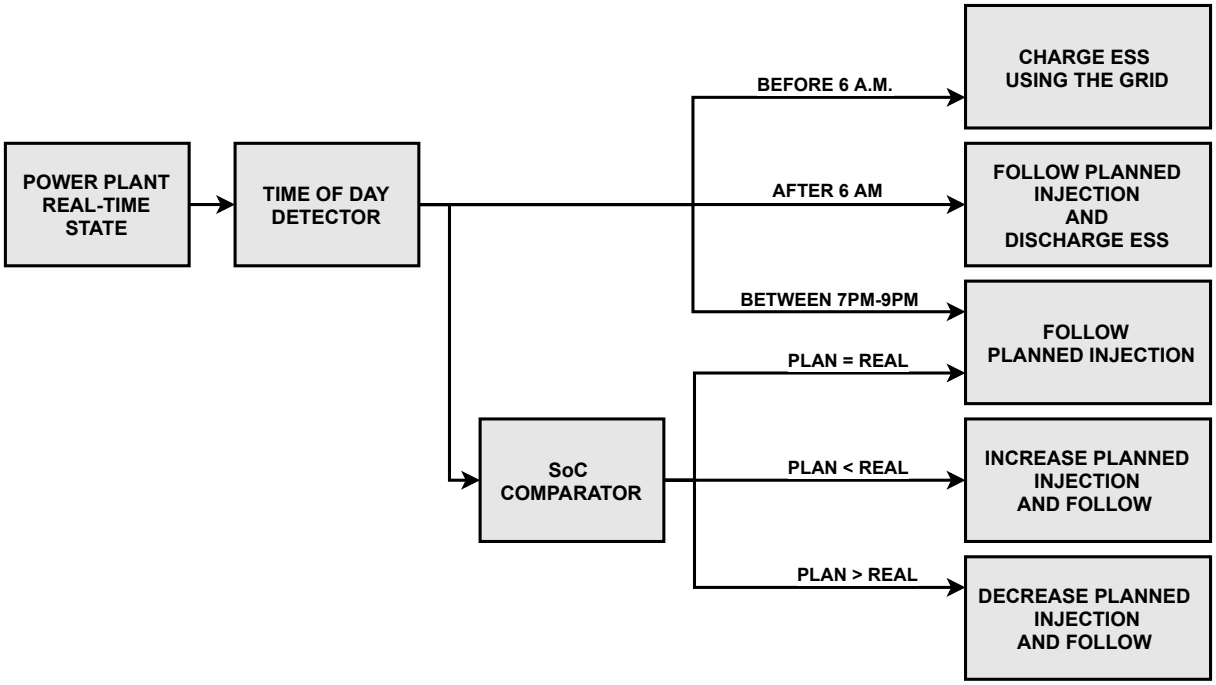

FIGURE 2.13 – Real-time logic used to decide whether to follow or to modify the scheduled objective power of the installation. EMS version from 14/09/2020.

in the morning disappeared through these modifications, proving the effectiveness of the measures applied.

The modifications here presented are however not the last iteration of the EMS deployed. The feedback and state of the system is a screenshot of the central in November 2020. As the sites remain under the warranty period and within a maintenance service, the EMS in each site will continue to evolve as the specific needs and behaviour of the central change.

2.4.2.4 Observable thermal behaviour

Unfortunately, the results from the surface temperature from the deployed BESS did not show any meaningful data regarding their thermal behaviour. In the first 6-month initial operational window, the surface temperature followed the recorded ambient temperature. Figure 2.15 shows the recorded values for a winter day, showing the very weak influence the power requested from the batteries had on the measured temperature. The systematic difference between the two temperatures is a consequence of the BESS heating system located within the cabinets to avoid extreme temperatures. Annex F expands on these measurements and shows the different temperature distributions, as well as daily examples for these sites.

As mentioned just before, this lack of significant thermal signals can be then associated

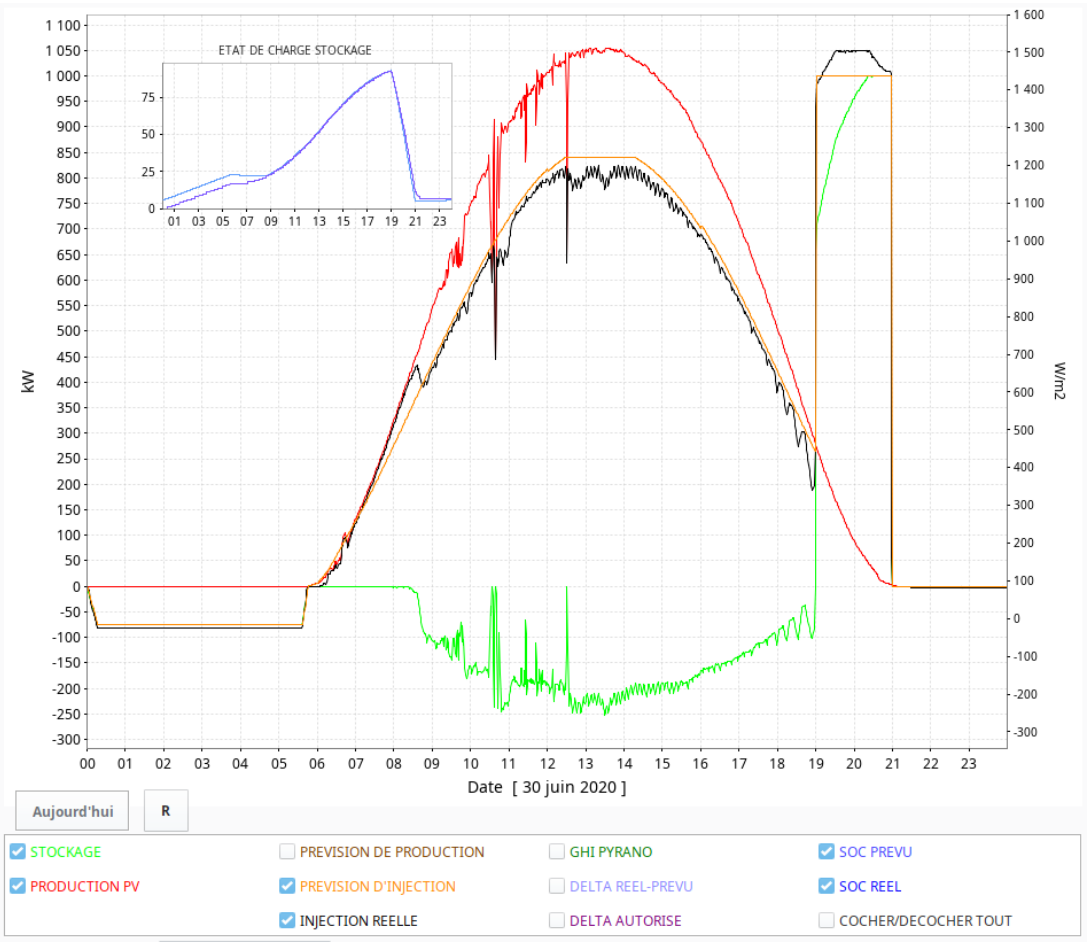

FIGURE 2.14 – Observed behaviour after updating the real-time control logic given the initial feedback.

directly to the presence of the ventilation and internal refrigeration/heating system. These systems avoid the internal cabinet temperature to rise outside what is normally expect given the ambient temperature. As consequence of this, no reasonable thermal model calibration and validation is foreseeable for the BESS in the Corsican hybrid PV sites due to the trivial nature of the measurements.

2.5 BESS Characterisation

One of the first steps in Hybrid PV+Storage project development, and in the finalized project commissioning before the start of nominal operation, is the characterization of the different production systems. For the Battery Energy Storage System (BESS) of such centrals, this generally translates to determining the efficiency, energy capacity, and power capabilities of the whole system.

By default the BESS offered by the manufacturer are submitted to a series of charac-

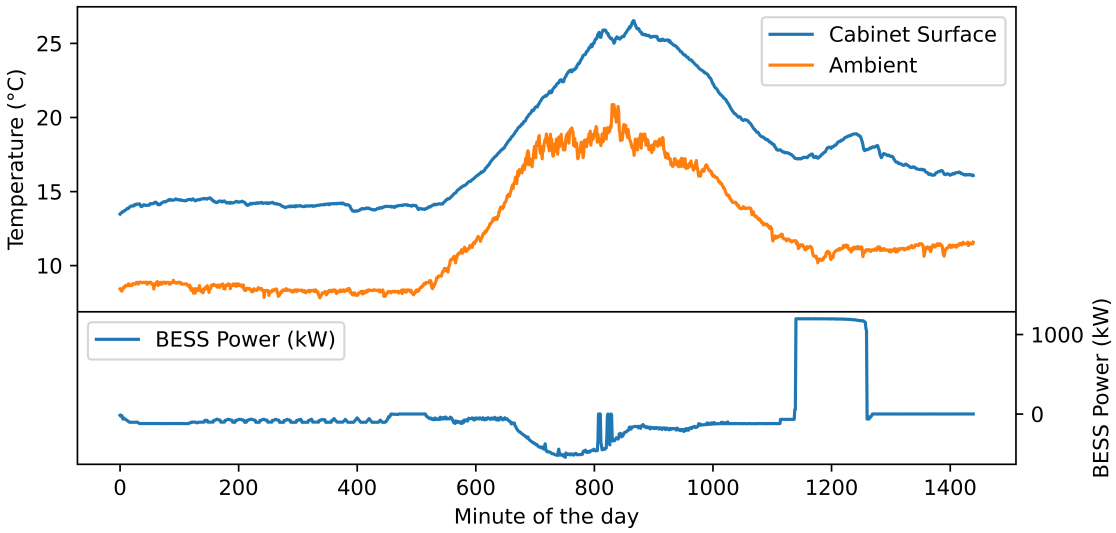

FIGURE 2.15 – Measured battery cabinet surface temperature and the ambient temperature (top), and requested BESS power for the period (bottom). Both temperatures share the same behaviour regardless of the BESS power.

terization protocols with laboratory conditions in the initial product Research & Development (R&D). The results are then published as the specification sheet for the BESS, which in turn are used by vRES investores to correctly size their projects. The data found in the specification sheet also provides the means to quickly, albeit shallowly, compare the different solutions, models, and configurations for the specific project needs.

Once the BESS are chosen and installed for their application, an on-site characterization for commissioning is usually done or requested by the manufacturer and/or the investor. This ensures that the system respects the minimal warrantied performance, and that the systems are fully operational. Otherwise, indemnities or equipment replacements can be requested by the owner. Additionally, the parameters found via these procedures create the referential values for Beginning-of-Life (BoL), which are later used for model fitting and parameterization.

Because of these reasons, the characterization protocol is a vital element on the life of BESS. Unfortunately for hybrid PV+Storage power plants, besides these situations the frequency at which the protocols are done depends entirely on the owner of the project. This often means that the characterization procedure will be done only when it is strictly necessary. That is, either to demonstrate an overall under-performance of the system (which means a reclamation to the BESS manufacturer), or because of a maintenance procedure is being done. More often than not, the financial impact of the BESS downtime is too high to justify a characterization procedure.

Regardless of this scarcity of characterization in operational hybrid PV+Storage sites, following the procedure does offer a useful snapshot of the BESS. This image of the system will depend on the protocol and setup that is used and/or available, and thus the parameters of interest that can be extracted are limited by it too. The choice of which protocol to apply becomes then a key element to determine based on the current needs of the owner, the control system on site, and the parameters exploited by it.

2.5.1 LiB Experimental Protocols : Historical Framework

As it's been noted by Bandhauer in its review of thermal issues in batteries belonging to Li-ion technologies [53], it is not rare in the literature to find simulations in which the results do not behave as a real battery cell. Furthermore, the corroboration of the different models is often a complicated task given the lack of rigor (or reporting) of the experimental procedures used. In some cases, important parameters are left static and thus a direct comparison is not viable, while in others the temporal resolution used is not shared and thus the reproduction of the results is compromised.

A difference in the battery internal design represents a factor too that disturbs the results and hurts the applicability from the models. This lack of common methodology and variability of cell technology is not only present in thermal related articles, but it is a generalized problem that can be observed in the literature concerning the different proposed estimation methods for critical li-ion battery state indicators as the State Of Charge (SoC) or the State Of Health (SoH) where some information is available but it is rarely enough to replicate the experiments [72, 74, 103, 75, 70, 73, 102, 109].

The absence of systematic experimental procedures can be linked to missing well-known protocols or norms outside the domain of electric vehicles. Whilst in 1996 a battery test manual for electric vehicles was already in its second revision [110], similar documentation was non-existent for general-purpose Energy Storage System (ESS), including those for stationary usage. In recent years however, the maturity and penetration of the technology has led to documentation to standardize the information available from the storage systems.

The Institute of Electrical and Electronics Engineers (IEEE) published in 2010 a series of recommendations for the characterization and evaluation of ESS [112], but it limited itself to listing the kind of information and tests that should be made available without defining any specific procedures. In 2012, the Pacific Northwest National Laboratory (PNNL) in union with the Sandia National Laboratory (SNL) published a series of protocols to measure and express the performance of ESS, in which its latest iteration

Application	Brief Description
Peak Shaving	Reduce maximal power withdrawal.
Volt/Var	Ensure voltage stability via VAr.
Frequency Control/Regulation	Ensure frequency stability via VA injection/withdrawal.
Renewables Firming	Ensure the output capavility of vRES.
Islanded Microgrids	Provide reliability to a microgrid.
Power Quality	Compensate voltage/frequency variations.
PV Smoothing	Reduce peaks and valleys of PV power outputs.

TABLE 2.5 – Energy Storage System Applications as identified by [111].

(April 2016) includes metrics considering Renewable Energy Sources (RES) oriented applications [111] amongst others (see table 2.5 for the identified applications by the PNNL). This document, as well as the recently published European standard NF EN 62933 [113] deal with the EES in a general way, not being reserved for any specific technology and providing a stable framework allowing a simpler comparison between technologies.

A Li-ion specific guide to characterize and evaluate their behaviour in stationary applications was also recently made available by the IEEE [114], but it focuses primarily on listing the areas that must be covered by a characterization without detailing how to do this. Nonetheless, this guide refers to the mentioned protocols by the PNNL and SNL for the industry-accepted procedures to follow.

Based on the different European Norm and the protocol by the PNNL [111, 114], the parameters shown in table 2.6 represent the minimum amount of information necessary to form an image of an ESS performance.

All these different characteristics can be classified in two different kinds : power system parameters, and battery system parameters. The former establishes the capabilities of the physical equipment installed, and the latter a static image of the batteries.

The estimation of instantaneous internal battery states will be briefly presented in section 2.5.1.3, but a deeper view is reserved for chapter 3.

2.5.1.1 ESS Power Parameters

The parameters that are considered to fall under this category are the input/output power ratings, the system response, auxiliary power consumption, and voltage/frequency range. They are highly dependent on the power electronics and the BMS provided by the BESS manufacturer. These values are often static unless there is some level of material malfunction or BMS software deficiency. A characterization at the beginning of life of the

Parameters	Definition
- Nominal Energy Capacity	Base energy that the system can restore.
- Input and Output Power Rating	Max. power the system can inject or withdraw.
- Round-trip Efficiency	Ratio between the energy restored per energy withdrawn.
- Expected Service Life	Years before reaching EoL capacity under the expected operation.
- System Response Performance	Time between a setpoint signal is received and the moment it is fulfilled.
- Auxiliary Power Consumption	Power and energy used by the system to keep itself running on when idle or in operation.
- Self-Discharge Rate	Loss of SoC when in an idle state.
- Voltage Range	Voltages at which the system is expected to operate.
- Frequency Range	Frequencies at which the system is expected to operate.

TABLE 2.6 – Energy Storage System common basic parameters.

system would be required just to ensure it follows the specification sheet of the system.

Input/Output Power Rating : Measures the maximal charge (input) and discharge (output) power the system can obtain from the batteries.

System Response Performance : It quantifies the time between when a power order is received, and the moment the system fulfills the requested power as expected. It encompasses notions such as dead time [10], settling time [11] and ramp rate [12].

The system response performance, and all the notions it implies, has a high importance for ESS that aim to provide voltage or frequency support to the electric grid.

10. Time between the order an initial change in output power
11. Time until the output power stays within a tolerance level from the order
12. Output power variation per second after the dead time and until the power reaches the requested set-point for the first time, regardless of an overshoot.

Auxiliary Power Consumption : Measures the amount of power the BESS needs to maintain its equipment in nominal operation. This parameter is often non negligible if the system has an AC or heating system.

Voltage/Frequency Range : These ranges determine the physical limits at which the Power Conversion System (PCS) can inject or withdraw power from the grid. In most of scenarios, the specific grid code (i.e., the grid manager specifications) constraints the operation within some predefined limit values.

A more detailed description of the protocols for the parameters can be found in annex C.

2.5.1.2 ESS Battery Parameters

The battery parameters that are treated by the characterization protocols discussed are the following : Nominal energy capacity , self-discharge, round-trip efficiency, and expected service life. All these depend on the current technology and state of the battery packs and cells, as well as their specific long-term behaviour. The round-trip efficiency parameter does have an efficiency component that depends on the AC/DC conversion process, but it is included as it is a necessary part of the BESS. In the case of the expected service life, it is determined by the limits at which the battery capacity does no longer satisfy the usage, which is a consequence of the battery behaviour.

A brief description of what each parameter implies as described by the IEC [113] can be seen here below, and a detailed description of the protocols for the parameters can also be found in annex C.

Nominal Energy Capacity : The International Electrotechnical Commission (IEC) defines this parameter as the energy in the EES when utilized in continuous operating conditions at the rated active power and going from a complete state of charge to a completely discharged state [113]. The fact that is measured at the rated active power is important because, in some cases the PCS lowers the power when batteries are almost discharged. This effectively reduces the energy capacity as there is a range of stored energy that cannot be accessed at the rated power.

Figure 2.16 shows the general protocol used to obtain this parameter. It is formed of four main phases : a first stand-by or resting period, followed by continuous charge until full. Then a second resting period, and lastly the discharge phase at nominal power until empty.

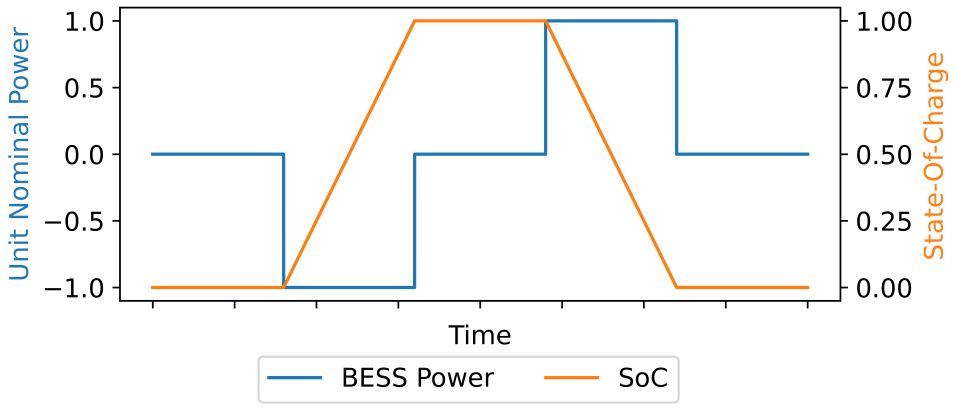

FIGURE 2.16 – Power profile and State of Charge profile used in energy capacity tests.

Self-discharge : Rate at which the BESS losses part of its accumulated energy due to phenomena independent from power injection.

Round-trip efficiency : Is the ratio between the energy discharged and the energy absorbed in a specific charging/discharge cycle (2.5), which normally involves the full capacity of the storage. It effectively represents the percentage of energy that can be used given the energy sent to the system.

$$\eta_{rt} = \frac{\int_{t(SoC=0)}^{t(SoC=100)} P \text{ dt}}{\int_{t(SoC=100)}^{t(SoC=0)} P \text{ dt}} \tag{2.5}$$

Although the standard definition implies a full charge/discharge just as mentioned, it is possible to have round-trip efficiencies for smaller subsets of cycles that go between charge point a and b as in (2.6).

$$\eta_{a\to b} = \frac{\int_{t(SoC=a)}^{t(SoC=b)} P \text{ dt}}{\int_{t(SoC=b)}^{t(SoC=a)} P \text{ dt}} \tag{2.6}$$

Expected Service Life T_{SL} : It is the duration of the BESS until it reaches end of life values. These last values, as the name implies, define the limits at which the storage is expected to be replaced in order to continue fulfilling the current usage. The nature of the values varies, but it often involves the capacity retention and rated power.

2.5.1.3 BESS State Indicators

What differentiates the BESS state indicators presented below from the parameters in sections 2.5.1.1-2.5.1.1 is that they offer the instantaneous operational image of the storage instead of a more general system characteristic. The information obtained by the state indicators allow to adapt and change in real time the setpoints and power demanded from the storage solution. They represent then a necessary element of any control system that aims to use BESS.

To generate such indicators there must exist either a direct measurement sensor or a model that estimates it. The nature of the state model and sensor depends entirely on the manufacturer, and the way they consider it is best to estimate the actual status of their battery configuration. Currently it does not exist standardized state models for the indicators presented below, although the most used rely heavily on mathematical or physical approaches. Chapter 3 will dive deeper into the modelling of these state indicators within the scope of hybrid PV-BESS capacity firming sites.

Internal Battery Temperature : Estimates the internal temperature within the cell or pack. Temperature sensors can be placed around the cells or packs, but they would still reflect the surface cell temperature. This real measurement (or estimated value if no sensor is installed) allows to avoid operation outside predefined ranges.

State Of Charge (SoC) : Represents the amount of energy the system has currently in storage (E_t) relative to the maximal energy the system can hold at the time ($E_t^{\max}$). This is useful as allows to know whether the storage can still absorb energy, or if a backup energy source needs to be launched as the stored energy reaches dangerously low values.

$$\text{SoC} = \frac{E_t}{E_t^{\max}} \tag{2.7}$$

State Of Health (SoH) : This indicates the current maximal energy capacity of the BESS ($E_t^{\max}$) relative to the "nameplate" or initial storage capacity ($t = 0$). It indicates the degradation the system has had given its past usage.

$$\text{SOH} = \frac{E_t^{\max}}{E_0^{\max}} \tag{2.8}$$

Remaining Useful Life (RUL) $T_{textRUL}$ **:** Strongly related with the SoH and the expected service life, this indicator offers the estimated remaining time at which the system

will reach its End-of-Service (EoS) values. The distinction from T_{SL} is that it offers this window of operation given the specific present and past usage of the system, and not the manufacturer foreseen use case scenario.

$$\mathrm{RUL} = \hat{t}\left(SoH = SoH_{\mathrm{EoS}}\right) - t \tag{2.9}$$

2.5.2 BESS characterization results from PV+BESS site

As a mean to establish the differences between the published or nameplate values for BESS and their real performance in operation, several characterization protocols that focus on the battery and power parameters were applied to the experimental PV+BESS site presented in section 2.3. The characterization of the 3 BESS on site was possible due to the lack of a financial constraints that discourages the out-of-service time the protocol requires, unlike the Corsican sites presented in section 2.4. The modelling of the BESS is not treated here but in further chapters.

The protocols applied to the three BESS were to measure the *Nominal Energy Capacity* and the *System Response* via the ramp rate and response time. These were the point of interest given that their values have a direct impact on the Energy Management System (EMS) and Power Management System (PMS) deployed in the experimental site. The PV capacity firming framework followed by the experimental hybrid site requires the energy capacity for the scheduling phase, and the system response for both the scheduling and the real time operation.

The tests were done during a 4-day period between 17/01/2019 and 21/01/2019. As the beginning of operation for the experimental site was at the end of the first trimester in 2018, this means the three BESS had less than 1 year in nominal operation.

2.5.2.1 Nominal Energy Capacity

The protocol as specified by the IEC (annex C) was followed. Given that the manufacturer does not specify a particular state of charge to consider it completely discharged, a value of 5% was supposed given the BESS is still able to operate at nominal power at this level. The three batteries of the site were subjected to the same charge-discharge duty cycle and same data-collection method. The specific parameters used for the protocol are summarized in table 2.7.

The capacity test was done 3 times per BESS and the results of such tests are seen in tables 2.8 - 2.10.

Capacity Test Conditions and Parameters of the BESS	
Nominal Energy (Manufacturer)	6.5 kWh
Nominal Charge/Discharge Power	2.2 kW / 2.2 kW
Charge/Discharge Current	37.8 A / 37.8 A
Lower SOC limit	5%
Rest Time Between Charge/Discharge	120 seconds

TABLE 2.7 – Nominal Energy Capacity Test Results

	LiBESS B01			
	Test #1	Test #2	Test #3	Average
Charge [kWh]	-7.255	-7.067	-7.177	-7.166
Discharge [kWh]	5.971	5.971	5.971	5.971
Performance	**82.31%**	**84.48%**	**83.19%**	**83.33%**

TABLE 2.8 – Capacity test results for LiBESS #01

2.5.2.2 System Performance : Ramp Rate and Response Time

The three BESS performances were evaluated via the ramp rate and response time as they are useful for the EMS on site. The reported data by the manufacturer of the BESS is a response time between 2-10 seconds and a ramp rate of 1kW/s [106]. The test as described in appendix C was followed and tables 2.11, 2.12 summarize the results for the three batteries. Both the charge and discharge regime were subject to the test.

In general, the response time was homogeneous amongst the ESS (around 5 seconds, average of two tests), and the ramp rate oscillated between 1kW/s and 1.5kW/s. The step response was calculated using the values reported by the BMS itself, while a power monitor was used for the ramp rate given its higher refresh rate of 1 second.

	LiBESS B02			
	Test #1	Test #2	Test #3	Average
Charge [kWh]	-7.361	-7.083	-7.157	-7.201
Discharge [kWh]	5.979	5.982	5.990	5.984
Performance	**81.22%**	**84.46%**	**83.69%**	**83.12%**

TABLE 2.9 – Capacity test results for battery #02

	LiBESS B03			
	Test #1	Test #2	Test #3	Average
Charge [kWh]	-7.068	-7.002	-7.050	-7.040
Discharge [kWh]	5.912	5.915	5.918	5.915
Performance	**83.64%**	**84.47%**	**83.94%**	**84.02%**

TABLE 2.10 – Capacity test results for battery #03

		Battery B01	**Battery B02**	**Battery B03**
Zero to $-P_{\text{nom}}$	Response Time	5s.	6s.	5s.
	Ramp Rate	-2.2kW/s	-1.98kW/s	-1.46kW/s
$-P_{\text{nom}}$ to zero	Response Time	5s.	5.s	4s.
	Ramp Rate	1.29kW/s	1.5kW/s	1.47kW/s

TABLE 2.11 – Response Rate and Ramp Rate for ESS **Charge**.

2.6 Conclusion

In this chapter, a presentation of five hybrid PV+Storage power plants was done. These sites were built while answering a call for tenders for non-interconnected French islands, in which the operational requirements expected from hybrid centrals establishes a PV capacity firming framework in which day-ahead engagements are requested.

A main particularity of the framework is the remuneration scheme proposed to the operators. By having a non-linear penalty in the case of power under-production and a very severe penalty for over-production, the behaviour from the associated BESS during diurnal production has a very characteristic profile. The charge will follow the variability of the solar production and absorb any excess power until it is no longer able to store more energy to respect the engagement and, at the same time, it will not systematically compensate any missing power as it is not advantageous. At night the BESS will systematically have a full discharge cycle with a duration of 2 hours. This essentially means that the power profile is almost categorically divided for the whole duration of the projects into a highly variable charge-only phase, and a full discharge phase.

		Battery B01	**Battery B02**	**Battery B03**
Zero to P_{nom}	Response Time	5s.	9s.	5s.
	Ramp Rate	1.27kW/s	1.48kW/s	1.21 kW/s
P_{nom} to zero	Response Time	5s.	5s.	5s.
	Ramp Rate	-2.021kW/s	-1.94kW/s	-1.3kW/s

TABLE 2.12 – Response Rate and Ramp Rate for ESS **Discharge**.

The regularity of the cycles the BESS have when operating under this framework offer a unique possibility to capture the evolution and system response under the specific stress. As power profile is different to other BESS common usages, it is normal to expect deviations from the advertised performance and capacity retention. By understanding the behaviour of these deviations, as well as the scale and time-horizons at which they occur, it is possible to improve the overall value obtained from hybrid PV capacity firming sites.

As seen in this chapter, the real-time operation can avoid unnecessary penalties via a precise and up-to-date BESS model on the daily scheduling process. On the project development and planning side, knowledge of the instantaneous and probable evolution of the BESS behaviour will render more precise business plans and a better budget control for power plants that expect to have a very repetitive behaviour for long periods of time.

One of the limiting factors to develop the BESS models for specific applications was however re-confirmed with the development and construction of these sites. Data-availability is dependent on the openness from the BESS manufacturer, and non-trivial battery measurements are not necessarily available to the EMS/PMS developer for the power sites. It is then the developer endeavour to build the control system and the battery model around the data provided by the specific BMS of the LiBESS. The missing information limits then the kind of phenomena that could be analysed, as well as separates the results from the physical reality of the cells. For instance, in the LiBESS here presented on the industrial sites, any thermal modelling is impossible given the lack of temperature measurements. For other parameters such as SoC and SoH, without direct battery-related measurements the models have to estimate directly the value the BMS will publish for each. The usefulness of the BESS models under these constraints does not decrease due to the missing direct physical and chemical relation. It however misses the opportunity to shine light on the specific reasons for the degradation and performance changes it can suffer.

The development of mandatory protocols which enforce the availability of direct physical battery measurements could alleviate this ailment in the future. Applications of such directives could facilitate the interoperability and generalisation of the EMS/PMS regardless of the manufacturer. Battery behaviour could be better understood from the investor perspective, and it could help him to weight the cost of auxiliary or supplementary systems to try and counter-act the physical mechanisms impacting the BESS performance.

Conclusion on BESS Characterization In the last section of this chapter the focus was given to Electrical Energy Storage System (EESS) characterization protocols. As

mentioned, it is possible to represent the BESS via its Power Conversion System (PCS) or its battery qualities. These two kinds of parameters are commonly found on the technical specification sheets from commercial systems, and they represent the majority of the efforts done to standardize and industrialize the meaning of the data published by the battery manufacturers.

PCS characterization aims to inform about the power limits and capabilities of the internal BMS and PMS embedded in the system, while the battery qualities reflect the battery cell/pack configuration, chemistry, and electrical characteristics.

The results from the characterization tests done to the three BESS in the experimental hybrid PV+Storage site help to showcase the importance of BoL commissioning and regular testing through the life of the systems. For the three LiBs the response time fell within the range published by the manufacturer although it was significantly slower ($\tilde{+}$200%) than the best-case scenario of 2 seconds, and the ramp rates were in average 1.5 times faster. The difference in response time is not important for the PV capacity firming framework used in the experimental site as the power is averaged per minute and the impact of this delay can be compensated by a temporary over- or unde-production. It is however possible to imagine cases in which an increased delay could have stronger consequences.

An example of this are BESS that operate under a Primary Frequency Regulation (PFR) regime in a grid composed in part by solar plants. As solar inverters disconnect themselves after an average period of 1.4 second when the grid presents an abnormal grid [115], a BESS with a response time of 500ms-1000ms could not afford a 200% time deviation as it is unable to prevent the solar inverter disconnection. This in turn could generate a critical grid failure. BESS for which the response time is critical should then have regular testing of its PCS capabilities to avoid any hardware malfunction that impedes the use originally intended.

For the capacity test results, the three tested systems showed an average energy retention of 6.2 kWh (5.9 kWh with a Depth of discharge of 95%) which means that 4% of the original capacity was already lost by the time the protocol took place. As the formation of SEI takes places in the initial cycles of a Li-ion battery system, a regular capacity test becomes almost a necessity for BESS projects in the early phases of the project.

An interesting result which highlight the need for characterization protocols is the round-trip efficiency that resulted from the capacity tests. The published round-trip of the manufacturer is 95% with a discharge rate of C/3, but at the nominal power of

2.2 kW (slightly higher than C/3) the efficiency decreased by 10%. This difference is significant, and it has to be considered by any existing EMS to reduce possible performance penalties. In this case, more solar production and a bigger storage would be needed in hybrid PV+BESS plants that use this battery manufacturer if specific capacity or energy requirements must be met.

The insights gained from the protocol results, and their deviation from the published value, highlight the need for more openness in battery characterization data from manufacturers. It is very difficult for hybrid project investors and constructors to have trustworthy financial and operational projections when it is unknown the expected behaviour the BESS will have for their application. The protocols offer a base characterization in which to develop a project, but it is unrealistic for them to offer valid characterization data for every possible usage the system can have.

Instead, what can be offered by the manufacturer is a parameterized BESS model. Although it would still have limitations and be dependent on the data and model the manufacturer used, it would streamline the sharing of the BESS behaviour in a multitude of scenarios and not be restrained to the information that can be written on a sheet of paper. For project developers this would reduce uncertainty due to the LiB behavior in the short and long term of their projects. Nevertheless, this does not solve all the problems as any non-modelled physical malfunction in the operational site would still need an on-site diagnostic, characterization, implementation in the deployed EMS.

Chapitre 3

LIBESS Modelling

Résumé en français

Afin d'obtenir une intégration efficace des LiBESS dans des systèmes industriels, il est nécessaire de connaitre et maitriser leur comportement. Ce chapitre présente les trois paramètres principaux identifies comme nécessaires pour accomplir cela : la température interne, l'état de charge (SoC), et l'état de santé (SoH). La première partie explore le comportement thermique des batteries, présentant divers modèles thermiques et leurs applications. Un modèle thermique spécifique pour les LiBESS est proposé et les résultats de simulations sont discutés.

Par la suite, le SoC et les différentes techniques de modélisation sont explorés. Le modèle retenu est une version modifiée d'un intégrateur de Coulomb exprimé en termes de la puissance active. Deux versions de ce modèle ont été testés ensuite : une version avec un paramètre thermique pour refléter l'effet que la température interne peut avoir sur la batterie et une autre sans cet élément. En dernier la modélisation du SoH, indicateur qui évalue la dégradation et la capacité à maintenir une performance optimale sur le long terme, est exposé. En utilisant les cycles de charge/décharge, la température, le courant et la capacité réelle observée sur les LiBESS à disposition, un modèle qui estime la capacité future selon les cycles attendues a été développé.

Ce chapitre se conclut par une discussion sur les modèles développés et leurs interactions entre eux. Les résultats obtenus montrent que les modèles thermiques, SoC et SoH proposées offrent une meilleure maitrise du comportement du stockage comparé avec les modèles et paramètres fournis par le fabricant. De la même façon, une co-estimation des paramètres a montré des bons résultats malgré une légère perte en précision. Grace à la relative simplicité des modèles, leur intégration dans des systèmes de gestion de batte-

rie (BMS) et de l'énergie (EMS) est facilement envisageable. Cette meilleure maitrise du comportement des LiBESS permettra d'améliorer l'efficacité des LiBESS dans les diverses applications industrielles.

3.1 Introduction

Previous chapters have shined light on the importance of BESS models for both hybrid PV+BESS projects and the control systems that are deployed in such sites. In all the scenarios mentioned, what remains of vital importance for BMS and/or EMS are the estimation of the State Of Charge (SoC) and State Of Health (SoH), as they allow a correct management of the ESS resource [116]. SoC estimation is unavoidable for any real-time battery management, and SoH modelling is essential if any long-term visibility and planning is wished.

In addition to these two, and as mentioned in the state of the art in chapter 1, attention must be given to modelling the battery internal temperature too. This additional parameter impacts both SoC and SoH estimation and can improve the overall accuracy of the models. Advanced Battery Management System (BMS) should integrate a thermal component to avoid LiBESS operation that can endanger its safety.

In existing literature, focus is given primarily to these three parameters and the different methods and techniques to estimate the state of the Li-ion battery cell. Each one of it uses different underlying parameters, but they usually are composed by determining either some kind of resistance (or impedance), voltage, and/or dynamics of the cell to mention a few [117, 56, 89, 118, 119]. These however are done with laboratory-grade characterisation methods and/or data collection setups.

When focus needs to be given to their applicability for industrial scenarios, it is necessary to address each parameter individually due to the different nature of the models and the specific procedure required for each. The synergy between models also has to be re-thought and adapted for said industrial scenarios such as large-scale hybrid PV+BESS sites. The models need to be compatible between each other as well as with the technological and economical constraints common in the remote sites of PV applications.

3.2 Objectives and chapter structure

In this chapter the subjects of thermal, SoC, and SoH modelling for Lithium-ion Battery Energy Storage System (LiBESS) in PV+BESS scenarios is treated. For each of these

BESS indicators, the same basic structure is followed for its respective section. At first an extended state of the art of the different methods and techniques used in the literature are provided. Afterwards, the retained modelling approach for the discussed parameter is developed while considering the technological constraints present in the intended use. At last, the model is applied and validated using the experimental data obtained from the experimental and industrial sites presented in chapter 2.

The resulting models here presented aim to be a stepping stone for a more robust LiBESS model that, by taking into account an explicit thermal component, improves the accuracy of the SoC/SoH estimation and avoids any abusive usage. The purpose of the different models is to increase the performance of the real-time state estimation, as well as the performance of the scheduling and simulation process used in the EMS in both the exploration and production phases of vRES projects.

In summary, the main contributions and objectives presented in this chapter address the industrial and research gaps **IG1**, **RG1**, **RG2**, and **RG3**. These can be expressed as :

— Development of a thermal, SoC, and SoH BESS model that are coherent with constraints commonly faced in industrial PV+BESS hybrid sites.
— Use of real industrial operational data to training and validate the LiBESS models, something traditionally done only with laboratory data and setups.
— Validate the applicability of the LiBESS models for PV capacity frameworks and evaluate the deviation the system exhibits to the manufacturer published and guaranteed specifications.

The structure of this chapter is separated by LiBESS parameter of interest. Section 3.3 covers the development and validation of a thermal model for LiBESS able to estimate the operating temperature, as well as the maximal expected temperature in operation. Afterwards, section 3.4 presents the development of a SoC model that is both suitable for the expected industrial application and can incorporate the previous thermal model. At last, the construction and parameterization of a SoH LiBESS model is presented in section 3.5. This using both the SoC and thermal models to simulate the behaviour of the ESS under specific power curves. A conclusion and discussion of the general findings and their applicability is then presented in section 3.6.

3.3 Thermal Modelling of Li-ion Batteries

The thermal management of Li-ion batteries is one of the most crucial elements in any BMS. The temperature at which the batteries are either stored or used heavily impacts the

life expectancy and performance of the battery in the short and long-term, not including the safety concerns that arise when the temperature is left unchecked. The most known effects can be boiled down to a capacity/power fade, an increase of the rate of self-discharge, a thermal runaway, an electrical balance, and low temperature performance. All these phenomena have been the subject of numerous studies through the years. Bandhauer et al did a review on the different publications done regarding the different effects [53].

The capacity fade is usually caused by the loss of active material (often in the form of SEI inside the cells) while the power fade is related to the increase of internal impedance. Both these kinds of degradation showed a strong relationship with temperature at either storage conditions or in operation. The capacity fade increase reported in the literature when the batteries are cycled at high temperatures (>45°) were values that ranged from 4% up to 40% compared to those when cycled at about half the temperature (around 25°). This variability is strongly dependent on the chemistry of the cells, as well as rate and number of cycles used. When special profiles with a low DoD (depth of discharge) were used, the capacity remains stable while the most prominent phenomenon was a fade in available power probably due to the mechanical stress in the cathodes due to the cycles. [120, 121].

For storage conditions, the temperature is an important factor in power fade, accelerating the rate at which the degradation occurs in the beginning. However, the SoC at which the batteries are stored is also of importance, reporting a power fade of up to 55% when temperature is above 45°and the battery is fully charged [122]. For the capacity fade, the nature of the electrolyte has a major role in the reaction of the battery to high temperature storage conditions [54]. On this note, the self-discharge is often linked to the conductivity of the electrolyte, value that also increases at high temperatures due to partial dissolution of the SEI.

The aforementioned effects, although important from a performance point of view, lackluster when considering the possible safety consequences a thermal runaway can have. This event materializes itself when the cells reach a critical internal temperature that creates an uncontrollable exothermic feedback within the electrolyte and the anodes. These critical temperatures, usually above 90°for Li-ion, imply an abusive usage of the battery packs and therefore keeping track of the current as well as the internal temperatures are of interest to avoid reaching this situation.[81, 123]

On the other side of the spectrum, low temperatures have an impact primarily in the performance of the cells. Low temperature charging cannot be performed at the same rate as a low temperature discharge. It has been reported that charging under cold tem-

peratures induces SEI formation at the electrodes[124]. Lithium plating, the formation of a solid coating in the anode, is another important reaction that is exacerbated by low temperatures and reduces the cell capacity in an irreversible way[125].

Because of all these mentioned phenomena, BESS manufacturers who wish to ensure the longevity of their product and a safe nominal operation have to include some kind of sensor or measurement of the cell temperature. By monitoring the temperature, the BMS can stop the battery from working under unsafe conditions and avoid future complaints from users due to unmet performance and fast degradation.

This real-time thermal monitoring alleviate concerns for BESS operators and owners, but it does not address the needs of the pre-construction period of the BESS project or the optimal operation of the system once deployed. For both of these, a comprehension of the storage behaviour needs to be had for any financial projection. A knowledgeable BESS model could make use of a thermal component to better tailor the foreseen usage to the project and maximise profitability and reliability, subject that is seldom explicitly treated in the literature, and vital for any Energy Management System (EMS).

3.3.1 LiB Thermal Behaviour & Modelling

As mentioned before, the effects that temperature has on LiB is no negligible affair. Consequences can go from relatively mundane power fade to a critical thermal runaway that endangers human life [53, 126]. The exact electro-chemical and physical mechanisms that come into play in critical thermal failures is out of the scope of this work, but the interested reader can refer to the works of Spotnitz and Franklin [81], Pasquer et al. [127], or Richard et al. [128] for more details on the phenomena. Generally speaking, very high temperatures of more than 80 °C [1] on LiB creates exothermic reactions due to different elements decomposition (e.g., SEI, electrolyte) and also generates conditions for the lithium to react with other elements present.

For the case of LiB under non-critical temperatures, the possible reactions impacting the power, capacity, and self-discharge vary from one cell chemistry to another. Aurbach et al [129] did a review of the reactions for common cathode materials, and showed how these are more prominent at higher temperatures. The details of such chemical reactions also fall outside the scope of this work, and focus will be given primarily to the macro-scale thermal behaviour of LiBESS.

Under this particular optic, a vast amount of research has been devoted to cha-

1. The exact temperature depends on the exact chemistry, but electrolyte decomposition is estimated to start at this value [126].

racterising the impact that temperature has on performance for the cells in different charge/discharge regimes. A review of different LiB thermal studies was done by Bandhauer et al. [53], and part of the compilation of findings in the review were :

— For high temperature scenarios :
    1. Capacity fade is weakly impacted by Depth of Discharge (DoD), and high temperatures have a small impact if DoD remains under 75% .
    2. Electrolyte selection can reduce capacity fade at high temperatures (e.g., high concentrations of Ethylene Carbonate (EC) reduces capacity fade at high temperatures).
    3. Power fade at the BoL depends strongly on temperature, and later the fault is shared between both time and temperature.
— For low temperature scenarios :
    1. Charge performance decreases more than discharge performance.
    2. Capacity fade is significant due to lithium plating at the interface between the electrolyte and the electrode, regardless of weak rates of charge/discharge [124]. Optimal charging strategies for such cases can be implemented to reduce the phenomena [130].

Although these findings are common amongst a wide variety of cell chemistry, it is worth nothing that the experimental setups and the results often refer to a specific cell. The expected capacity and power fades reported are therefore hard to extrapolate to other battery systems, but the importance of knowing the temperature at which the system operates stands as a key finding for model development and implementation.

3.3.1.1 LiB heat generation and exchanges

To estimate the temperature it is necessary to model the heat exchanges the system experiences. The general approach is to use the energy balance equation seen in (3.1) [131, 132] in which the change in temperature per unit of volume is equal to difference between the heat transfer ($\nabla(h\nabla T)$) and the different heat generation mechanisms ($\dot{Q}$). This equation then becomes the more commonly seen equation (3.2) when taking into account a homogeneous internal temperature and heat exchange coefficient in all axes for a definite volume or system.

$$\rho C_p \frac{\partial T}{\partial t} = \nabla(\lambda \nabla T) + \sum \dot{Q} \tag{3.1}$$

$$m\ C_p \frac{\partial T}{\partial t} = \sum_j \dot{Q}_j \tag{3.2}$$

For a LiB, the heat generation can be separated in two kind of sources it presents : the battery cell itself (Q_{cell}) and the environment (Q_{amb}) as in (3.3).

$$m\ C_p \frac{\partial T}{\partial t} = \dot{Q}_{cell} + \dot{Q}_{amb} \tag{3.3}$$

To determine the different heat sources for the cell $\dot{Q}_{cell}$, this is often done via an electrochemical approach [133, 134]. This heat can be further separated as the reversible heat $\dot{Q}_{rev}$ (3.4) and irreversible heat $\dot{Q}_{irrev}$(3.5) linked to both reactions taken place inside the materials and the performance due to efficiency and ohmic resistance [134]. These translate to the equations in (3.6).

$$\dot{Q}_{rev} = I\ T \frac{\mathrm{d}E_0}{\mathrm{d}T} \tag{3.4}$$

$$\dot{Q}_{irrev} = I(E - E_0) \tag{3.5}$$

$$m\ C_p \frac{\partial T}{\partial t} = IT \frac{\mathrm{d}E_0}{\mathrm{d}T} + I(E - E_0) + \dot{Q}_{amb} \tag{3.6}$$

with I being the current, E_0 as the open voltage circuit and E the voltage during operation [2]. The reversible heat can be thought as the entropic heat, and the irreversible as the polarisation heat [87].

The heat exchanges that occur with the exterior $\dot{Q}_{amb}$ can be represented by the equation (3.7), in which the first term is the heat loss due to convection and the second represents the heat loss due to radiation [135].

$$\dot{Q}_{amb} = hA\left(T - T_{amb}\right) + \varepsilon\sigma A\left(T^4 - T_{amb}^4\right) \tag{3.7}$$

where $h\left[\frac{W}{m^2 K}\right]$: Heat Exchange Coefficient ; ε : Emission coefficient ; $\sigma\left[\frac{W}{m^2 K^4}\right]$: Stefan-Boltzman and $A[m^2]$: represents the surface area of the battery pack. This can be then rewritten as in (3.8) with $h^*\left[\frac{W}{K}\right]$ and $\varepsilon^*\left[\frac{W}{K^4}\right]$, where the constants are specific to the system as the surface area is integrated in the parameter.

$$\frac{dQ_{air}}{dt} = h^*\left(T_{ambient} - T_{battery}\right) + \varepsilon^*\left(T_{ambient}^4 - T_{battery}^4\right) \tag{3.8}$$

The thermal equation that describes a LiB behaviour becomes then (3.9)

$$m\ C_p \frac{\partial T}{\partial t} = IT \frac{\mathrm{d}E_0}{\mathrm{d}T} + I(E - E_0) + h^*\left(T_{ambient} - T_{battery}\right) + \varepsilon^*\left(T_{ambient}^4 - T_{battery}^4\right) \tag{3.9}$$

2. Also referenced as V_{ocv} and V for open voltage circuit voltage and operational voltage

Reversible Heat As seen in equation (3.4), the reversible heat can be determined by the change in open circuit voltage E_0 given the temperature. Schuster et al. [134] determined the value by experimentally measuring the voltage at an SoC of 20% at different temperatures, founding a value of -0.14mV/K for a commercial 40 Ah NMC LiB.

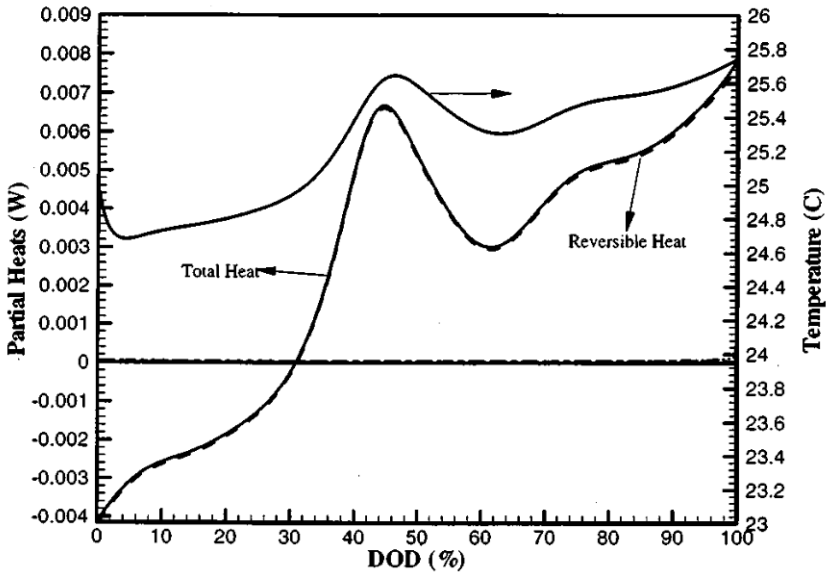

FIGURE 3.1 – Partial Heat during a simulated 0.01 C discharge. Source : [136]

In a more general approach, the reversible heat can be expressed directly by the change in entropy as in (3.10). Using the entropy relation in (3.11) we find then the previously seen equation depending on the voltage[134].

$$\dot{Q}_{rev} = \frac{\mathrm{d}}{\mathrm{d}t}(T\Delta S) \tag{3.10}$$

$$\Delta S = nF\frac{\mathrm{d}E_0}{\mathrm{d}T} \tag{3.11}$$

An example of the reversible heat in a LiB can be seen in figure 3.1. As the discharge rate is low, almost all the total heat generation is reversible heat. Noteworthy is that at the beginning of the discharge, the LiB absorbs heat, and that at a SoC of 40% (DoD 60%) the heat generation decreases. This is coherent with the entropy change reported by Schuster [134] and seen in figure 3.2, for which $\frac{\mathrm{d}\Delta S}{\mathrm{d}t}$ is positive for a high SoC during discharge, and then changes sign later on.

However, and as also noted by Schuster in his work, the entropy change reported can vary. It is then hard then to dissociate the reversible heat to the specific cell chemistry.

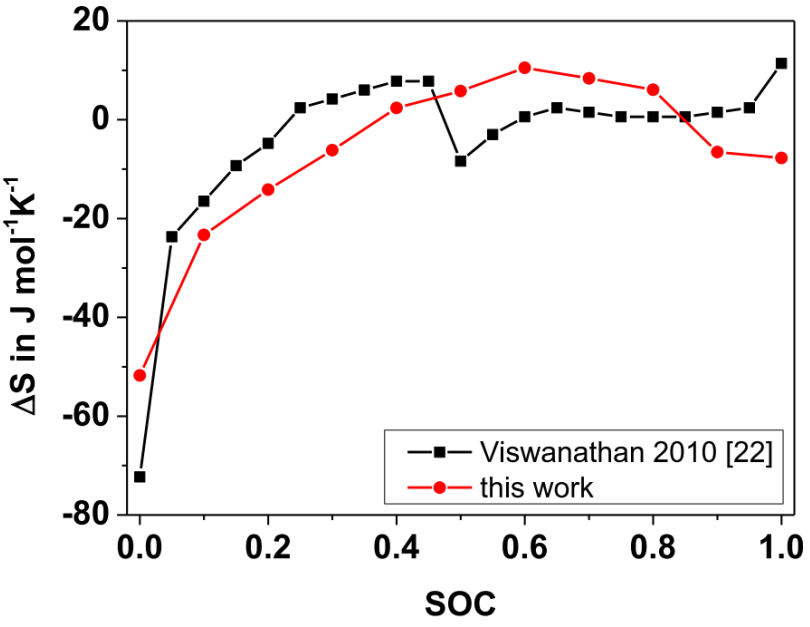

FIGURE 3.2 – Example of entropy change at different SoC levels. Source : [134]

Irreversible Heat The irreversible heat, or polarisation heat, can be thought of as the results of joule heating and energy losses at the electrodes. It includes the inefficiencies due to mass transfer, charge transfer and ohmic resistances [137]. By using Ohms law (3.12), it is possible to determine the resistance of an element given the voltage before (E_0) and after the resistive element (E).

$$I = V/R \tag{3.12}$$

$$R = I(E_0 - E) \tag{3.13}$$

This transforms equation (3.5) into (3.14) using an internal resistance R_{int}.

$$\dot{Q}_{irrev} = I(E - E_0) = I^2 R_{int} \tag{3.14}$$

As one can expect, this internal resistance is not a static value as it regroups multiple internal loss phenomena. The resistance can be seen as a function of the SoC and/or current, showing in most cases a substantial increase in resistance when the LiB decreases below 30% [87, 103]. Figure 3.3 shows an example of internal resistance given the DoD.

Heat exchanges The two most predominant exchanges the LiB has with the exterior are due to convection and radiation. As BESS are often protected from direct solar radiation, the heat gained from this source $\dot{Q}_S$ is seldom included. Otherwise, the different

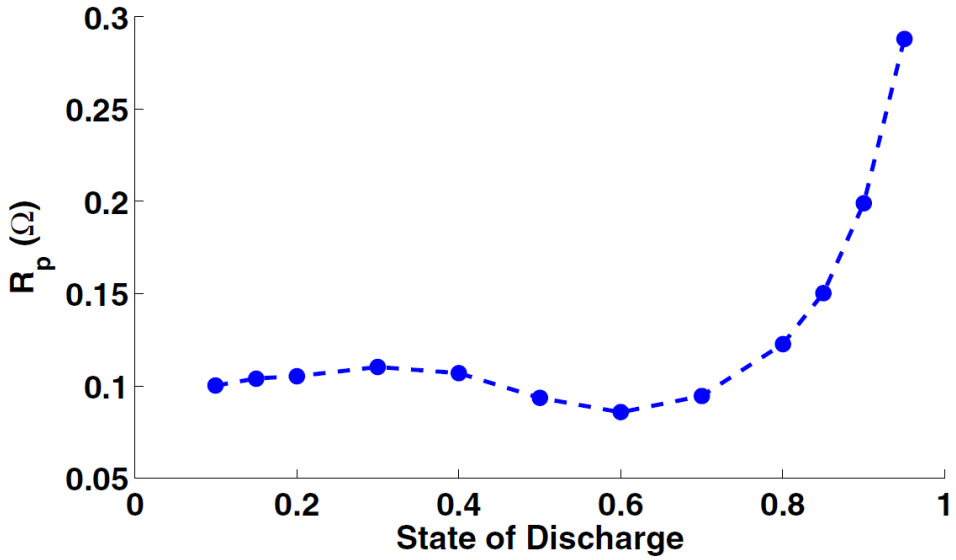

FIGURE 3.3 – Internal resistance given the Depth of Discharge. Source : [87]

heat sources would need to include this element which can be characterised by the solar irradiance W_s, an absorption coefficient α and the surface as in (3.15) [135].

$$\dot{Q}_S = \alpha \, A \, W_S \tag{3.15}$$

As for the convection, the order of magnitude for different heat transfer convection methods can be seen in table 3.1. For the heat transfer due to radiation, aLiB in standard operational conditions (<45°C) would have an energy loss of less than 60 W/m^2 when supposing à deviation of 10°to the ambient temperature.

Type	h [W/(m^{2}K)]
Free Convection (Gas)	2-25
Free Convection (Liquid)	10-1,000
Forced Convection (Gas)	25-250
Forced Convection (Liquid)	50-20,000
Boiling and Condensation	2,500-100,000

TABLE 3.1 – Heat exchange coefficients for different types of convection. Obtained from [138]

Given the relative weak heat transfer due to radiation compared to convection, the term is often ignored or taken into account by a combined heat transfer coefficient h_{comb}[138].

3.3.2 Proposed LiBESS Heat Model

Given the different insights and points mentioned before, it is possible to compose a suitable heat equation for a LiB depending on the scenario. The approach used in this work, a LiBESS for PV capacity firming framework, belongs to the case of rates that fall within a range of 0.3C- 1C as the constraints impose a charge that responds to the solar overproduction and a discharge of 2 hours at constant power.

It has been noted that when the current is below 0.2C, the entropic heat generation matches roughly 1 :1 to the irreversible heat. Under higher scenarios >0.5 the heat contribution by irreversible process passes to be at least 66% of the total heat generation[47]. Due to this small entropic heat, and by supposing that the heat exchange coefficient includes a part of the radiating term, we can express a LiB thermal model as in (3.16).

$$m\ C_p \frac{\partial T}{\partial t} = I^2 R_{int} + h^*_{comb}\Big(T_{ambient} - T_{battery}\Big) \tag{3.16}$$

This last form allows making temperature predictions by finding two parameters : the internal resistance and the heat environment exchange coefficient divided both by the specific heat and mass. The heat model through this work and subsequent chapters will be based primarily on this equation.

Alternatively, equation (3.16) can be rewritten as in (3.17) by including the mass and specific heat on the internal resistance and heat exchange coefficient. These new coefficients are represented as R^{**}_{int} and h^{**}_{comb}.

$$\frac{\partial T}{\partial t} = I^2 R^{**}_{int} + h^{**}_{comb}\Big(T_{ambient} - T_{battery}\Big) \tag{3.17}$$

3.3.2.1 Heat Model Parameter Identification

As mentioned before, the heat model for a LiB under the constraints of the PV capacity framework will follow the equation proposed in (3.17). The two values that need to be determined experimentally are the parameters depending on the specific heat and the internal resistance, and several approaches will be presented in this section.

Linear Thermal Model with DoD-dependent R_{int} To correctly reflect the thermal behaviour by using the relation expressed in (3.17), it is necessary to obtain the constants $R^{**}_{int} = R_{int}/mC_p$, $h^{**}_{comb} = h_{comb}/mC_p$. It can be then found that there are three scenarios that allow to approximate this set of values :

— The first scenario belongs to the case where there is no current flowing into or out of the battery ($I = 0$) storage (3.18).

$$\frac{\partial T}{\partial t} = h^{**}_{comb}\left(T_{ambient} - T_{battery}\right) \tag{3.18}$$

— The second case is when there is a strong current ($I > 0.5C$) so the change in temperature is mainly due to irreversible heat generation and not the convection loss, i.e. :

$$\frac{\partial T}{\partial t} = I^2 R^{**}_{int} \tag{3.19}$$

— Third case is when there is no observed change in temperature in the battery pack $\frac{\partial T}{\partial t} = 0$ even though a current is flowing as in (3.20).

$$I^2 R^{**}_{int} = h^{**}_{comb}\left(T_{ambient} - T_{battery}\right) \tag{3.20}$$

In consequence, by using (3.18), (3.19) we get the next relations for the constants :

$$\frac{h^{**}}{C^{*}_{p}} = \frac{dT/dt}{T_{ambient} - T_{battery}}, \text{ for } I \sim 0 \tag{3.21}$$

$$\frac{R_{int}}{C^{*}_{p}} = \frac{dT/dt}{I^2}, \text{ for } I >> 0 \tag{3.22}$$

In addition, as it's been noted in sections 3.3.1.1 and 3.3.1.1, the thermal behaviour changes depending on the state of charge of the battery and whether it is undergoing a discharge or charge current. Given this, it is proposed here to take into account these variations via an OC dependent internal resistance $R^{**}_{int}(SOC)$. This R^{**}_{int} is calculated for different scenarios of charge and discharge.

To find this parameter, a specific data treatment can be done by separating experimental data into two subsets : a discharging set and a charging set. Each set is then subsequently separated by their respective state of charge range (in sections of 10%). Then it is classified again by either a high or low current in order to estimate the wished parameters. This data treatment procedure is summarized in figure 3.5, and the schematic for the validation procedure can be seen in figure 3.4

Continuous-time Temperature State Space Model A second approach can be implemented to estimate the LiB temperature by using a state space model[3] described by

3. See annex A for a more detailed view of state space models.

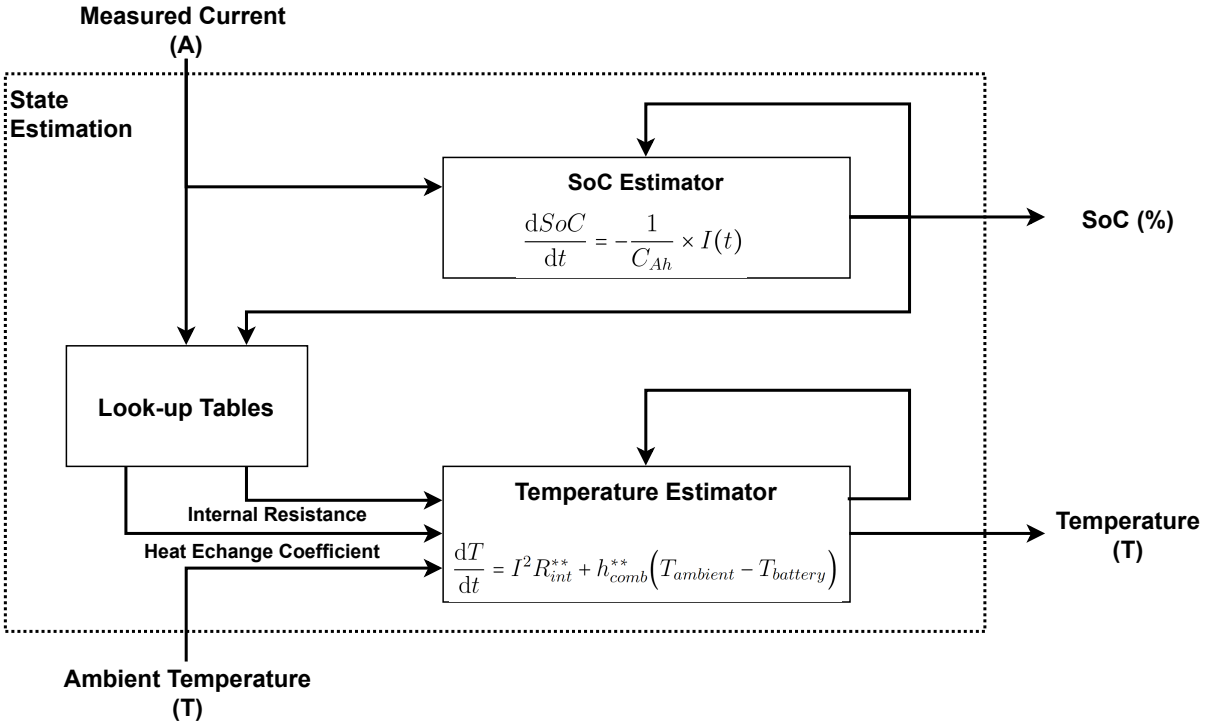

FIGURE 3.4 – Simulation Schematic for DoD-dependent model with a look-up table.

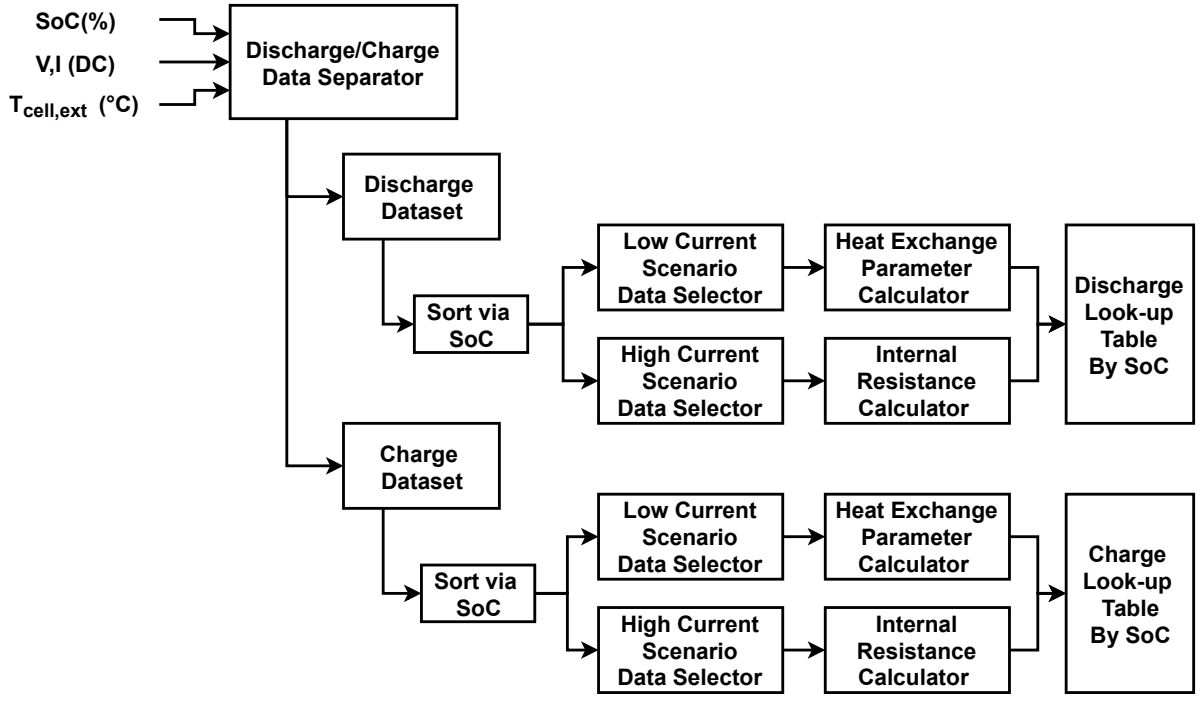

FIGURE 3.5 – Data treatment procedure used to obtain estimated value of the different model's variables.

equations (3.23), (3.24). The inputs for this state model are the square of the current going from or into the battery, as well as the ambient temperature. By focusing on a first

order state-model as seen in equation, a direct physical significance can be drawn between the parameters to estimate and the battery characteristics.

$$\frac{dx}{dt} = -\frac{h^{**}}{C_p^*}x(t) + \begin{bmatrix} \frac{R_{int}}{C_p^*} & \frac{h^{**}}{C_p^*} \end{bmatrix} \begin{bmatrix} I^2 \\ T_{ambient} \end{bmatrix} \tag{3.23}$$

$$T(t) = C\ x(t) \tag{3.24}$$

The determination of the parameters here discussed can then be obtained through the use of mathematical software such as MATLAB.

3.3.2.2 Max. Temperature Model via Neural Networks (NN)

Besides the heat equation presented, which is able to represent the instantaneous temperature, a secondary approach using Machine Learning techniques can be used to estimate and predict the temperature. In this instance, the focus is given to the maximal temperature of the LiB as this value can help to avoid operation or expected operation that can endanger the safety of the equipment.

Given the PV capacity framework which entails an almost static discharge behaviour, a Neural Network (NN) can be trained to predict the maximal temperature for this usage. The data that can be used for this are :

— Starting temperature before discharge.
— Average discharge power.
— Average ambient temperature during discharge.
— Time of discharge until.

The target for this neural network is defined as the daily maximal temperature $\max(T_B)$.

3.3.3 LiB Thermal Model Results

The thermal model and max. temperature predictor were parameterised with the real operational data collected from the experimental site discussed in chapter 2.3. The site is equipped with three individual LiBESS of 126Ah (6.5 kWh). The three follow a charge profile that is highly dependent on the weather, and a discharge profile at almost a constant power as per the specifications of the PV capacity framework in place.

The LiBESS from the sites presented in 2.4 are not taken into accounts as there are no temperature measurements available.

3.3.3.1 Observed Thermal LiB Behaviour

The thermal behaviour of the batteries, given the site operational constraints, was as expected. The ohmic heat generally increased the temperature, however under certain conditions an unexpected decrease was observed even when discharging at a quasi-constant power.

The figures in 3.6 show the battery pack temperature in 3 different ambient temperatures, each belonging to a different season of the year. Remarkable from these figures is the decline in temperature near the last peak of the day for the set (a) and (b). This phenomenon does not seem logic given that the current increases (and thus the ohmic heat (3.14) too) as the cell voltage decreases. Nevertheless, as seen in section 3.3.1.1, this behaviour could be expected under certain circumstances where the predominance of reversible heat allows the room temperature to play an important role if the discharge current is low enough [136].

Given that the LiB internal resistance reaches a minimal value when the Depth of Discharge (DoD) is in the range between 40-70%, this behaviour seems coherent with a lower ohmic heat generation. A higher cell temperature also reduces the internal resistance which can exacerbate the phenomenon [139].

With regards to the entropic heat itself, its value is highly dependent on the materials composing the anode/cathode of the cell. Extensive studies of this property have been made [53, 136, 140, 141, 142, 55, 134] and although the values vary strongly between each other, some remarkable points are to distinguish that support the temperature decrease when discharging :

— The entropic heat coefficient can be positive (exothermic) or negative(endothermic) and it depends on the DoD. It follows that in the range between 30% and 60% of SoC, this entropic heat either is weaker or has a different behaviour than in other ranges.
— Some cells present a more erratic behaviour (change in sign and slope) in entropy than others. The presence of Manganese (Mn) seems to have a strong influence as can be seen on the work of Lu [140].

The previous evidence suggests that a thermal model that considers the entropic heat, as well as the changing internal resistance should be able to simulate and predict the temperature decrease observed.

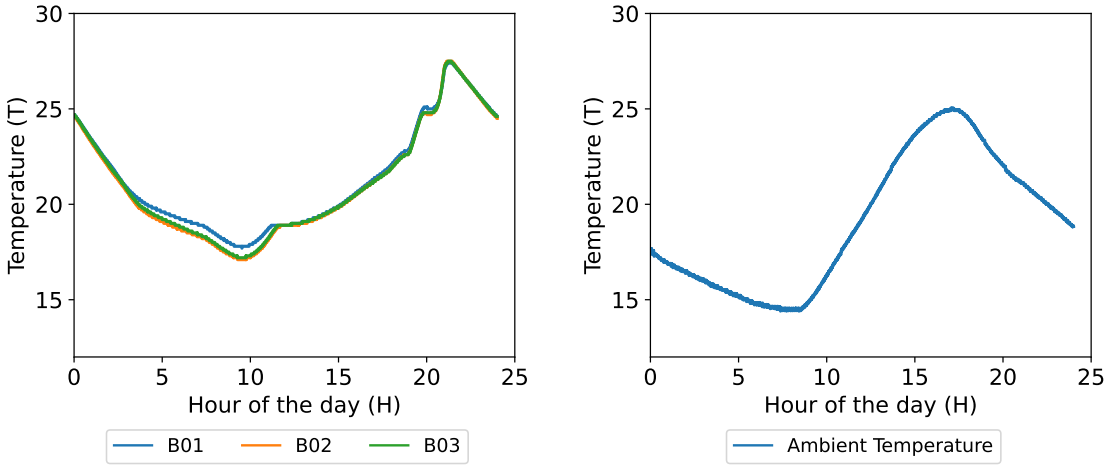

(a) Day 95

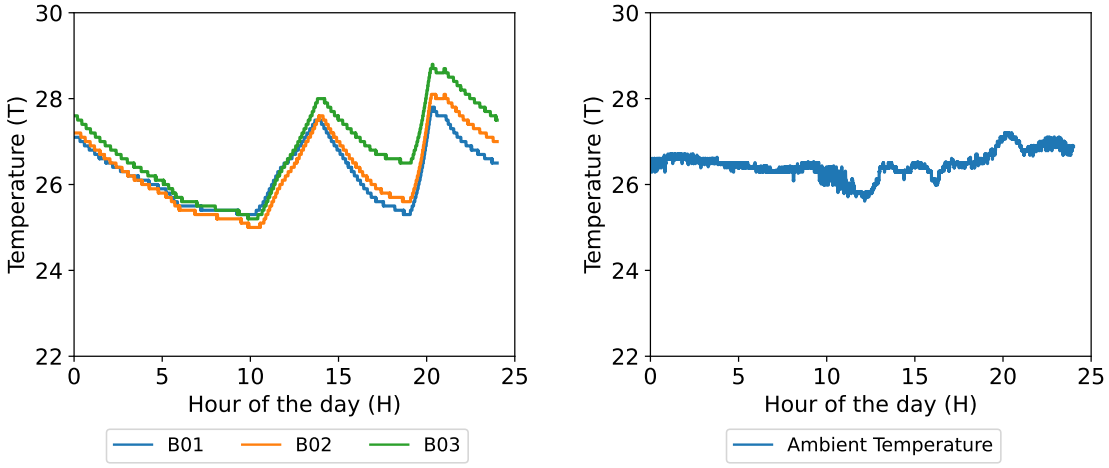

(b) Day 185

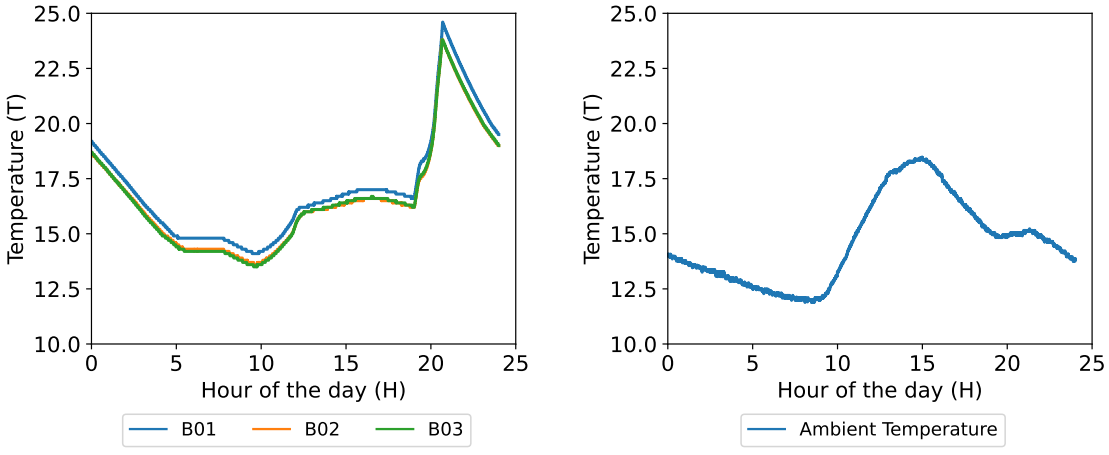

(c) Day 330

FIGURE 3.6 – Battery Packs' temperature (left) and Ambient Temperature (right) recorded for different days in a year for the PoC site.

DoD Range	Discharge		Charge	
	$\frac{h^{**}}{C_p^*}$	$\frac{R_{int}}{C_p^*}$	$\frac{h^{**}}{C_p^*}$	$\frac{R_{int}}{C_p^*}$
(00 – 10)	2.37x10−4	3.58x10−7	6.81x10−4	-4.98x10−5
(10 – 20)	1.76x10−4	-4.15x10−7	3.86x10−4	-3.61x10−5
(20 – 30)	2.51x10−4	-8.43x10−7	2.51x10−4	-6.78x10−6
(30 – 40)	5.7x10−4	-2.25x10−6	1.433x10−3	1.37x10−6
(40 – 50)	3.59x10−4	1.31x10−6	4.13x10−4	1.34x10−6
(50 – 60)	5.445x10−3	4.97x10−7	1.126x10−3	1.04x10−6
(60 – 70)	1.02x10−4	3.52x10−7	2.158x10−3	2.1e-08
(70 – 80)	4.09x10−3	2.23x10−6	2.24x10−4	4.42x10−6
(80 – 90)	4.74x10−4	3.83x10−6	3.65x10−3	7.64x10−6
(90 – 100)	3.23x10−4	-1.44x10−5	1.01x10−4	-6.29x10−5

TABLE 3.2 – DoD-dependent thermal parameters based on a 100-days sample

3.3.3.2 Linear Thermal Model with DoD-dependence

The parameters found for the three battery packs of the experimental site by using the procedure previously described can be seen in the table 3.2. These values were then applied in a simple thermal model where a look-up function for the table was used. The SoC prediction was calculated by following a simple Coulomb counter with Q being the capacity in Ah (3.25) and the temperature (3.17), rewritten as here below in (3.26).

$$\frac{dSOC}{dt} = \frac{I}{Q} \tag{3.25}$$

$$\frac{dT}{dt} = I^2 * \frac{R_{int}}{C_p^*} + \frac{h^{**}}{C_p^*} \left(T_{ambient} - T_{battery}\right) \tag{3.26}$$

This approach was implemented in Python for validation with a different 100-day set of currents and temperatures. The average daily RMSE between the SoC prediction and the real value was of 4.44%, whilst the temperature prediction had an average RMSE of 1.71°. However, as seen in figure 3.7, this model doesn't reflect properly the temperature. The rate of change in temperature isn't strong enough and the decrease in temperature due to reversible heat isn't replicated. Increasing the amount of SoC divisions could help to alleviate the lack of temperature decrease, but the amount of data needed to calculate each parameter per section increases substantially.

3.3.3.3 Continuous-time Temperature State Space Model

For this model, the different values for the variables were calculated by using MATLAB Parameter Estimation Toolbox. The parameter C was manually fixed to 1 for the

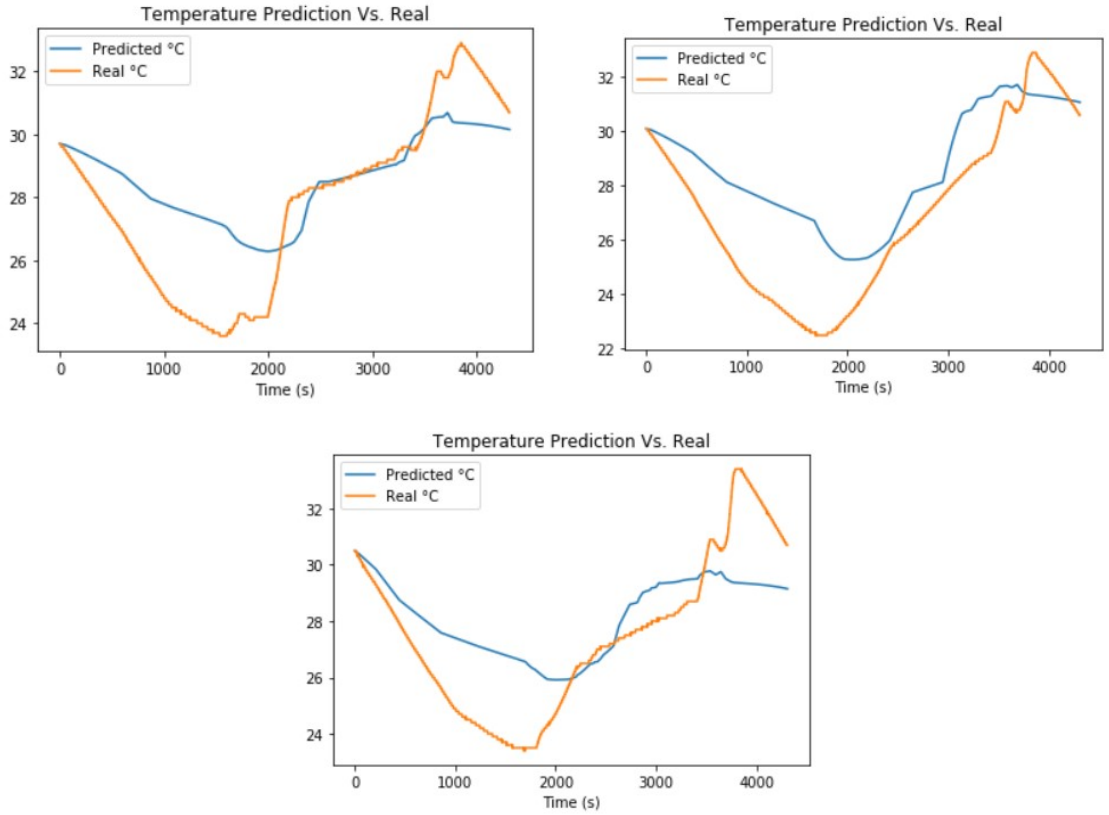

FIGURE 3.7 – Examples of the expected and real value for Temperature

models and a maximum of 2000 iterations after fixing C were allowed for it to converge. The training data for each pack was composed of 252 chronological days, with a sample time of 900, 600, 300, 60, 20, 10 and 1 second. The data for each point is the instantaneous value at t. For the validation process, a set of 101 days were used. The tables 3.3, 3.4, 3.5 summarize the different parameters found for each battery at different sampling times, and the figure 3.8 shows the procedure followed for the subsequent validation.

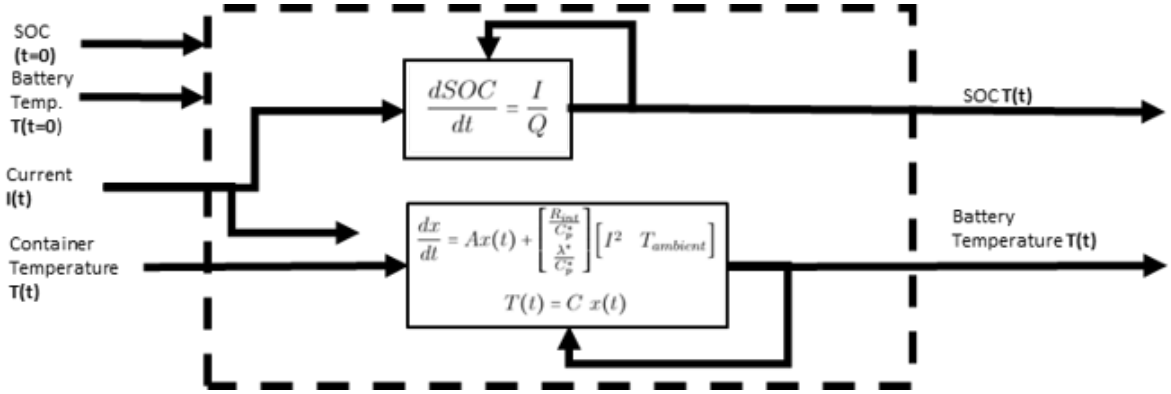

FIGURE 3.8 – Schematic of the temperature's prediction procedure.

When observing the output of the model (figure 3.9), the behaviour of the predicted

Timestep (s)	A	$\frac{R_{int}}{C_p}$	$\frac{h}{C_p}$
900	-2.42x10^{-5}	3.74x10^{-7}	2.30x10^{-5}
600	-2.46x10^{-5}	3.80x10^{-7}	2.33x10^{-5}
300	-2.45x10^{-5}	3.85x10^{-7}	2.31x10^{-5}
120	-2.42x10^{-5}	3.88x10^{-7}	2.28x10^{-5}
60	-1.73x10^{-5}	3.75x10^{-7}	1.60x10^{-5}
20	-2.42x10^{-5}	3.90x10^{-7}	2.28x10^{-5}
10	-2.42x10^{-5}	3.90x10^{-7}	2.28x10^{-5}
1	-2.42x10^{-5}	3.90x10^{-7}	2.28x10^{-5}

Table 3.3 – Parameters for battery B01

Timestep (s)	A	$\frac{R_{int}}{C_p}$	$\frac{h}{C_p}$
900	-2.63x10^{-5}	3.95x10^{-7}	2.49x10^{-5}
600	-2.65x10^{-5}	4.04x10^{-7}	2.50x10^{-5}
300	-2.62x10^{-5}	4.07x10^{-7}	2.47x10^{-5}
120	-2.61x10^{-5}	4.09x10^{-7}	2.45x10^{-5}
60	-1.94x10^{-5}	3.95x10^{-7}	1.79x10^{-5}
20	-2.60x10^{-5}	4.10x10^{-7}	2.44x10^{-5}
10	-2.60x10^{-5}	4.10x10^{-7}	2.44x10^{-5}
1	-2.60x10^{-5}	4.10x10^{-7}	2.44x10^{-5}

Table 3.4 – Parameters for battery B02

Timestep (s)	A	$\frac{R_{int}}{C_p}$	$\frac{h}{C_p}$
900	-3.20x10^{-5}	3.97x10^{-7}	3.10x10^{-5}
600	-3.22x10^{-5}	4.03x10^{-7}	3.12x10^{-5}
300	-3.19x10^{-5}	4.04x10^{-7}	3.08x10^{-5}
120	-3.16x10^{-5}	4.06x10^{-7}	3.05x10^{-5}
60	-3.16x10^{-5}	4.07x10^{-7}	3.04x10^{-5}
20	-3.15x10^{-5}	4.06x10^{-7}	3.04x10^{-5}
10	-3.15x10^{-5}	4.06x10^{-7}	3.04x10^{-5}
1	-3.16x10^{-5}	4.06x10^{-7}	3.04x10^{-5}

Table 3.5 – Parameters for battery B03

temperature follows closely the real temperature. The RMSE stays below the 2 degrees Celsius for the validation set. The predicted daily minima and maxima temperature are also close, with the most notable difference being that the real battery temperature has more pronounced slopes and peaks.

The state of charge is not shown given that there is not a difference between the results shown in section 3.3.2.1. This because the temperature is not a parameter yet in the prediction of the state of charge.

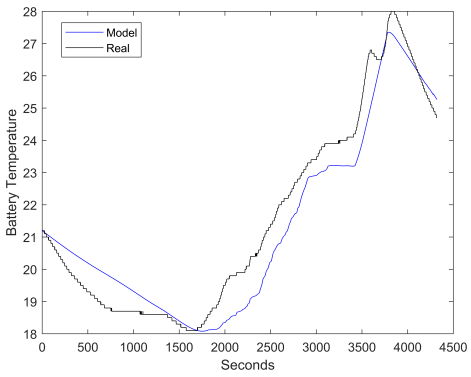

B01, Day 90

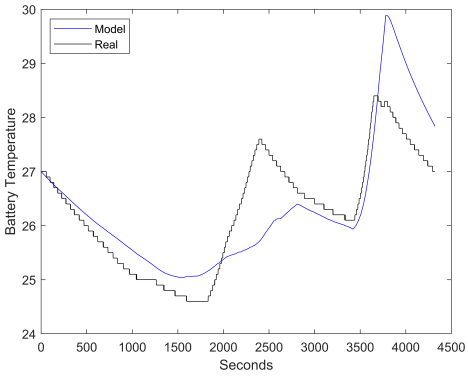

B02, Day 180

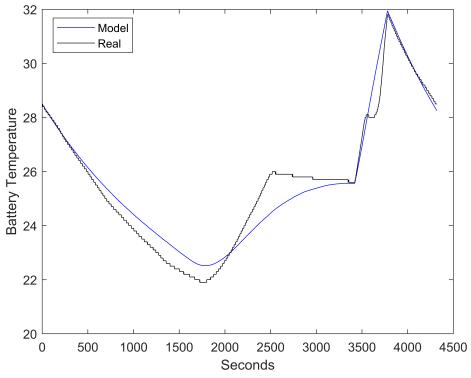

B03, Day 270

FIGURE 3.9 – Examples of the expected and real value for Temperature

Model performance with different timesteps To test the model performance, the measured data obtained in 2019 was used for validation of the model trained with 2018 data. As can be seen by the results in table 3.6, the different RMSE found did not show a visible improvement pattern by changing the training sample time. Only the 20 seconds, and 1 second timestep demonstrated a better performance. These two scenarios showed similar (and better) performances than the others for the battery B02 and B03, however for the battery B01 the results showed an inverted behaviour being these two cases the one that showed the worst performance.

	Model's Training Time-step							
	900	600	300	120	60	20	10	1
B01	0.7477	0.7372	0.7361	0.7382	0.7424	**1.4339**	0.7448	**1.1495**
B02	1.5418	1.5282	1.5767	1.6033	2.2859	**0.9919**	1.4063	**1.3051**
B03	1.2375	1.2227	1.2643	1.2933	1.303	**0.7266**	1.1269	**0.7775**

TABLE 3.6 – RMSE found for each different trained model (2018 data) when validated (2019 data).

Maxima and minima analysis In addition to the global error analysis showed before by using the RMSE, the estimated daily maxima and minima were compared between the simulation and the real measured values. The purpose of this is, given that the operation and storage temperature have a huge impact on the battery performance and life expectancy, a model that can correctly predict the highest temperature the battery pack will reach can be used to optimize the charge/discharge profile.
The table 3.7 here below shows the values for the models with the best performance. For the complete tables see appendix D.

	B01		**B02**		**B03**	
	Average	RMSE	Average	RMSE	Average	RMSE
$\mathbf{T}_{max}$	1.0471	1.4043	0.2102	1.1589	0.3744	1.111
$\mathbf{T}_{min}$	-1.7342	1.8	0.7568	0.9131	0.2365	0.502

TABLE 3.7 – Average difference between estimated Maxima and Minima for the batteries' temperatures. Results of the model trained and tested with 20 seconds between data points.

When considering the training time as part of the metric for the performance, it is obvious that the first order state space model trained with a data interval of 20 seconds offers the best compromise between training time and temperature prediction. Furthermore, the model is robust enough to perform well when used to generate estimations with smaller timesteps.

3.3.3.4 Maximal Daily Temperature Prediction via NN

The trained neural networks were tested with the data of 2019 for each battery. The RMSE for the three trained neural networks are reported in table 3.8 and figures 3.10 showcase the predicted values against the real measured ones.

As it can be concluded by these results, the average error was less than 1°C and no significant improvement was shown by increasing the number of layers. The case with 10 layers had worse results but it is due to aberrant points which are easily identifiable as they deviate very strongly from the ambient temperature. By filtering these points, the 10 layers NN show comparable results to the others (table 3.9).

3.3.4 Model Conclusion and Discussion

DoD-dependent constants The parameters found usually stayed one order of magnitude higher than the ones obtained by the state-space model. This difference could be explained

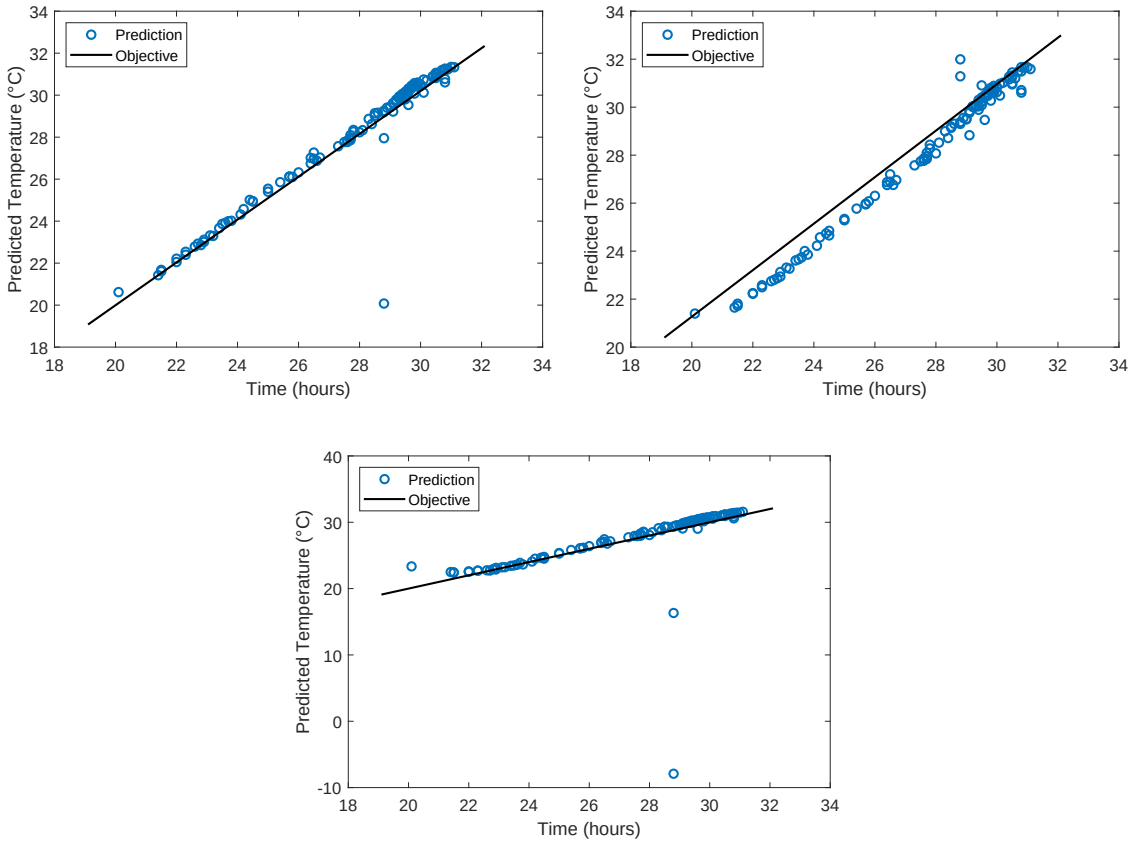

B03, Day 270

FIGURE 3.10 – Predicted max. temperature with 3 (top left),5 (top right), and 10 (bottom) hidden layers.

	B01	B02	B03
3 Hidden Layers	0.925689	0.94784	0.951052
5 Hidden Layers	0.701285	1.113553	0.764068
10 Hidden Layers	3.657472	0.596238	1.760227

TABLE 3.8 – RMSE when validation is done using data of 2019.

Output Treatment	B01	B02	B03
Unfiltered	4.045615	0.57	0.936216
Filtered	0.672978	0.57	0.936216

TABLE 3.9 – RMSE for a **10 hidden layer** neural network with and without filter applied to its output.

by the lack of the previous state contribution A seen in (3.23).

A noisier prediction can then be expected from this approach Noteworthy is the change of sign in the R_int constant. The negative value found in higher depths of discharge can be correlated to the changes in entropy in the cell, which is coherent with the predominance

of this heat source over the ohmic losses.

State-Space Thermal Model The first order state-space model showed that, although with plenty room of improvement, it can be an easy approach to have a thermal prediction of a battery pack. Even if this model is not able to reproduce the decrease in temperature correlated to the reversible heat and the environment temperature, the results show a predicted temperature that follows closely the real one. Just as important as this, the highest and lowest temperatures were predicted with a margin of error of ± 1 °Celsius for most cases.

Another remarkable result is the non-existent improvement by using data with a time-step of 1 second. For batteries #2 and #3, the best results were shown with 20 seconds between the data, while for the battery #1 the best results were systematically better if the time-step was superior to 20 seconds. This strongly suggests that for high-capacity Li-ion storage, data collection with a period higher than 20 seconds is a probably a waste of resources in memory and processing power. Reliable real time applications can be built with less resolution in training data.

Neural Network Maximal Temperature Predictor The results obtained by this method showed a similar performance to the state-space model in terms of RMSE. It provides a relatively fast way to predict the maximal temperature by using only four parameters. Furthermore, of these four parameters, two are directly controlled by the scheduled usage of the battery and thus provides an opportunity for a two-variable optimization given a predefined cost function.

The number of hidden layers didn't showcase a substantial improvement in prediction, but it made the bad predictions easily identifiable by taking them out of the domain of the realistic. As a consequence, a high number in layers could provide an aberrant point identification method. This however would be specific to each trained neural network, so its reliability isn't guaranteed.

3.4 State-of-Charge Modelling of Li-ion Batteries

As mentioned before, the notion of SoC is fundamental for any storage system regardless of the element being accumulated. The IEEE defines the SoC as the actual capacity of a battery expressed as a percentage of a fully-charged capacity [143]. Similarly, the International Renewable Energy Agency (IRENA) defines this parameter as the ratio of stored energy in a storage system (kWh) to its usable capacity (kWh) [4]. Noteworthy from these definitions are the terms of usable capacity or fully-charged capacity. Both of these are directly related to the SoH of the battery, which itself is a parameter to be estimated and/or observed and will be further discussed in section 3.5.

In SoC estimation, the aim is to obtain a reliable value for the currently stored energy parameter E_t as in (3.27), while mostly considering the maximal stored energy $E_{\max,t}$ as a constant for the cycle.

$$\text{SoC} = \frac{E_t}{E_{\max,t}} \tag{3.27}$$

The evaluation of the SoC or stored energy is critical for all applications using a LiBESS. For Hybrid Electric Vehicles (HEV) and Electric Vehicle (EV), the integrated BMS needs the parameter so it can display the remaining kilometres prediction for the user. This avoids abusive behaviour on the battery (over-charge and over-discharge) and helps the driver to efficiently plan his trips. Generally speaking, a correct SoC estimation improves the reliability, safety, and efficiency of the LiBESS whether in an EV context or in Renewable Energy Sources (RES), and is deemed essential for any BMS [90, 144, 145, 116].

3.4.1 SoC Behaviour and Modelling

The complexity of SoC estimation comes directly from the fact that it cannot be directly observed given the evolving non-linear physical and chemical characteristics in the LiB cells, as well as environmental conditions [90]. Furthermore, the complications increase when one starts to consider the inconsistencies and variability that can be present between cells in battery packs. Naguib et al. identified cell material impurities, tolerances in the manufacturing process, welding processes, and cell grouping methods as sources for battery pack inconsistency. Equally, once the battery packs are formed, the operation of the ensemble increases the discrepancy between individual cells as the current distribution is not uniform. This results in uneven operational temperatures and Depth of Discharge (DoD) between cells impacting not only the difficulty of SoC estimation but also the general performance and aging of battery packs [146].

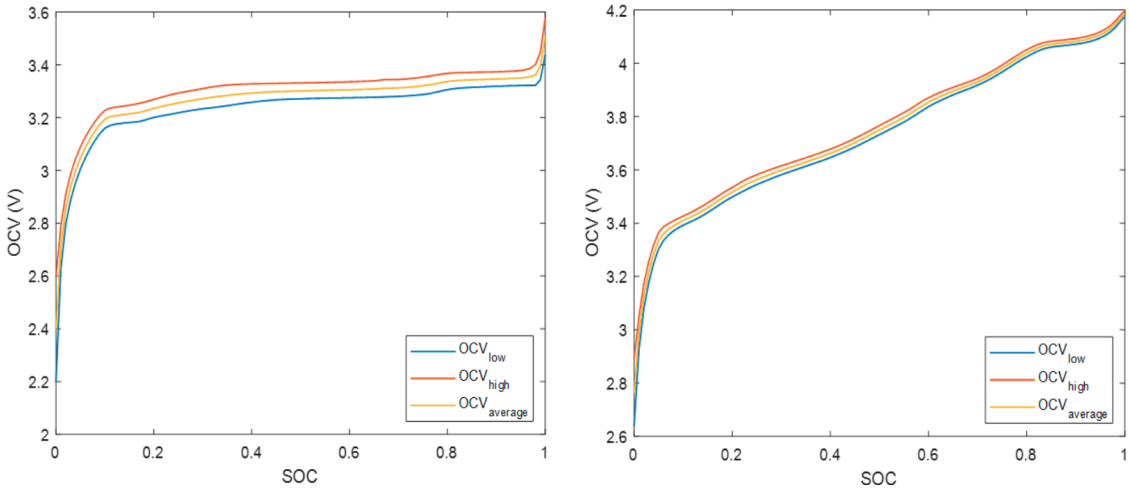

FIGURE 3.11 – OCV voltage profile for a LFP cell (a) and an NMC cell (b) when discharging (OCV_{low}, charging (OCV_{high}, and the average value of both ($OCV_{average}$). Source : [147].

When focusing on a single cell, the SoC estimation process must consider the behaviour the cell experiences under different circumstances. The OCV and the terminal voltage, two of the most common parameters used for SoC estimation, are influenced by factors such as the chemistry used, operating temperature, and age. The cell chemistry dictates the overall voltage profile the cell will experience and makes some kinds of cells harder to estimate than others. For example, and as seen in figure 3.11, Lithium Iron Phosphate (LFP) batteries exhibit a very constant OCV in a wide range of SoC while Nickel Manganese Cobalt (NMC) show a more progressive change given the state of charge. This makes the former more difficult to determine its current SoC using only the measured voltage.

In addition, it can also be observed in the same figure 3.11 that the tension observed at the terminals is dependent on the current use given to the cell. A charge regime generates a higher voltage at the terminal compared to the cell while discharging. If a battery follows a strict charge-discharge cycle such as in mobile phones, this is not much of an issue. However, for EVs and/or systems that alternate between charge/discharge frequently, the change in SoC can trouble the SoC estimation.

The ambient temperature (and temperature of the cell) also has an impact on the observed voltage at the terminals. Feng et al. [87] while simulating the battery dependence on temperature, reported a decrease in voltage at the terminals with the decrease in ambient temperature for an NCA battery as seen in figure 3.12 (a). Related to this are the findings by Shen et al. in which the estimated internal ohmic resistance for their LiBESS EC model increased with low temperatures regardless of the current SoC for an NMC

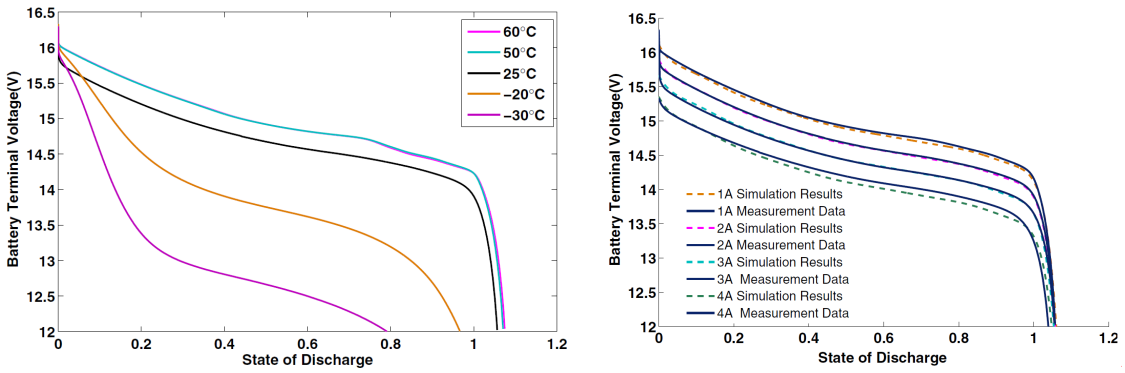

(a) (b)

FIGURE 3.12 – Voltage measured at the terminals of an NCA battery. (a) Shows the voltage given different ambient temperatures and a constant current discharge of 2A. (b) Exhibits the measured voltage (continuous line) for different discharge currents. Source : [87].

LiB. This behaviour repeated even for complementary resistances in their model [148]. Incidentally, temperature also has an impact on the total capacity of the storage impacting any state estimation of SoC [149].

Finally, a third important factor that influences the SoC behaviour is the current at which it is used. For the case of an NCA battery, the cell voltage at the terminals decreases almost linearly as the current is increased [87], here seen in figure 3.12 (b).

These three phenomena need to be considered for accurate and reliable SoC estimation of LiBESS in operation. The interrelationships between them are something that can also negatively impact the state estimation. As an example, high discharge currents can increase the operating temperature of a LiB. This in turn can raise the voltage seen at the terminals and imply a DoD [4] weaker than the reality.

3.4.1.1 SoC Estimation Methods

Given the mentioned complexity and lack of direct way to measure the SoC, multiple approaches to estimate it have been developed through the years. As mentioned in chapter 1, the classification adopted in this works divides the methods into 4 families : Look-up tables, ampere-hour integrals, model based, and data driven estimation methods [56].

Other classification different to this one have also been reported, but they share strong similarities with the one here adopted. Qays et al. in its review of SoC estimation methods divided them in direct measurement based, adaptive estimations, filter-based estimations, and model based [150]. This estimation includes the coulomb-counting methods in the

4. As a reminder, DoD = 1 – SoC

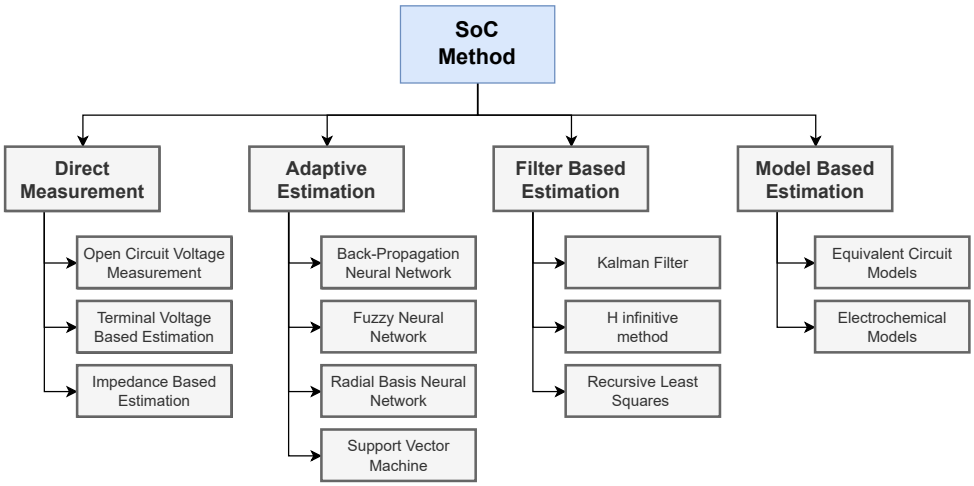

FIGURE 3.13 – SoC estimation methods by category. Adapted from : [150].

direct measurements group and separates data-driven methods into adaptive and filter-base methods. Kassim et al. in addition to the four in figure 3.13 isolated the adaptive filter methods in a separate category [145]. Wang et al. in their review of state estimation approaches created a family for filter-based and observer based methods in addition to data driven [144], and in the review by Girijaprasanna and Dhanamjayulu the methods analysed were classification into the conventional methods, adaptive filters, learning algorithms, non-linear observers, deep-learning algorithms and hybrid methods [90].

All the classified methods in the different reviews can however be re-classified into the four families retained. Table 3.10 shows a summary of the methods within each family after the reclassification. A small description of the method is also provided. Although methods are classified in a single family, it is common to have overlaps and the classification is done given the main principle that differentiates it from other methods.

Table 3.10: SoC estimation methods reported in the literature by family. Adapted from : [56, 150, 145, 144, 90]

Family	Method Description	Description
Look-up Tables	Open Circuit Voltage Method (OCVM)	Determines the SoC by looking at or estimating the open circuit voltage at the terminals.
	Terminal Voltage Estimation	Determines the SoC by using the observed voltage at the terminals in operation.

Continued on next page

Table 3.10: SoC estimation methods reported in the literature by family. Adapted from : [56, 150, 145, 144, 90] (Continued)

Family	Method Description	Description
	Electrical Impedance Analysis (EIA)	The current impedance of the LiB is used to determine the SoC. Often requires specialized equipment.
	Resistance-Based Estimation	Similar to EIA, but the resistance is measured or estimated instead. Depending on the equivalent circuit model used, one or more resistance values can be used.
Ampere-hour Integrals	Coulomb Counting	The total charge in and out from the LiB is integrated to determine the SoC. Its main drawback is an accumulative error if not calibrated frequently enough. Otherwise, it is easy to implement.
Model-Based	Electrochemical models (EChM)	Simulates the physical and chemical reactions inside the LiB cell to determine its state. The most common are the Doyle-Fuller-Newman (DFN) method and the single particle model (SP) in 1 and 2-dimensions.
	Equivalent Circuit Model (ECM)	The LiB is represented by classical circuit elements (e.g. resistors, capacitors). Afterward, the internal state or voltages are estimated to determine the associated SoC.
	Support Vector Machines (SVM)	Supervised learning methods that can approximate the SoC given a multivariate function of the available data.
	Recursive Least Squares (RLS)	As its name suggests, the model parameters are chosen by recursively minimizing the squared error between the estimated and the real output. Once the model is parameterized, it can be used to estimate the OCV or SoC.

Continued on next page

Table 3.10: SoC estimation methods reported in the literature by family. Adapted from : [56, 150, 145, 144, 90] (Continued)

Family	Method Description	Description
	Observer Methods (Luenberg, Sliding, Nonlinear)	These methods define a system for which the available measurements or observations are used to estimate its state. They use two phases : system state estimation and then a feedback loop that corrects the model real measurements.
	Kalman Filters (KF)	These are one specific kind of observers (estimation followed by correction via the real output) for which the parameterisation process includes Gaussian behavior on the errors and disturbances. Many implementations of this filter exist (linear, extended, unscented to mention a few). SoC is commonly obtained after estimating the OCV through the KF.
	Particle Filter (PF)	Just as KF, they are a subset of observer methods, but they have a more probabilistic approach. In PF, discrete sampling (particle) points in the state space are sampled given the initial data distribution and are later adjusted and resampled given the newer measurements and distinguish the useful particles. They are particularly adapted for non-linear and non-gaussian systems.
	Neural Networks (NN)	These methods predict the wished output (OVC, SoC) by determining the weights of several activation functions (neurons) applied to the inputs and reducing the errors as much as possible. The specific implementation of the input-output mapping and the operations in between generates a subset of methods such as back-propagation NN or fuzzy NN.

Continued on next page

Table 3.10: SoC estimation methods reported in the literature by family. Adapted from : [56, 150, 145, 144, 90] (Continued)

Family	Method Description	Description
	Deep Learning	These methods transform the inputs into secondary features through NN, which will be further treated by other NN or used at last to generate the input-output mapping. The name comes from the number of layers that these techniques require, and one of the most known is convolutional neural networks.

A focus of selected SoC estimation methods from table 3.10 is presented below. The highlighted methods were chosen due to their prominence and appearance as the building blocks in more advanced methods as the building blocks. .

Open-Circuit Voltage Method This technique works by establishing a relationship between the SoC and the current state of charge of the battery. This is done by measuring the OCV at many different conditions and SoC to generate a reference look-up table to match any subsequent measurements.

$$SoC_t = f\left(V_{\mathrm{OC}}\right) \tag{3.28}$$

Although simple and fast, a pure OCV-SOC method has a series of disadvantages. For accurate OCV measurements, the LiB needs a long time of inactivity which is not practical for real-time applications. Also, the OCV hysteresis and temperature need also to be accounted for as they impact the measurement. At last, given that the LiBs evolve through their life, the aging of the cell adds deviations from the look-up tables [144, 154].

Impedance-based methods are very similar to the OCV-SoC methods. Because of this, they share the same disadvantages with the additional constraint of the impedance test requiring specialized equipment. They however offer lore insight in the actual state of the battery.

Coulomb Counting As its name suggests, this method consists in using the amount of current that flows from or to the batteries to provide a State of Charge estimation. As consequence, the accuracy of this method is highly reliant not only in the current

measurement quality but also knowledge of the initial state.

$$SOC(t) = SOC_{t=0} + \frac{\int_{t=0}^{t} \eta_I I(t)dt}{C} \tag{3.29}$$

where C is the nominal capacity of the battery system.

The main disadvantage of the method is that small deviations in the current measurements due to noise can impose important accumulative errors. Constant calibration can avoid this problem, but changes in efficiency, temperature, and capacity can also impact the accuracy. Nevertheless, the principle followed by this method is the foundation for other kind of SOC estimation algorithms [90, 144]

Electrical Equivalent Circuits (ECMs) The method aims to reproduce the LiB behaviour by using components of electrical circuits (resistor, inductors, capacitors, voltage sources) and estimate the SoC usually via the estimated OCV. The exact configuration of the electric components will depend on the desired complexity and behaviour to mimic. In 2012, Hu et al. did a review of 12 different ECM for LiB that go from a simple model (fig. 3.14) with one resistance per current direction, up to a third order RC model with a one-state hysteresis.In the comparative study, the best results were given by the first order RC model (fig.3.15). Higher-order RC models showed similar results but were not significantly better [88].

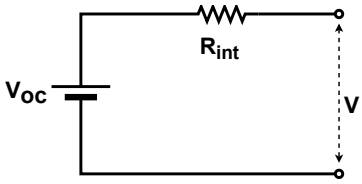

FIGURE 3.14 – Simple EC Model.

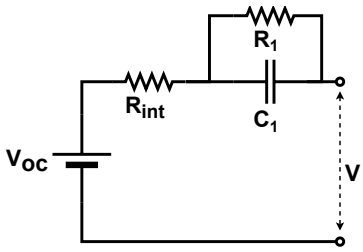

FIGURE 3.15 – First Order EC Model.

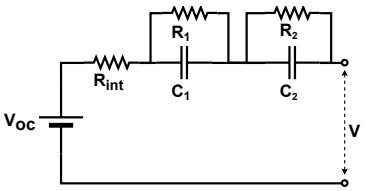

FIGURE 3.16 – Second Order EC model.

Part of the limitations of ECM have been their inability to reproduce and follow the LiB cell behaviour as it ages. The joint use of ECM and filters, specially of Kalman Filter (KF), has been reported to counteract this drawback while allowing accurate real-time estimations [155, 156, 89] with an SoC error of less than 2% [157].

State and Filter-based methods A state model describes the output of a system given the current and precedent inputs it had. It generates an internal state x based on inputs u and errors e, which is then used to determine a measurable output y. This system is

schematized as in figure 3.17 and described by equations (3.30), (3.31), where A,B,C, and D are free parameters to effectively determine the contributions of the inputs, current estimated state, and disturbances have on the estimated output [153]. However, because LiB are non-linear dynamical systems, different linear constructions of state models can be used.

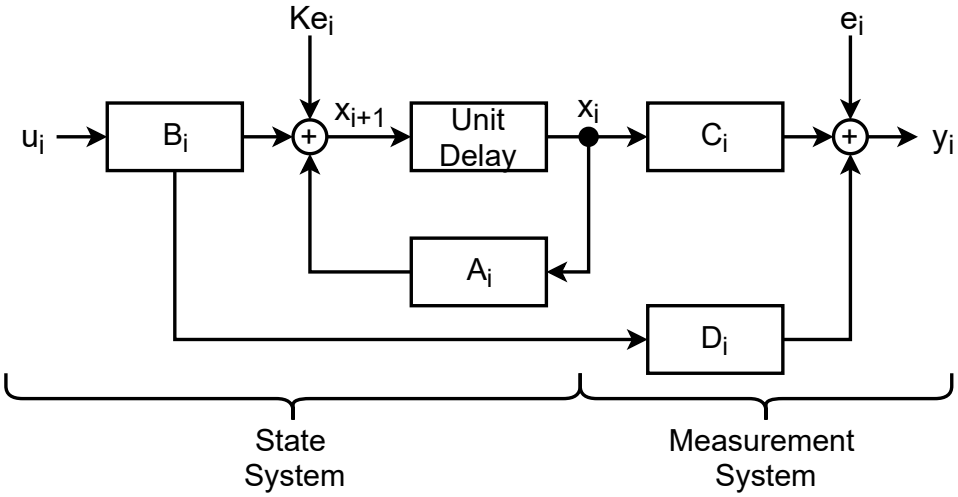

FIGURE 3.17 – State space schema of a linear discrete time system. Adapted from : [158].

$$\frac{dx}{dt} = A\ x(t) + B\ u(t) + K\ e(t) \tag{3.30}$$

$$y(t) = C\ x(t) + Du(t) + e(t) \tag{3.31}$$

Barillas et al. used a first order EC model (fig. 3.15) with an OCV approach in order to get a linear estimator. This model requires to determine the LiB parameters R_{int}, R_1 and C_1 from characterization tests. It uses then these values to determine the outputs of interest : the SoC, and the capacitor voltage V_i, and the voltage V_i at the terminals. This discrete linear state space representation space is defined as follows :

$$x_{i+1} = f(x_i, u_i, Ke_i) \tag{3.32}$$

$$y_i = g(x_i, u_i, e_i) = V_{OC,i} = OCV(SOC_i) + R_0 I_i + V_{1,i} \tag{3.33}$$

Where the state x is defined as in (3.34) and the SoC is calculated using a coulomb integrator as in (3.35). A look-up table that based on the SoC is used to determine the OCV.

$$x_k = \begin{pmatrix} x_{1,i} \\ x_{2,i} \end{pmatrix} = \begin{pmatrix} SOC_i \\ U_{1,i} \end{pmatrix} \tag{3.34}$$

$$SOC_{i+1} = SOC_i + \frac{\Delta t}{C} I_i \tag{3.35}$$

Filter methods, in addition to using the system model, also employ statistical insights from all previous states and measurements to estimate the current state of a system. KF-based methods [5] are the most common examples, and they focus in real-time state estimation given past and current data without the control or implicit "prediction" nature of observers. KF has shown good results for LiBESS SoC state estimation under a wide use-case scenarios results and models. For application on EVs, Extended Kalman Filters (EKF) [6] approaches have reported errors of $< 1\%$ in average [90, 159], with the error being highest for $LiFePO_4$ with up to 2.5% [160]. Unscented Kalman Filters (UKF), filters adapted for non-linear systems, have been reported for SoC estimation under varying temperature with errors of less than 5% [154]. However, it is important to note the importance of the SoC estimation model used. Naguib et al. showed that, while using EKF or UKF, the error of four estimation methods varies in a significant way. The method used for EKF or UKF can reduce (or increase) the RMSE and maximal error by about 2% [146].

Artificial Neural Networks (ANN) & Data-driven methods Characterised by the absence of a physical model, these methods rely entirely on the available data and the quality of the information fed to them to "learn" and estimate or predict the wished output. The main virtue they present is the ability to adapt to the complex and non-linear behaviour that Li-ion cell chemistry exhibits, with the main drawback of requiring extensive datasets. Processing these datasets is computationally expensive, but once this phase is done the resulting model is fast and easy to deploy [90, 150, 161].

NNs are composed of inputs to which a series of hidden layers are applied to get an output, and can be defines as in (3.36). In this equation the output y of a node located in the layer j is the result of an activation function $\mathcal{F}$, commonly the hyperbolic tangent sigmoid function in (3.37), that acts on the result of a node x_i from the previous layer to which a weight $W_{i,j}$ was applied.

$$y_j = \mathcal{F}\left(\sum_i W_{i,j} x_i + b_j\right) \tag{3.36}$$

$$\mathcal{F}_{tansig}(u) = \frac{2}{1 + e^{-2u}} - 1 \tag{3.37}$$

5. Chapter 4 of [153] provides an extensive view on the theory of Kalman Filters.
6. A linearization of the Kalman Filter applied to non-linear stochastic systems

The errors found by using NN depends on the specific form the system takes. Standard NN have reported an average error of < 3%, recursive back propagating neural networks (RBPNN) under EV constraints exhibited a MAE of < 5% while a wavelet neural network (WNN) showed a MAE of 0.59% with a maximum error of 3.13%. Deep learning methods, versions of NN that uses several hideen layers, has consistently show less errors for SoC prediction. Deep neural networks, long short term memory network (LSTM), recurrent NN with gated recurrent unit (GRU) and deep belief network (DBN), all showed a MA of less than 1% [85]. Table 3.11 summarizes these errors found per architecture.

Architecture	MAE
NN	$\leq 3\%$
RBPNN	$\leq 5\%$
WNN	$\leq 0.6\%$
WNN	$\leq 0.6\%$
DNN	$\leq 0.61\%$
LSTM	$\leq 0.57\%$
GRU	$\leq 0.84\%$
DNN	$\leq 0.57\%$

Table 3.11 – Summary of SoC estimation MAEs given the NN architecture used. Adapted from : [85]

In addition to NN, other data-driven methods for SoC estimation are support vector machines (SVM) which operate by classification and regression of nonlinear problems thanks to a linearisation on higher dimensional spaces [162] , fuzzy logic (FL) algorithms which are rule-based input-output systems in which both the input and output are categorized into broad or fuzzy groups [163], and genetic algorithms (GA) in which optimal parameters of complementary models are found by stochastic search algorithms [85]. All these three methods result in high accuracy with an average errors of 4.3%, but their main disadvantage remains the need of high memory and computational power [90].

3.4.2 Proposed LiBESS SoC Model

From all the different methods seen before, we can distinguish the coulomb counter approach as the more versatile and adapted method to estimate the SoC for industrial LiBESS. As seen in chapter 2, the use-case of interest in this work confronts data and measurements constraints which render other SoC estimation methods less interesting. Given that LiBESS under industrial constraints do not always offer DC measurements of any kind, equation (3.29) needs to be adapted to the AC power measurement as it

is always available. This is especially true for power production applications in which it necessary to control and supervise the net energy from the system.

The resulting power integrator in differential form useful to determine the SoC can be seen in (3.38). In here, the capacity in ampere hours Ah becomes the capacity in watt-hours E_0, and the current efficiency parameters η_I is expressed in terms of power η_P. .

$$\frac{\mathrm{d}SoC}{\mathrm{d}t} = \frac{\eta_P \ P}{E_0(t)} \tag{3.38}$$

In this approach, it is possible to consider self-discharge losses with a thermal dependence as in (3.39), where ν_T is a self-discharge thermal coefficient and the EC for this model can be seen in figure 3.18. This thermal dependence requires only the operating temperature of the BESS, which can be estimated using the model presented in section 3.3.2.

$$\frac{\mathrm{d}SoC}{\mathrm{d}t} = \frac{\eta_P \ P}{E_0(t)} + \nu_T \ T^B \tag{3.39}$$

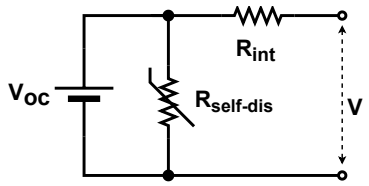

FIGURE 3.18 – Simple EC Model with a temperature-dependent self-discharge.

To accommodate the difference in behaviour under a charge or discharge regime, phenomena discussed before in section 3.4.1, the power efficiency coefficient can be separated into a charge/discharge coefficient ($\eta_{P,-}$,$\eta_{P,+}$). Although the presence of diodes in the EC make the circuit non-linear by definition [7], the resulting model is essentially the superposition of two mutually exclusive simple linear systems. Estimating the SoC via this requires then to identify the three efficiency parameters and the current maximal capacity the storage can hold $E_0(t)$. This can be done using the AC and BESS measurements available from the sites of interest.

$$\frac{\mathrm{d}SoC}{\mathrm{d}t} = \frac{\eta_{P,+} \ P_+ + \eta_{P,-} \ P_-}{E_0(t)} + \eta_T \ T^B \tag{3.40}$$

An additional advantage from this model is the capability to extend its application to other scenarios. In long-term forecasts, where measurement and re-calibration steps used in filter-based methods are unavailable, the model here proposed can play the required

7. Diodes are non-linear elements.

role to generate the previsions. To accurately represent the LiBESS operation through the life of a project, the issue becomes estimating the efficiency and capacity changes over time. The evolution of the parameters will be further discussed and presented in section 3.5. The results presented below for the SoC estimation presume static parameters for the short-term window of interest.

3.4.3 LiB SoC Model Results

In contrast to the thermal model, all seven sites studied in this work can be used to find the SoC model parameters. To identify the parameters of the model, the AC power output from the LiBESS was separated depending on the direction of the power flow. The reported value for the the SoC as reported by the BMS was used as the output for the power counter. The parameters were found using MATLAB parameter identification toolbox given the mentioned power inputs and the SoC as output. The values for the parameters given a the power integrator in (3.38) can be seen in table 3.12.

LiBESS	$\eta_{P,+}$	$\eta_{P,-}$	Roundtrip Efficiency	Δ in Efficiency
B01	87.69 %	95.75 %	83.96 %	-11.04 %
B02	84.4 %	95.92 %	80.95 %	-14.05 %
B03	86.02 %	95.99 %	82.58 %	-12.42 %
B04	100.61 %	89.57 %	90.12 %	-1.88 %
B05	98.81 %	89.6 %	88.53 %	-3.47 %
B06	98.04 %	90.32 %	88.55 %	-3.45 %
B07	98.9 %	88.83 %	87.85 %	-4.15 %

TABLE 3.12 – Efficiency parameters for the SoC model, round-trip efficiency, and change of efficiency compared to the published manufacturer round-trip efficiency.

For the LiBESS from the experimental sites, given the presence of the required data, the parameter identification was repeated with an additional input of the reported internal temperature measurement in order to obtain the parameters of the temperature dependent SoC equation in (3.40). Table 3.13 summarizes this findings.

LiBESS	$\eta_{P,+}$	$\eta_{P,-}$	ν_T
LiBESS #1	97.46%	97.46%	-7.16x10^{-4}
LiBESS #2	88.8%	92.37%	-4.00x10^{-4}
LiBESS #3	88.05%	92.06%	-2.46x10^{-4}

TABLE 3.13 – Parameters for the SoC model with thermal dependence.

The error of using these parameters for SoC estimation with and without thermal consideration was evaluated next. Following sections summarize these findings. The two horizons studied were a 1-day estimation and a 7-day continuous estimation. The former

aims to represent the behaviour when a daily calibration is done, while the latter aims to show the deviation of the model for longer forecasts.

3.4.3.1 SoC-only estimation

When considering only the parameters reported in table 3.12, a significant improvement was observed when compared to the performance reported by the LiBESS manufacturer. When doing 7-continuous days SoC estimations without considering the thermal dependence, the average error for all sites was reduced from 10.1% to 4.6%. If distinction is given to the manufacturer and model of the LiBESS, two different changers are observed. Systems B01-B03, which belong all to the PoC site, showed the most improvement by using the improved SoC model and reducing the error from 15% to 3%. In contrast, the improvement in systems B04-B07 was more subtle going from 6.5% to 5.7%.

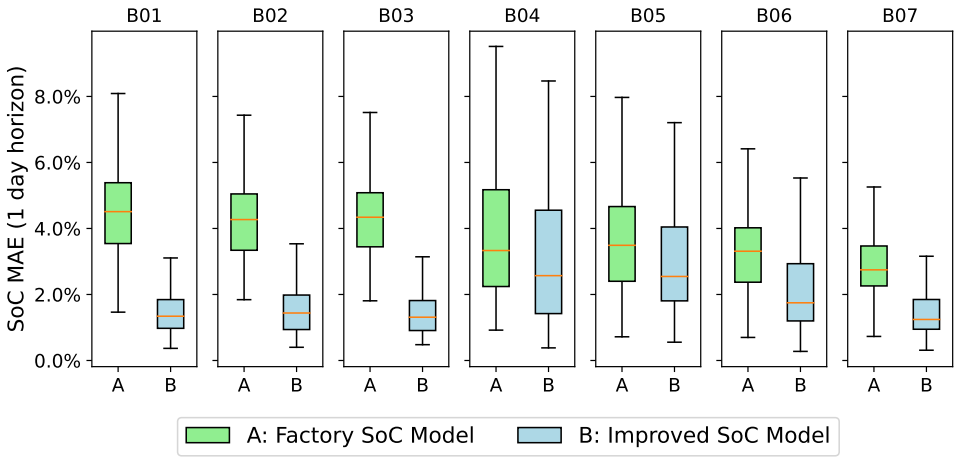

FIGURE 3.19 – SoC estimation MAE distribution for periods of 1 day. The improved SoC model does not consider the temperature of the LiBESS.

This difference in behaviour, although in a lesser manner, is also visible for daily SoC estimation for the two different brands of LiBESS studied. As it can be seen in figure 3.19, B01-B03 still show the better improvement with an error reduction in average of 2.5% compared to 0.5% for the others. The average error for all was then contained to less than 3% when using the improved SoC model.

3.4.3.2 SoC-Temperature co-estimation

As a thermal model to estimate the internal temperature is available, we can simultaneously estimate its value with the current SoC. The process, seen in figure 3.20, relies on using the SoC in the previous step to determine the internal resistance for heat generation.

At the same time, the SoC for the instant i used the temperature on the previous step for calculation.

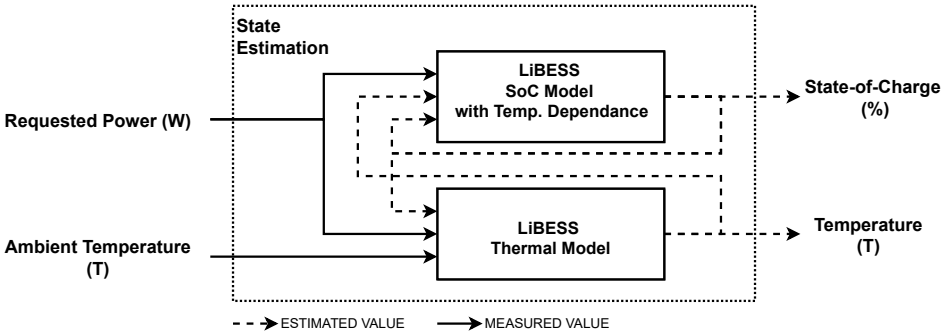

FIGURE 3.20 – SoC and temperature co-estimation procedure. Both the output of the thermal and SoC model are used at the step i+1.

By following this approach, the MAE error in SoC estimation increased slightly when using an estimated temperature instead of the recorded one. Seen in figure 3.21, the error increased slightly. Being in average this increase of 0.14% for a 7-day horizon and only 0.04% for a daily horizon.

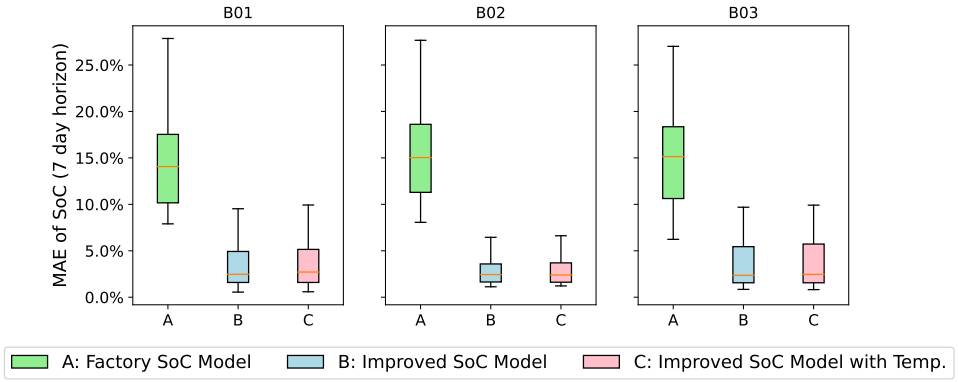

FIGURE 3.21 – MAE distribution for 7-day continuous SoC estimation without thermal consideration for each BESS.

In what concerns the internal temperature prediction, the use of the thermal dependent SoC (improved SoC Model with Temp.) instead of the factory SoC model to determine the current SoC had no significant improvement. In a 7 day horizon the MAE reduction was of less than 0.01 °C, and the reduction was even lower for a 1-day horizon. Table 3.14 shows this results.

3.4.4 Model Conclusion and Discussion

The SoC estimation approach in this chapter aimed to provide an accessible and easily adaptable model that is suitable for industrial usage regardless of the manufacturer,

	Factory SoC		Improves SoC w/ Temp.	
LiBESS	1-day	7-day	1-day	7-day
LiBESS #1	1.935 °C	1.803 °C	1.934 °C	1.802 °C
LiBESS #2	1.917 °C	1.854 °C	1.913 °C	1.849 °C
LiBESS #3	2.00 °C	1.891 °C	1.998 °C	1.888 °C

TABLE 3.14 – MAE for the temperature prediction depending on the origin of the SoC, either the Factory SoC Model or the Improved SoC Model with temperature dependence.

brand, or configuration of the LiBESS. By using the AC measurements and the reported SoC value from the LiBESS BMS, an adaptation of a coulomb counter was built. The performance parameters, which can be seen as resistances in an EC model for the battery, where parameterised given the real performance of the LiBESS in operation. In addition, for the LiBESS where thermal measurements were available, the temperature was used to identify a thermal-dependant self-discharge resistance in an EC model as it is a parameter that can be co-estimated for modelling and forecasting purposes.

From the results obtained through the use of the parameterised models, a general improvement can be seen for SoC estimation in all cases. In both 1 and 7-day horizons, the parameterised models showed improvement compared to a simple model that uses the manufacturer-issued values and limited the MAE to less than 5% in both cases. Also, as seen from the results, the data published from the manufacturer can deviate strongly from the real performance of the system. To improve a power plant performance, an SoC model becomes necessary to correct the deviation one could incur if this step is omitted or too much trustiness is given to the manufacturer.

At last, in what concerns the thermal consideration for the LiBESS, a slight degradation in SoC estimation was observed due to this inclusion. This SoC estimation degradation can be explained by the co-estimation as error is added from both the SoC and the thermal model. It however remains an improvement compared to the factory model and, if thermal information is required for LiBESS modelling, a small penalty in SoC precision can be an acceptable trade-off for operational temperature estimation.

3.5 State-of-Health Modelling of Li-ion Batteries

In addition to the thermal behaviour and the state-of charge covered in sections 3.3-3.4, attention also needs to be given to the estimation of the LiBESS degradation and health. As time and power goes through the storage system, the capacity and general performance of the system evolve due to changes in the internal chemistry and the stress from cycling. Even if these changes are slow and barely impact the day-to-day operation of an industrial LiBESS already deployed, it is important for the longevity and profitability of projects to have an overview of the current and expected behaviour from the system.

This degradation from the LiBESS is commonly represented by the SoH and defined as in (3.41). This value indicates the maximal current energy capacity E_i the system can hold relative to the initial maximal capacity E_0 published by the manufacturer. An SoH of between 60% and 70% is often used to determine the End-of-Service (EoS) or End-Of-Life (EoL) from an electrochemical storage system. At this point the BESS is still operational, but the capacity loss is considered too high for the system to continue its intended purpose.

This way of defining the SoH is not the only one though. As noted in [164], it is common as well to express the SoH relative to the expected capacity loss at EoL as in (3.42). In here a SoH of 0% indicates that the battery reaches its useful life regardless the fact that it can continue to store and deliver energy. It is also easy to see how this implementation is less practical when studying degradation across applications as different applications establish different EoL limits. As consequence, it is impossible to know the current remaining capacity for two batteries of the same kind without also knowing the EoL percentage.

$$\mathrm{SoH}_i = \frac{E_i}{E_0} \tag{3.41}$$

$$\mathrm{SoH}_i = \frac{E_i - E_0}{E_0 - E_{\mathrm{EoL}}} \tag{3.42}$$

The complexity of determining the SoH of a LiBESS comes from the impact the external conditions and the specific usage have on the system. The temperature, just as in the case of SoC estimation, can also change the available capacity of a LiBESS at any given time. This in addition to the fact that integrated BMS can artificially reduce the capacity to avoid damages or extended capacity loss. Battery cycling and the specific power profile are other elements that, depending on the stress they imply, can increase or reduce the degradation to what is expected by the manufacturer.

Because of this, SoC modelling approaches need to understand the different phenomena that impact and cause the capacity of a LiBESS to change. Development of these models would help not only to determine the SoH at an instant i, but also to estimate the short and long-term LiBESS behaviour on applications and scenarios outside of what the manufacturer envisioned.

3.5.1 SoH Behaviour and Modelling

Capacity fade in LiBESS is generated by side reactions and degradation of the elements that happen naturally with ageing and cycling of the cells. Some of the different identified phenomena, seen in figure 3.22, depend on the electrode they occur, the specific state of the electrochemical cell, and the materiel from which the components are made of. Electrolyte oxidation and solid lithium deposition on the electrodes are accentuated when the cell voltage is high (overcharge) [52, 165]. Likewise, high temperature increases the oxidation process at the electrodes which increases degradation on storage condition and raises the impedance in operation [166].

In what concerns the phenomena relative to phase changes, current collectors, electrolyte reduction, and active material dissolution, all impact the energy capacity by reducing the cell capability to react even without any loss in lithium due to SEI formation. Phase changes on the electrodes change the crystal structure and reduce the contact between the materials. Current collectors, when a cell is over-discharged, can dissolve reducing the general performance, safety, and capacity of the cell. At last, both electrolyte reduction and active material dissolution both reduce capacity by generating irreversible by-products, such as in $LiMn_2O_4$ where the dissolution of manganese is identified as a driving factor on capacity loss [52]

From the previous mechanisms, the electrolyte decomposition and loss of active surface due to volume changes have been identified as the main driving factors for capacity loss. These work by reducing the available lithium, increase the cell impedance, and also diminish the number of elements available to react. Some mitigation can be done through electrolyte stabilisers and pressurised cell containers, but they do not eliminate them completely [167].

Power fade is also a degradation and health indicator besides capacity loss, although it is more commonly used for applications that are power-based such as HEV. Defined as a decrease in the maximal output power from the cell or LiBESS, this phenomenon is strongly related to the increase of the impedance in the cell. This increase in resistance naturally impacts the capacity (and by consequence the SoH) as there are non-reversible

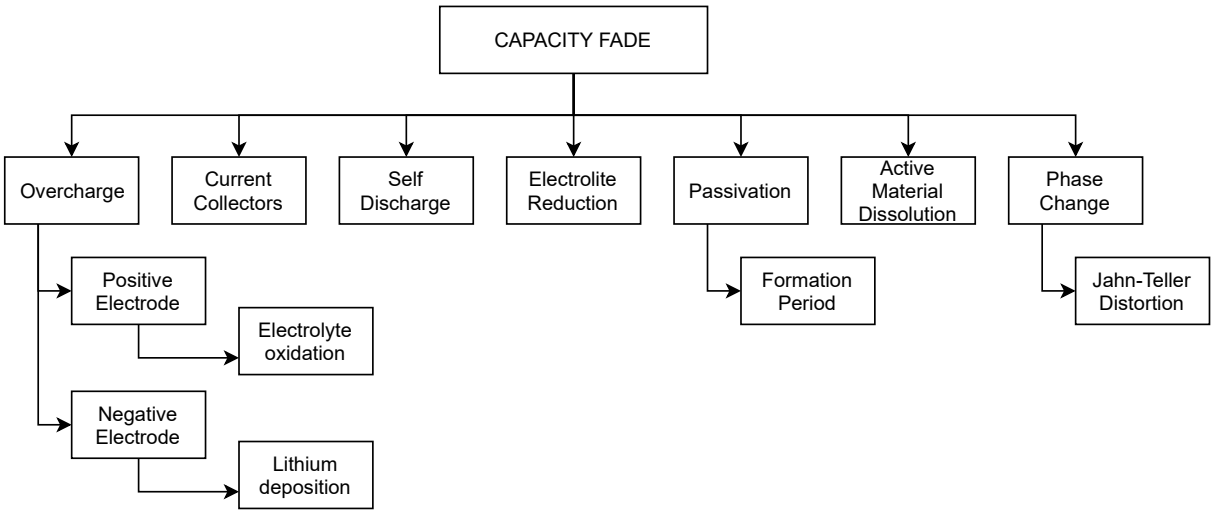

FIGURE 3.22 – Different phenomena reported as the cause for capacity fade in LiBESS. Adapted from : [52].

losses due to heat increase. SEI growth has been identified as the main source for its increase, and the EoL is reached when the resistance double to that at the BoL for the LiBESS [167, 164]

3.5.1.1 LiBESS Degradation behavior

As hinted, the impact and apparition of the different phenomena discussed before depend strongly on the conditions and chemistry of the LiB. Han et al. compared 5 different cells and each one showed a very distinct degradation curve as seen in figure 3.23. An NCM battery showed the least degradation, while an LMO cell with carbon anode degraded the fastest. The terminal voltage at each SoC also followed this with the former barely changing, and the latter showing a great deviation from the voltage from a fresh cell [104].

In the case where there are no cycles, the degradation is promoted by the temperature at which the LiBESS is stored. Broussely et al. [166] compared for 4 years the Li loss when stored at 40 °Cagainst 60 °Cas visible in (a) in figure 3.24. In this timeframe, the degradation doubled thanks to the hot temperature. Likewise, when cycling was involved, the higher temperatures reduced the global capacity.

The power fade is also impacted by the temperature of the LiB cell. As visible in (b) in figure 3.24, high temperatures decrease the relative power expected from a LiB cell [122], and even in storage conditions the phenomena is observed [166]. In the case of low temperatures, upon cycling under sub-zero temperatures create even faster degradation and capacity loss than under high temperatures [168]. The cold temperatures increase the internal resistance of LiB cell at all levels of SoC (specially low SoC), which create further

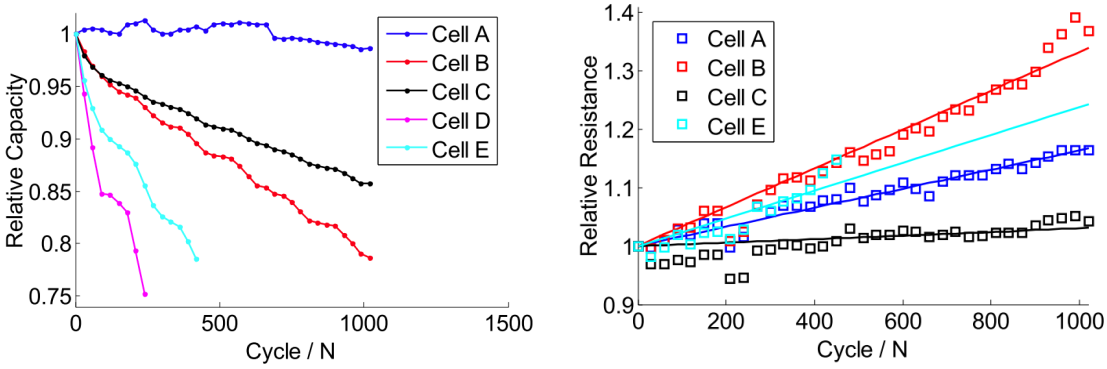

(a) (b)

FIGURE 3.23 – (a) Capacity loss for 5 different cells at 25 °Cand 1/3 C. (b) Resistance increase at 50% SoC. A : NCM with 20Ah, B : LFP with 60Ah, C : LFP with 11Ah, D : LMO with 35Ah, E : LMO with 10Ah. Source : [104].

capacity loss as each cycle generates more heat [169, 148, 170].

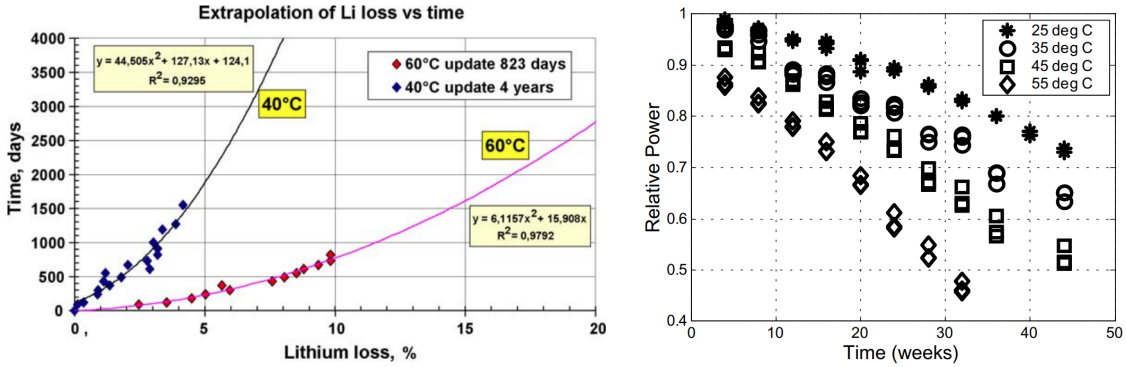

(a) (b)

FIGURE 3.24 – (a) Capacity loss at two different storage temperatures for a Ni-based LiB cell. Source : [166]. (b) Power loss at different temperatures for an SoC of 60% and a custom-made NCA LiB cell. Source : [122]

Because the degradation and SEI formation happens both at idle conditions and when cycled as seen just before, the aging is often classified into two different kinds : calendar aging, and cyclical aging [171]. The former encompasses the capacity and power fade from the LiB by the passing of time, and the latter is the degradation linked to the power profiles the cell is subjected to. Although both kind of degradation occur simultaneously when in use, calendar aging is considered more important for EV as the resting periods are longer [172]. Likewise, methods and procedures exist for EVs to standardize the meaning and data availability of these kinds of LiB degradation [173].

Spotnitz in [174] described the two behaviours of the degradation as in (a) for calendar and (b) for cyclical in figure 3.25. The calendar aging is more pronounced at the BoL and then it becomes a slow loss. In cyclical capacity loss, 4 different periods are common. An

initial fast degradation (A), followed by a weaker but still consequential capacity loss (B) which evolves into a very weak degradation (C). At last, after the period of stability a period of fast degradation is also expected (D).

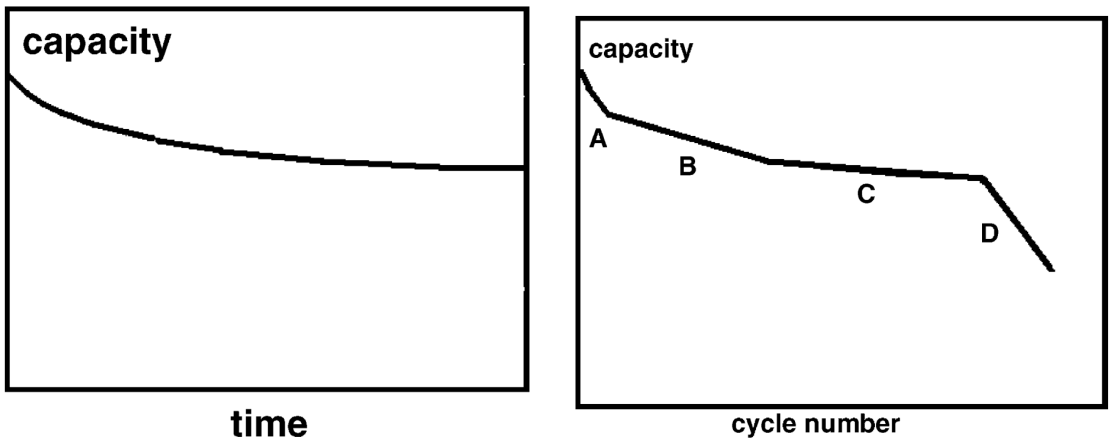

(a) (b)

FIGURE 3.25 – (a) Calendar capacity loss. (b) Cyclical capacity loss behaviour. Source : [174].

3.5.1.2 SoH Estimation & Modelling

Just as in the case with SoC, the modelling of the SoH for a LiBESS has a plethora of approaches and techniques. Berecibar et al. in their review of SoH health estimations methods [91] categorized the techniques into experimental and adaptive as seen in figure 3.26, classification adopted in this work. Although other categorizations separate the SoH estimation methods in four families such as direct, model-based, data-driven and adaptive filters [145], the differences between these families is subtle and the overlapping is more prominent making less clear to which category techniques fall within.

For the two here presented, the distinction lays fundamentally on the application and way to operate The experimental methods use databases of measurements from the LiBESS to foresee the future performance. This makes them easy to implement on the BMS if the needed measurement for the SoH model is available. On the other side, adaptive methods rely on the calculation and update of parameters of a model given the observed measurements. Although more precise, these are computationally expensive and the implementation is less straightforward.

As briefly presented in 1.3.2.3, within the experimental methods there are resistance and impedance techniques which are based on direct measurements, and techniques which use measurements such as data maps, SVA, coulomb counting, etc. SoH can also be

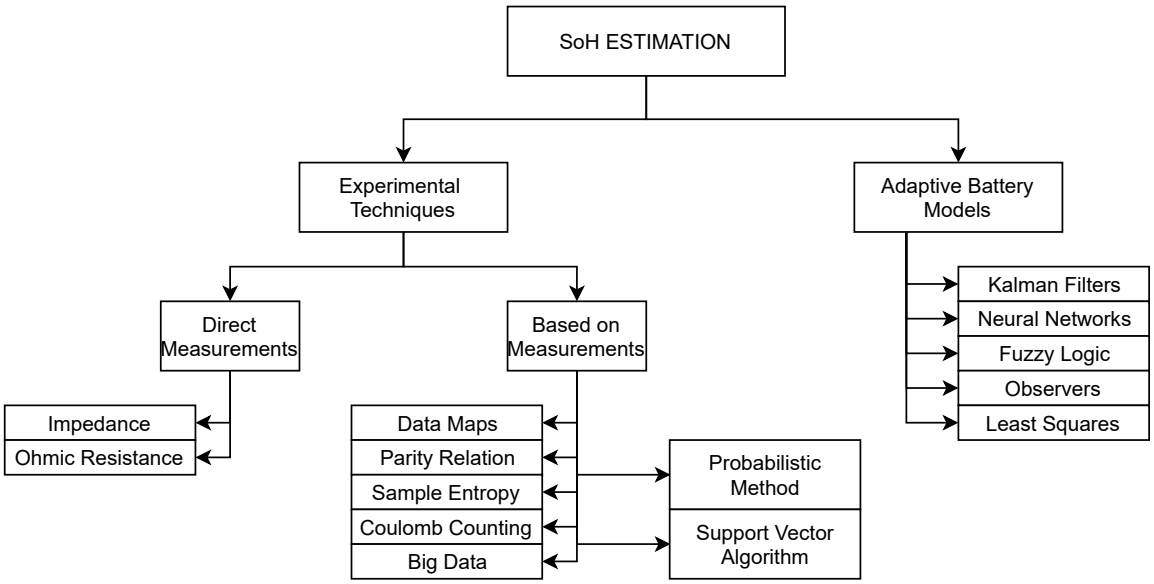

FIGURE 3.26 – SoH estimation methods. Source : [91]

determined through destructive experimental methods, but they will not be covered as they are incompatible with LiBs in operation. On the adaptive side of techniques, just as with the case of SoC estimation, they are built around Kalman Filters (KF), observers and ANN to mention a few. A comparison on the performance of these was also previously presented in figure 1.12 in the introduction chapter.

A more in-depth review of some SoH estimation methods based on experimental techniques are presented below. Adaptive models will not be presented as the core is the same but with the inclusion of processes to estimate and correct deviations given the newer measurements. Further details of these methods can be found in the review [91] by Berecibar et al.

Impedance & Ohmic Resistance. A SoH estimation can be done through its relation to the internal resistance R_{int}. As the cell ages and it is cycled, the internal resistance increases for any state of charge and temperature relative to a new cell under the same conditions [170]. Given a known SoH - R_{int} relationship (obtained through extensive experimental datasets), the problem shifts to the method used to determine the resistance.

$$R_{int} = \frac{\Delta U}{\Delta I} \tag{3.43}$$

Two of the methods commonly used to determine the internal resistance are the Hybrid Pulse Power Characterisation (HPPC) and Direct Current Internal Resistance (DCIR). HPPC, proposed for EVs by the United States Advances Battery Consortium (USBAC) in [175], studies the voltage at the terminals after 30-seconds discharge pulses

followed by a 10-seconds charge pulses at each 10% SoC. In the case of DCIR, the discharge and charge periods have the same duration (5 to 10 seconds) and intensity, and are repeated at higher currents for the same SoC level [176]. In both of these test profiles, seen in figures 3.27-3.28, the internal resistance is obtained through Ohm's Law given the observed voltage and current during the tests as in (3.43).

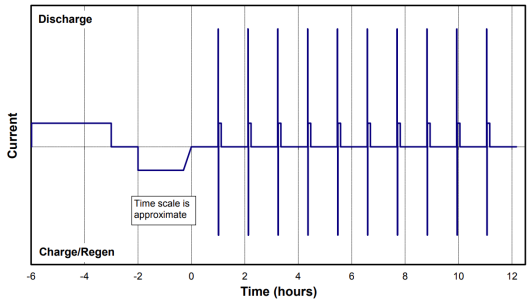

FIGURE 3.27 – (a) HPPC Test Profile. Source : [175]

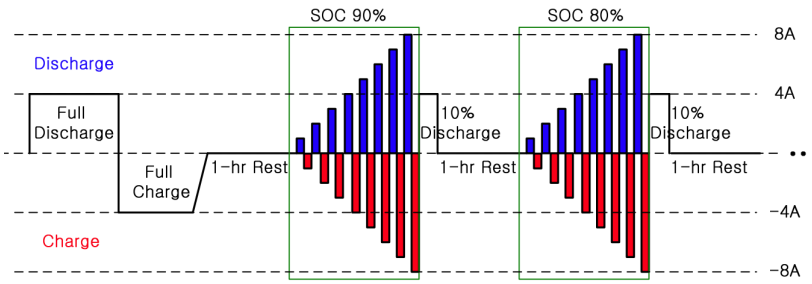

FIGURE 3.28 – (b) DCIR Test Profile. Source : [176]

The internal resistance and capacity measured through these two techniques are then used to create models of R_{int} [177], SoH and capacity models upon cycling [84], and also can be used to determine the power capabilities of the LiB [178]. Besides HPPC and DCIR, Gismero et al. used electrochemical impedance spectroscopy (EIS) to characterise the relationship between SoH and internal resistance, and proposed and model that estimates R_{int} given time, temperature and SoC with an RMSE of 2.5% [172]. Lee et al. also reported an SoH estimation error of 3.7% after 250 cycles for an SoC-R_{int} model [179] when obtaining the resistance measurement through a different measurement protocol.

Differential Voltage Analysis The voltage seen at the terminals can also be used to determine capacity of the LiB without the need of calculating the internal resistance. Given that the LiB cells have a characteristic voltage-capacity curves, the evolution of this curve as the cell ages gives insight of the SoH. Figures 3.29 show the voltage and differential voltage (DV) curve for a charging LFP batteries at different SoH, and in these it can be seen how the most important differences in energy storage occur when the SoC

of the LiB is high. The current SoH can then be determined, with a reported error of 1%, by analysing the energy charged/discharged within this short range of high SoC until the DV reaches the last peak on charge (or first in discharge). In figure 3.29 (b) this means the peak at most right. Using only the small SoC window is possible as the capacity on the remaining SoC range that is not analysed remains almost static as the cell ages [180].

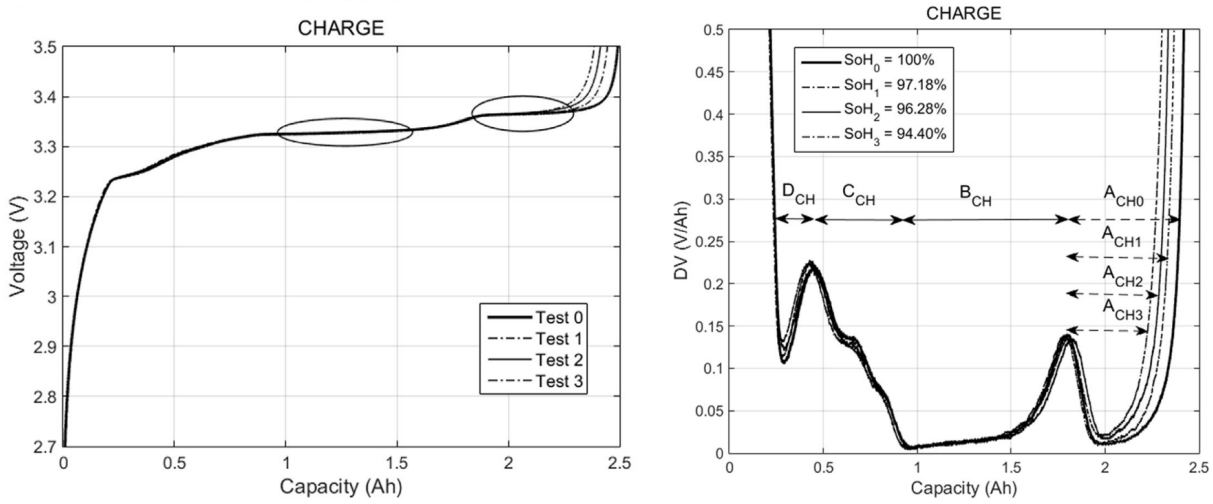

(a) (b)

FIGURE 3.29 – (a) Charge Voltage-Capacity curves for LFP cells with different SoH. (b) Charge DV-Capacity curves for the LFP cells. Source : [180].

In addition to SoH estimation, it DV analysis can also be used to identify the location of the degradation the LiB cell suffers. This can be used afterwards to gain insight on the precise process responsible for the capacity loss [181].

Coulomb counting This SoH technique follows closely the definition seen in (3.45). The energy measured when going from the high cut-off voltage to the low cut-of voltage (SoC from 100% to 0%) can be used to directly determine the current maximal capacity of the LiB at the specific operation conditions.

The coulomb efficiency, the relation between the discharged capacity C_d and the charged capacity C_c in the same cycle (3.44), can also be used to estimate the current degradation of the LiB. As degradation and capacity losses increase, the CE decreases as well with a strong correlation. This makes the CE a strong indicator of the SoH which allows to generate SoH estimation models function of the CE [182]

$$\text{CE} = \frac{C_d}{C_e} \tag{3.44}$$

Ageing Modelling : Calendar & Cyclic Given that the degradation of the LiB is driven mainly by SEI formation in time (calendar) and through charge/discharge cycles (cyclic), these two can be used to model and estimate the SoH of the cell. Xu et al. expressed these behaviours using two SEI growth parameters α_{sei}, β_{sei} and a unit cycle deterioration function $f_{d,1}$ in eq. (3.45), with N the number of full charge/discharge cycles the BESS has had [183]. This approach is also not exigent in operational data, as only a health indicator and the AC power through the BESS is needed.

$$SoH = \alpha_{sei} e^{N\beta_{sei} f_{d,1}} + (1 - \alpha_{sei}) e^{-N f_{d,1}} \tag{3.45}$$

More simpler approaches for the cyclical degradation have also been reported. In [184], the capacity loss is modelled via two parameters a,b given N cycles as in (3.46). In [169] a proportionality coefficient β was used with the number of cycles (3.47) to determine the capacity loss. This equation can be then applied to many temperatures to generate a 2-d model (T,N).

$$Q_{\text{loss}} = a \cdot N^b \tag{3.46}$$

$$Q_{\text{loss}} = \beta \cdot N \tag{3.47}$$

Relative to calendar aging, when isolated from cyclical aging, a common approach is to express it as the square root of t as in (3.48). Here kf is a proportional factor impacted by the storage SoC and temperature, which its thermal dependence is often linked directly to Arrhenius law (3.49) [171, 185]. This calendar aging expression is however not the only one. More complex polynomials have also been reported to better fit the behaviour by the LiB cells [169].

$$Q_{\text{loss}}(t) = kf * t^{1/2} \tag{3.48}$$

$$\upsilon = A \cdot e^{\frac{-Ea}{RT}} \tag{3.49}$$

3.5.2 Proposed LiBESS SoH Model

The approach used in this work is the one seen in (3.45) with calendar and cyclical aging expressed in exponential terms. This model is able to reproduce the fast initial degradation due to SEI formation in the first term, and the continuous cycle-dependent degradation in the second. An advantage of this approach is that it does not require in-depth DC measurements, as only a health indicator and the AC power through the BESS

are enough to train the model and obtain the fitted parameters.

In this formulation, the individual calendar aging is not expressed explicitly as it is included in the cycle degradation. The regularity and homogeneity of the cycles in the dataset used in this work (as the sites follow the AO ZNI 2015 operational framework presented in chapter 2) allows this simplification. For the cases where the LiB operation profile is not regular, which is not the case in this work, it is possible to use expression f_d in eq. (3.50) to replace $Nf_{d,1}$, where δ_i is the depth of discharge, σ_i is the average SoC, and $T_{c,i}$ is the average temperature for the ith cycle. This allows to express the degradation given the particular use of the storage.

$$f_d(t, \delta, \sigma, T_c) = f_t(t, \hat{\sigma}, \hat{T_c}) + \sum_{i}^{N} n_i f_c(\delta_i, \sigma_i, T_{c,i}) \tag{3.50}$$

To identify the parameters in the equation of interest (3.45), traditional curve fitting techniques can be used with the life degradation observations as the amount of the LiBESS regular cycles increase.

3.5.3 LiB SoH Model Results

Equation (3.45) was parameterised for BESS #4-#7 since these systems provide the data needed for the model. The training data to determine the parameters presented here came from the first year of operation, and the kind of behaviour it has can be seen in fig. 3.30. In this figure it is possible to see the off-line periods (SoH of zero), the malfunction of battery racks (decrease in SoH down to 70%) as well as the introduction of fresh cells (steep increase in SoH seen for instance in cycles 45 or 60).

The parameterized values can be seen in Table 3.15, and they describe the expected SoH evolution given the constant cycling behaviour associated with the PV capacity firming framework that the sites follow. In half of the cases, these values showed the strong expected initial degradation linked to SEI formation (α_{sei}), going up to 5% energy capacity loss in the first year when considering an average of 1 cycle per day, as well as the subsequent softer degradation. For the other two, the initial degradation observed was even higher (> 10%) for one, and lower for the other (3%).

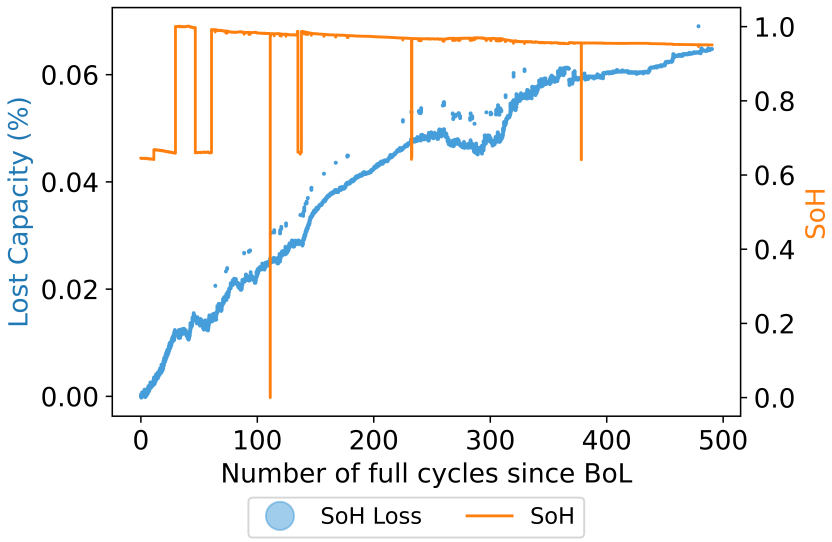

FIGURE 3.30 – SoH and loss in capacity as reported by the BMS used to parameterize the SoH model for the LiBESS #4. LiBESS #5 - #7 share a similar behaviour.

TABLE 3.15 – Degradation parameters

	α_{sei}	β_{sei}	$f_{d,1}$
LiBESS #4	0.0509	149.994	3.64e-05
LiBESS #5	0.0473	0.9968	8.419e-05
LiBESS #6	0.1213	149.991	1.546e-04
LiBESS #7	0.0266	141.92	2.426e-04

However, the parameters reported in table 3.15 took as input the reported SoH regardless of its behavior. It is possible to see in figure 3.30that, when failure occurs on battery packs, the reported SoH by the BMS jumps up and down which pollutes the input data. When considering that any sudden change in capacity superior to 0.5% of E_0 is due to a malfunction and thus is not to be included, we can better characterise the continual degradation parameters β_{sei} and $f_{d,1}$. Table 3.16 shows the changing values when applying the described filter, and figure 3.31 shows the estimation and predictions given these new values for a horizon of 5 years.

The expected degradation over 10 years of cycles for the four LiBESS can be seen in figure 3.32 in page 128, where the broken green line indicates the maximal capacity loss accepted by the manufacturer warranty. It is easy to see in these results that the deviation from the warranty values as the LiBESS health does not degrade as quickly. The training data for these figures was set to the first year of available data. When reducing the amount of training data to less than a year, the SoH model predicted behaviour more

TABLE 3.16 – Degradation parameters

	α_{sei}	β_{sei}	$f_{d,1}$
LiBESS #4	0.1440	148.85	6.02e-06
LiBESS #5	0.002	0.961	1.2e-04
LiBESS #6	0.4907	129.95	3.19e-06
LiBESS #7	0.0490	149.99	1.93e-06

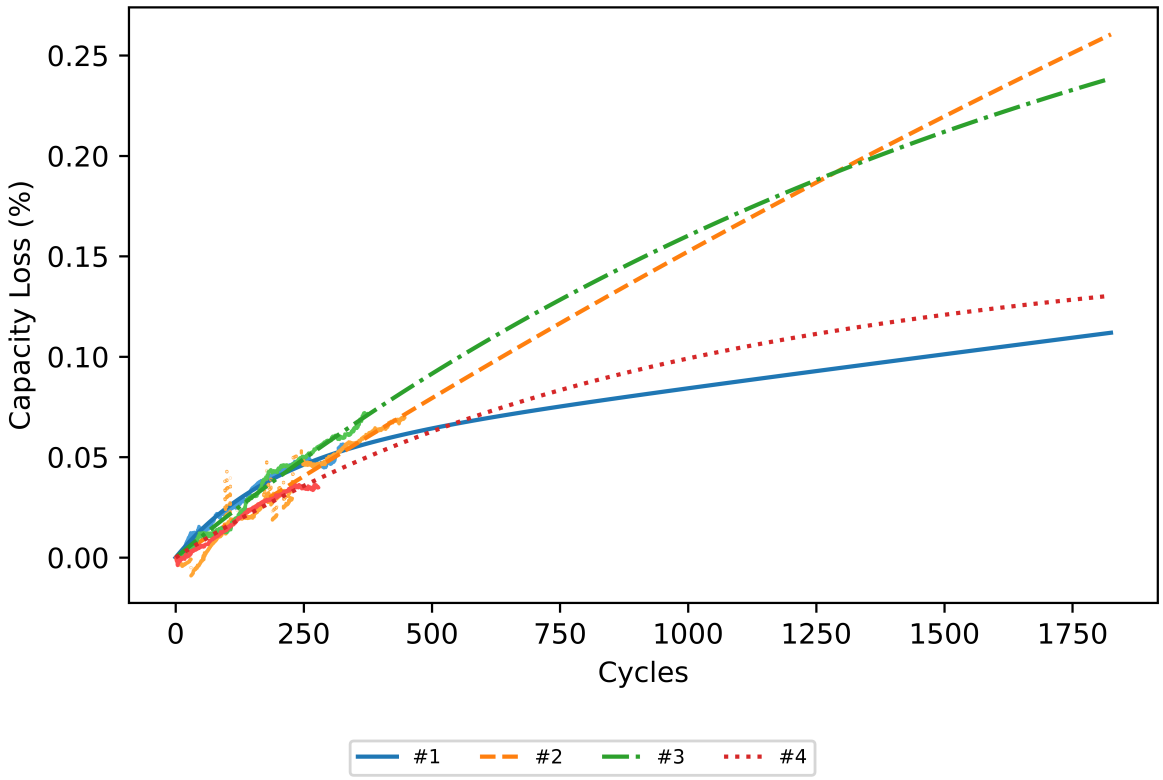

FIGURE 3.31 – Predicted SoH for batteries # 4 to # 7 in a 5 year horizon. The parameters are found on table 3.16.

closely related to the warranty expected loss (figure 3.33, page 129) near the BoL, but less as time passes on the error increased. This can be explained due to the SEI formation phase still being predominant, which is less dependent on the LiBESS use.

For these 4 LiBESS, the reference values are considered to be the warranty issued by the manufacturer. This warranty depends only on the total energy throughput the system has experienced, which can also be expressed in cycles as each cycle is considered to have exported a definite amount of energy. The MAE for both the model trained with 3 months and 1 year of data can be seen in tables 3.17, 3.18 [8]. From these results, we can see how the

8. Notable from these tables is the fact that the warranty MAE was lower for some sites in table 3.17.

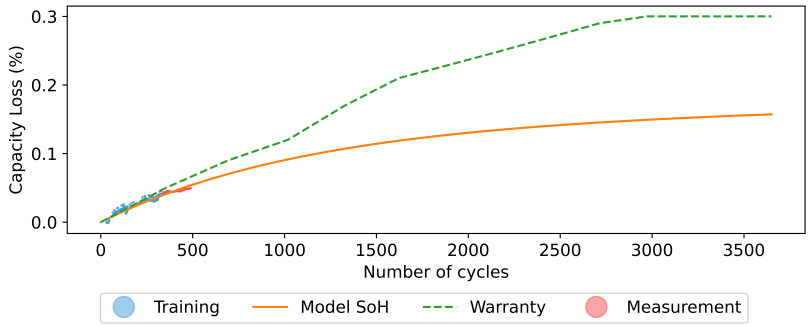

(a)

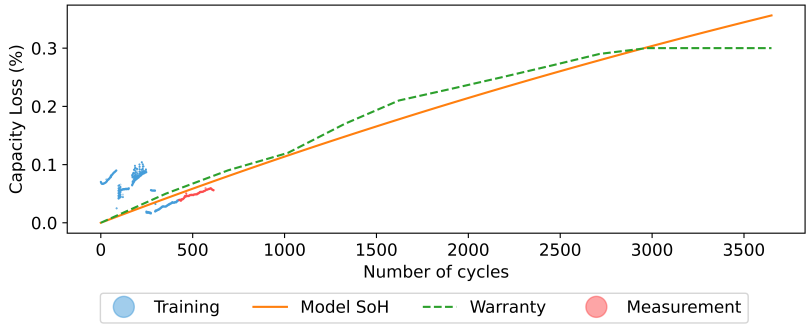

(b)

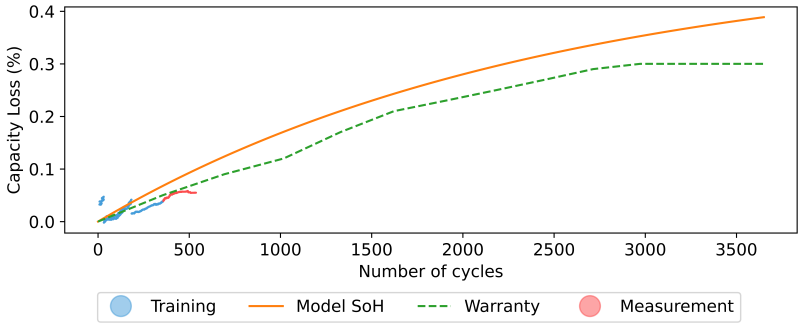

(c)

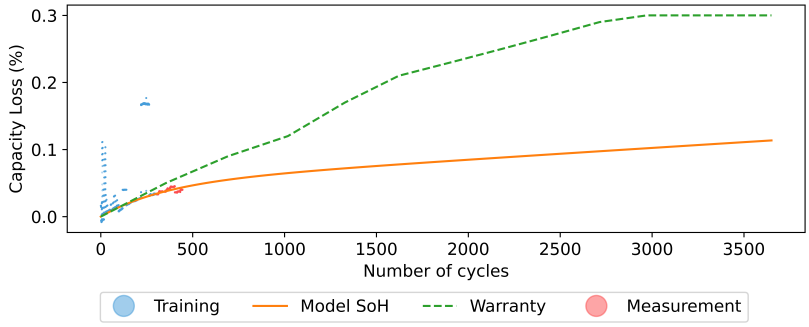

(d)

FIGURE 3.32 – Predicted SoH for LiBESS #4 - #7 in a 10-year horizon with **1-year of training data**. The blue dots represent the training set, and the red dots the validation set : (a) LiBESS #4 ; (b) LiBESS #5 ; (c) LiBESS #6 ; (d) LiBESS #7.

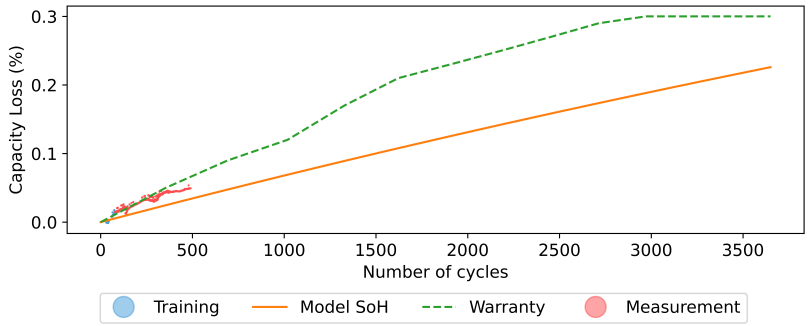

(a)

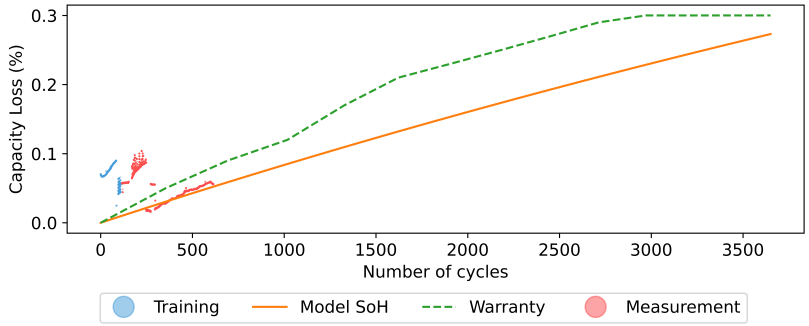

(b)

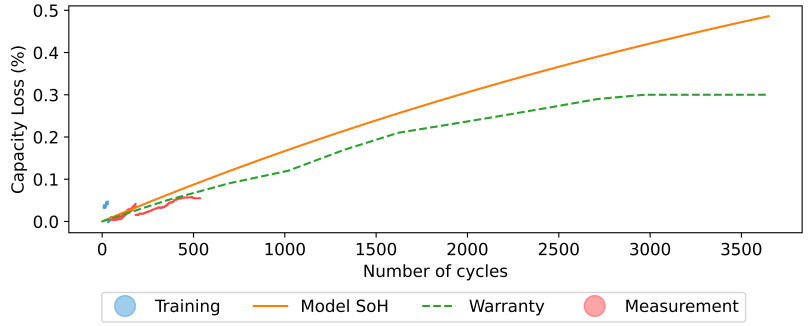

(c)

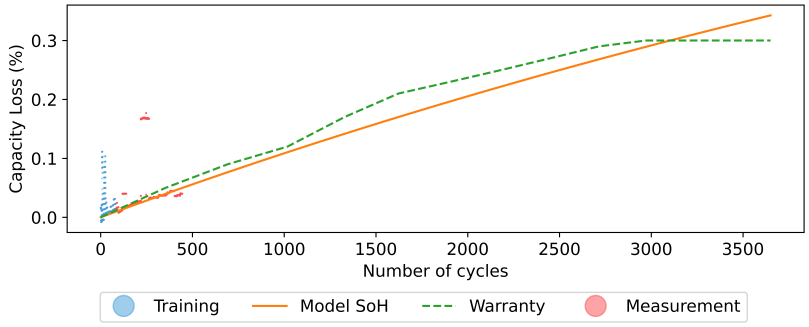

(d)

FIGURE 3.33 – Predicted SoH for LiBESS #4 - #7 in a 10-year horizon with **6 months of training data**. The blue dots represent the training set, and the red dots the validation set : (a) LiBESS #4 ; (b) LiBESS #5 ; (c) LiBESS #6 ; (d) LiBESS #7.

model parameterized with less data exhibited errors that were similar or higher than the warranty, with a difference being as high as 1% in capacity. An improvement was observed when training with 1 year, as the SoH error by the model decreased of 1% compared to the warranty in all but 1 BESS. The BESS for which the error increased is related due to a major repair the BESS had, which replaced an important number of battery packs. This slowed the degradation initially observed and basically meant that the initial data was no longer applicable.

	Model	Warranty
LiBESS #4	1.42	0.68
LiBESS #5	1.8	2.61
LiBESS #6	1.88	0.85
LiBESS #7	2.33	2.66

TABLE 3.17 – SoH MAE in % for the model trained with **3 months of data**.

	Model	Warranty
LiBESS #4	0.24	1.15
LiBESS #5	1.08	1.97
LiBESS #6	3.06	0.79
LiBESS #7	0.28	1.33

TABLE 3.18 – SoH MAE in % for the model trained with **1 year of data**.

3.5.4 Model Conclusion and Discussion

The SoH model here proposed and trained showed a better performance at mirroring the real behaviour the LiBESS exhibited after 2 years of operation, and proved adequate for the conditions met in PV+Storage sites under capacity firming frameworks. The average deviation of 1%-2% from the SoH from the warrantied value, although can seem insignificant, represents on the long term a significant amount of energy and revenue. E.G. For a 1MWh storage cycled upon daily with a 10-year expected life-time, a lower real capacity of 1% would translate to 36.5MWh of annual energy. Given the decreasing cost of the storage, this energy at current market price [9] could represent 3% of the CAPEX of the storage.

Furthermore, the deviation causes two different sets of problems with particular difficulties. If the SoH error is positive (more energy than expected), then there could be wasted available energy if this difference is unexploited by the EMS. The ROI could in this case increase and render more attractive storage related projects. For the case of negative SoH error, the financial loss due to the missing exploitable energy is amplified by potential sanctions due to the inability to fulfil energy engagements.

This is logical as more datapoints from the early life of the BESS are used to calculate the error. In such early phases, behaviour is expected to be close to the warranty values.

9. Electricity cost of 252.5eur per MWh in Europe [186]

By using an SoH model as the presented here, it is also possible to generate a range of operating scenarios useful to formulate the EMS in which the LiBESS are deployed. The warranty values can be used as a *worst-case scenario* and the trained model as the realistic capacity projection if no further failures occur. Operators and EMS developers could then use these projections to improve the risk-management strategies used to determine the operation of the systems.
All this with the also advantage of not needing to realize specific capacity tests, which imply the storage unavailability and the costs that this entails.

3.6 Conclusion and Discussion

In this chapter, three main indicators used for the performance and management of LiBESS were presented : the internal temperature, the SoC, and the SoH. For each, the different physical and chemical mechanisms involved, as well as their impact on the behaviour of the LiB were introduced. In the case of temperature, high and low operating temperatures have been shown to generate undesirable side reactions that reduce the performance, longevity, and can even endanger the safety of the battery packs. The SoC, being an indicator of the current energy stored, is crucial for any management of the power system. It is impacted by the current state of the storage (temperature, degradation, internal resistance) and its expected charge/discharge profile amongst others. At last, the SoH, which indicates the current maximal capacity, was displayed as the result of Li loss and the increase in internal resistance due to side reactions that happen when idle or under operation. These phenomena boosted by certain LiB temperatures and state of charge. .

The different estimation methods for the three battery states of interest were also discussed through the chapter. For temperature estimation, the methods rely heavily on heat generation modelling in which irreversible heat generation is expressed via Ohm's Law. Because of this, it is necessary to model and/or determine the internal resistance under the many operation conditions the LiBESS can be found. The other two parameters, SoC and SoH, are estimated and calculated following similar techniques. DC and AC measurements are used for both to determine the relationship between the measure and the parameter of interest. Afterwards, the relationship is used with numerical and EC models that estimate the physical measurement and the LiB indicator of interest. Additionally, for all three parameters, black-box models via ML are also possible but their exposure in this work was limited as physical insights from the system are limited.

From the operational constraints and data scarce scenarios found within vRES pro-

jects with LiBESS integration, only certain techniques can be reasonably be expected to be applied and deployed in the EMS and PMS on site. With the collected data and operational sites at disposal seen in chapter 2, the retained parameter models were as follows : an irreversible heat generation model based on the estimated internal resistance (temperature), a power-integrator SoC estimation with a thermal dependant self-discharge parameter, and an aging model that incorporates together the calendar and cyclical degradation due to the uniformity of the behaviour of the LiB. These, when trained and applied to the deployed LiBESS, showed lower MAE as the observed behaviour of the systems diverged from the foreseen and published by the manufacturer.

The results from the models strongly suggest then that the specific purpose and usage of the LiBESS has a non-negligible impact on the short- and long-term performance of the LiBESS. Although in the prospecting and study phase of vRES+LiBESS projects it is reasonable to consider only the published and guaranteed performance values, in the production phase the deviations from these parameters can mean under-exploited resources. If the degradation and performance of the system is better that the "bought" from the system, this can be used to further optimize the management system. A better performance could invite the vRES developer to add more LiBESS to the current system to increase revenue, and even to green-light similar projects as the ROI is better than expected. In the case of a less advantageous performance, developers can turn to the LiBESS manufacturer for indemnities. Similar projects would become less attractive, and this would open the door for exploration for alternative storage solutions.

By using the three models simultaneously under a co-estimation framework, it is also possible to study the impact of different scenarios and charge/discharge profiles can have on the LiBESS. Similar vRES + LiBESS project located on other regions with or without different power profiles would behave differently thermally speaking, which impacts both SoC and SoH as seen in this chapter. This different behaviour could be weighed in the early phases of the projects when the three models are available, allowing to study and analyse the expected operating conditions in a way that was not done previously.

Next chapter will explore the impact and integration of these advanced LiBESS models on the operational framework of the experimental and industrial sites of this work. The applicability of such models for other use-cases that can benefit heavily by the usage of LiBs will also be treated.

Chapitre 4

LiB scheduling & Operation

Résumé en français

Ce chapitre explore l'utilisation optimale des systèmes de stockage d'énergie par batteries lithium-ion (LiBESS) dans le cadre de l'intégration des sources d'énergie renouvelable variables (vRES) au réseau électrique. L'objectif principal du chapitre est d'intégrer les modèles de température, de SoC (état de charge) et de SoH (état de santé) développés dans les chapitres précédents dans un algorithme d'optimisation adaptatif à des différentes scenarios et besoins. Le premier scenario simule le cas présenté dans le deuxième chapitre, l'appel d'offres pour les Zones Non Interconnectées (AO ZNI 2015), afin de maximiser le gain financier du système grâce à une utilisation optimale du stockage. Le second scenario présente un micro-réseaux composé de plusieurs LiBESS, une vRES ainsi que d'une consommation locale, cela avec l'objectif de retrouver le cout minimal de l'énergie afin de satisfaire les contraintes locales. L'impact financier et à long terme de l'intégration des différents modèles est évalué pour illustrer les risques et les écarts par rapport aux paramètres de performance publiés par les fabricants.

Les résultats obtenus montrent que le comportement thermique des BESS et les paramètres de performance réel ont un impact significatif dans les performances attendues des sites. Cela permet donc un meilleur pilotage quand ils sont intégrés dans les systèmes de contrôle. En cas de meilleures performances que celles garanties par le fabricant et prévues initialement, une utilisation plus agressive des LiBESS peut etre imaginé afin d'augmenter le revenu. Inversement, des performances moins avantageuses invitent vers une utilisation plus conservatrice du stockage pour fiabiliser le système dans le temps, ainsi que demander des indemnités du fabricant de LiBESS.

Le chapitre termine par une discussion sur l'intégration de ces modèles avancés de

LiBESS pour des sites expérimentaux et industriels. Les bénéfices potentiels pour d'autres scenarios d'utilisation est discuté, ainsi que les limites que ces intégrations peuvent avoir.

4.1 Introduction

Recent vRES integration into the electrical grid has promoted the apparition of capacity firming frameworks to mitigate the unpredictability in production they bring to the grid[39]. These frameworks incentivize the deployment of adjoin BESS thanks to more advantageous remuneration schemes at specific times of the day, as well as penalties related to unmet scheduled power engagements. The framework presented in chapter 2.4 is an example of this kind of projects, and they showcase the synergy needed between power scheduling and operation of the vRES/BESS.

This subject of BESS scheduling has been widely discussed in the literature. Ngoran et al. described the optimal engagement and operation problem for the AO ZNI 2015 framework, proposing a comparative study of the different strategies to solve the problem [187]. Other works have focused on similar optimization problems for li-ion storage systems [188, 189, 190], changing the vRES to wind [191] or including different financial perspectives and constraints such as the one from the aggregator[40, 192]. When addressing the subject of coordination of multiple BESS in a network to propose flexibility services, the schedule algorithm and process has been referred before as Network Battery Aggregator (NBA) [193]. This name will be adopted in this work to refer to any BESS + vRES scheduling procedure in a local network with a single point of connection, no matter the amount of individual BESS present.

In all the mentioned optimisation and scheduling cases, the BESS model incorporated was mostly restricted to the SoC and its charge/discharge power efficiency. Thermal behaviour of li-ion BESS due to specific use profile is not considered in scheduling frameworks, and its impact hasn't been properly accounted.

4.2 Objective and chapter structure

In this chapter, the models developed in previous sections 3.3 and 3.4 are integrated in two different NBA optimisation frameworks that maximize the profits of the system. The first aims to emulate the real-case scenario of the Call for tenders for the Non-Interconected Zones published by the Energy Regulation Commision (AO ZNI) 2015 for a single storage and vRES system, and the second follows a LV load network with multiple

BESS and a vRES. The cost of energy and remuneration in both frameworks was estimated, and the impact of the integration of the different models was measured. This aims to illustrate the financial and long-term impact of not explicitly considering the thermal behaviour of the BESS, as well as the risks and deviations of considering the factory-issued performance parameters for the earning estimations in the life of a hybrid project.

The main contributions can be summarised as :

— Two open-source based optimisation frameworks that incorporate the intra-day operational temperature
— BESS thermal impact analysis in scheduling applications for load response systems.
— Exploration of the degradation and thermal impact on flexibility scenarios.

The developed optimisation framework and results will be discussed in the following sections. First, the optimisation frameworks and specific constraints for the use-cases of interest will be presented in section 4.3. Afterwards, the results of these frameworks when applying the advanced LiBESS models is shown in section4.4. At last, a conclusion and discussion of the optimisation results is presented in 4.5

4.3 Optimization Framework

The general optimisation problem can be defined as a set of decision variables x we wish to determine to minimize an objective function f while respecting a set of constraints [194]. This can be translated into the formulation seen in (4.1).

Depending on the nature of the objective function or the constraints, the problem can be categorized as a Linear Problem (LP), Non-Linear Problem (NLP), Mixed Integer Linear Problem (MILP) and Mixed Integer Non-Linear Problem (MINLP). An LP problem is, as its name suggests, a problem for which the objective function and constraints follow a linear form. When having any non-linear variable (e.g., square, e, log), the problem is categorized as NLP. If in any of these two scenarios a binary variable is needed, then the problem receives the Mixed Integer prefix (MILP, MINLP). Depending on the complexity of the problem, modern solvers are able to find global or local minimum. In addition, several reformulations can be used to transform certain subset of problems into simpler forms [1] that are able to converge.

1. Leo Liberti in [194] did a comprehensive review on reformulations for mathematical programming problems used in optimisation frameworks. An in-depth view of such reformulations can be found in [195, 196].

$$\min_{x} \quad f(x) \tag{4.1a}$$

subject to :

$$g_i(x) \leq 0 \quad \forall i \leq m \tag{4.1b}$$

$$L \leq x \leq U \quad \forall x \tag{4.1c}$$

$$x_j \in \mathbb{R} \quad \forall j \in \mathbb{Z} \tag{4.1d}$$

For the case of hybrid centrals or hybrid local networks, structuring the problem in this formalism requires to identify and translate the possible power flow interactions (see figure 4.1 for the general case). This system can by represented by equations (4.2) - (4.5), in which the direction of power was set from the energy producer perspective : positive (+) when the power goes from the generator element to the grid, and negative (-) otherwise. The general constraints are that the load L can't have a positive value as it is not a generator element, and the solar resource S behaves exclusively as a generator. Both the grid and the associated storage can behave as both.

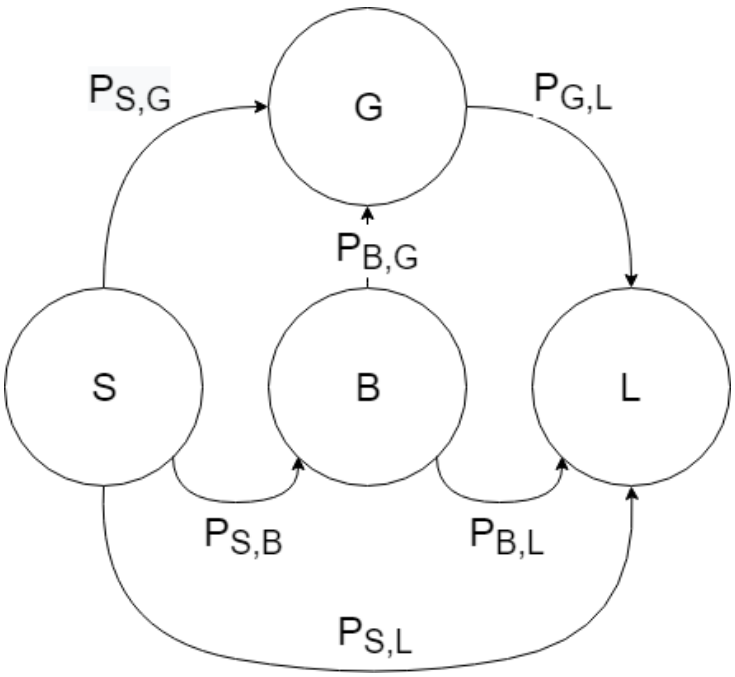

FIGURE 4.1 – Power Flows present in a LV network grid G with a load L, an energy storage B, and a solar resource S.

$$P^G = P^S + P^B + P^L, \qquad P^G \in \mathbb{R} \tag{4.2}$$

$$P^S = P^{S\to B} + P^{S\to G} + P^{S\to L}, \qquad P^S \in \mathbb{R}_{\geq 0} \tag{4.3}$$

$$P^B = P^{B\to G} + P^{B\to L} - P^{S\to B}, \qquad P^B \in \mathbb{R} \tag{4.4}$$

$$P^L = -(P^{G\to L} + P^{S\to L} + P^{B\to L}), \qquad P^L \in \mathbb{R}_{\leq 0} \tag{4.5}$$

The objective function was defined depending on the specific scenario, and the constraints imposed to it will be discussed in the next subsections.

4.3.1 Solar model constraints

The solar production P^S is dependent on the solar radiation and the installed inverter rating. As such, we can distinguish different solar profiles that encapsulate the behaviour under different weather scenarios. The good (a), average(b) and ugly(c) weather profiles used can be seen in figure 4.2, and represent the power input $P^{S,in}(i)$ in the optimisation framework.

When modelling the solar resource behaviour, the only limiting factor is the instantaneous available solar resource $P_i^{S,in}$. If curtailment is accepted for the vRES plant, then the notions of exploited ($P^{S,out}$) and unexploited (P^{S*}) solar resource are introduced to quantify the solar performance. These solar constraints can be seen in (4.6).

$$P_i^{S,in} = P^{S,in}(i) \quad \forall i \tag{4.6a}$$

$$0 \leq P_i^{S,out} \leq P_i^{S,in} \quad \forall i \tag{4.6b}$$

$$P_i^{S,out} = P_i^{S,in} - P_i^{S*} \quad \forall i \tag{4.6c}$$

As there is no uncertainty management in the PV production nor the optimisation framework, the three solar profiles offer the best behaviour possible given a specific production.

4.3.2 BESS model constraints

Unlike the solar resource that is naturally limited by the solar irradiation, or the grid that is an infinite [2] power source/sink, the BESS model has to include an SoC estimator to determine its capacity to absorb and inject energy. The other limits are dependent on the power rating and current state of health.

2. For the purpose of the optimisation framework

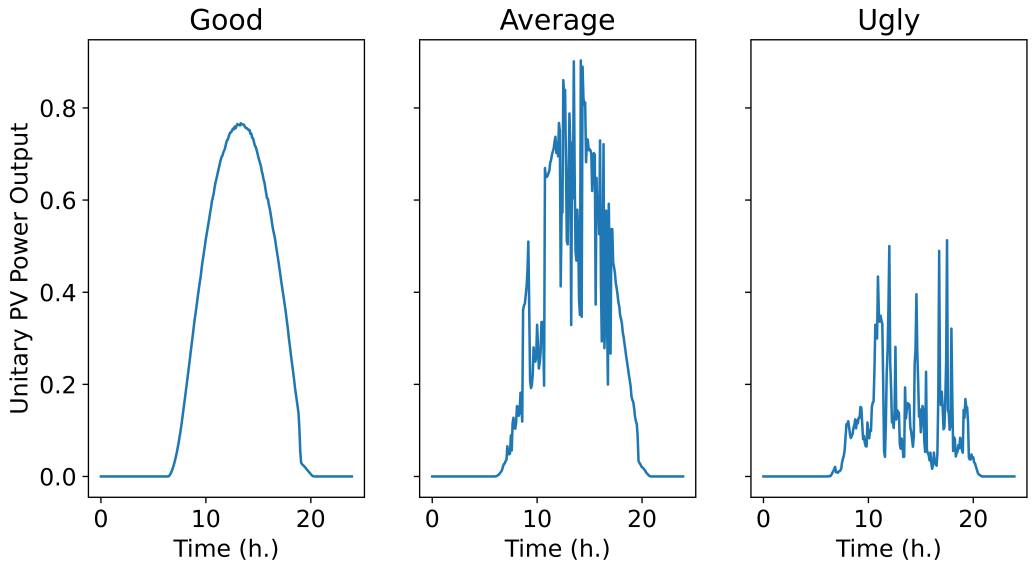

FIGURE 4.2 – Different behaviours of PV Production for a good(left), average (middle) and ugly (right) weather.

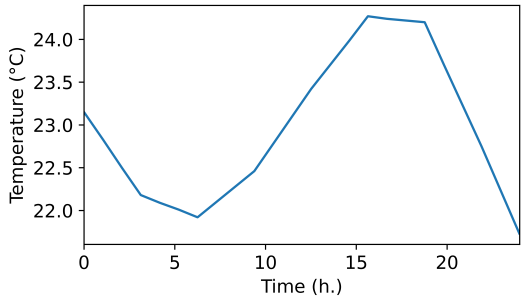

FIGURE 4.3 – Amb. Temperature in the LV Node

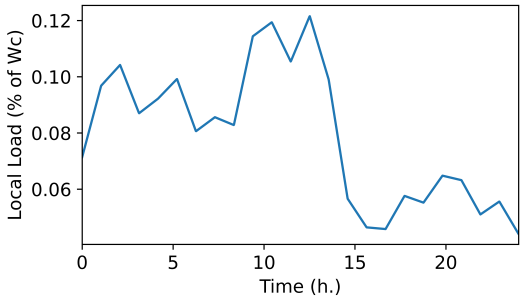

FIGURE 4.4 – Local Load in the LV Node

The model used to predict the SoC is a finite-difference version of those seen in section 3.4. To reduce the problem complexity, the non-linearity of the charge/discharge efficiency was simplified to the average value. The resulting SoC discretized model for a BESS j can be seen in (4.7) when incorporating the thermal effect. In the formulation, η_T is the thermistor self-discharge coefficient, η_P the charge/discharge efficiency, and $C_0^{B,j}$ the initial capacity in kWh.

$$SoC_{i+1}^{B,j} = SoC_i^{B,j} + \frac{\eta_T T_i^{B,j} + \eta_P P_i^{B,j}}{C_0^{B,j}} \tag{4.7}$$

For the thermal behaviour, the internal resistance was also averaged to create a quadratic thermal equation and maintain convergence for the problem. This transformed the equation (3.26) from chapter 3.3 into the expression (4.8). Here $\bar{R}_{int}^{*,j}$ and $\bar{\lambda}^{*,j}$ represent

the aforementioned average internal resistance for all SoC and the average heat exchange coefficient.

$$T_{i+1}^{B,j} = T_i^{B,j} + \bar{R}_{int}^{*,j} {I_i^{B,j}}^2 + \bar{\lambda}^{*,j}(T_{ext,i} - T_i^{B,j}) \tag{4.8}$$

$$\bar{R}_{int}^{*,j} = \int_0^1 R_{int}^{*,j}(SoC)\ dSoC \tag{4.9}$$

The formalised constraints including the physical limits of the BESS are then seen in (4.10).

$$P_{min}^{B,j} \leq P_i^{B,j} \leq P_{max}^{B,j} \quad \forall i \forall j \tag{4.10a}$$

$$SoC_{i+1}^j = f(T, SoC_i^j) \quad \forall i \forall j \tag{4.10b}$$

$$0 \leq SoC_i^j \leq 1 \quad \forall i \forall j \tag{4.10c}$$

$$T_{i+1}^{B,j} = g(T_i^{B,j}, SoC_i^j, T_{amb}) \quad \forall i \forall j \tag{4.10d}$$

4.3.3 AOZNI Optimisation Framework

As a reminder, the AOZNI 2015 capacity firming framework establishes three unique characteristics for the hybrid PV centrals that wish to operate within its specifications :

1. Schedule has to be done with a temporal resolution of 1 minute and respect rate of change limitations, as well as in a day-ahead fashion with limited changes allowed
2. Remuneration and penalty are evaluated per minute. They are calculated following the revenue and penalty equations (eq. (2.2), (2.3), and (2.1))
3. Price of energy is increased by 200€/MWh between 19 :00 and 21 :00

As a result of these characteristics particularly the first two, the optimisation framework can be considered in a two-step structure : 1) Identify the best power schedule E_i^G given a known PV forecast, 2) and determine the optimal operation P_i^G given a predefined schedule and a PV production. In both steps the objective function is defined as maximizing the revenue while minimizing the penalty. For the former case, penalty is systematically zero as it is calculated directly using the schedule. The resulting cost represents the best possible expected revenue given a forecast. For the second scenario, schedule is considered as static and penalty reduction by power control is done. As the constraints are sequential and differ from one step to the next, a specific optimization framework was built for each step (see following sections 4.3.3.1, 4.3.3.2) to reduce the problem's complexity and offer a solution for the two different use cases.

Following this, the AOZNI optimisation problem including scheduling and power control can be generalized as follows :

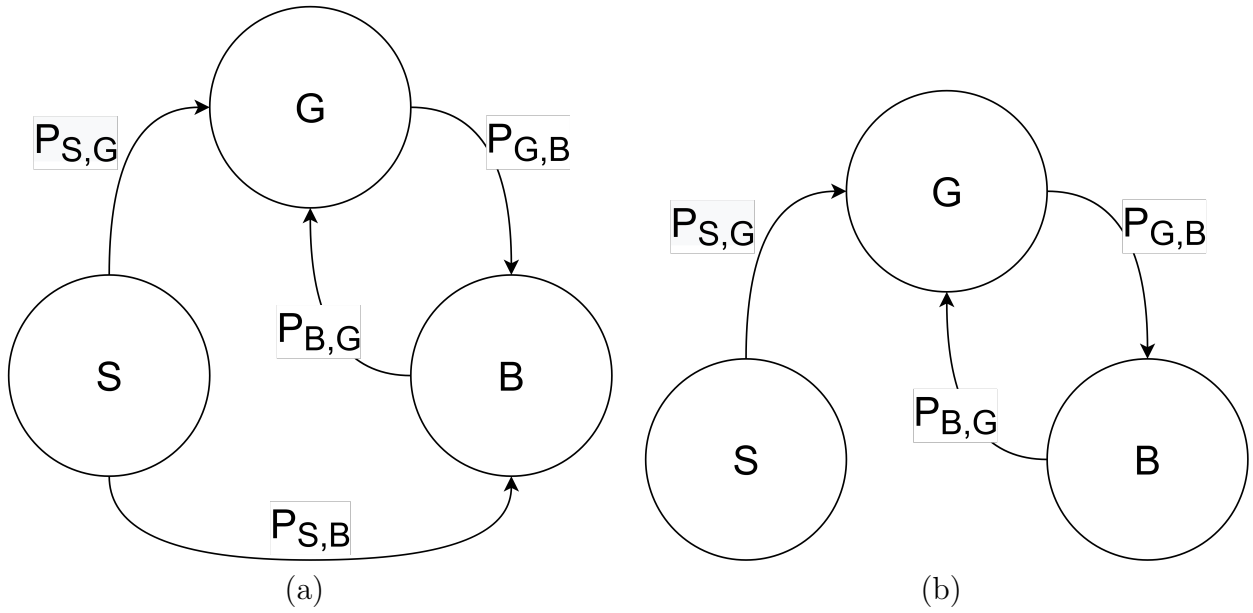

FIGURE 4.5 – Power Flow In AOZNI Framework and b) Simplified power flow.

4.3.3.1 Optimal schedule given a known PV forecast

In this case, the power engagement from the hybrid central E^G (i.e., the power schedule) is established as the decision variable. The PV production forecast is introduced as the solar production P_i^S and the specific schedule constraints are added. [3]. The formulation of this optimisation problem can be seen in (4.11).

$$\max \quad \sum \left(r_i * \left(E_i^G - c\left(E_i^G, P_i^G\right)\right)\right) \tag{4.11a}$$

s.t.

$$E_{min,i}^G \leq E_t^G \leq E_{max,i}^G \quad \forall i \tag{4.11b}$$

$$\Delta E_i^{G,-} \leq E_{i+1}^G - E_i^G \leq \Delta E_i^{G,+} \quad \forall i \tag{4.11c}$$

$$E_t^G = P_i^{S,in} + P_i^B \quad \forall i \tag{4.11d}$$

$$P_i^G = P_i^G + P_i^B \quad \forall i \tag{4.11e}$$

$$P_{min,i}^B \leq P^B \leq P_{max,i}^B \quad \forall i \tag{4.11f}$$

$$P_{min,i}^G \leq P^G \leq P_{max,i}^G \quad \forall i \tag{4.11g}$$

$$SoC_{i+1} = f(SoC_i, P_i^B) \quad \forall i \tag{4.11h}$$

$$0 \leq SoC_i \leq 1 \quad \forall i \tag{4.11i}$$

In this optimization, the cost function represents the maximal revenue possible if the PV production behaves exactly as the forecast. Given that the real production is

3. See chapter 2.4.1.1 for the full description of the schedule requirement.

unknown the moment the schedule is done, the engagements E_t are later used in the operation optimization.

4.3.3.2 Optimal operation given a known PV Production

The schedule optimization problem expressed before is a more constrained version of the one seen in this section. E^G is no longer a decision variable and is instead an input in the system. By removing all related schedule constraints and using the real PV production as P^S, we obtain the optimisation problem in (4.12).

In this framework the planned output power maximizes the revenue constrained by the enveloped defined by the schedule, and thus defines the ceiling of the performance given a specific PV production. Real-time operation has to work with the uncertainty of the future production, but it could never have a better performance than the one resulting here. This upper value can be used as an indicator unto which evaluate a deployed EMS/PMS.

$$\max \quad \sum \left(r_t * \left(P_i^G - c\left(E_i^G, P_i^G \right) \right) \right) \tag{4.12a}$$

s.t.

$$P_i^G = P_i^S + P_i^B \quad \forall i \tag{4.12b}$$

$$P_{min,i}^B \leq P^B \leq P_{max,i}^B \quad \forall i \tag{4.12c}$$

$$P_{min}^G \leq P^G \leq P_{max}^G \quad \forall i \tag{4.12d}$$

$$SoC_{i+1}^b = f\left(SoC_i, P_i^B \right) \quad \forall i \tag{4.12e}$$

$$0 \leq SoC_i^B \leq 1 \quad \forall i \tag{4.12f}$$

Objective function reformulations To ensure convergence and keep the problem solvable, a reformulation of the objective function was used. The main problem arises from the non-linearity as well as the discontinuities present in the penalty calculation.

4.3.4 LV Load Optimisation Framework - Nice Grid Scenario

The paradigm treated in this case, in contrast with the last one presented, aims to have a net power injection to the grid of zero $P^G = 0$, use the locally available resources in an efficient manner, and reduce grid congestion. The Nice grid scenario [197] embodies this intention and establishes a NBA for multiple BESS scenario, a vRES and local load, all with a single Point of Common Coupling (PCC). The interactions reflected in this framework follow those presented in figure 4.1. The multiple BESS interactions can be

seen in figure 4.5, in which interactions batteries is not explicitly expressed as it is rarely optimal. The cases in which such exchanges can be beneficial is for long term storage to reduce self-discharge and or to avoid operation under prohibited SoC.

The objective function is defined to reduce the LCOE while satisfying the local load. A cost was designed to unexploited solar resource because of two reasons : 1) curtailment increases heat generation in the PV panels and increases the risk of degradation, and 2) unexploited solar resource impacts the current revenue and lengthens the time of operation before net gains. By establishing this cost as higher than the one from BESS, we incentivize the use of the battery to create an energy reserve for horizons longer than 1 day.

The complete optimisation problem, including the thermal estimation for each BESS j as well as the power contributions per BESS by the solar resource or the grid, can be seen in (4.13).

In this use case, no voltage or frequency control is included explicitly, but the needs of the DSO can be addressed by managing the grid congestion as explained in section 4.3.4.1.

$$\text{min.} \quad \sum_{i=1}^{n} \left(€^{G} P_i^{G} + €^{S} P_i^{S} + €_i^{S*} P_i^{S*} + €^{B} P_i^{B} \right) \tag{4.13a}$$

$s.t.$

$$P_i^{G} = L_i - P_i^{S} - P_i^{B} \qquad \forall i \tag{4.13b}$$

$$P_i^{S} = P_i^{S,out} - P_i^{S \to B} \qquad \forall i \tag{4.13c}$$

$$P_i^{B} = \sum_j P_i^{B,j \to L} \qquad \forall i, \forall j \tag{4.13d}$$

$$P_i^{S \to B} = \sum_j P_i^{S \to B,j} \qquad \forall i, \forall j \tag{4.13e}$$

$$P_i^{S*} = P_i^{S,in} - P_i^{S,out} \qquad \forall i, \forall j \tag{4.13f}$$

$$P_i^{B,j} = P_i^{S \to B,j} - P_i^{B,j \to L} \qquad \forall i, \forall j \tag{4.13g}$$

$$0 \leq P_i^{S,out} \leq P_i^{S,in} \qquad \forall i \tag{4.13h}$$

$$P_{min}^{B,j} \leq P_i^{B,j} \leq P_{max}^{B,j} \qquad \forall i, \forall j \tag{4.13i}$$

$$SoC_{i+1}^{j} = f(T, SoC_i^{j}) \qquad \forall i, \forall j \tag{4.13j}$$

$$0 \leq SoC_{i+1}^{j} \leq 1.0 \qquad \forall i, \forall j \tag{4.13k}$$

$$T_{i+1}^{B,j} = g(T_i^{B,j}, SoC_i^{j}) \qquad \forall i, \forall j \tag{4.13l}$$

4.3.4.1 Flexibility integration and grid congestion management

To address the needs of the DSOs and TSOs, the NBA framework expressed before is capable to generate operation schedules that answer to the needs of the grid. The originally expressed problem is mainly a self-supply scenario where the grid covers the missing energy needs, but by adding a need for specific power at the PCC it is possible to answer to the flexibility need.

$$P_i^G = k_i \quad \forall i \in (a, b) \tag{4.14a}$$

$$P_i^F = k_i \quad \forall i \in (a, b) \tag{4.14b}$$

$$P_i^F = 0 \quad \forall i \notin (a, b) \tag{4.14c}$$

$$\text{min.} \quad \sum_i \left(€^G (P_i^G - P_i^F) + €^S P_i^S + €_i^{S*} P_i^{S*} + €^B P_i^B \right) \tag{4.15}$$

This flexibility constraint, or power requirement by the grid, was incorporated by adding the constraint and parameter seen in (4.14) and changing the objective function to (4.15). In here, the power seen by the grid at the wished period between a, b is set to a pre-known value and parameter P^F is used in the objective function to penalize any deviation from the engaged value. Otherwise, the price of injected or withdrawn energy during this period is considered free and only the cost of production is taken into account. This scenario is reasonable as the grid could ask for this flexibility as a condition to obtain the right of connection.

The two key parameters are then the power requested k_i and the time of request. By modifying these two elements, the cost of flexibility and its sensibility can be obtained. The analysis can be repeated when incorporating or not the BESS thermal dependence to obtain its impact.

4.4 Optimization Results

The optimisation problem was coded using python's open-source library PYOMO [198, 199], and the solver used IPOPT [200] is able to solve the NLP problem and find feasible local minima. The default timestep was chosen to be 1 minute for the AOZNI framework and 15 minutes for the NBA, both with a 1-day horizon as it allows to exhibit the variability of the vRES which can be softened by higher timesteps. The parameters for each BESS model including the maximal power charge and discharge P^B_{max}, P^B_{min}, can

Table 4.1 – Convection heat exchange coefficients.

BESS	#1	#2	#3	#4	#5	#6	#7
Factory η_P	92%	92%	92%	92%	96%	96%	96%
Improved η_P	90.12%	88.52%	88.55%	87.85%	83.98%	80.96%	82.58%

Table 4.2 – Convection heat exchange coefficients.

	LiBESS #5	LiBESS #6	LiBESS #7
η_T	-2.44$x10^{-8}$	-1.18$x10^{-8}$	-1.52$x10^{-8}$
$\bar{R}_{int}^{*,j}$	-5.93$x10^{-7}$	4.03$x10^{-7}$	4.81$x10^{-7}$
$\bar{\lambda}^{*,j}$	1.12$x10^{-3}$	6.77$x10^{-4}$	9.85$x10^{-4}$

be seen in table 4.1.

Both optimisation frameworks were evaluated with the three weather scenarios, and the ambient temperature used was the same for all the cases (fig. 4.3) The more relevant results are presented in the following sections.

4.4.0.1 AOZNI Framework

As discussed, for each of the 3 weather patterns in section 4.3.1 we can associate a PV production forecast issued by a third-party forecaster the day before. This forecast allows to generate the power engagement required by the DSO and fixes the amount of benefit the hybrid power plant will have for the next day. Given this condition, we can distinguish three results of interest :

1. Optimal revenue and schedule if the forecast is 100% accurate.
2. Optimal revenue with vRES production and a predefined schedule.
3. Optimal revenue and schedule given the vRES production.

The scenarios were done for the four different site configurations of the sites in chapter 2.4 section 2.4.1.1. The BESS were set to have an initial state of charge of 0% . The expected revenue for each configuration with the factory-issued parameters can be seen in figure 4.7 [4] The 4.6, and the specific schedule, BESS profile, PV output and injection for one of these sites can be seen in fig. 4.6 on page 146.

As it can be appreciated through these results, the benefit of a high knowledge of the real PV production is most valuable when the weather has low variance (good and

4. See annex E for the tables with the exact results.

ugly weather) and the total energy difference is the driving factor for the revenue. In the scenario with a very high variance (second line in figure 4.6), there was no significant advantage to tailor a schedule to this production.

When including the trained SoC model's parameters, we could observe an average decrease in revenue of 1.28% for the portfolio. This is coherent as the results in chapter 3.4 showed a weaker charge/discharge performances for three out of four sites.

4.4.0.2 NBA algorithm

The NBA scenario used 3 BESS for whose characteristics can be seen in table 4.3. The initial state of charge was set different for each BESS (75%, 50%, 25%) but the external temperature was the same as a LV grid is geographically small and no significant weather changes are to be expected. The load to meet at the PCC remained also unchanged between executions (see figure 4.4).

TABLE 4.3 – Charge/discharge performance parameters.

	LiBESS #1	LiBESS #2	LiBESS #3
η_{cha}	-0.9576	-0.9592	-0.96
η_{dis}	-0.877	-0.8441	-0.8603

The LCOE per energy source in (4.15) was set as follows : 40€/MWh for the grid ($€^G$) , 7€/MWh for the vRES ($€^S$), 14€/MWh for unexploited vRES ($€^{S*}$) and 12€/MWh for the BESS ($€^B$). These prices were chosen to do the two functions mentioned in section 4.3.4 : incentivize the use of local power production, and to favour the storage of energy when a surplus of solar resource is available.

The optimisation problem was solved for the 4 different weather cases [5] and after execution, the total cost of energy was analysed when including or not the added cost of degradation for the storage. This last one was defined as the lost capacity of the battery without including the conversion system, in this case set at 505.46€/kWh, and was evaluated after determining the best possible power profile for each production equipment. The cost of energy per scenario, with figure 4.9 (in page 148) showing the different profiles per equipment that the NBA optimisation algorithm finds as optimal solution.

When introducing the thermal component to the BESS models, a general increase in cost was observed thanks to the higher self-discharge. The average cost increase was of 0.11%, with table E.3 in annex E detailing the specific cost of energy observed for each case. The three BESS with the NBA algorithm with thermal consideration was shown to

5. As a reminder, these are 1) Forecast, 2) Good Weather, 3) Average Weather ; and 4) Ugly Weather

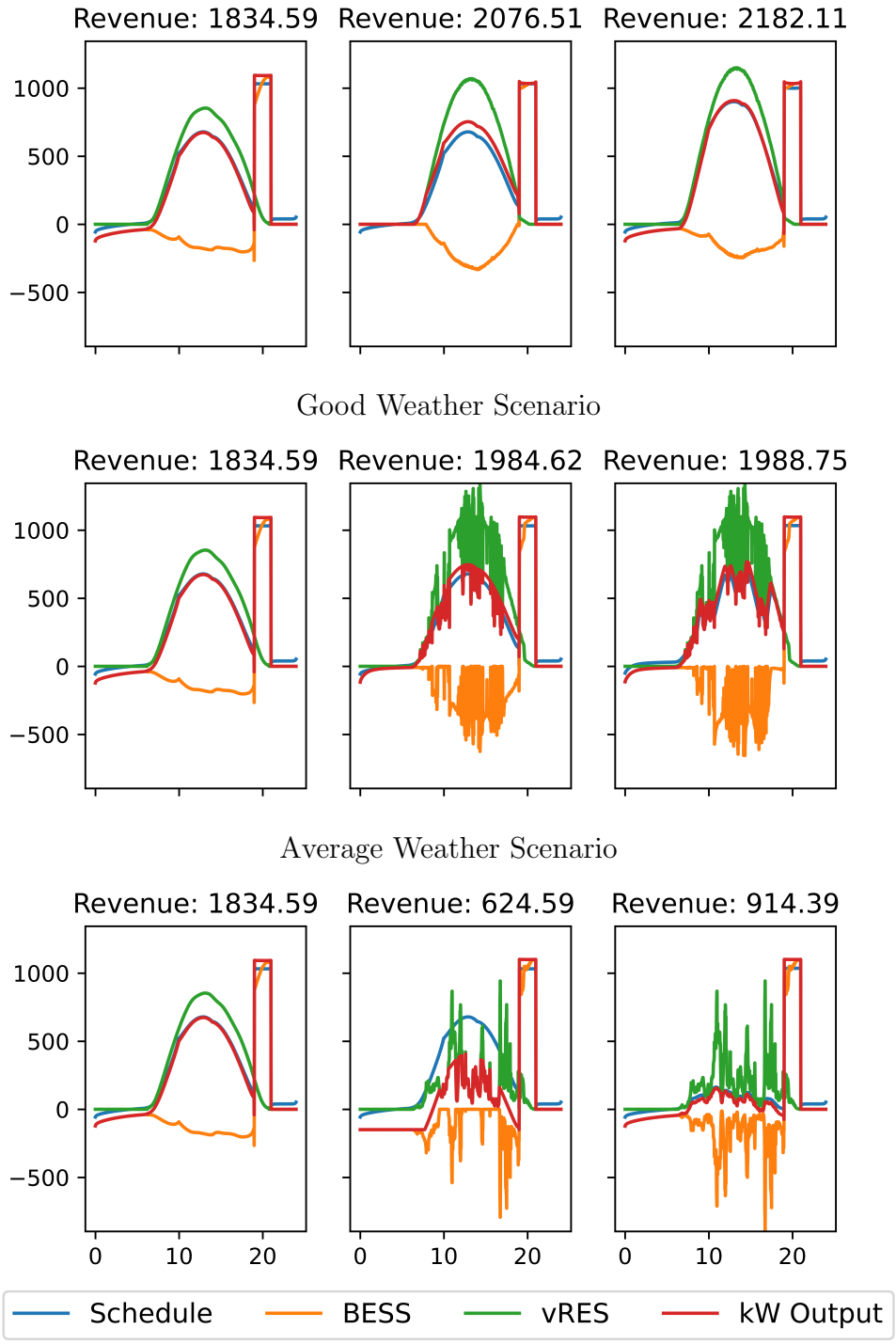

FIGURE 4.6 – Different results from the AOZNI optimization scenario. The left column optimizes the plan given the forecast (same for all cases), the middle column optimizes the injection given the previous schedule and the real vRES production, and the right column optimizes both the schedule and injection to maximize profits given the production.

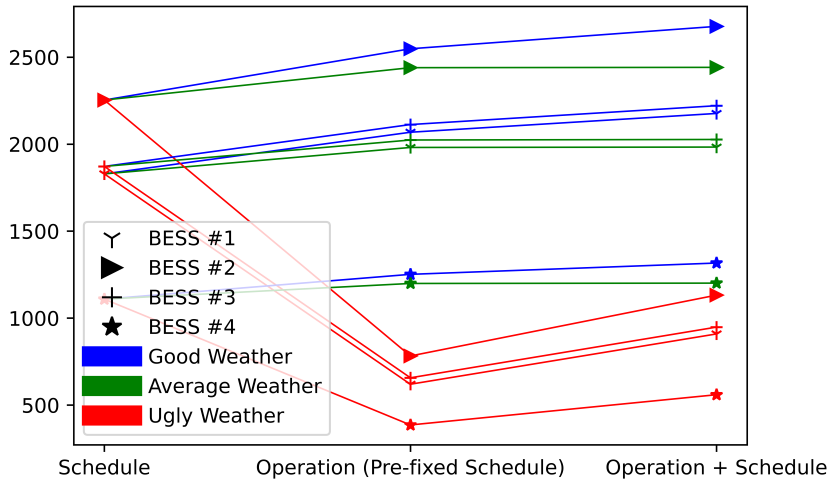

FIGURE 4.7 – Revenue evolution for each site and each weather scenario with the factory issued BESS parameters.

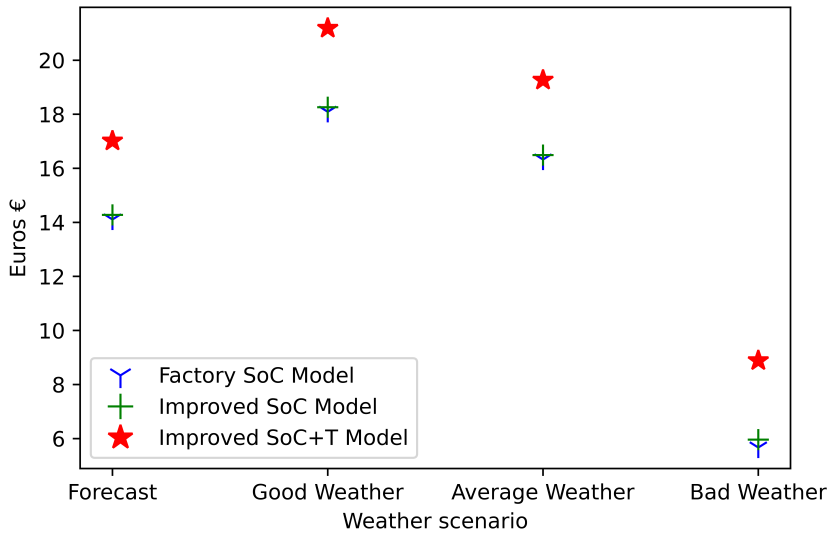

FIGURE 4.8 – Cost of Energy to satisfy the local load depending on the type of weather and BESS model used in the NBA algorithm.

follow a more relay-like behaviour (fig. 4.10), i.e., power usage was not simultaneous unless strictly necessary. This behaviour can be explained by the BESS efficiency decreasing at higher temperatures, and as consequence the charge stops to let the BESS relax and reach the minimal temperature possible (the ambient temperature).

BESS Degradation. From the resulting power profiles, the number of total cycles was quantified and introduced into the degradation model previously mentioned. The accumulated degradation from the three BESS was found to increase compared to the case using only the factory performance in the BESS model (see table 4.4). Including the thermal

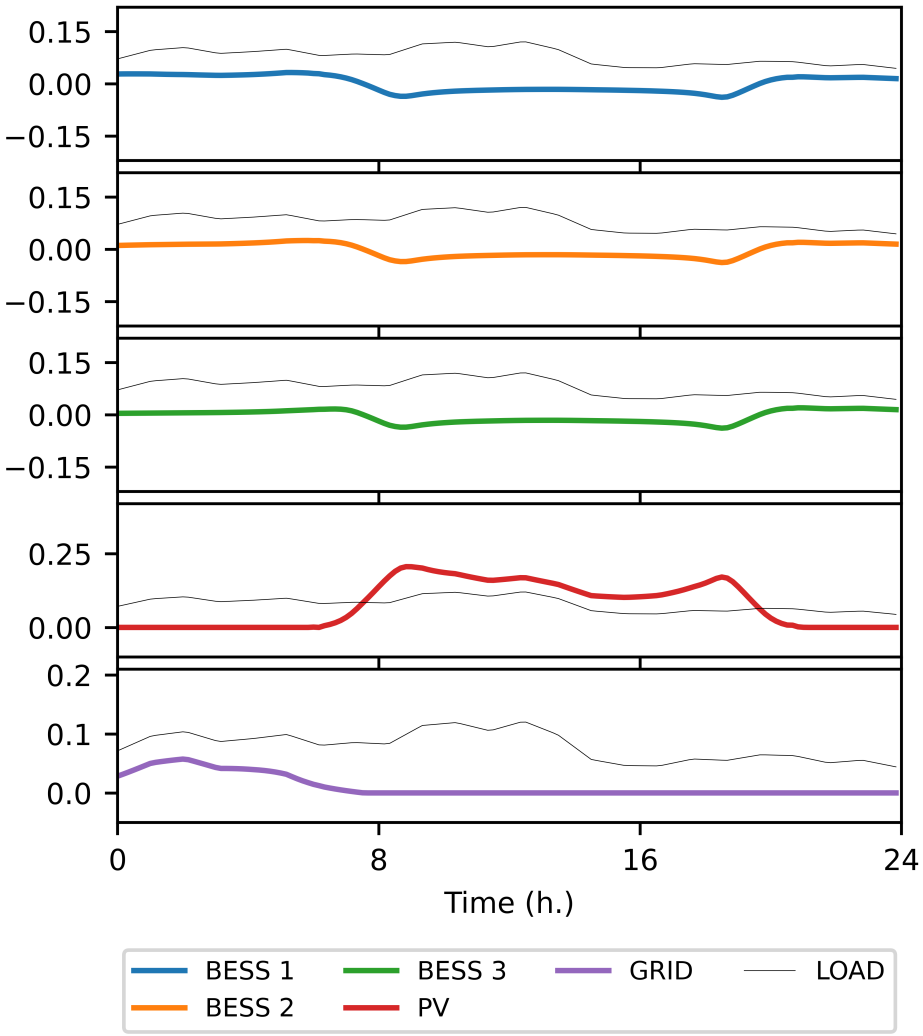

FIGURE 4.9 – Predicted power contributions per energy source for the load by the optimisation framework.

component did not change this trend, but it softened it as the expected capacity loss was 0.5%, 0.25% and 0.01% less than the power-only parameterized SoC model.

One reasonable explanation for the last values mentioned is the decrease in net energy that flowed through the storage. This naturally decreases the degradation as total energy throughput usage is the main driving factor. Warranties of recent batteries also use this metric as reference, as modern BMS greatly reduce the influence of micro-cycles or DoD.

Flexibility Cost. When evaluating the cost of flexibility, both excess offer and demand are considered. The parameter k was defined as a percentage of the installed vRES injection power (-1.0, 1.0) as it is assumed the LV node can withstand *at least* this amount of power. The duration was set to 1 and 2 hours, and the time of flexibility request was set

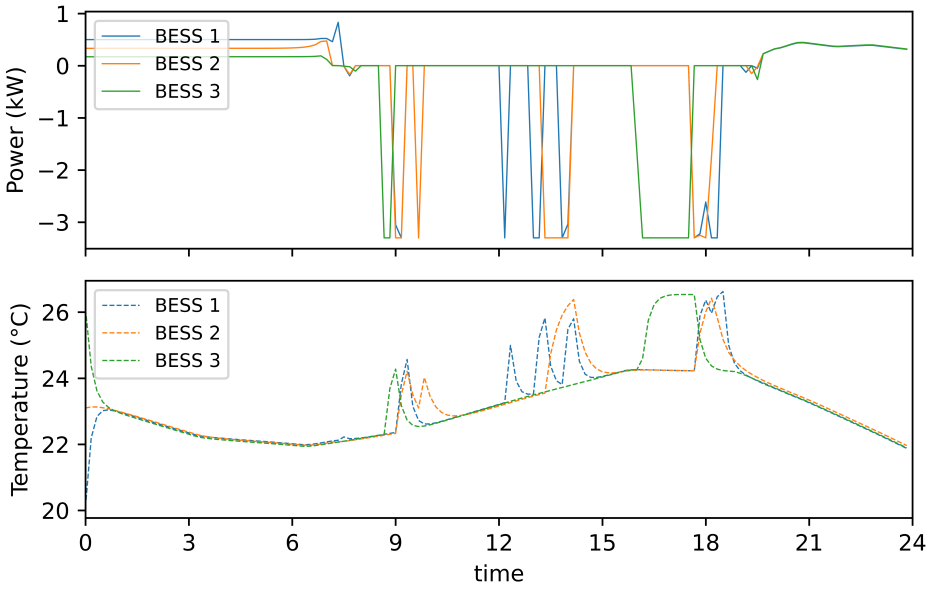

FIGURE 4.10 – Predicted power contributions per BESS and expected internal temperature when a surplus of vRES is present. BESS behaviour is not synchronous as it is not needed by the grid.

TABLE 4.4 – Cumulated SoH Loss change by weather and BESS model for a 1-day horizon. Less is better.

Day	Factory SoC (% of C_0)	Improved SoC (change %)	Improved SoC + T (change %)
Good	1.75×10^{-4}	+4.91%	+4.58%
Average	1.71×10^{-4}	+5.02%	+4.64%
Ugly	1.73×10^{-4}	+1.71%	+1.99%

in the morning (8 a.m.), in the middle of the day (12 p.m.) and lastly at the end of the day (7 p.m.). The three different hours are meant to represent the classical consumption scenarios of people arriving at work, lunch time, and the peak consumption after work.

The resulting energy cost was compared to a 0 kW power request by the grid using the factory performance. The cost increase followed the same behaviour between the improved SoC model and the SoC + °C, with a slightly higher increase in the latter. Nevertheless, this average cost increase was less than 0.1%. When including the cost of BESS degradation in such calculation, the increase was only slightly reduced (δ0.001%). Figure 4.12 shows the cost increase given the flexibility requested by the DSO in the different scenarios and with the different BESS models. The weak impact from the operational temperature can be observed in these figures.

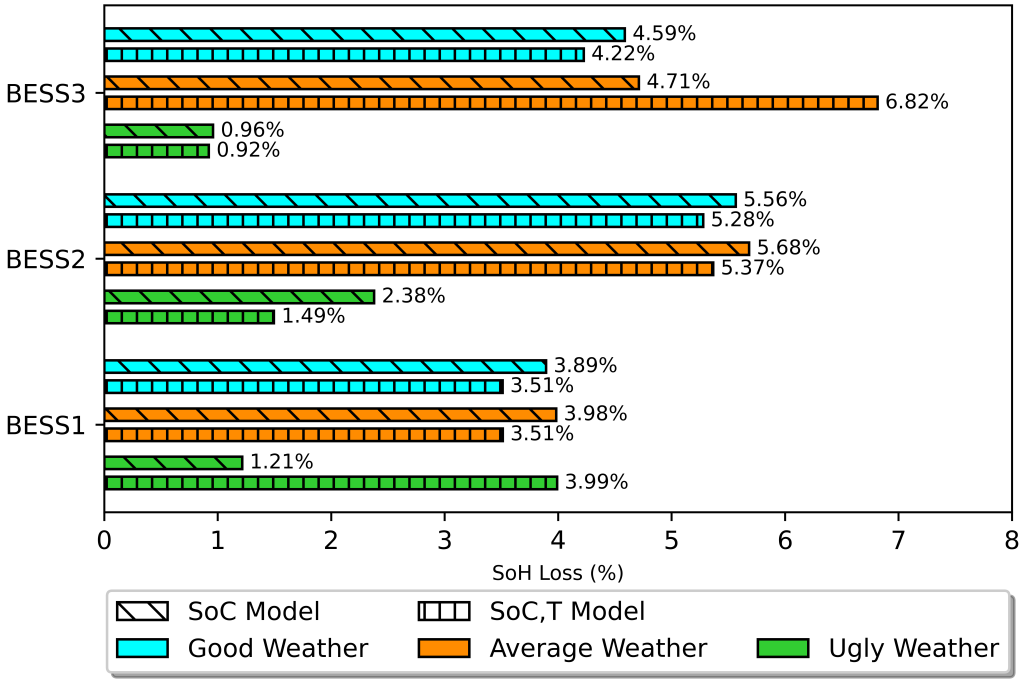

FIGURE 4.11 – SoH Loss per BESS in the optimisation problem when using different SoC models and in different weathers.

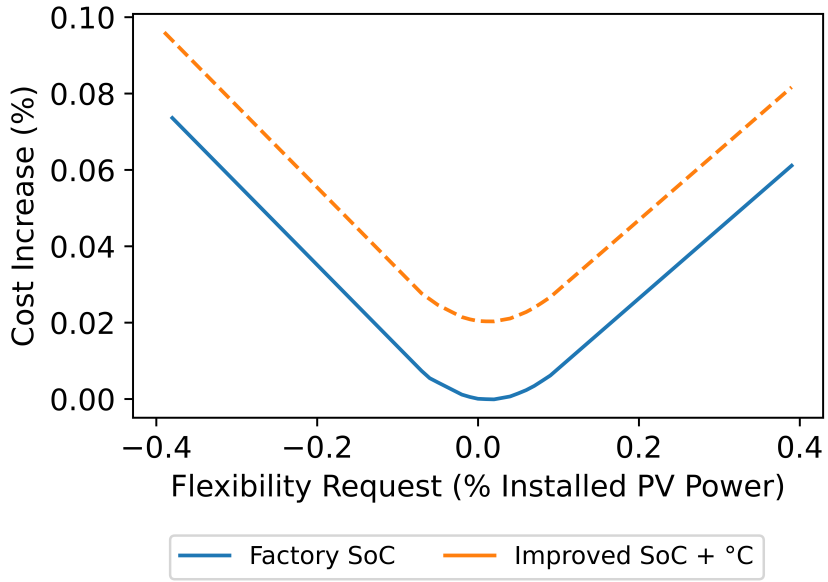

FIGURE 4.12 – Increase (in %) of energy cost when imposing a flexibility constraint with different storage models

4.5 Conclusion and Discussion

In this chapter, an optimisation framework based on open-source solutions was developed to determine the best possible schedule and operation for PV plants with adjacent

BESS for two different scenarios : the AO ZNI capacity firming framework of 2015 in which a power injection engagement is needed and earnings are calculated given the real power production deviation from such values, and a LV grid node with a vRES and several BESS nodes in which the objective is to reduce the total cost of energy while satisfying the local load. The different BESS models trained and developed in precedent chapters using real operational data from 5 different hybrid plants were incorporated in these frameworks and the resulting expected revenues and/or LCOE were analysed depending on the depth and precision of the integrated models.

For the AO ZNI scenario, the operational temperature of the BESS was not initially included, and only the integration of the improved SoC models against the factory values was studied. The maximal possible revenue for all weathers decreased by an average of 1.31%, and the average optimal operation given the optimistic forecast showed a similar decrease in revenue of 1.48%. The bad weather scenario showed the worst impact from the improved BESS as it reduced the expected revenue of 2.81% given the forecast.

It is also possible to appreciate the reduced financial impact that deviation from the factory BESS performance has in the AO ZNI framework. Although the error on the SoC by the model was reduced by 3 points, the loss in maximal revenue was only of 1%. The efficient use of the storage, in addition to the large margin of error allowed in the capacity firming framework, reduces the overall impact this deviation has in the final financial performance. Given a more constrained environment with less accepted deviation before penalties, or an increase in penalty price, the impact is expected to be accentuated.

For the LV node optimisation framework, the LCOE to satisfy the local load was defined as the objective function to optimize, and the impact of the different BESS models was studied as well. The increase in energy cost when using the improved SoC instead of the factory issued model was of 1.97%, and including the thermal dependence to the SoC further increased the cost of 0.06%. If the BESS degradation is taken into account given the power profiles expected from them, the cost compared to the base case without degradation rose to 2.079% without temperature and to 2.138% with it.

The impact different weathers had on the costs were also analysed. Naturally for the average and ugly weather scenarios, the cost was systematically higher as either more vRES production had to be curtailed or missing energy had to be completed by the grid. Complementary, a good weather profile reduces the cost as the vRES production is the least expensive energy source in the scenario. The cost increase related to the BESS model remained in the same range as before except for when the weather was harsher. Here the use of the operational temperature dependence increases by 1% the total cost. Noteworthy

is however how the BESS degradation slightly reduces the impact of the improved battery models. The cost increase is between 0.05% and 0.3% *less* when compared to base model if it includes the capacity loss.

When the cost of flexibility under the same constraints and scenarios was evaluated for both grid power injection and withdrawal, the average cost increase was of 0.211% per each grid absorption request of 1% the vRES installed capacity. For a grid injection request this value was of 0.167%. The impact of the thermal consideration changed these cost increase rate to 0.20% and 0.184%, but the degradation's impact was very negligible as before.

From the different results discussed it is possible to appreciate the importance of integrating an upgraded SoC model behaviour in optimisation and scheduling frameworks. The 1% decrease in revenue (or increase in LCOE) due to the more realistic charge/discharge efficiency is a parameter not negligible for hybrid vRES centrals. Often business plans for these kinds of project foresee an ROI after at least 10 years, and overestimating revenue stream in the pre-construction phase exposes the project to financial difficulties and uncertainty. As the time needed to recover from the initial investment is increased, the possibility of equipment malfunction and operational related costs increases. Even if such business plans foresee a leeway of 5%, this safety prevision is diminished right from the start when such considerations are not weighed in.

The same conclusion however cannot be said about considering the operational temperature in the BESS model. The financial impact of an additional 0.05% decrease in revenue is not insignificant, but it is small compared to the impact of the improved SoC model alone. The operational time needed to compensate the lost revenue for a 20 year horizon project is less than a week, and doesn't represent a strong financial argument unless the size and expected revenue of the concerned installation is big enough [6]. If such financial precision is not needed, the results suggest that the added value of this parameter is very limited as it also implies an increase in computational effort due to the non-linearity of the temperature.

Nonetheless, it is important to remind that the timestep evaluated was relatively large compared to the behaviour of the vRES of choice. A finer timestep would force the BESS to experience more sudden power demands, and the impact from the thermal behaviour could increase as a consequence. Other use case scenarios with more constrained power requirements or a stronger vRES variability could be explored to discover the threshold

6. E.G. an AOZNI constrained plant of 15 MWc would miss around 45k€in the lifetime of the project (20 years), in which case the absolute amount of revenue represents a significant amount.

at which the thermal component's impact becomes stronger. Future works could be based in this unknown, as well as in the capacity sizing component which would also impact the temperature as C ratings would change for the same requested power.

Chapitre 5

Conclusions

Résumé en français

Le chapitre 5 résume les contributions clés de la thèse, offrant une vue d'ensemble des résultats obtenus et des perspectives futures pour la recherche et l'application des systèmes de stockage par batteries lithium-ion.

Les principales conclusions incluent l'efficacité des modèles unifiés développés pour l'estimation simultanée du SoC, du SoH et de la température, ainsi que leur applicabilité dans des environnements industriels et de micro-réseaux. Le chapitre discute également de l'impact financier de la gestion thermique et de la dégradation sur les opérations des LiBESS, démontrant comment ces facteurs influencent les coûts et la viabilité des projets de stockage d'énergie.

Enfin, les recommandations pour les travaux futurs sont présentées, suggérant des pistes pour améliorer les modèles existants et explorer de nouvelles applications des LiBESS dans les réseaux électriques intelligents.

5.1 General conclusions

Chapter 1 introduced ESS in the context of vRES applications, and how they are essential to achieve and sustain the vRES penetration needed in the energy mix if environmental goals of CO_2 reduction are to be achieved. Electrochemical energy storage solutions, in particular lithium-based, possess advantageous characteristics that allow the DSOs and TSOs to build services and frameworks which reduce the negative impact intermittent energy sources can have on the electrical grid. One of these frameworks, and the pivotal subject of these thesis , is the capacity firming of photovoltaic power plants (PV

Capacity Firming). In these, the global availability, or capacity, of the PV power plant is increased through the guarantee and smoothing of the output power via the usage of LiBESS.

PV capacity firming sites are however not very common. The need for such operating and regulatory frameworks is more prominent in medium- to small-sized electrical grids. In these, the resiliency of the grid is small compared to a continental grid and it is easier to have a higher share of renewables. A natural consequence of this is the lack of hindsight regarding the performance, behaviour, and longevity of the associated LiBESS. This weak understanding is exacerbated by the fact that lithium-based BESS are still a fairly recent technology for many domains in which their presence was unusual due to the high costs they used to represent. It is under this novelty and uncertainties revolving around LiBESS that the need for models tailored for the new applications arises.

From the review of the existing literature, it was possible to distinguish two sets of questions linked to missing knowledge. The first set is related to the industrial needs and interrogations around integrating LiBESS for vRES projects, whilst the second set revolves primarily around the research gaps. The industrial questioning (IQ) can be summarised then in the following :

IQ1 : How can a BESS be modelled in a way that is both easy to deploy in vRES industrial systems and accurate enough to embed within the control applications ?

IQ2 : How can a BESS model be used to optimize the financial results of vRES power plants ?.

For the identified research gaps, the questions (RQ) they incite are :

RQ1 : What, if any, is the impact of the thermal behaviour on large-scale LiBESS and what is a suitable method for thermal modelling for such systems ?

RQ2 : How much do complete LiBESS models can be trusted knowing most related modelling literature is built for an individual cell or a single battery pack ?

RQ3 : What is a suitable alternative to data-driven LiBESS models when data is scarce and in pre-deployment stages ?

RQ4 : Does LiBESS ageing behaves differently due to their integration in vRES capacity firming applications ?

RQ5 : What is the impact of operational conditions (temperature, power profile, equipment maintenance and replacement) on the reliability of the ageing models for LiBESS ?

Following the industrial and research questions identified in the state of the art, the general objective can be distilled and formulated to address them. This objective is then to provide LiBESS models of key parameters which are fit to be used in industrial applications (especially for PV capacity firming scenarios) and that are able to be integrated in control systems both at pre- and post-production stages of the sites to evaluate past, present, and future performances.

With this previous objective in mind, in Chapter 2 the vRES capacity firming framework of interest in this thesis, a PV capacity firming scenario designed for the French Islands, was presented. The development and the construction of a PoC site and four industrial PV+BESS sites under this framework was needed to obtain real data about the LiBESS behaviour under these circumstances. In addition to the data collected, this provided the insight needed to address Research Question 3 in further chapters as the constraints of such environments were met first-handed and incorporated in the thought-process involved.

The modelling of the LiBESS, treated in Chapter 3, was built upon three cornerstone parameters for any management system in which LiB are part of (e.g., BMS, EMS, PMS). The thermal behaviour of the studied LiBESS proved to be a challenging topic by itself, as it is difficult to have temperature measurements on commercial large-scale LiBESS. Such kind of systems are not required to publish all their internal measurements to the end-user, with the additional constraint that most are closed climate-controlled systems in which any external sensor voids the warranty. Using the temperature measurements from the compatible BESS (i.e., those that publish the LiB operational temperature), a thermal estimation model and approach that is more easily compatible with large-scale LiBESS is proposed. In addition to the reported temperature, by using only the DC current and ambient temperature, two parameters that can be independent from the published data by the BMS [1], it was found to be possible to estimate the internal temperature within an acceptable margin of error. Even if this error on the temperature estimation seems important, it can be used as reference to avoid thermal danger zones and to estimate other temperature dependant parameters in more complex systems.

The second section of the chapter saw the development of a SoC model for the LiBESS. The approach presented prioritizes only the AC measurements easily accessible in any BESS system. It is also able to incorporate a thermal dependence through a self-discharge element in the EC when the data and thermal model is available, which improves the

1. Ambient temperature sensors and, if DC current is not reported, use of the AC power measurement to estimate it via the LiB nominal voltage.

accuracy of the SoC estimation and addresses Research Question 1. The estimation of temperature had a stronger impact on the SoC than the other way around and, thanks to their relatively simple modelling approach, the co-estimations and integration of both in embedded systems is achievable.

The subject of assessing the LiBESS ageing, i.e., SoH estimation, was treated at the end of this chapter. A model based on calendar and cyclical ageing was proposed to follow the real behaviour of the observed industrial LiBESS more closely. The model proposed takes advantage of the regularity in operation and cycles expected for BESS under the foreseen capacity firming scenario. It also benefits from the fact that commercial industrial LiBESS offer, in one way or another, a capacity indicator which is the only real requirement of the modelling approach here presented. Through the observed degradation and SoH model results, it was observed how the expected degradation from LiBESS is less extreme than the accepted degradation by the manufacturer. PV capacity firming scenarios under the AO ZNI 2015 framework impose less strain on the LiBESS systems, which can be a key element to include in business plans for newer projects and shines light upon the Research Question 4.

In the three models for LiBESS here developed, these were the results of the adaptation and reworking of the modelling approaches applied to single LiB cells, which by their relative simplicity answer the needs of industrial sites (Industrial Question 1). In response to Research Question 2, it is remarked that the approaches differ mainly due to the nature and granularity of the physical measurements available. A direct application of most reported modelling frameworks for LiBs need to be interpreted with a whole system perspective, and either equivalent or proxy parameters have to be used to substitute unavailable data which is ordinarily obtainable through specialized characterisation equipment.

Chapter 4 saw the application of the LiBESS models developed and validated in the previous chapter in order to study the impact they could have on the operation of vRES power plants in both short- and long-term. To achieve this, an optimal scheduling and operation framework for AO ZNI 2015 PV capacity firming sites was developed. With the objective of maximizing the revenue from the sites given some known vRES production forecast, the optimisation framework generates an expected power, SoC, and temperature profile for the LiBESS. By changing the LiBESS model embedded in the optimisation framework, from one based on the LiBESS datasheet to the one developed in this work, the expected revenue was influenced accordingly and afterwards reviewed. This highlighted the importance of post-deployment assessment of the LiBESS performance due to the non-

negligible revenue deviations when using the manufacturer base specifications against the latest parameters found.

In the same chapter, the optimisation framework was also adapted to a microgrid in which a vRES (PV) and multiple LiBESS participate to satisfy the local load and reduce the consumption from the grid. This framework, referenced as NBA due to the coordination of multiple batteries, also incorporated a flexibility requirement which helped to quantify the extra cost such demand would have for the grid. In the same logic as before, the focus of interest was on the cost increase from using the improved LiBESS compared to a generic model. Through these two optimisation frameworks and the implementation of the LiBESS model, the Industrial Question 2 and the Research Question 5 were addressed. The framework allows to selectively include parameters in the LiBESS models, which permits to evaluate the influence of each one of them in the ending financial result and the expected degradation from the different LiBESS. The thermal influence for instance, even if it does reduce the error on the SoC estimation, was seen to have a very minor impact on financial results in both scenarios. The change in degradation due to the improved SoC model and expected energy throughput was weak too. These results encourage the final implementation to avoid these calculations unless they are explicitly required for other processes and/or the external conditions are harsh (e.g., unusual high/low ambient temperatures) and thus it is needed to avoid specific operation temperatures.

5.2 Analysis of contributions

From this thesis, the contributions from the inquiries done in the Research and Industrial Questions can be identified as the following :

Increase the dataset of LiBESS in operation under industrial constraints.

The vast majority of LiBESS data for modelling comes from laboratory setups in which only cells or packs are addressed. The whole LiBESS system is seldom treated and as consequence little data from their behaviour is available. Although these industrial datasets could be tainted due to the unavoidable BMS [2] which can filter and hinder the operation on certain ranges, they still provide valuable insights on the LiBESS.The constraints in measurements available, their resolution, and their range of operation embedded in the dataset allow for models to consider part of the underlying logic of BMS.

LiBESS models compatible with industrial constraints.

The models proposed and trained in this work all answer to the data limitations that

2. Always present for safety reasons.

can be found on large-scale LiBESS deployed in vRES applications. They are lightweight and can be parameterised with ease after the initial deployment without the need of specialized characterisation protocols or equipment. Co-estimation of these is also possible and relatively straightforward when the required data is available. The simplicity of the models makes them to be also a good fit as embedded models in supervision systems.

PV capacity firming and multi-LiBESS LV microgrid optimisation frameworks with flexibility requirements.

The optimisation scenarios presented in this work, in particular the AO ZNI 2015 framework, belong to a set of problems for which few literature exists and their representation within an Operational Research (OR) lens is limited. The frameworks here presented serve then as a stepping stone on which further analysis can be done through the refinement of the LiBESS model, the vRES source, and/or the inclusion of multiple energy sources.

Insights on the impact of thermal co-estimation on LiBESS models in deployed applications.

Through the optimisation frameworks and the LiBESS models, it was found that the increase in accuracy due to the thermal co-estimation had a very low impact on the final financial results including the case of the cost of flexibility. Optimizing the power profile by considering the temperature decreased the total energy throughput and thus degradation was slightly lower, but it required a more intense usage which can create equipment malfunction more easily due to the mechanical stress. This without mentioning the fact that the computational effort of thermal co-estimation is important, and in embedded systems the slight margin of improvement does not seem worth it compared to the extra load.

5.3 Perspectives

Several future research opportunities are possible when departing from the building blocks exposed in this work. A brief description of them is given below.

Determination of power conditions for augmented thermal influence on the LiBESS performance.

Given that the influence of thermal consideration in SoC had a weak impact in the use-case scenarios studied, the question of determining the operational constraints in which this influence starts to become non-negligible becomes more prominent. Through more demanding scenarios, e.g., one in which the LiBESS is under-sized, one could expect the system to charge and discharge at higher C. This could generate temperature scenarios in

which the thermal effect considerably degrades the total energy expected from the system whilst in operation. Otherwise, if the LiBESS is applied to a different use case such as primary frequency response, this kind of scenarios could arrive more easily. It would be interesting then to be able to recognize the frontier in which this happens and be able to adapt the models and systems accordingly.

SoH modelling with seasonal temperature consideration.

The SoH model developed in this work relies heavily on the regularity of operation in which the batteries operate. It however does not incorporate explicitly the seasonal changes in ambient temperature. Just as it was seen in [53, 124], the temperature can impact the available capacity without directly increasing the overall degradation. Further research on seasonal SoH modelling for large-scale LiBESS seems then appropriate as temporary capacity losses could be estimated while also improving their general operation.

Stochastic scheduling optimisation with advanced LiBESS models.

Under the optimisation frameworks, the vRES behaviour was considered to be known. This generated an expected revenue and optimal LiBESS operation that did not consider the possible variability of the vRES source. The subject of solar production forecasting techniques, treated for example in [201], could then be used in the optimisation framework to further study the effects that advanced LiBESS models can have.

LiBESS usage optimisation to maximize its life expectancy.

The objective function evaluated in chapter 4 did not consider at any moment the degradation from the LiBESS at the end of the operation. Maximizing daily revenue could negatively impact the health of the LiB as more extreme power requests and cycles are required because of that. Integrating the cost of the capacity loss, in addition to evaluating long-term horizons ($\geq$ 1 year) could extend the service life of the systems. It would be possible then to study of the financial ramifications of this and the longer replacement cycles.

Project sizing and financial prospecting of vRES+LiBESS given regional temperatures.

Given that the PV capacity firming framework focused in this work remains relatively rare, the pertinence on the wide deployment of such kind of sites remains an open question. Due to the LiBESS sensibility to the temperature, insight can be won over the expected performance and revenues given the location and the meteorological characteristics of the site. An analysis of the LiBESS size, cost and location could be foreseen given this approach, which can help investors and grid managers to establish the regulatory frameworks to make them viable.

Annexe A

SOC estimation algorithms

In this section, a compilation of multiple SoC estimation algorithms with a brief description is presented. Further details can be consulted in [73, 70, 88, 101, 151, 152, 153].

Coulomb Counting

As its name suggests, this method consists in using the amount of current that flows from or to the batteries to provide a State of Charge estimation. As consequence, this method's accuracy is highly reliant not only in the current measurement's quality but also a knowledge of the initial state.

$$SOC(t) = SOC_{t=0} + \frac{\int_{t=0}^{t} i(t)dt}{C} \tag{A.1}$$

where C is the nominal capacity of the battery system.

As it can be seen from the expression, even small deviations in the current measurements can impose important accumulative errors and thus constant calibration needs to be done. Nevertheless, the principle followed by this method is the foundation for other kind of SOC estimation algorithms.

State-based Methods

Luenberger observer

Starting from the described electric equivalent system, the Luenberger observer is an estimation method where a constant gain is proportional to the model error. The state vector is then described as

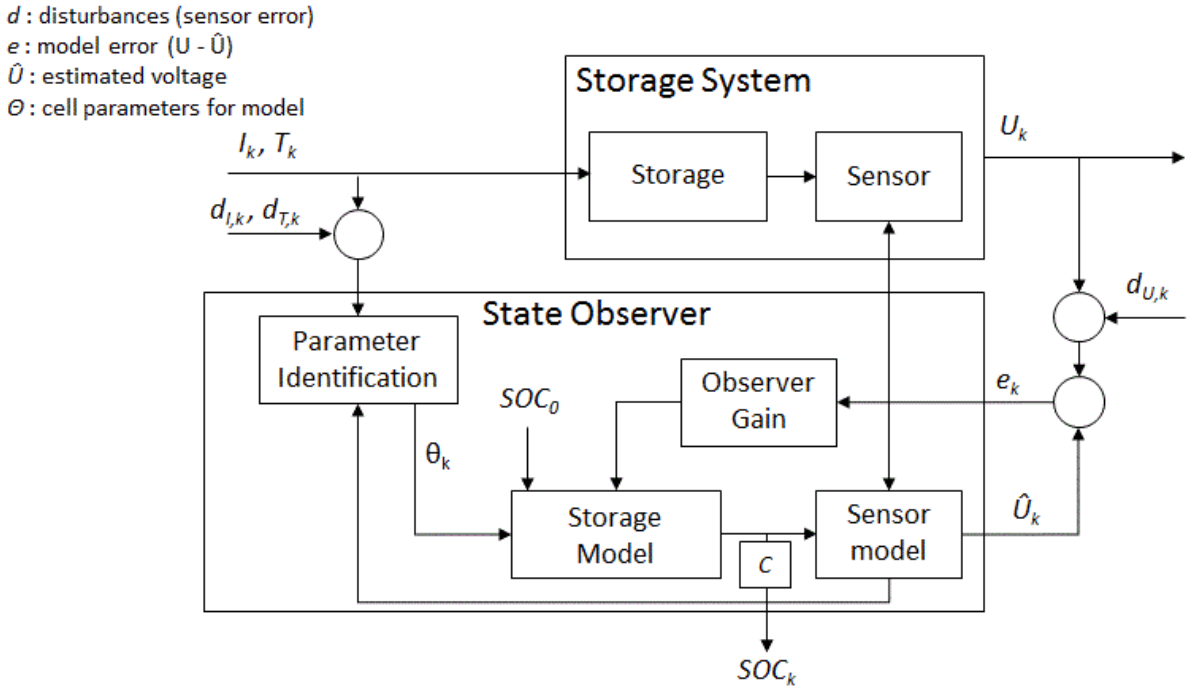

FIGURE A.1 – State Observer Flowchart

$$\hat{\mathbf{x}}_{\mathbf{k+1}} = \mathbf{f}(\hat{\mathbf{x}}_{\mathbf{k}}, \hat{\mathbf{u}}_{\mathbf{k}}) + \mathbf{L} \cdot \mathbf{e}_{\mathbf{k}} \tag{A.2}$$

where $e_k = y_k - \hat{y}_k$ is the model error.

This kind of system, when an observer is present, can be represented as in figure A.1

Sliding-mode observer

The feedback gain in this method is described by a non-linear function **H**, which is then applied to a switching function based in the system's error. The Lyapunov functions are usually used as the feedback gain for switching system.

$$\hat{\mathbf{x}}_{\mathbf{k+1}} = \mathbf{f}(\hat{\mathbf{x}}_{\mathbf{k}}, \hat{\mathbf{u}}_{\mathbf{k}}) + \mathbf{H} \cdot sgn(e_k) \tag{A.3}$$

Kalman Filters

State Estimate Update	$\hat{x}_k^+ = \hat{x}_k^- + K_k[z_k - H_k\hat{x}_k^-]$
Error Covariance Update	$P_k^+ = [I - K_k H_k] P_k^-$
Kalman Gain	$K_k = P_k^- H_k^T \left[H_k P_k^- H_k^T + R_k\right]^{-1}$

Where $\mathbf{H_k}$ is the measurement matrix at time t_k, $\mathbf{P_k}$ is the error covariance and $\mathbf{R_k}$ is the noise's covariance.

Unscented Kalman Filter [73]

$\chi_0 = \bar{\mathbf{x}}$	$i = 0$
$\chi_i = \bar{\mathbf{x}} + (\sqrt{(L+\lambda)\mathbf{P_x}})_i$	$i = 1, 2...L$
$\chi_i = \bar{\mathbf{x}} - (\sqrt{(L+\lambda)\mathbf{P_x}})_{i-L}$	$i = 1, 2...2L$
Error Covariance Update	$P_k^+ = [I - K_k H_k] P_k^-$
Kalman Gain	$K_k = P_k^- H_k^T \left[H_k P_k^- H_k^T + R_k\right]^{-1}$

Extended Kalman Filter

These systems are usually described by :

$$\dot{\underline{x}} = \underline{f}(\underline{x}(t), t) + \underline{w}(t) \tag{A.4}$$

$$\dot{\underline{z}}_k = \underline{h}(\underline{x}(t_k)) + \underline{v}_k \tag{A.5}$$

with $\underline{f}$ being a nonlinear function, $\underline{w}$ is a zero mean gaussian noise and the measurements are given by $\underline{z}$ with $\underline{v}_k$ is a random sequence of zero mean variables. The linearization is then obtained by using Taylor series approximations to compute the estimates.

Continuous-Discrete Extended Kalman Filter	
State Estimate Update	$\hat{\underline{x}}_k^+ = \hat{\underline{x}}_k^- + K_k[\underline{z}_k - \underline{h}_k(\hat{\underline{x}}_k^-)]$
Error Covariance Update	$P_k^+ = [I - K_k H_k(\hat{\underline{x}}_k^-)] P_k^-$
Kalman Gain	$K_k = P_k^- H_k^T(\hat{\underline{x}}_k^-) \left[H_k(\hat{\underline{x}}_k^-) P_k^- H_k^T(\hat{\underline{x}}_k^-) + R_k\right]^{-1}$

TABLE A.1 – Extended Kalman Filter Summary

Where the matrix H_k is defined as follows :

$$H_k(\hat{\underline{x}}_k^-) = \left.\frac{\delta \underline{h}_k(\underline{x}(t_k))}{\delta \underline{x}(t_k))}\right|_{\underline{x}(t_k)=\hat{\underline{x}}_k^-} \tag{A.6}$$

The Kalman gain shown in A.1 is recalculated at each iteration of this procedure, so a faster convergence and accuracy is expected.

Linearized Kalman Filter

A special case of the Extended Kalman Filter exists when instead of an estimation vector $\hat{\underline{x}}$, a known mean vector $\bar{\underline{x}}$ is used. This allows the pre-calculation of the Kalman Gain in

order to save processing power. The next table summarizes the update estimators as well as the Kalman Gain.

Continuous-Discrete Linearized Extended Kalman Filter	
State Estimate Update	$\underline{\hat{x}}_k^+ = \underline{\hat{x}}_k^- + K_k[\underline{z}_k - \underline{h}_k(\underline{\bar{x}}(t_k)) - H_k(\underline{\bar{x}}(t))[\underline{\hat{x}}_k^- - \underline{\bar{x}}(t_k)]]$
Error Covariance Update	$P_k^+ = [I - K_k H_k(\underline{\bar{x}}_k(t_k))]\, P_k^-$
Kalman Gain	$K_k = P_k^- H_k^T(\underline{\bar{x}}(t_k))\left[H_k(\underline{\bar{x}}(t_k)) P_k^- H_k^T(\underline{\bar{x}}(t_k)) + R_k\right]^{-1}$

TABLE A.2 – Extended Kalman Filter Summary

The disadvantage lies in the often-not-negligible differences that occur between the mean values and the expected values, whose behavior is closer to the reality.

Autoregressive Integrated Moving Average (ARIMA)

In linear dynamic systems, an empirical model can be used to fit empirical time series data. In the equation A.7, $\mathbf{z_k}$ is the observation at $\mathbf{t_k}$ with $\mathbf{r_k}$ being an uncorrelated gaussian variable (called the residual). The values **p**,**q**,**b**,**c** are free variables for model fitting. [153]

$$z_k = \sum_{i=1}^{p} b_i z_{k-1} + r_k - \sum_{i=1}^{q} c_i r_{k-i} \tag{A.7}$$

From this principle, a series of different processes can be defined, each one built around different characteristics of the wished system. The Autoregressive Process (**AR**) is used for systems where the present is defined by a linear combination of past measurements and a gaussian random variable A.8. In the Moving Average Process (**MA**) the observations are considered as a linear combination of past and present inputs A.9. The method that is a combination of both is called Mixed Autoregressive Moving Average (**ARMA**), and its equation is the same as shown in A.7, with the exception that the range of coefficients is restricted to make the process stationary and invertible.

$$z_k = \sum_{i=1}^{p} b_i z_{k-1} + r_k \tag{A.8}$$

$$z_k = r_k - \sum_{i=1}^{p} c_i r_{k-i} \tag{A.9}$$

When talking about **ARIMA**, this process is a generalization of the ARMA methodology for non-stationary systems. The key of this procedure lies in that, even if the observations don't have stationary statistics, the differentiation of the observation (A.10) shows the same behavior as in equation A.7. [101]

$$d_k = z_k - z_{k-1} \tag{A.10}$$

Data-driven Estimation Methods

Relevance Vector Machine (RVM)

A vector machine belongs to the classifiers in the machine learning realm. The Relevance Vector Machine, even though more advanced method exists (Support Vector Machine SVM), can be implemented in favorable frameworks to obtain probabilistic outputs.

$$F(\underline{t};\underline{w}) = \sum_{i=1}^{N} w_i K(\underline{t}, t_i) + w_0 \tag{A.11}$$

In an RVM, the model used is given by equation A.11, where $\underline{w}$ is a weight vector and $K(\underline{t}, t_i)$ is the kernel function. The training targets (θ) used are supposed to have the form in equation A.12. here ε is a zero-mean random Gaussian noise sample.

$$\theta = F(t_n;\underline{w}) + \varepsilon_n \tag{A.12}$$

Bayesian Regression

The Bayes theorem states that the probability for an event A given that B has occurred can be stated as the probability of the probability of A and B both occurring independently divided by the probability of B happening naturally, that is :

$$P(A|B) = \frac{A \cap B}{P(B)} \tag{A.13}$$

Given this base, expected values can be obtained by generating probability distributions for each possible output state of the system.

Supervised Learning methods

A review of different supervised learning methods is presented below. A more in-depth review of these methods and their variants can be found in the source material [202].

Least Squares

Given a linear system, the output Y can be estimated via an input vector X using

$$\hat{Y} = \hat{\beta}_0 + \sum_{j=1}^{p} X_j \hat{\beta}_j \tag{A.14}$$

where β_0 is the bias or intercept and β is a vector of coefficients.
Written in matrix form, this equation becomes :

$$\hat{Y} = X^T \hat{\beta} \tag{A.15}$$

which, given its linear nature, the gradientis given by β.
The least square method consists then in finding a set of β that minimizes the square error RSS (equations A.16). Here $\mathbf{X}$ represents an $N \times p$ matrix for each p-dimensional input vector and $\mathbf{y}$ is an N-vector of the outputs.

$$\begin{aligned} \text{RSS}(\beta) &= \sum (y_i - x_i^T \beta)^2 \\ \text{RSS}(\beta) &= (\mathbf{y} - \mathbf{X}\beta)^T (\mathbf{y} - \mathbf{X}\beta) \end{aligned} \tag{A.16}$$

Differentiating A.16 with respect to β we get the equation A.17 to which the vector solution $\hat{\beta}$ can be obtained using A.18 if $\mathbf{X}^T\mathbf{X}$ is not singular.

$$X^T (\mathbf{y} - \mathbf{X}\beta) = 0 \tag{A.17}$$

$$\hat{\beta} = \left(\mathbf{X}^T \mathbf{X}\right)^{-1} \mathbf{X}^T \mathbf{y} \tag{A.18}$$

K-Nearest Neighbor Method

Given a training set $\mathcal{T}$, the predicted output $\hat{Y}$ is obtained by averaging the k nearest neighbors from the input space x (A.19). The neighborhood $N_k(x)$ is defined by a closeness metric, usually the euclidean distance.

$$\hat{Y}(x) = \frac{1}{k} \sum_{x_i \in N_k(x)} y_i \tag{A.19}$$

Annexe B

Equivalent Circuit Battery Models

In this section, the mathematical formulation of multiple equivalent circuit models are presented. More information regarding them can be found in [88].

In the mathematical representations below, the following nomenclature is used :

— V_k : battery terminal voltage at time k.

— z_k : state of charge at time k.

— I_k : battery current at time k.

— θ : optimization vector.

Simple model

$$V_k = OCV(z_k) - R_0 I_k \tag{B.1}$$

Combined model

$$V_k = K_0 - \frac{K_1}{z_k} - K_2 z_k + K_3 ln(z_k) + K_4 ln(1 - z_k) \tag{B.2}$$

where $\theta = [K_0, K_1, K_2, K_3, K_4, R_0]$.

Zero-state hysteresis model

$$V_k = OCV(z_k) - R_0 I_k - s_k M, \qquad \text{where } s_k \begin{cases} 1 & I_k > \epsilon \\ -1 & I_k < \epsilon \\ s_{k-1} & |I_k| \leq \epsilon \end{cases} \tag{B.3}$$

One-state hysteresis model

$$V_k = OCV(z_k) - R_0 I_k + h_k \tag{B.4}$$

$$h_{k+1} = \exp(-|\kappa I_k \Delta t|) h_k + [1 - \exp(-|\kappa I_k \Delta t|)] H \tag{B.5}$$

Enhances Self-Correcting (ESC) model

$$\begin{vmatrix} f_{1,k+1} \\ f_{2,k+1} \\ h_{k+1} \end{vmatrix} = \begin{vmatrix} \alpha_1 & 0 & 0 \\ 0 & \alpha_2 & 0 \\ 0 & 0 & \exp(-|\kappa I_k \Delta t|) \end{vmatrix} \begin{vmatrix} f_{1,k} \\ f_{2,k} \\ h_k \end{vmatrix} + \begin{vmatrix} 1 & 0 \\ 1 & 0 \\ 0 & 1 - \exp(-|\kappa I_k \Delta t|) \end{vmatrix} \begin{vmatrix} I_k \\ H \end{vmatrix} \tag{B.6}$$

Two state low-pass filter

$$V_k = OCV(z_k) - R_0 I_k + h_k + g_1 f_{1,k} + g_2 f_{2,k} \tag{B.7}$$

Four state low-pass filter

$$V_k = OCV(z_k) - R_0 I_k + h_k + g_1 f_{1,k} + g_2 f_{2,k} + g_3 f_{3,k} + g_4 f_{4,k} \tag{B.8}$$

Nth-order RC model

$$U_{1,k+1} = \exp(\Delta t/\tau_1) U_{1,k} + R_1 [1 - \exp(-\Delta t/\tau_1)] I_k \tag{B.9}$$

$$V_k = OCV(z_k) - R_0 I_k - \left(\sum_{i=1}^{n} U_{i,k} \right) \tag{B.10}$$

One-state hysteresis

$$V_k = OCV(z_k) - R_0 I_k - \left(\sum_{i=1}^{n} U_{i,k} \right) + h_k \tag{B.11}$$

Annexe C

NF EN62933 BESS Characterisation Procedures

The following procedures are as described in the European standard NF EN62933-2-1[114]., with some notations and precisions corresponding to the industry standards defined in the Protocol for Uniformly Measuring and Expressing the Performance of Energy Storage Systems by the Pacific Northwest National Laboratory (PNNL)[111].
The values and parameters here reported obey the sign convention as seen in figure C.1, and are calculated at the Point of Connection (POC) unless specified otherwise.

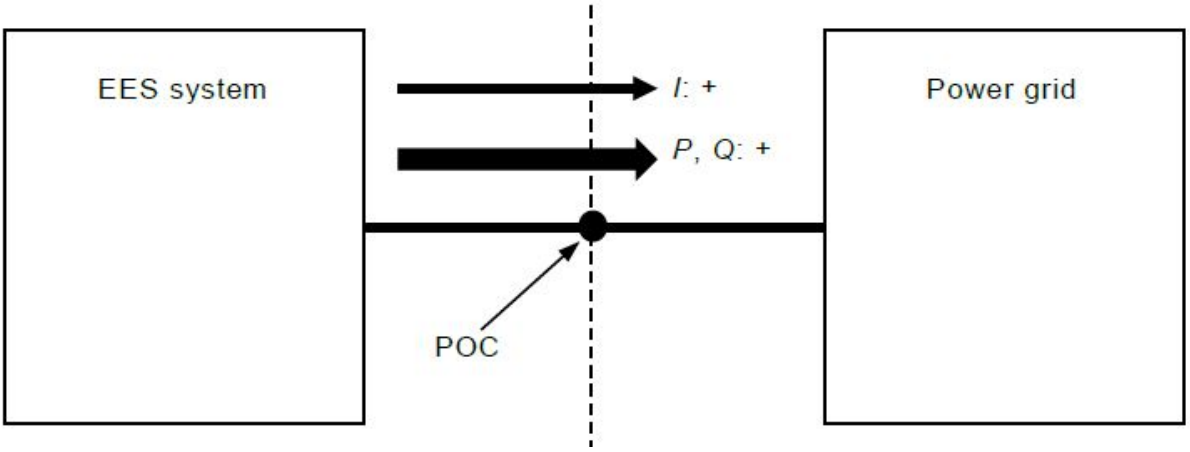

FIGURE C.1 – POC and sign convention used in the procedures

Energy Capacity Test

1. Discharge the ESS to its lower energy level.
2. Charge the ESS to its maximum state of charge at the rated input power.
3. Discharge at the rated power until the storage system reaches its lowest energy state

under normal operating conditions [1]. The energy capacity is then calculated as :

$$E_o = \sum_{i=1}^{n} P_{Oi} \times \Delta t \tag{C.1}$$

with E_o being the energy capacity at the POC (Wh), P_Oi is the active power output, Δt is the sampling time and n is the discharge time samples.

Input/Output Power Rating

These values are to be reported according to the Energy Capacity Test and the constant powers used to charge (step # 2) and discharge (step # 3) the storage system.

— **The input and output Power at the POC, as well as their corresponding times, should be measured.**

Round-trip Efficiency

This test should be done at the same time as the energy capacity test.

$$\eta_{rt} = \frac{E_O}{E_I} \tag{C.2}$$

$$\eta_{rt} = \frac{E_O - E_{aux_O}}{E_i + E_{aux_I}} \tag{C.3}$$

	E_o (Wh)	E_I (Wh)	E_{aux_I} (Wh)	E_{aux_o} (Wh)	Roundtrip efficiency η_{rt} (%)
Test 1					
Test 2					
Average					

FIGURE C.2 – Example Table as found in IEC 62933-2-1 to report the Roundtrip Efficiencies

Response Time and Ramp Rate

1. At a given State of Charge, preferred 50%, get the output power of the system to 0 (±2% of rated power).

1. The PNNL specifies that the discharge should be done up until the point where the system is able to produce 98% of the rated power, being this the SOC of reference.

2. Change the ESS setpoint to the nominal charge power. The setpoint is to be maintained until the power falls within ±2% range.
3. Change the ESS setpoint to zero. The setpoint is to be maintained until the power falls within ±2% range.
4. Change the ESS setpoint to nominal output power. The setpoint is to be maintained until the power falls within ±2% range.
5. Change the ESS setpoint to zero. The setpoint is to be maintained until the power falls within ±2% range.

The values to recover from this test, as defined by the norm IEC 62933-2-1 :2017 are :

— *Step Response Time (SRT)*
  — $SRT_1 = t(P_{out} = P_{Charge} \pm 2\%) - t(Order = P_{Charge})$
  — $SRT_2 = t(P_{out} = \pm 2\% P_{Charge}) - t(Order = 0)$
  — $SRT_3 = t(P_{out} = P_{Discharge} \pm 2\%) - t(Order = P_{Discharge})$
  — $SRT_4 = t(P_{out} = \pm 2\% P_{Discharge}) - t(Order = 0)$
— *Ramp Rate (RR)*
  — When operating at $P = 0$:

$$RR_1 = \frac{80\% P_{Charge}}{t(P = 90\% P_{Charge}) - t(P = 10\% P_{Charge})} \tag{C.4}$$

  — When operating at P_{Charge} :

$$RR_2 = \frac{80\% P_{Charge}}{t(P = 10\% P_{Charge}) - t(P = 90\% P_{Charge})} \tag{C.5}$$

  — When operating at $P = 0$:

$$RR_3 = \frac{80\% P_{Discharge}}{t(P = 90\% P_{Discharge}) - t(P = 10\% P_{Discharge})} \tag{C.6}$$

  — When operating at $P_{Discharge}$:

$$RR_4 = \frac{80\% P_{Discharge}}{t(P = 10\% P_{Discharge}) - t(P = 90\% P_{Discharge})} \tag{C.7}$$

Annexe D

Thermal State-Space Model Performance by Timestep

This section compiles all the results found for the thermal state-space model depending on the timestep used to train the models as well the timestep of the data used to validate such models.

Intra-day temperature RMSE.

		Model's Timestep used for Training							
		900	600	300	120	60	20	10	1
Dataset's Timestep	900	0.74	0.74	0.73	0.73	0.73	**1.33**	0.73	1.28
	600	0.74	0.73	0.73	0.73	0.73	**1.36**	0.73	1.24
	300	0.73	0.73	0.73	0.73	0.73	**1.39**	0.73	1.19
	120	0.73	0.73	0.73	0.73	0.73	**1.41**	0.73	1.17
	60	0.73	0.73	0.74	0.74	0.74	**1.42**	0.74	1.16
	20	0.74	0.74	0.74	0.74	0.74	**1.43**	0.74	1.15
	10	0.73	0.73	0.74	0.74	0.74	**1.43**	0.74	1.15
	1	0.73	0.73	0.74	0.74	0.74	**1.43**	0.74	1.14

Table D.1 – RMSEs for the intra-day temp. predictor of LiBESS #01.

Dataset's Timestep	Model's Timestep used for Training							
	900	600	300	120	60	**20**	10	1
900	1.54	1.51	1.53	1.53	2.18	**1.10**	1.33	1.23
600	1.55	1.52	1.53	1.54	2.20	**1.05**	1.33	1.23
300	1.58	1.56	1.57	1.58	2.25	**1.01**	1.37	1.26
120	1.60	1.58	1.59	1.60	2.27	**1.00**	1.39	1.28
60	1.61	1.59	1.60	1.61	2.28	**0.99**	1.39	1.29
20	1.62	1.59	1.61	1.61	2.29	**0.99**	1.40	1.30
10	1.62	1.60	1.61	1.61	2.29	**0.98**	1.40	1.30
1	1.62	1.60	1.61	1.62	2.29	**0.98**	1.40	1.30

TABLE D.2 – RMSEs for the intra-day temp. predictor of LiBESS #02.

Dataset's Timestep	Model's Timestep used for Training							
	900	600	300	120	60	**20**	10	1
900	1.23	1.21	1.22	1.23	1.23	**0.81**	1.30	0.77
600	1.24	1.22	1.23	1.24	1.24	**0.77**	1.24	0.75
300	1.27	1.25	1.26	1.27	1.27	**0.74**	1.18	0.76
120	1.29	1.27	1.28	1.29	1.29	**0.73**	1.15	0.76
60	1.30	1.28	1.29	1.30	1.30	**0.72**	1.14	0.77
20	1.30	1.28	1.29	1.30	1.30	**0.72**	1.13	0.77
10	1.31	1.29	1.30	1.31	1.31	**0.72**	1.12	0.77
1	1.31	1.29	1.30	1.31	1.31	**0.72**	1.12	0.77

TABLE D.3 – RMSEs for the intra-day temp. predictor of LiBESS #03.

Average error of the Daily Maximal Temperature Prediction.

Dataset's Timestep	Model's Timestep used for Training							
	900	600	300	120	60	20	10	1
900	0.93	0.9	0.86	0.85	0.81	**1.13**	0.83	0.37
600	0.94	0.90	0.86	0.84	0.81	**1.10**	0.82	0.40
300	0.90	0.86	0.81	0.80	0.76	**1.01**	0.78	0.39
120	0.92	0.88	0.83	0.82	0.78	**1.01**	0.80	0.43
60	0.96	0.92	0.87	0.86	0.82	**1.04**	0.84	0.47
20	0.97	0.93	0.89	0.87	0.84	**1.05**	0.85	0.48
10	0.95	0.91	0.87	0.86	0.82	**1.04**	0.84	0.46
1	0.95	0.91	0.87	0.86	0.82	**1.04**	0.84	0.46

TABLE D.4 – Average error for the maximal temp. prediction of LiBESS #01.

		Model's Timestep used for Training							
		900	600	300	120	60	20	10	1
Dataset's Timestep	900	1.18	1.08	1.04	1.00	0.82	**0.21**	0.97	0.95
	600	1.09	1.00	0.96	0.92	0.72	**0.20**	0.89	0.87
	300	0.95	0.85	0.81	0.76	0.54	**0.13**	0.74	0.73
	120	0.94	0.84	0.80	0.76	0.52	**0.16**	0.74	0.73
	60	0.97	0.87	0.83	0.79	0.55	**0.19**	0.77	0.76
	20	0.97	0.88	0.83	0.79	0.55	**0.21**	0.78	0.76
	10	0.96	0.86	0.82	0.78	0.55	**0.17**	0.76	0.75
	1	0.96	0.87	0.82	0.78	0.55	**0.18**	0.77	0.75

Table D.5 – Average error for the maximal temp. prediction of LiBESS #02.

		Model's Timestep used for Training							
		900	600	300	120	60	20	10	1
Dataset's Timestep	900	1.22	1.17	1.16	1.15	1.13	**0.54**	0.22	0.83
	600	1.10	1.04	1.03	1.02	1.00	**0.46**	0.17	0.73
	300	0.92	0.87	0.86	0.84	0.82	**0.34**	0.08	0.59
	120	0.89	0.84	0.83	0.81	0.79	**0.34**	0.10	0.57
	60	0.92	0.86	0.85	0.84	0.81	**0.37**	0.13	0.60
	20	0.92	0.86	0.85	0.83	0.81	**0.37**	0.13	0.60
	10	0.90	0.84	0.83	0.82	0.79	**0.34**	0.09	0.57
	1	0.90	0.84	0.83	0.82	0.79	**0.34**	0.09	0.58

Table D.6 – Average error for the maximal temp. prediction of LiBESS #03.

RMSE of the Daily Maximal Temperature prediction.

		Model's Timestep used for Training							
		900	600	300	120	60	20	10	1
Dataset's Timestep	900	1.42	1.39	1.36	1.35	1.32	**1.59**	1.33	1.34
	600	1.39	1.36	1.32	1.31	1.28	**1.50**	1.29	1.32
	300	1.37	1.34	1.30	1.28	1.26	**1.41**	1.27	1.33
	120	1.36	1.32	1.28	1.26	1.24	**1.37**	1.25	1.31
	60	1.38	1.34	1.30	1.29	1.26	**1.40**	1.27	1.32
	20	1.38	1.35	1.30	1.29	1.26	**1.40**	1.27	1.31
	10	1.37	1.33	1.29	1.28	1.25	**1.39**	1.26	1.31
	1	1.37	1.34	1.29	1.28	1.25	**1.39**	1.26	1.31

Table D.7 – RMSEs for the maximal temp. predictor of LiBESS #01.

Dataset's Timestep	Model's Timestep used for Training: 900	600	300	120	60	20	10	1
900	1.65	1.59	1.57	1.55	1.64	**1.18**	1.48	1.43
600	1.51	1.45	1.43	1.41	1.46	**1.16**	1.34	1.31
300	1.38	1.32	1.30	1.28	1.34	**1.15**	1.22	1.19
120	1.36	1.30	1.28	1.26	1.31	**1.14**	1.20	1.17
60	1.39	1.32	1.30	1.28	1.33	**1.15**	1.22	1.20
20	1.39	1.32	1.30	1.28	1.32	**1.15**	1.22	1.19
10	1.37	1.31	1.29	1.26	1.31	**1.15**	1.21	1.18
1	1.37	1.31	1.29	1.27	1.31	**1.15**	1.21	1.19

TABLE D.8 – RMSEs for the maximal temp. predictor of LiBESS #02.

Dataset's Timestep	Model's Timestep used for Training: 900	600	300	120	60	20	10	1
900	1.64	1.60	1.59	1.59	1.57	**1.32**	1.40	1.39
600	1.48	1.43	1.43	1.42	1.40	**1.22**	1.32	1.25
300	1.31	1.26	1.25	1.24	1.23	**1.14**	1.28	1.13
120	1.26	1.22	1.21	1.20	1.18	**1.10**	1.25	1.09
60	1.28	1.24	1.23	1.22	1.20	**1.11**	1.25	1.10
20	1.27	1.23	1.22	1.21	1.19	**1.11**	1.25	1.09
10	1.26	1.21	1.20	1.19	1.18	**1.10**	1.25	1.08
1	1.26	1.21	1.21	1.19	1.18	**1.10**	1.25	1.08

TABLE D.9 – RMSEs for the maximal temp. predictor of LiBESS #03.

Average error in the Daily Minimal Temperature prediction.

Dataset's Timestep	Model's Timestep used for Training: 900	600	300	120	60	20	10	1
900	0.32	0.29	0.22	0.19	0.17	**-1.58**	0.18	1.37
600	0.29	0.26	0.19	0.16	0.15	**-1.61**	0.15	1.35
300	0.26	0.22	0.16	0.12	0.11	**-1.66**	0.11	1.32
120	0.23	0.20	0.13	0.10	0.09	**-1.69**	0.09	1.30
60	0.23	0.19	0.12	0.09	0.08	**-1.70**	0.08	1.29
20	0.22	0.18	0.12	0.08	0.07	**-1.71**	0.07	1.28
10	0.21	0.17	0.11	0.07	0.06	**-1.72**	0.06	1.28
1	0.20	0.17	0.10	0.07	0.06	**-1.73**	0.06	1.27

TABLE D.10 – Average error for the minimal temp. prediction of LiBESS #01.

		Model's Timestep used for Training							
		900	600	300	120	60	20	10	1
Dataset's Timestep	900	-1.90	-1.85	-1.86	-1.87	-3.08	**0.84**	-1.46	-1.26
	600	-1.92	-1.87	-1.89	-1.89	-3.10	**0.81**	-1.49	-1.28
	300	-1.97	-1.92	-1.93	-1.94	-3.16	**0.78**	-1.53	-1.33
	120	-2.00	-1.94	-1.96	-1.97	-3.18	**0.76**	-1.56	-1.35
	60	-2.01	-1.95	-1.97	-1.98	-3.20	**0.76**	-1.57	-1.36
	20	-2.01	-1.96	-1.98	-1.98	-3.20	**0.75**	-1.57	-1.37
	10	-2.03	-1.97	-1.99	-2.00	-3.22	**0.74**	-1.58	-1.38
	1	-2.03	-1.98	-1.99	-2.00	-3.22	**0.74**	-1.59	-1.38

Table D.11 – Average error for the minimal temp. prediction of LiBESS #02.

		Model's Timestep used for Training							
		900	600	300	120	60	20	10	1
Dataset's Timestep	900	-1.50	-1.45	-1.46	-1.48	-1.48	**0.31**	0.97	-0.32
	600	-1.53	-1.48	-1.49	-1.51	-1.51	**0.29**	0.95	-0.35
	300	-1.56	-1.51	-1.53	-1.55	-1.55	**0.26**	0.93	-0.38
	120	-1.59	-1.54	-1.56	-1.57	-1.57	**0.24**	0.91	-0.40
	60	-1.60	-1.55	-1.57	-1.58	-1.58	**0.23**	0.90	-0.41
	20	-1.60	-1.55	-1.57	-1.58	-1.59	**0.23**	0.90	-0.41
	10	-1.61	-1.56	-1.58	-1.60	-1.60	**0.22**	0.89	-0.42
	1	-1.62	-1.57	-1.58	-1.60	-1.60	**0.22**	0.89	-0.42

Table D.12 – Average error for the minimal temp. prediction of LiBESS #03.

RMSE in the Daily Minimal Temperature prediction.

		Model's Timestep used for Training							
		900	600	300	120	60	20	10	1
Dataset's Timestep	900	0.50	0.48	0.43	0.41	0.41	**1.65**	0.40	1.47
	600	0.48	0.46	0.42	0.40	0.39	**1.68**	0.39	1.45
	300	0.47	0.44	0.40	0.39	0.38	**1.73**	0.38	1.42
	120	0.45	0.42	0.39	0.38	0.37	**1.76**	0.37	1.40
	60	0.44	0.42	0.39	0.37	0.37	**1.77**	0.37	1.39
	20	0.44	0.42	0.38	0.37	0.37	**1.78**	0.37	1.38
	10	0.43	0.41	0.38	0.37	0.36	**1.79**	0.36	1.37
	1	0.43	0.41	0.38	0.37	0.36	**1.79**	0.36	1.37

Table D.13 – RMSEs for the minimal temp. predictor of LiBESS #01.

Dataset Timestep	Model's Timestep used for Training							
	900	600	300	120	60	20	10	1
900	1.97	1.92	1.93	1.94	3.18	**0.99**	1.53	1.33
600	1.99	1.94	1.96	1.96	3.20	**0.97**	1.55	1.35
300	2.04	1.99	2.00	2.01	3.25	**0.93**	1.60	1.40
120	2.07	2.01	2.03	2.04	3.28	**0.92**	1.62	1.42
60	2.08	2.02	2.04	2.05	3.29	**0.91**	1.63	1.43
20	2.08	2.03	2.05	2.05	3.29	**0.91**	1.64	1.43
10	2.09	2.04	2.06	2.07	3.30	**0.90**	1.65	1.45
1	2.10	2.05	2.06	2.07	3.31	**0.90**	1.65	1.45

TABLE D.14 – RMSEs for the minimal temp. predictor of LiBESS #02

Dataset Timestep	Model's Timestep used for Training							
	900	600	300	120	60	20	10	1
900	1.56	1.51	1.53	1.54	1.54	**0.54**	1.13	0.50
600	1.59	1.54	1.56	1.57	1.57	**0.53**	1.11	0.51
300	1.63	1.58	1.59	1.61	1.61	**0.52**	1.09	0.54
120	1.65	1.60	1.62	1.64	1.64	**0.50**	1.07	0.55
60	1.66	1.61	1.63	1.64	1.64	**0.50**	1.07	0.56
20	1.66	1.61	1.63	1.65	1.65	**0.50**	1.07	0.56
10	1.68	1.63	1.64	1.66	1.66	**0.49**	1.06	0.57
1	1.68	1.63	1.64	1.66	1.66	**0.49**	1.06	0.57

TABLE D.15 – RMSEs for the minimal temp. predictor of LiBESS #03.

Annexe E

Optimisation Results

In this section, the different results obtained via the Optimisation Framework are included. This includes both the results from the AO ZNI 2015 framework and the LV Hybrid Grid framework.

AOZNI Framework

Factory Issued BESS parameters

PV Behaviour	Optimization	SITE #1	SITE #2	SITE #3	SITE #4
Good Weather	Schedule	1829.0€	2253.5€	1872.0€	1108.8€
	Injection	2068.4€	2548.3€	2112.6€	1251.4€
	Schedule + Injection	2176.5€	2677.1€	2221.0€	1316.4€
Average Weather	Schedule	1829.0€	2253.5€	1872.0€	1108.8€
	Injection	1981.0€	2439.7€	2023.8€	1198.9€
	Schedule + Injection	1983.1€	2441.5€	2026.8€	1200.9€
Ugly Weather	Schedule	1829.0€	2253.5€	1872.0€	1108.8€
	Injection	619.6€	782.1€	656.6€	385.4€
	Schedule + Injection	908.8€	1131.9€	948.0€	559.3€

TABLE E.1 – Financial results when using the factory-issued values and different weather scenarios.

Parameterized SoC BESS Model

PV Behavior	Optimization	SITE #1	SITE #2	SITE #3	SITE #4
Good Weather	Schedule	1834.5€	2238.0€	1836.4€	1087.7€
	Injection	2076.5€	2551.7€	2080.6€	1232.9€
	Schedule + Injection	2182.1€	2668.9€	2185.3€	1295.2€
Average Weather	Schedule	1834.5€	2238.0€	1836.4€	1087.7€
	Injection	1984.6€	2422.3€	1988.5€	1177.9€
	Schedule + Injection	1988.7€	2424.5€	1991.2€	1179.8€
Ugly Weather	Schedule	1834.5€	2238.0€	1836.4€	1087.7€
	Injection	624.5€	766.7€	623.5€	366
	Schedule + Injection	914.3€	1113.3€	912.3€	538.2€

TABLE E.2 – Financial results when using the improved LiBESS model and different weather scenarios.

Parameterized SoC + Thermal BESS Model

LV Hybrid Grid Framework

Cost of Energy

PV Production	Factory SoC	Improved SoC	Improved SoC + T
Forecast	14.11€	14.28€	17.01€
Good Weather	18.09€	18.26€	21.18€
Average Weather	16.32€	16.49€	19.26€
Ugly Weather	5.67€	5.96€	8.88€

TABLE E.3 – Cost of energy under different BESS models in the NBA optimization framework.

Annexe F

BESS Cabinet Temperatures

A sample of the recorded temperatures for ambient air and the LiB cabinet surface for BESS #4-#7 located in the island of Corsica is seen here. For each plot, the power profile from the BESS is shown below. Through these images it is easy to see how thermal modelling for these LiBESS is not adequate. The cabinet surface temperature follows closely the behavior of the air temperature, and only in cold temperatures a slight different behavior can be seen. However such differences are not enough to parameterize a thermal model and reliably estimate the LiB internal temperature inside the cabinet.

As a reminder, installing any kind of temperature sensor was forbidden by the manufacturer. Any external system inside the cabinet would void the warranty.

BESS #4

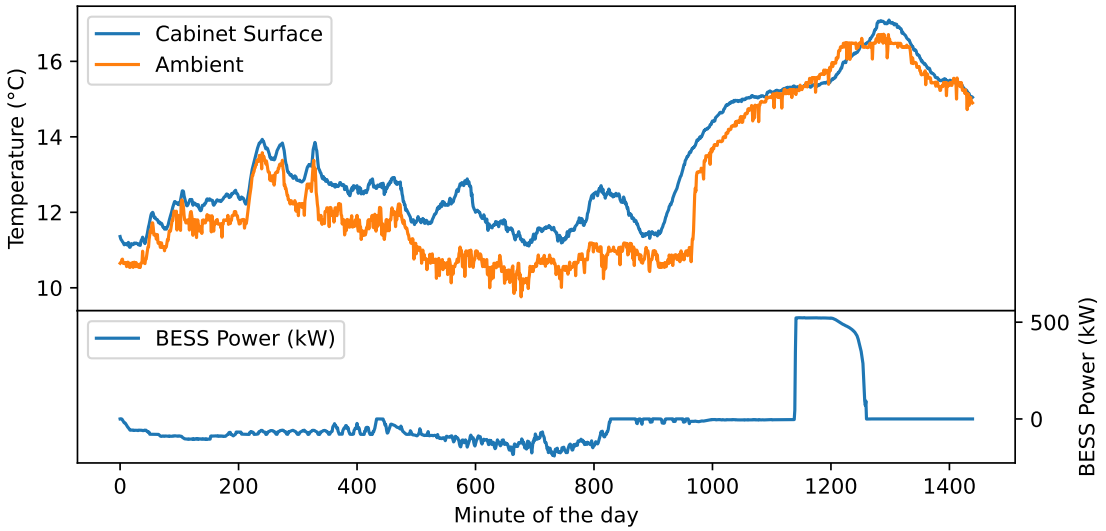

FIGURE F.1 – Recorded temperatures and power for a **summer** day for for BESS #4.

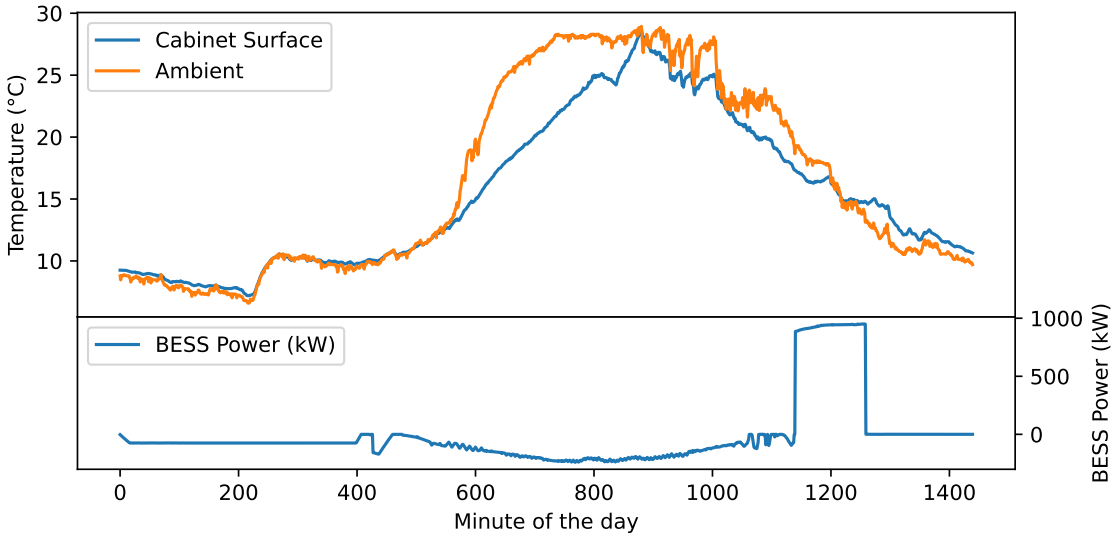

FIGURE F.2 – Recorded temperatures and power for a **winter** day for for BESS #4.

BESS #5

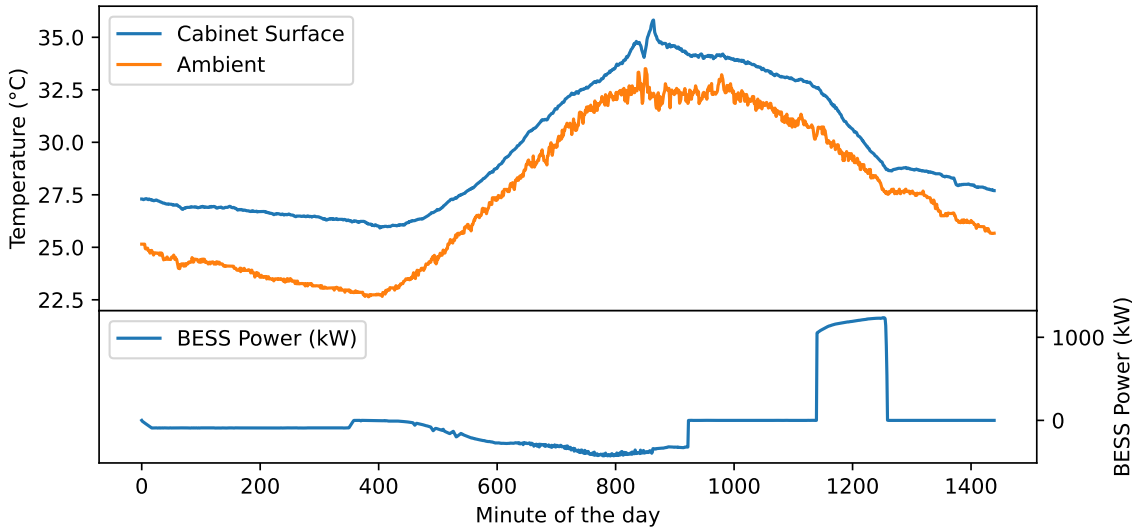

FIGURE F.3 – Recorded temperatures and power for a **summer** day for for BESS #5.

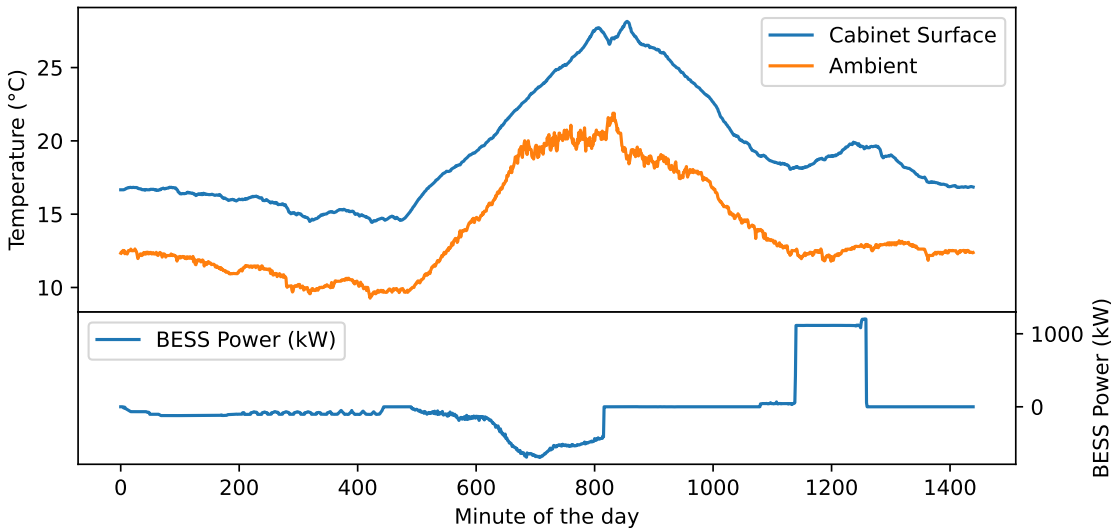

FIGURE F.4 – Recorded temperatures and power for a **winter** day for for BESS #5.

BESS #6

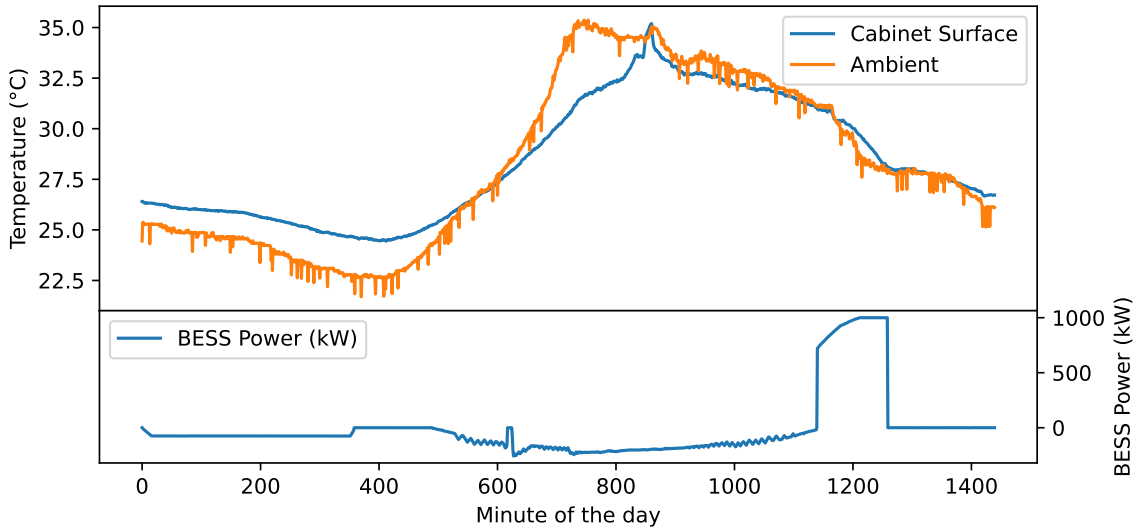

FIGURE F.5 – Recorded temperatures and power for a **summer** day for for BESS #6.

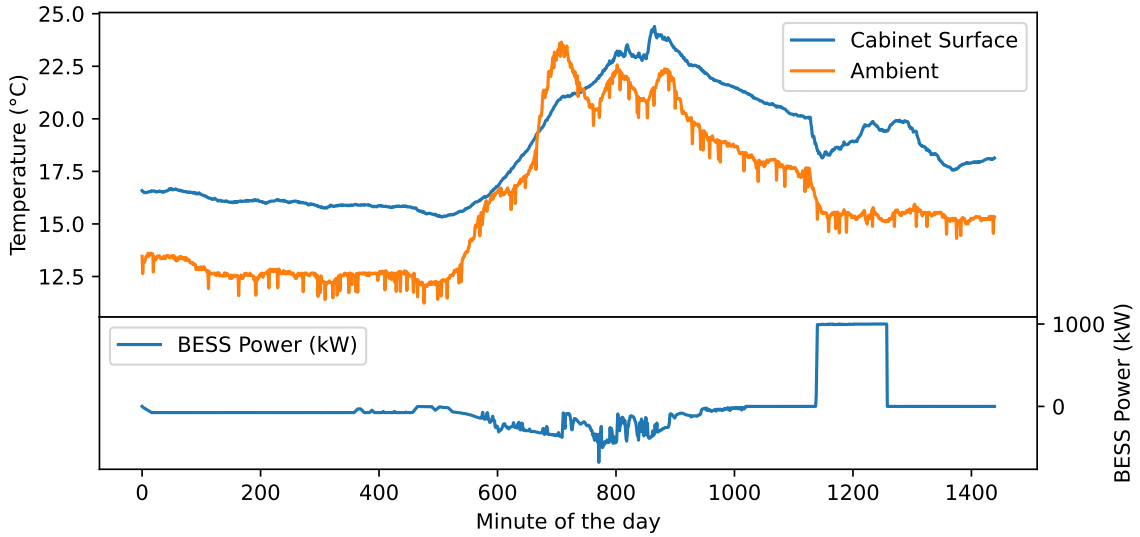

FIGURE F.6 – Recorded temperatures and power for a **winter** day for for BESS #6.

BESS #7

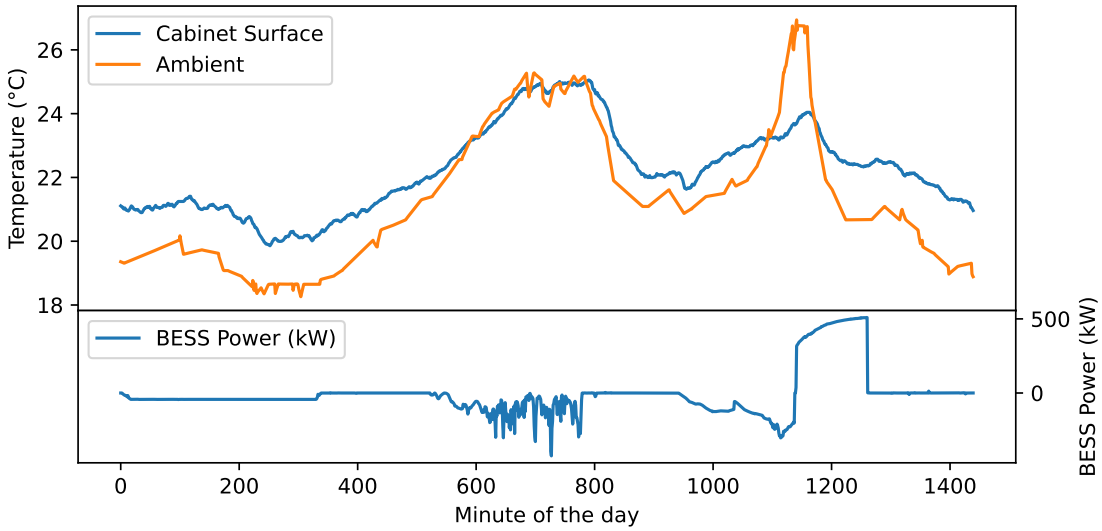

FIGURE F.7 – Recorded temperatures and power for a **summer** day for for BESS #7.

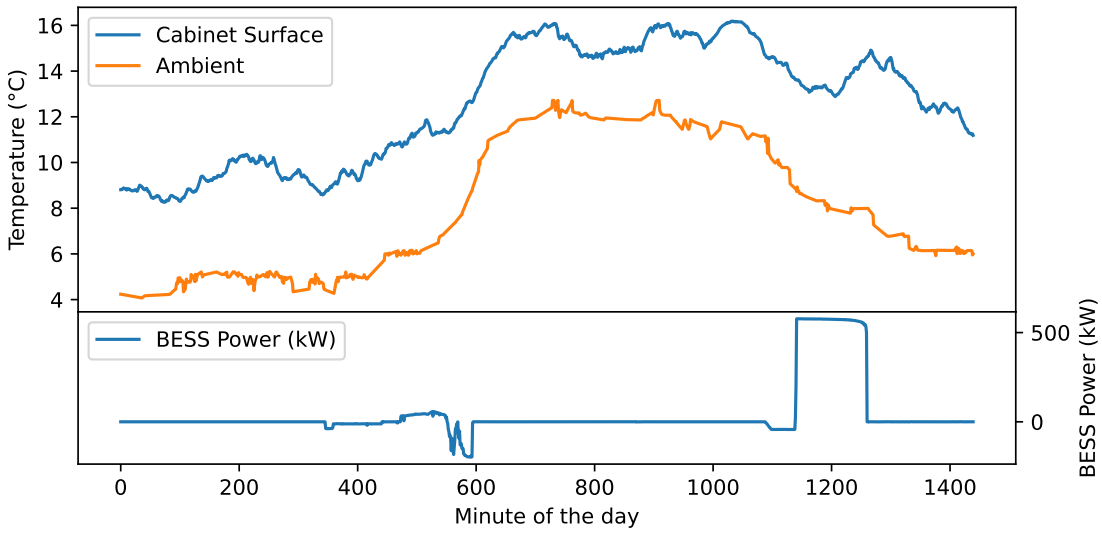

FIGURE F.8 – Recorded temperatures and power for a **winter** day for for BESS #7.

Bibliographie

[1] Statistical Review of World Energy BP. *BP Statistical Review of World Energy 2021*. Rapp. tech. June. London : Statistical Review of World Energy BP p.l.c, 2021. URL : https://www.bp.com/content/dam/bp/business-sites/en/global/corporate/pdfs/energy-economics/statistical-review/bp-stats-review-2021-full-report.pdf.

[2] *The Paris Agreement | UNFCCC*. URL : https://unfccc.int/process-and-meetings/the-paris-agreement/the-paris-agreement.

[3] *Renewable energy targets*. URL : https://energy.ec.europa.eu/topics/renewable-energy/renewable-energy-directive-targets-and-rules/renewable-energy-targets_en#documents.

[4] IRENA. *Electricity storage and renewables : Costs and markets to 2030*. October. 2017, p. 132. ISBN : 978-92-9260-038-9. URL : http://irena.org/publications/2017/Oct/Electricity-storage-and-renewables-costs-and-markets%0Ahttps://www.irena.org/-/media/Files/IRENA/Agency/Publication/2017/Oct/IRENA_Electricity_Storage_Costs_2017.pdf.

[5] Cour des COMPTES. *La politique de développement des énergies renouvelables*. Rapp. tech. Paris : Cour des Comptes, 2013, p. 241.

[6] Steven STOFT. *Power System Economics : Designing Markets for Electricity*. United States : Wiley-IEEE Press, 2002, p. 496. ISBN : 978-0-471-15040-4.

[7] Philip HEPTONSTALL, Robert GROSS et Florian STEINER. *The costs and impacts of intermittency – 2016 update : A systematic review of the evidence on the costs and impacts of intermittent electricity generation technologies*. Rapp. tech. February. UK Energy Reseach Centre, 2017. URL : www.eti.co.uk.

[8] ECOFYS. « Energy Storage Opportunities and Challenges ». In : *A West coast Perspective White Paper* (2014), p. 1-61.

[9] Siavash Asiaban et al. *Wind and solar intermittency and the associated integration challenges : A comprehensive review including the status in the belgian power system*. T. 14. 9. 2021, p. 1-41. isbn : 3292643422. doi : 10.3390/en14092630.

[10] Samuel C Johnson, Joshua D Rhodes et Michael E Webber. « Understanding the impact of non-synchronous wind and solar generation on grid stability and identifying mitigation pathways ». In : *Applied Energy* 262.December 2019 (2020), p. 114492. issn : 0306-2619. doi : 10.1016/j.apenergy.2020.114492. url : https://doi.org/10.1016/j.apenergy.2020.114492.

[11] Jean Franeois Toubeau et al. « Forecast-Driven Stochastic Scheduling of a Virtual Power Plant in Energy and Reserve Markets ». In : *IEEE Systems Journal* (2021), p. 1-12. issn : 19379234. doi : 10.1109/JSYST.2021.3114445.

[12] Brendan Fox et Damian Flynn. « Wind intermittency - Mitigation measures and load management ». In : *2005 IEEE Russia Power Tech, PowerTech* (2005), p. 9-11. doi : 10.1109/PTC.2005.4524796.

[13] Sunil G. Solanki et al. « Power smoothing techniques to mitigate solar intermittency ». In : *Proceedings - 2019 International Conference on Electrical, Electronics and Computer Engineering, UPCON 2019* (2019), p. 3-8. doi : 10.1109/UPCON47278.2019.8980080.

[14] Viet T Tran et al. « Mitigation of Solar PV Intermittency Using Ramp-Rate Control of Energy Buffer Unit ». In : 34.1 (2019), p. 435-445.

[15] Jun Shimizukawa et al. « Mitigation of intermittency of wind power generation using battery energy storage system ». In : *Proceedings of the Universities Power Engineering Conference* (2010).

[16] Joseph Mossoba, Milan Ilic et Leo Casey. « PV plant intermittency mitigation using constant DC voltage PV and EV battery storage ». In : *2010 IEEE Conference on Innovative Technologies for an Efficient and Reliable Electricity Supply, CITRES 2010* (2010), p. 297-301. doi : 10.1109/CITRES.2010.5619791.

[17] Joseph Mossoba et al. « Analysis of solar irradiance intermittency mitigation using constant DC voltage PV and EV battery storage ». In : *2012 IEEE Transportation Electrification Conference and Expo, ITEC 2012* (2012). doi : 10.1109/ITEC.2012.6243473.

[18] Michael Caramanis et Justin M. Foster. « Management of electric vehicle charging to mitigate renewable generation intermittency and distribution network congestion ». In : *Proceedings of the IEEE Conference on Decision and Control* iii (2009), p. 4717-4722. issn : 25762370. doi : 10.1109/CDC.2009.5399955.

[19] Yimin Zhou et Xiaoyun Li. « Vehicle to grid technology : A review ». In : *Chinese Control Conference, CCC* 2015-September (2015), p. 9031-9036. issn : 21612927. doi : 10.1109/ChiCC.2015.7261068.

[20] Aqsa Naeem et Naveed Ul Hassan. « Renewable Energy Intermittency Mitigation in Microgrids : State-of-the-Art and Future Prospects ». In : *Proceedings of 2020 4th International Conference on Green Energy and Applications, ICGEA 2020* (2020), p. 158-164. doi : 10.1109/ICGEA49367.2020.239699.

[21] Yih-huei Wan. *Analysis of Wind Power Ramping Behavior in ERCOT*. Rapp. tech. March. NREL, 2011. url : http://www.nrel.gov/wind/systemsintegration/pdfs/2011/wan_wind_power_ramping.pdf.

[22] Dae Kyeong Kim et al. *Handbook on Battery Energy Storage System*. December. 2018, p. 1-92. isbn : 9789292614713. url : https://www.adb.org/publications/battery-energy-storage-system-handbook.

[23] Abbas A Akhil et al. *DOE / EPRI 2013 Electricity Storage Handbook in Collaboration with NRECA*. Rapp. tech. July. New Mexico : Sandia National Laboratories, 2013. url : https://www.sandia.gov/ess/publications/doe-oe-resources/eshb/doe-epri-nreca.

[24] Ingeteam Power Technology. « Storage, FACTS & Custom Power, SSSC : Glossary of Terms ». In : (2012).

[25] Paul Denholm et al. *The Four Phases of Storage Deployment : A Framework for the Expanding Role of Storage in the U.S. Power System*. Rapp. tech. 2021. url : https://www.nrel.gov/docs/fy21osti/77480.pdf.

[26] Wesley Cole et A Will Frazier. « Cost Projections for Utility- Scale Battery Storage ». In : *National Renewable Energy Laboratory* June (2019), NREL/TP–6A20-73222. url : https://www.nrel.gov/docs/fy19osti/73222.pdf.

[27] Geoffrey J. May, Alistair Davidson et Boris Monahov. « Lead batteries for utility energy storage : A review ». In : *Journal of Energy Storage* 15 (2018), p. 145-157. issn : 2352152X. doi : 10.1016/j.est.2017.11.008. url : http://dx.doi.org/10.1016/j.est.2017.11.008.

[28] A. K. Padhi, K. S. Nanjundaswamy et J. B. Goodenough. « Phospho-olivines as Positive-Electrode Materials for Rechargeable Lithium Batteries ». In : *Journal of The Electrochemical Society* 144.4 (avr. 1997), p. 1188-1194. issn : 0013-4651. doi : 10.1149/1.1837571. url : https://doi.org/10.1149/1.1837571.

[29] IRENA. « Utility-Scale Batteries Innovation Landscape Brief ». In : *International Renewable Energy Agency* (2019), p. 7. url : https://www.irena.org/-/media/Files/IRENA/Agency/Publication/2019/Sep/IRENA_Utility-scale-batteries_2019.pdf.

[30] Jan Ahlen et al. *Battery Energy Storage Overview*. Rapp. tech. April. National Rural Electric Cooperative Association, 2019.

[31] J Donald et al. « The Lithium-Ion Battery Modeling Challenge : a Dynamic Systems and Contorl Perspective ». In : *Mechanical Engineering* (2014).

[32] Marco Stecca et al. « A Comprehensive Review of the Integration of Battery Energy Storage Systems into Distribution Networks ». In : *IEEE Open Journal of the Industrial Electronics Society* 1.February (2020), p. 1-1. issn : 2644-1284. doi : 10.1109/OJIES.2020.2981832. url : https://ieeexplore.ieee.org/document/9040552/.

[33] University of Massachusetts at Amherst Renewable Energy Research Laboratory. *Wind Power : Capacity Factor, Intermittency, and what happens when the wind doesn't blow ?* Rapp. tech. University of Massachusetts at Amherst, 2009, p. 1-3.

[34] Richard Green et Nicholas Vasilakos. « Market behaviour with large amounts of intermittent generation ». In : *Energy Policy* 38.7 (juill. 2010), p. 3211-3220. issn : 03014215. doi : 10.1016/j.enpol.2009.07.038. url : http://dx.doi.org/10.1016/j.enpol.2009.07.038%20https://linkinghub.elsevier.com/retrieve/pii/S0301421509005461.

[35] Milos Pantos et al. « Capacity firming of intermittent generation by dispersed energy storage ». In : *2017 Australasian Universities Power Engineering Conference (AUPEC)*. March. IEEE, nov. 2017, p. 1-6. isbn : 978-1-5386-2647-4. doi : 10.1109/AUPEC.2017.8282510. url : http://ieeexplore.ieee.org/document/8282510/.

[36] Jonathan Dumas et al. « A Probabilistic Forecast-Driven Strategy for a Risk-Aware Participation in the Capacity Firming Market ». In : *IEEE Transactions on Sustainable Energy* 13.2 (avr. 2022), p. 1234-1243. issn : 1949-3029. doi : 10.

1109/TSTE.2021.3117594. arXiv : arXiv:2105.13801v5. URL : https://ieeexplore.ieee.org/document/9562566/.

[37] Jonathan DUMAS et al. « Stochastic and deterministic formulations for capacity firming nominations ». In : *2020 International Conference on Probabilistic Methods Applied to Power Systems (PMAPS)*. IEEE, août 2020, p. 1-7. ISBN : 978-1-7281-2822-1. DOI : 10.1109/PMAPS47429.2020.9183646. arXiv : 2106.02425. URL : https://ieeexplore.ieee.org/document/9183646/.

[38] Sherif A. ABDELRAZEK et Sukumar KAMALASADAN. « Integrated PV Capacity Firming and Energy Time Shift Battery Energy Storage Management Using Energy-Oriented Optimization ». In : *IEEE Transactions on Industry Applications* 52.3 (mai 2016), p. 2607-2617. ISSN : 0093-9994. DOI : 10.1109/TIA.2016.2531639. URL : http://ieeexplore.ieee.org/document/7412704/.

[39] Matt BRUERS. *Firming renewables : A commercial perspective*. Rapp. tech. March. EnergyAustralia, 2019. URL : https://assets.cleanenergycouncil.org.au/documents/events/event-docs-2019/WIF19/Matt-Bruers-UPDATE.pdf.

[40] Clay CAMPAIGNE et Shmuel S. OREN. « Firming renewable power with demand response : an end-to-end aggregator business model ». In : *Journal of Regulatory Economics* 50.1 (août 2016), p. 1-37. ISSN : 0922-680X. DOI : 10.1007/s11149-016-9301-y. URL : http://link.springer.com/10.1007/s11149-016-9301-y.

[41] Alexandra ZABLOCKI. *Energy Storage | Energy Storage*. Rapp. tech. February. 2019, p. 1-8.

[42] Commision de Regulation de l'Energie CRE. *Appel d'offres portant sur la réalisation et l'exploitation d'installations de production d'électricité à partir de techniques de conversion du rayonnement solaire d'une puissance supérieure à 100 kWc et situées dans les zones non interconnectées*. 2015.

[43] Commision de Regulation de l'Energie CRE. *Rapport de synthèse : Appel d'offres portant sur la réalisation et l'exploitation d'installa- tions de production d'électricité à partir de l'énergie solaire et situées dans les zones non interconnectées*. Rapp. tech. Commision de Regulation de l'Energie, 2020, p. 1-35.

[44] Christopher L HETH. « Energy on demand : A brief history of the development of the battery ». In : *Substantia* 3.2 SE - (2019), p. 77-86. DOI : 10.13128/Substantia-280. URL : https://riviste.fupress.net/index.php/subs/article/view/280.

[45] Mogalahalli V. Reddy et al. « Brief History of Early Lithium-Battery Development ». In : *Materials* 13.8 (avr. 2020), p. 1884. issn : 1996-1944. doi : 10.3390/ma13081884. url : https://linkinghub.elsevier.com/retrieve/pii/S2451910321001721%20https://www.mdpi.com/1996-1944/13/8/1884.

[46] K BRANDT. « Historical development of secondary lithium batteries ». In : *Solid State Ionics* 69.3-4 (août 1994), p. 173-183. issn : 01672738. doi : 10.1016/0167-2738(94)90408-1. url : https://linkinghub.elsevier.com/retrieve/pii/0025540896800080%20https://linkinghub.elsevier.com/retrieve/pii/0167273894904081.

[47] Christian Julien et al. *Lithium Batteries*. 1re éd. Cham : Springer International Publishing, 2016. isbn : 978-3-319-19107-2. doi : 10.1007/978-3-319-19108-9. url : https://www.springer.com/fr/book/9783319191072%20http://link.springer.com/10.1007/978-3-319-19108-9.

[48] T. Editors of Encyclopaedia Britannica. *Electronegativity*. 2011.

[49] Aquino Todd et al. *Battery Energy Storage Technology Assessment*. Rapp. tech. 2007, p. 61-78.

[50] Languang Lu et al. « A review on the key issues for lithium-ion battery management in electric vehicles ». In : *Journal of Power Sources* 226 (2013), p. 272-288. issn : 03787753. doi : 10.1016/j.jpowsour.2012.10.060.

[51] D Grazioli, M Magri et A Salvadori. « Computational modeling of Li-ion batteries ». In : *Computational Mechanics* 58.6 (2016), p. 889-909. issn : 1432-0924. doi : 10.1007/s00466-016-1325-8. url : http://dx.doi.org/10.1007/s00466-016-1325-8.

[52] Pankaj Arora, Ralph E. White et Marc Doyle. « Capacity Fade Mechanisms and Side Reactions in Lithium-Ion Batteries ». In : *Journal of The Electrochemical Society* 145.10 (1998), p. 3647-3667. issn : 0013-4651. doi : 10.1149/1.1838857.

[53] Todd M Bandhauer, Srinivas Garimella et Thomas F Fuller. « A Critical Review of Thermal Issues in Lithium-Ion Batteries ». In : *Journal of The Electrochemical Society* (2011). doi : 10.1149/1.3515880.

[54] M.C. Smart et al. « The effect of high temperature exposure upon the performance of lithium ion cells ». In : *Seventeenth Annual Battery Conference on Applications and Advances. Proceedings of Conference (Cat. No.02TH8576)*. IEEE, p. 53-58. doi : 10.1109/BCAA.2002.986368. url : http://ieeexplore.ieee.org/document/986368/.

[55] Ahmadou Samba. « Battery Electrical Vehicles-Analysis of Thermal Modelling and Thermal Management ». Theses. LUSAC (Laboratoire Universitaire des Sciences Appliquées de Cherbourg), Université de caen Basse Normandie ; MOBI (the Mobility, Logistics et Automotive Technology Research Centre), Vrije Universiteit Brussel, mars 2015. URL : https://hal.archives-ouvertes.fr/tel-01298416.

[56] Rui Xiong et al. « Critical Review on the Battery State of Charge Estimation Methods for Electric Vehicles ». In : *IEEE Access* 6 (2017), p. 1832-1843. ISSN : 21693536. DOI : 10.1109/ACCESS.2017.2780258.

[57] Matthew T. Lawder et al. « Battery Energy Storage System (BESS) and Battery Management System (BMS) for Grid-Scale Applications ». In : *Proceedings of the IEEE* 102.6 (juin 2014), p. 1014-1030. ISSN : 0018-9219. DOI : 10.1109/JPROC.2014.2317451. URL : http://ieeexplore.ieee.org/document/6811152/.

[58] C F Chiasserini et R R Rao. *Energy efficient battery management*. 2001. DOI : 10.1109/49.932692.

[59] Max Jung et Simon Schwunk. « High End Battery Management Systems for Renewable Energy and EV Applications ». English. In : *Green* 3.1 (2013), p. 19-26. ISSN : 1869876X. DOI : http://dx.doi.org/10.1515/green-2012-0028. URL : http://0-search.proquest.com.millenium.itesm.mx/docview/1703449162?accountid=41938.

[60] A T Elsayed, C R Lashway et O A Mohammed. *Advanced Battery Management and Diagnostic System for Smart Grid Infrastructure*. 2016. DOI : 10.1109/TSG.2015.2418677.

[61] Ajay Raghavan et al. « Embedded fiber-optic sensing for accurate internal monitoring of cell state in advanced battery management systems part 1 : Cell embedding method and performance ». In : *Journal of Power Sources* 341 (fév. 2017), p. 466-473. ISSN : 03787753. DOI : 10.1016/j.jpowsour.2016.11.104. URL : https://linkinghub.elsevier.com/retrieve/pii/S0378775316316718.

[62] Marc Doyle, Thomas F Fuller et John Newman. « Modeling of Galvanostatic Charge and Discharge of the Lithium/Polymer/Insertion Cell ». In : *Journal of The Electrochemical Society* 140.6 (juin 1993), p. 1526. DOI : 10.1149/1.2221597. URL : https://dx.doi.org/10.1149/1.2221597.

[63] L. Xia et al. « A Computationally Efficient Implementation of an Electrochemistry-Based Model for Lithium-Ion Batteries ». In : *IFAC-PapersOnLine* 50.1 (2017), p. 2169-2174. ISSN : 24058963. DOI : 10.1016/j.ifacol.2017.08.276. URL : https://doi.org/10.1016/j.ifacol.2017.08.276.

[64] Michelle A. Kehs, Michael D. Beeney et Hosam K. Fathy. « Computational efficiency of solving the DFN battery model using descriptor form with Legendre polynomials and Galerkin projections ». In : *Proceedings of the American Control Conference* (2014), p. 260-267. issn : 07431619. doi : 10.1109/ACC.2014.6858858.

[65] Joel C. Forman et al. « Reduction of an Electrochemistry-Based Li-Ion Battery Model via Quasi-Linearization and Padé Approximation ». In : *Journal of The Electrochemical Society* 158.2 (2011), A93. issn : 00134651. doi : 10.1149/1.3519059.

[66] Woosuk Sung et Chee Burm Shin. « Electrochemical model of a lithium-ion battery implemented into an automotive battery management system ». In : *Computers and Chemical Engineering* 76 (2015), p. 87-97. issn : 00981354. doi : 10.1016/j.compchemeng.2015.02.007. url : http://dx.doi.org/10.1016/j.compchemeng.2015.02.007.

[67] Björn Weisshar et Wolfgang G. Bessler. « Model-based lifetime prediction of an LFP/graphite lithium-ion battery in a stationary photovoltaic battery system ». In : *Journal of Energy Storage* 14 (2017), p. 179-191. issn : 2352152X. doi : 10.1016/j.est.2017.10.002. url : http://dx.doi.org/10.1016/j.est.2017.10.002.

[68] Aishwarya Panday, Hari Om Bansal et Pramod Srinivasan. « Thermoelectric Modeling and Online SOC Estimation of Li-Ion Battery for Plug-In Hybrid Electric Vehicles ». In : *Modelling and Simulation in Engineering* 2016 (2016). issn : 16875605. doi : 10.1155/2016/2353521.

[69] Ximing Cheng et al. « Novel Parametric Circuit Modeling for Li-Ion Batteries ». In : *Energies* 9.7 (2016), p. 539. issn : 1996-1073. doi : 10.3390/en9070539. url : http://www.mdpi.com/1996-1073/9/7/539.

[70] Joaquín Klee Barillas et al. « A comparative study and validation of state estimation algorithms for Li-ion batteries in battery management systems ». In : *Applied Energy* 155 (2015), p. 455-462. issn : 03062619. doi : 10.1016/j.apenergy.2015.05.102.

[71] Jian Guo, Zhaojun Li et Michael Pecht. « A Bayesian approach for Li-Ion battery capacity fade modeling and cycles to failure prognostics ». In : *Journal of Power Sources* 281 (2015), p. 173-184. issn : 03787753. doi : 10.1016/j.jpowsour.2015.01.164.

[72] Chao Hu et al. « Data-driven method based on particle swarm optimization and k-nearest neighbor regression for estimating capacity of lithium-ion battery ». In : *Applied Energy* 129 (2014), p. 49-55. ISSN : 03062619. DOI : 10.1016/j.apenergy.2014.04.077. URL : http://dx.doi.org/10.1016/j.apenergy.2014.04.077.

[73] Wei He et al. « State of charge estimation for Li-ion batteries using neural network modeling and unscented Kalman filter-based error cancellation ». In : *International Journal of Electrical Power and Energy Systems* 62 (2014), p. 783-791. ISSN : 01420615. DOI : 10.1016/j.ijepes.2014.04.059. URL : http://dx.doi.org/10.1016/j.ijepes.2014.04.059.

[74] Jiani Du, Zhitao Liu et Youyi Wang. « State of charge estimation for Li-ion battery based on model from extreme learning machine ». In : *Control Engineering Practice* 26.1 (2014), p. 11-19. ISSN : 09670661. DOI : 10.1016/j.conengprac.2013.12.014. URL : http://dx.doi.org/10.1016/j.conengprac.2013.12.014.

[75] Suresh Daravath et al. « Lithium-Ion Battery Modelling and Online Battery Management Systems ». In : (2017), p. 1800-1806.

[76] Carolyn R. Pals et John Newman. « Thermal Modeling of the Lithium/Polymer Battery : I . Discharge Behavior of a Single Cell ». In : *Journal of The Electrochemical Society* 142.10 (1995), p. 3274-3281. ISSN : 0013-4651. DOI : 10.1149/1.2049974.

[77] S.C. Chen, C.C. Wan et Y.Y. Wang. « Thermal analysis of lithium-ion batteries ». In : *Journal of Power Sources* 140.1 (jan. 2005), p. 111-124. ISSN : 03787753. DOI : 10.1016/j.jpowsour.2004.05.064. URL : https://linkinghub.elsevier.com/retrieve/pii/S0378775304008596.

[78] Nicolas Damay et al. « Thermal modeling and experimental validation of a large prismatic Li-ion battery ». In : *IECON 2013 - 39th Annual Conference of the IEEE Industrial Electronics Society*. IEEE, nov. 2013, p. 4694-4699. ISBN : 978-1-4799-0224-8. DOI : 10.1109/IECON.2013.6699893. URL : http://ieeexplore.ieee.org/document/6699893/.

[79] Matteo Muratori. « Thermal Characterisation Of Lithium-Ion Battery Cell ». Thèse de doct. Politecnico Di Milano, 2009, p. 171.

[80] Manh-Kien Tran et al. « A Review of Lithium-Ion Battery Thermal Runaway Modeling and Diagnosis Approaches ». In : *Processes* 10.6 (juin 2022), p. 1192. ISSN : 2227-9717. DOI : 10.3390/pr10061192. URL : https://www.mdpi.com/2227-9717/10/6/1192.

[81] R Spotnitz et J Franklin. « Abuse behavior of high-power , lithium-ion cells ». In : 113 (2003), p. 81-100.

[82] Muhammad Umair Ali et al. *Towards a Smarter Battery Management System for Electric Vehicle Applications : A Critical Review of Lithium-Ion Battery State of Charge Estimation*. 2019. isbn : 8251510236. doi : 10.3390/en12030446.

[83] Jun Xu et al. « A new method to estimate the state of charge of lithium-ion batteries based on the battery impedance model ». In : *Journal of Power Sources* 233 (2013), p. 277-284. issn : 0378-7753. doi : 10.1016/j.jpowsour.2013.01.094. url : http://dx.doi.org/10.1016/j.jpowsour.2013.01.094.

[84] Yun Bao, Wenbin Dong et Dian Wang. « Online Internal Resistance Measurement Application in Lithium Ion Battery Capacity and State of Charge Estimation ». In : *Energies* 11.5 (avr. 2018), p. 1073. issn : 1996-1073. doi : 10.3390/en11051073. url : http://www.mdpi.com/1996-1073/11/5/1073.

[85] Dickson N T How, M A Hannan et Senior Member. « State of Charge Estimation for Lithium-Ion Batteries Using Model-Based and Data-Driven Methods : A Review ». In : *IEEE Access* 7 (2019), p. 136116-136136. doi : 10.1109/ACCESS.2019.2942213.

[86] Yanhui Zhang et al. « A novel model of the initial state of charge estimation for LiFePO4 batteries ». In : *Journal of Power Sources* 248 (fév. 2014), p. 1028-1033. issn : 03787753. doi : 10.1016/j.jpowsour.2013.09.135. url : http://dx.doi.org/10.1016/j.jpowsour.2013.09.135%20https://linkinghub.elsevier.com/retrieve/pii/S037877531301642X.

[87] X Feng, H B Gooi et S X Chen. « An improved lithium-ion battery model with temperature prediction considering entropy ». In : *2012 3rd IEEE PES Innovative Smart Grid Technologies Europe (ISGT Europe)*. Oct. 2012, p. 1-8. doi : 10.1109/ISGTEurope.2012.6465668.

[88] Xiaosong Hu, Shengbo Li et Huei Peng. « A comparative study of equivalent circuit models for Li-ion batteries ». In : *Journal of Power Sources* 198 (2012), p. 359-367. issn : 0378-7753. doi : 10.1016/j.jpowsour.2011.10.013. url : http://dx.doi.org/10.1016/j.jpowsour.2011.10.013.

[89] Tarun Huria et al. « Simplified Extended Kalman Filter Observer for SOC Estimation of Commercial Power-Oriented LFP Lithium Battery Cells ». In : (2013). issn : 09284931. doi : 10.4271/2013-01-1544. url : http://papers.sae.org/2013-01-1544/.

[90] T Girijaprasanna et C Dhanamjayulu. « A Review on Different State of Battery Charge Estimation Techniques and Management Systems for EV Applications ». In : (2022).

[91] M. Berecibar et al. « Critical review of state of health estimation methods of Li-ion batteries for real applications ». In : *Renewable and Sustainable Energy Reviews* 56 (2016), p. 572-587. issn : 18790690. doi : 10.1016/j.rser.2015.11.042.

[92] K. Saqli et al. « Critical review of ageing mechanisms and state of health estimation methods for battery performance ». In : *Smart Innovation, Systems and Technologies* 163 (2020), p. 507-518. issn : 21903026. doi : 10.1007/978-981-32-9868-2_43.

[93] Xiaoli Qin et al. « Prognostics of remaining useful life for lithium-ion batteries based on a feature vector selection and relevance vector machine approach ». In : *2017 IEEE International Conference on Prognostics and Health Management, ICPHM 2017* (2017), p. 1-6. doi : 10.1109/ICPHM.2017.7998297.

[94] Dong Wang, Qiang Miao et Michael Pecht. « Prognostics of lithium-ion batteries based on relevance vectors and a conditional three-parameter capacity degradation model ». In : *Journal of Power Sources* 239 (2013), p. 253-264. issn : 03787753. doi : 10.1016/j.jpowsour.2013.03.129. url : http://dx.doi.org/10.1016/j.jpowsour.2013.03.129.

[95] Guangxing Bai et al. « A generic model-free approach for lithium-ion battery health management ». In : *Applied Energy* 135 (2014), p. 247-260. issn : 03062619. doi : 10.1016/j.apenergy.2014.08.059.

[96] Wei He et al. « Prognostics of lithium-ion batteries based on Dempster-Shafer theory and the Bayesian Monte Carlo method ». In : *Journal of Power Sources* 196.23 (2011), p. 10314-10321. issn : 03787753. doi : 10.1016/j.jpowsour.2011.08.040.

[97] S. Castano et al. « Dynamical modeling procedure of a Li-ion battery pack suitable for real-time applications ». In : *Energy Conversion and Management* 92 (2015), p. 396-405. issn : 01968904. doi : 10.1016/j.enconman.2014.12.076. url : http://dx.doi.org/10.1016/j.enconman.2014.12.076.

[98] Changhao Piao et al. « Lithium-ion battery cell-balancing algorithm for battery management system based on real-time outlier detection ». English. In : *Mathematical Problems in Engineering* (fév. 2015). issn : 1024123X. url : http :

/ / 0 - go . galegroup . com . millenium . itesm . mx / ps / i . do ? p = ITOF & sw = w & u = itesm01 & v = 2 . 1 & it = r & id = GALE % 7CA456623504 & sid = summon & asid = 66e82e3ed6d8e6be66ac7f5ef0a470a0.

[99] M. Montaru et S. Pelissier. « Frequency and Temporal Identification of a Li-ion Polymer Battery Model Using Fractional Impedance ». In : *Oil & Gas Science and Technology – Revue de l'Institut Français du Pétrole* 65.1 (2010), p. 67-78. issn : 1294-4475. doi : 10.2516/ogst/2009056. url : http://ogst.ifpenergiesnouvelles.fr/10.2516/ogst/2009056.

[100] Systems Engineering Conference et al. « Bivariate Gamma Processes for Modeling Lithium Ion Battery Aging Mechanism ». In : (2017), p. 139-145.

[101] B. Saha, K. Goebel et J. Christophersen. « Comparison of prognostic algorithms for estimating remaining useful life of batteries ». In : *Transactions of the Institute of Measurement and Control* 31.3-4 (2009), p. 293-308. issn : 0142-3312. doi : 10.1177/0142331208092030.

[102] Xiaosong Hu, Shengbo Li et Yalian Yang. « Advanced Machine Learning Approach for Lithium-Ion Battery State Estimation in Electric Vehicles ». In : *IEEE Transactions on Transportation Electrification* 7782.c (2015), p. 1-1. issn : 2332-7782. doi : 10.1109/TTE.2015.2512237. url : http://ieeexplore.ieee.org/lpdocs/epic03/wrapper.htm?arnumber=7365487.

[103] Cunxue Wu et al. « Improved State of Charge Estimation for High Power Lithium Ion Batteries Considering Current Dependence of Internal Resistance ». In : *Energies* 10.10 (2017), p. 1486. issn : 1996-1073. doi : 10.3390/en10101486. url : http://www.mdpi.com/1996-1073/10/10/1486.

[104] Xuebing Han et al. « A comparative study of commercial lithium ion battery cycle life in electric vehicle : Capacity loss estimation ». In : *Journal of Power Sources* 268 (2014), p. 658-669. issn : 03787753. doi : 10.1016/j.jpowsour.2014.06.111. url : http://dx.doi.org/10.1016/j.jpowsour.2014.06.111.

[105] Alexander Farmann et al. « Critical review of on-board capacity estimation techniques for lithium-ion batteries in electric and hybrid electric vehicles ». In : *Journal of Power Sources* 281 (2015), p. 114-130. issn : 03787753. doi : 10.1016/j.jpowsour.2015.01.129. url : http://dx.doi.org/10.1016/j.jpowsour.2015.01.129.

[106] Nico Kreutzer, Claus Allert et Michael Ebel. « Using Modbus with Sunny Island 3.0M/4.4M/6.0H/8.0H ». In : (2015).

[107] Commision de Regulation de l'Energie CRE. *Rapport de synthèse : Appel d'offres portant sur la réalisation et l'exploitation d'installations de production d'électricité à partir de l'énergie solaire et situées dans les zones non interconnectées*. Rapp. tech. Commision de Regulation de l'Energie, 2015, p. 1-19.

[108] Yayuan Liu, Yangying Zhu et Yi Cui. « Challenges and opportunities towards fast-charging battery materials ». In : *Nature Energy* 4.7 (juill. 2019), p. 540-550. issn : 2058-7546. doi : 10.1038/s41560-019-0405-3. url : http://www.nature.com/articles/s41560-019-0405-3.

[109] Jian Guo et al. « Modeling Li-Ion Battery Capacity Fade Using Designed Experiments Western New England University ». In : *Proceedings of the 2014 Industrial and Systems Engineering Research Conference* (2014), p. 913-920.

[110] USABC et DOE National Laboratories. « Electric Vehicle Battery Test Procedures Revision 2 ». In : January (1996).

[111] A .J. Crawford et al. *Protocol for Uniformly Measuring and Expressing the Performance of Energy Storage Systems*. Rapp. tech. April. Pacific Northwest National Laboratory, Sandia National Laboratories, 2016.

[112] « IEEE Recommended Practice for the Characterization and Evaluation of Emerging Energy Storage Technologies in Stationary Applications ». In : *IEEE Std 1679-2010* (oct. 2010), p. 1-38. doi : 10.1109/IEEESTD.2010.5618903.

[113] Association Française de Normalisation. *IEC 62933-1 Electrical Energy Storage (EES) systems - Part 1 : vocabulary*. Rapp. tech. La Plaine Saint-Denis : AFNOR, 2018.

[114] Association Française de Normalisation. *NF EN 62933-2-1 Electrical energy storage (EES) systems - Part 2-1 : Unit parameters and testing methods - General specification*. Rapp. tech. La Plaine Saint-Denis : AFNOR, 2018.

[115] Australian Energy Market Operator (AEMO). « Response of Existing Pv Inverters To Frequency Disturbances ». In : April (2016), p. 1-34. url : https://aemo.com.au/-/media/Files/PDF/Response-of-Existing-PV-Inverters-to-Frequency-Disturbances-V20.pdf.

[116] Yuqing Yang et al. « Modelling and optimal energy management for battery energy storage systems in renewable energy systems : A review ». In : *Renewable and Sustainable Energy Reviews* 167.June (2022), p. 112671. issn : 18790690. doi : 10.1016/j.rser.2022.112671. url : https://doi.org/10.1016/j.rser.2022.112671.

[117] Seyed Madani, Erik Schaltz et Søren Knudsen Kær. « Review of Parameter Determination for Thermal Modeling of Lithium Ion Batteries ». In : *Batteries* 4.2 (avr. 2018), p. 20. issn : 2313-0105. doi : 10.3390/batteries4020020. url : http://www.mdpi.com/2313-0105/4/2/20.

[118] Ravi Methekar et al. « Optimum Charging Profile for Lithium-Ion Batteries to Maximize Energy Storage and Utilization ». In : *ECS Transactions* 25.35 (avr. 2010), p. 139-146. issn : 1938-5862. doi : 10.1149/1.3414012. url : https://iopscience.iop.org/article/10.1149/1.3414012.

[119] A Szumanowski et Y Chang. *Battery Management System Based on Battery Nonlinear Dynamics Modeling*. 2008. doi : 10.1109/TVT.2007.912176.

[120] Jeffrey R Belt et al. « A capacity and power fade study of Li-ion cells during life cycle testing ». In : 123 (2003), p. 241-246. doi : 10.1016/S0378-7753(03)00537-8.

[121] Jeffrey R Belt et al. « The effect of temperature on capacity and power in cycled lithium ion batteries ». In : 142 (2005), p. 354-360. doi : 10.1016/j.jpowsour.2004.10.029.

[122] E V Thomas et al. « Accelerated power degradation of Li-ion cells ». In : 124 (2003), p. 254-260. doi : 10.1016/S0378-7753(03)00729-8.

[123] D.P. Abraham et al. « Diagnostic examination of thermally abused high-power lithium-ion cells ». In : *Journal of Power Sources* 161.1 (oct. 2006), p. 648-657. issn : 03787753. doi : 10.1016/j.jpowsour.2006.04.088. url : https://linkinghub.elsevier.com/retrieve/pii/S0378775306006768.

[124] H.-p. Lin et al. « Low-Temperature Behavior of Li-Ion Cells ». In : *Electrochemical and Solid-State Letters* 4.6 (2001), A71. issn : 10990062. doi : 10.1149/1.1368736. url : https://iopscience.iop.org/article/10.1149/1.1368736.

[125] N. Legrand et al. « Physical characterization of the charging process of a Li-ion battery and prediction of Li plating by electrochemical modelling ». In : *Journal of Power Sources* 245 (2014), p. 208-216. issn : 03787753. doi : 10.1016/j.jpowsour.2013.06.130.

[126] Dongxu Ouyang et al. « A Review on the Thermal Hazards of the Lithium-Ion Battery and the Corresponding Countermeasures ». In : *Applied Sciences* 9.12 (juin 2019), p. 2483. issn : 2076-3417. doi : 10.3390/app9122483. url : https://www.mdpi.com/2076-3417/9/12/2483.

[127] A. Du Pasquier et al. « Differential Scanning Calorimetry Study of the Reactivity of Carbon Anodes in Plastic Li-Ion Batteries ». In : *Journal of The Electrochemical Society* 145.2 (fév. 1998), p. 472-477. issn : 0013-4651. doi : 10.1149/1.1838287. url : https://iopscience.iop.org/article/10.1149/1.1838287.

[128] M. N. Richard et J. R. Dahn. « Accelerating Rate Calorimetry Study on the Thermal Stability of Lithium Intercalated Graphite in Electrolyte. I. Experimental ». In : *Journal of The Electrochemical Society* 146.6 (juin 1999), p. 2068-2077. issn : 0013-4651. doi : 10.1149/1.1391893. url : https://iopscience.iop.org/article/10.1149/1.1391893.

[129] Doron Aurbach et al. « Review on electrode-electrolyte solution interactions, related to cathode materials for Li-ion batteries ». In : *Journal of Power Sources* 165.2 (2007), p. 491-499. issn : 03787753. doi : 10.1016/j.jpowsour.2006.10.025.

[130] Bharatkumar Suthar et al. « Optimal Low Temperature Charging of Lithium-ion Batteries ». In : *IFAC-PapersOnLine* 48.8 (2015), p. 1216-1221. issn : 24058963. doi : 10.1016/j.ifacol.2015.09.134. url : https://linkinghub.elsevier.com/retrieve/pii/S240589631501215X.

[131] Gi-Heon Kim, Ahmad Pesaran et Robert Spotnitz. « A three-dimensional thermal abuse model for lithium-ion cells ». In : *Journal of Power Sources* 170.2 (juill. 2007), p. 476-489. issn : 03787753. doi : 10.1016/j.jpowsour.2007.04.018. url : https://linkinghub.elsevier.com/retrieve/pii/S0378775307007082.

[132] Nanako Tanaka et Wolfgang G. Bessler. « Numerical investigation of kinetic mechanism for runaway thermo-electrochemistry in lithium-ion cells ». In : *Solid State Ionics* 262 (sept. 2014), p. 70-73. issn : 01672738. doi : 10.1016/j.ssi.2013.10.009. url : https://linkinghub.elsevier.com/retrieve/pii/S0167273813004852.

[133] W. B. Gu et C. Y. Wang. « Thermal-Electrochemical Modeling of Battery Systems ». In : *Journal of The Electrochemical Society* 147.8 (2000), p. 2910. issn : 00134651. doi : 10.1149/1.1393625. url : https://iopscience.iop.org/article/10.1149/1.1393625.

[134] Elke Schuster et al. « Thermal behavior and electrochemical heat generation in a commercial 40 Ah lithium ion pouch cell ». In : *Journal of Power Sources* 286 (2015), p. 580-589. issn : 03787753. doi : 10.1016/j.jpowsour.2015.03.170. url : http://dx.doi.org/10.1016/j.jpowsour.2015.03.170.

[135] Dave Roberts et al. « Dynamic Thermal Rating For Increasing Network Capacity And Delaying Network Reinforcements ». In : *SmartGrids for Distribution*. 2008.

[136] Venkat Srinivasan et C. Y. Wang. « Analysis of Electrochemical and Thermal Behavior of Li-Ion Cells ». In : *Journal of The Electrochemical Society* 150.1 (2002), A98. issn : 00134651. doi : 10.1149/1.1526512.

[137] D. Bernardi, E. Pawlikowski et J. Newman. « A General Energy Balance for Battery Systems ». In : *Journal of The Electrochemical Society* 132.1 (jan. 1985), p. 5-12. issn : 0013-4651. doi : 10.1149/1.2113792. url : https://iopscience.iop.org/article/10.1149/1.2113792.

[138] Yunus A Çengel et Afshin Ghajar. *Heat and Mass Transfer : Fundamentals and Applications*. Sixth Edit. New York : McGraw-Hill Education, 2020. isbn : 978-0-07-339819-8.

[139] Ruifeng Zhang et al. « Study on the Characteristics of a High Capacity Nickel Manganese Cobalt Oxide (NMC) Lithium-Ion Battery—An Experimental Investigation ». In : *Energies* 11.9 (août 2018), p. 2275. issn : 1996-1073. doi : 10.3390/en11092275. url : http://www.mdpi.com/1996-1073/11/9/2275.

[140] W. Lu et al. « Isothermal calorimetry investigation of Li1xMn2yAlzO4 spinel ». In : *Electrochimica Acta* 52.19 (mai 2007), p. 5837-5842. issn : 00134686. doi : 10.1016/j.electacta.2007.03.005. url : https://linkinghub.elsevier.com/retrieve/pii/S0013468607003635.

[141] Doris L. Britton, Thomas B. Miller et William R. Bennett. « Thermal Characterization Study of Lithium-Ion Cells ». In : *Thermal Characterization Study of Lithium-Ion Cells*. Sous la dir. de NASA Glenn Research Center. Williamsburg, VA. United States : 10th Electrochemical Power Sources Symposium, 2007, p. 26.

[142] Yvan Reynier et al. « Entropy of Li intercalation in LixCoO2 ». In : *Physical Review B* 70.17 (nov. 2004), p. 174304. issn : 1098-0121. doi : 10.1103/PhysRevB.70.174304. url : https://link.aps.org/doi/10.1103/PhysRevB.70.174304.

[143] IEEE. *The Authoritative Dictionary of IEEE Standards Terms*. 2000, p. 1-1362. isbn : 0738126012.

[144] Yujie Wang et al. « A comprehensive review of battery modeling and state estimation approaches for advanced battery management systems ». In : *Renewable and Sustainable Energy Reviews* 131.March (2020), p. 110015. issn : 18790690. doi : 10.1016/j.rser.2020.110015. url : https://doi.org/10.1016/j.rser.2020.110015.

[145] Mohamed Rawidean Mohd Kassim, Wan Adil Wan Jamil et Roslee Mohd Sabri. « State-of-Charge (SOC) and State-of-Health (SOH) Estimation Methods in Battery Management Systems for Electric Vehicles ». In : *2021 IEEE International Conference on Computing, ICOCO 2021* (2021), p. 91-96. doi : 10.1109/ICOCO53166.2021.9673580.

[146] Mina Naguib, Phillip Kollmeyer et Ali Emadi. « Lithium-ion battery pack robust state of charge estimation, cell inconsistency, and balancing : Review ». In : *IEEE Access* 9 (2021), p. 50570-50582. issn : 21693536. doi : 10.1109/ACCESS.2021.3068776.

[147] Manh-Kien Tran et al. « Comparative Study of Equivalent Circuit Models Performance in Four Common Lithium-Ion Batteries : LFP, NMC, LMO, NCA ». In : *Batteries* 7.3 (juill. 2021), p. 51. issn : 2313-0105. doi : 10.3390/batteries7030051. url : https://www.mdpi.com/2313-0105/7/3/51.

[148] Ping Shen et al. « The co-estimation of state of charge, state of health, and state of function for lithium-ion batteries in electric vehicles ». In : *IEEE Transactions on Vehicular Technology* 67.1 (2018), p. 92-103. issn : 00189545. doi : 10.1109/TVT.2017.2751613.

[149] Jan Leuchter et Pavol Bauer. « Capacity of Power-Batteries versus Temperature Keywords Method of Investigation ». In : *2015 17th European Conference on Power Electronics and Applications (EPE'15 ECCE-Europe)* (2015), p. 1-8.

[150] Md Ohirul Qays et al. « Recent progress and future trends on the state of charge estimation methods to improve battery-storage efficiency : A review ». In : *CSEE Journal of Power and Energy Systems* 8.1 (2022), p. 105-114. issn : 20960042. doi : 10.17775/CSEEJPES.2019.03060.

[151] Fabien Moutarde. « Deep-Learning : general principles + Convolutional Neural Networks ». In : Center for Robotics, MINES ParisTech, 2018.

[152] Jay L. Devore. *Probability and Statistics for Engineering and the Sciences*. Cengage Learning, 2016. doi : 978-1-305-25180-9.

[153] The Analytic Sciences Corporation et Arthur Gelb. *Applied Optimal Estimation*. The MIT Press, 1974.

[154] Yinjiao Xing et al. « State of charge estimation of lithium-ion batteries using the open-circuit voltage at various ambient temperatures ». In : *Applied Energy* 113 (2014), p. 106-115. ISSN : 03062619. DOI : 10.1016/j.apenergy.2013.07.008. URL : http://dx.doi.org/10.1016/j.apenergy.2013.07.008.

[155] Gregory L. Plett. « Extended Kalman filtering for battery management systems of LiPB-based HEV battery packs - Part 2. Modeling and identification ». In : *Journal of Power Sources* 134.2 (2004), p. 262-276. ISSN : 03787753. DOI : 10.1016/j.jpowsour.2004.02.032.

[156] Gregory L. Plett. « Extended Kalman filtering for battery management systems of LiPB-based HEV battery packs - Part 3. State and parameter estimation ». In : *Journal of Power Sources* 134.2 (2004), p. 277-292. ISSN : 03787753. DOI : 10.1016/j.jpowsour.2004.02.033.

[157] Mori W. Yatsui et Hua Bai. « Kalman filter based state-of-charge estimation for lithium-ion batteries in hybrid electric vehicles using pulse charging ». In : *2011 IEEE Vehicle Power and Propulsion Conference*. IEEE, juill. 2011, p. 1-5. ISBN : 978-1-61284-248-6. DOI : 10.1109/VPPC.2011.6042988. URL : http://ieeexplore.ieee.org/document/6042988/.

[158] Gregory L. Plett. « Extended Kalman filtering for battery management systems of LiPB-based HEV battery packs - Part 1. Background ». In : *Journal of Power Sources* 134.2 (2004), p. 252-261. ISSN : 03787753. DOI : 10.1016/j.jpowsour.2004.02.031.

[159] Jiani Du, Zhitao Liu et Youyi Wang. « State of charge estimation for Li-ion battery based on model from extreme learning machine ». In : *Control Engineering Practice* 26 (mai 2014), p. 11-19. ISSN : 09670661. DOI : 10.1016/j.conengprac.2013.12.014. URL : http://www.sciencedirect.com/science/article/pii/S0967066113002530%20https://linkinghub.elsevier.com/retrieve/pii/S0967066113002530.

[160] Xiaosong Hu et al. « Robustness analysis of State-of-Charge estimation methods for two types of Li-ion batteries ». In : *Journal of Power Sources* 217 (2012), p. 209-219. ISSN : 0378-7753. DOI : https://doi.org/10.1016/j.jpowsour.2012.06.005. URL : https://www.sciencedirect.com/science/article/pii/S0378775312009937.

[161] Mingyue Zhang et Xiaobin Fan. « Review on the State of Charge Estimation Methods for Electric Vehicle Battery ». In : *World Electric Vehicle Journal* 11.1 (mars 2020), p. 23. ISSN : 2032-6653. DOI : 10.3390/wevj11010023. URL : https://www.mdpi.com/2032-6653/11/1/23.

[162] J.N. Hu et al. « State-of-charge estimation for battery management system using optimized support vector machine for regression ». In : *Journal of Power Sources* 269 (2014), p. 682-693. ISSN : 03787753. DOI : 10.1016/j.jpowsour.2014.07.016.

[163] Alvin J. Salkind et al. « Determination of state-of-charge and state-of-health of batteries by fuzzy logic methodology ». In : *Journal of Power Sources* 80.1-2 (juill. 1999), p. 293-300. ISSN : 03787753. DOI : 10.1016/S0378-7753(99)00079-8. URL : https://linkinghub.elsevier.com/retrieve/pii/S0378775399000798.

[164] C. Pastor-Fernández et al. « A Study of Cell-to-Cell Interactions and Degradation in Parallel Strings : Implications for the Battery Management System ». In : *Journal of Power Sources* 329 (2016), p. 574-585. ISSN : 03787753. DOI : 10.1016/j.jpowsour.2016.07.121.

[165] Eric Prada. « Aging modeling and lifetime optimization of Li-ion LiFePO4-graphite batteries according to the vehicle use. » Theses. Université Pierre et Marie Curie, nov. 2012. URL : https://hal.archives-ouvertes.fr/tel-01091347.

[166] M. Broussely et al. « Main aging mechanisms in Li ion batteries ». In : *Journal of Power Sources* 146.1-2 (août 2005), p. 90-96. ISSN : 03787753. DOI : 10.1016/j.jpowsour.2005.03.172. URL : https://linkinghub.elsevier.com/retrieve/pii/S0378775305005082.

[167] J. Vetter et al. « Ageing mechanisms in lithium-ion batteries ». In : *Journal of Power Sources* 147.1-2 (sept. 2005), p. 269-281. ISSN : 03787753. DOI : 10.1016/j.jpowsour.2005.01.006. URL : https://linkinghub.elsevier.com/retrieve/pii/S0378775305000832.

[168] Carlos Vidal et al. « xEV Li-Ion Battery Low-Temperature Effects—Review ». In : *IEEE Transactions on Vehicular Technology* 68.5 (mai 2019), p. 4560-4572. ISSN : 0018-9545. DOI : 10.1109/TVT.2019.2906487. URL : https://ieeexplore.ieee.org/document/8671735/.

[169] Joris Jaguemont et al. « Lithium-Ion Battery Aging Experiments at Subzero Temperatures and Model Development for Capacity Fade Estimation ». In : *IEEE Transactions on Vehicular Technology* 65.6 (2016), p. 4328-4343. ISSN : 00189545. DOI : 10.1109/TVT.2015.2473841.

[170] Simone Barcellona et al. « Aging effect on the variation of Li-ion battery resistance as function of temperature and state of charge ». In : *Journal of Energy Storage* 50.March (2022), p. 104658. ISSN : 2352152X. DOI : 10.1016/j.est.2022.104658. URL : https://doi.org/10.1016/j.est.2022.104658.

[171] Hiroaki YOSHIDA et al. « Verification of Life Estimation Model for Space Lithium-Ion Cells ». In : *Electrochemistry* 78.5 (2010), p. 482-488. ISSN : 2186-2451. DOI : 10.5796/electrochemistry.78.482. URL : http://joi.jlc.jst.go.jp/JST.JSTAGE/electrochemistry/78.482?from=CrossRef.

[172] Alejandro GISMERO, Daniel-Ioan STROE et Erik SCHALTZ. « Calendar Aging Lifetime Model for NMC-based Lithium-ion Batteries Based on EIS Measurements ». In : *2019 Fourteenth International Conference on Ecological Vehicles and Renewable Energies (EVER)*. IEEE, mai 2019, p. 1-8. ISBN : 978-1-7281-3703-2. DOI : 10.1109/EVER.2019.8813635. URL : https://ieeexplore.ieee.org/document/8813635/.

[173] Jon P. CHRISTOPHERSEN. « Battery Test Manual For Electric Vehicles, Revision 3 ». In : (juin 2015). DOI : 10.2172/1186745. URL : https://www.osti.gov/biblio/1186745.

[174] R. SPOTNITZ. « Simulation of capacity fade in lithium-ion batteries ». In : *Journal of Power Sources* 113.1 (2003), p. 72-80. ISSN : 03787753. DOI : 10.1016/S0378-7753(02)00490-1.

[175] Jon P. CHRISTOPHERSEN. *Battery Test Manual For Electric Vehicles, Revision 3*. Rapp. tech. Idaho Falls, ID (United States) : Idaho National Laboratory, juin 2015. DOI : 10.2172/1186745. URL : http://www.osti.gov/servlets/purl/1186745/.

[176] JONG HOON KIM et al. « A new direct current internal resistance and state of charge relationship for the Li-ion battery pulse power estimation ». In : *2007 7th Internatonal Conference on Power Electronics*. November. IEEE, oct. 2007, p. 1173-1178. ISBN : 978-1-4244-1871-8. DOI : 10.1109/ICPE.2007.4692563. URL : http://ieeexplore.ieee.org/document/4692563/.

[177] Lin CHEN et al. « Estimation the internal resistance of lithium-ion-battery using a multi-factor dynamic internal resistance model with an error compensation strategy ». In : *Energy Reports* 7 (2021), p. 3050-3059. ISSN : 23524847. DOI : 10.1016/j.egyr.2021.05.027. URL : https://doi.org/10.1016/j.egyr.2021.05.027.

[178] Seongjun LEE, Jonghoon KIM et B.H. CHO. « Maximum pulse current estimation for high accuracy power capability prediction of a Li-Ion battery ». In : *Microelectronics Reliability* 55.3-4 (fév. 2015), p. 572-581. ISSN : 00262714. DOI : 10.1016/j.microrel.2014.12.016. URL : http://dx.doi.org/10.1016/j.microrel.2014.12.016%20https://linkinghub.elsevier.com/retrieve/pii/S0026271414005381.

[179] Hao Ji et al. « State of health prediction model based on internal resistance ». In : *International Journal of Energy Research* 44.8 (juin 2020), p. 6502-6510. ISSN : 0363-907X. DOI : 10.1002/er.5383. URL : https://onlinelibrary.wiley.com/doi/10.1002/er.5383.

[180] Maitane Berecibar et al. « State of health estimation algorithm of LiFePO4 battery packs based on differential voltage curves for battery management system application ». In : *Energy* 103 (2016), p. 784-796. ISSN : 03605442. DOI : 10.1016/j.energy.2016.02.163.

[181] Ira Bloom et al. « Differential voltage analyses of high-power, lithium-ion cells 1. Technique and application ». In : *Journal of Power Sources* 139.1-2 (2005), p. 295-303. ISSN : 03787753. DOI : 10.1016/j.jpowsour.2004.07.021.

[182] Fangfang Yang et al. « A study of the relationship between coulombic efficiency and capacity degradation of commercial lithium-ion batteries ». In : *Energy* 145.January 2019 (2018), p. 486-495. ISSN : 03605442. DOI : 10.1016/j.energy.2017.12.144. URL : https://doi.org/10.1016/j.energy.2017.12.144.

[183] Bolun Xu et al. « Modeling of lithium-ion battery degradation for cell life assessment ». In : *IEEE Transactions on Smart Grid* 9.2 (2018), p. 1131-1140. ISSN : 19493053. DOI : 10.1109/TSG.2016.2578950.

[184] M Berecibar, I Gandiaga et I Villarreal. « Realistic lifetime prediction approach for Li-ion batteries ». In : *Applied Energy* 162 (2016), p. 839-852. ISSN : 0306-2619. DOI : 10.1016/j.apenergy.2015.10.115. URL : http://dx.doi.org/10.1016/j.apenergy.2015.10.115.

[185] M. Broussely et al. « Aging mechanism in Li ion cells and calendar life predictions ». In : *Journal of Power Sources* 97-98 (2001), p. 13-21. ISSN : 03787753. DOI : 10.1016/S0378-7753(01)00722-4.

[186] Avr. 2023. URL : https://ec.europa.eu/eurostat/statistics-explained/index.php?title=Electricity_price_statistics.

[187] Arnold N'Goran et al. « Optimal engagement and operation of a grid-connected PV/battery system ». In : *IEEE PES Innovative Smart Grid Technologies Europe (ISGT-Europe 2019)*. Bucharest, Romania, sept. 2019. URL : https://hal-mines-paristech.archives-ouvertes.fr/hal-02318181.

[188] M Bruno Francois. « Développement d ' algorithmes de gestion optimale des systèmes de stockage énergétique basés sur des modèles adaptatifs ». In : (2016).

[189] Matteo Boaro et al. « Adaptive Dynamic Programming Algorithm for Renewable Energy Scheduling and Battery Management ». In : *Cognitive Computation* 5.2 (2013), p. 264-277. issn : 1866-9964. doi : 10.1007/s12559-012-9191-y. url : http://dx.doi.org/10.1007/s12559-012-9191-y.

[190] Carlos Adrian Correa-Florez et al. « Stochastic operation of home energy management systems including battery cycling ». In : *Applied Energy* 225 (sept. 2018), p. 1205-1218. issn : 03062619. doi : 10.1016/j.apenergy.2018.04.130. url : https://linkinghub.elsevier.com/retrieve/pii/S0306261918306597.

[191] Samuele Grillo et al. « Optimal management strategy of a battery-based storage system to improve renewable energy integration in distribution networks ». In : *IEEE Transactions on Smart Grid* 3.2 (2012), p. 950-958. issn : 19493053. doi : 10.1109/TSG.2012.2189984.

[192] Carlos Adrian Correa-Florez, Andrea Michiorri et George Kariniotakis. « Optimal Participation of Residential Aggregators in Energy and Local Flexibility Markets ». In : *IEEE Transactions on Smart Grid* 11.2 (mars 2020), p. 1644-1656. issn : 1949-3053. doi : 10.1109/TSG.2019.2941687. url : https://ieeexplore.ieee.org/document/8839865/.

[193] Andrea Michiorri, Georges Kariniotakis et Fiona Foucault. « An aggregator for distributed energy storage units under multiple constraints in the nice grid demonstrator ». In : *CIRED Workshop 2014 - Grid operation and congestion management* 0371 (2014), p. 11-12. url : https://hal-mines-paristech.archives-ouvertes.fr/hal-01016026.

[194] Leo Liberti. *Mathematical Progamming*. Ecole Polytechnique, 2018, p. 122. url : https://www.lix.polytechnique.fr/$%5Csim$liberti/teaching/dix/inf580-15/mathprog.pdf.

[195] Leo Liberti. « Reformulations in mathematical programming : Definitions and systematics ». In : *RAIRO - Operations Research* 43.1 (jan. 2009), p. 55-85. issn : 28047303. doi : 10.1051/ro/2009005. url : http://www.rairo-ro.org/10.1051/ro/2009005.

[196] Leo Liberti, Sonia Cafieri et Fabien Tarissan. « Reformulations in Mathematical Programming : A Computational Approach ». In : 2009, p. 153-234. doi : 10.1007/978-3-642-01085-9_7. url : http://link.springer.com/10.1007/978-3-642-01085-9_7.

[197] A. Michiorri et al. « A local energy management system for solar integration and improved security of supply : The Nice Grid project ». In : *2012 3rd IEEE PES Innovative Smart Grid Technologies Europe (ISGT Europe)*. IEEE, oct. 2012, p. 1-6. isbn : 978-1-4673-2597-4. doi : 10.1109/ISGTEurope.2012.6465667. url : http://ieeexplore.ieee.org/document/6465667/.

[198] Michael L Bynum et al. *Pyomo–optimization modeling in python*. Third. T. 67. Springer Science & Business Media, 2021.

[199] William E Hart, Jean-Paul Watson et David L Woodruff. « Pyomo : modeling and solving mathematical programs in Python ». In : *Mathematical Programming Computation* 3.3 (2011), p. 219-260.

[200] Andreas Wächter et Lorenz T. Biegler. « On the implementation of an interior-point filter line-search algorithm for large-scale nonlinear programming ». In : *Mathematical Programming* 106.1 (mars 2006), p. 25-57. issn : 0025-5610. doi : 10.1007/s10107-004-0559-y. url : http://link.springer.com/10.1007/s10107-004-0559-y.

[201] Thomas Carriere. « Towards seamless value-oriented forecasting and data-driven market valorisation of photovoltaic production ». Theses. Université Paris sciences et lettres, fév. 2020. url : https://pastel.archives-ouvertes.fr/tel-02988233.

[202] Trevor Hastie, Robert Tibshirani et Jerome Friedman. *The Elements of Statistical Learning*. Second Edi. Springer Series in Statistics. New York, NY : Springer New York, 2009, p. 745. doi : 10.1007/978-0-387-84858-7. url : http://link.springer.com/10.1007/978-0-387-84858-7.

RÉSUMÉ

Depuis plusieurs années, la présence des sources d'énergie renouvelable (EnR) variables dans le réseau électrique n'a fait qu'augmenter afin de réduire les émissions de gaz à effet de serre. En raison de leur nature intermittente, de nouveaux défis pour assurer la stabilité du réseau électrique sont apparus. Les systèmes de stockage d'énergie par batterie de type Li-ion (LiBESS) ont été fortement adoptés pour atténuer la dépendance des EnR aux conditions météorologiques, mais ces technologies sont toujours coûteuses et l'incertitude concernant l'optimisation de leur utilisation ainsi que leur durabilité restent un sujet de recherche. Pour intégrer efficacement les LiBESS dans des systèmes de production d'électricité, et compte tenu de l'engagement financier qu'ils impliquent pour les développeurs et exploitants, il est nécessaire de connaître leur comportement à court et à long termes. Cette maitrise de leur comportement est faite à travers des modèles qui estiment l'état de charge (SoC), l'état de santé (SoH) ou l'état thermique des batteries. Dans cette thèse, la génération d'un modèle LiBESS adapté aux applications de production d'électricité EnR et intégrant simultanément SoC, SoH et état thermique est étudié. Le processus d'étude suivi s'est d'abord concentré sur le développement de modèles indépendants du SoC, SoH ou de la température pour LiBESS de haute capacité, dans le contexte spécifique de LiBESS pour centrales photovoltaïques (PV) hybrides fonctionnant dans un cadre de sécurisation de de la capacité (Capacity Firming). Les modèles résultants de chaque paramètre indépendant ont ensuite été unifiés dans un modèle unique qui estime simultanément ces trois valeurs et auxquelles sont appliqué des tests et mesures d'erreur pour en valider précision et fiabilité. Enfin, ce modèle unifié a été utilisé pour l'optimisation de l'injection des systèmes de production hybrides. L'impact financier de la température et de la dégradation du LiBESS, dans le cas d'un usage optimal, a été évalué pour le scenario industriel de la sécurisation de la capacité PV. L'applicabilité de ce modèle a également été étendue et évaluée pour un scénario de micro-réseau avec plusieurs LiBESS, cela afin d'observer l'évolution des coûts en fonction des modèles de batterie.

MOTS CLÉS

Réseaux électriques intelligents Gestion intelligente de l'énergie Énergies Renouvelables Modelisation des batteries Optimisation d'injection Sécurisation de la capacité Centrales PV hybrides Photovoltaïque Stockage

ABSTRACT

The amount of variable renewable energy sources (vRES) integrated to the electrical grid has continued to increase to reduce greenhouse gas emissions. Because of their intermittent nature, new obstacles arise when ensuring the stability of the grid. High-capacity li-ion battery energy storage systems (LiBESS) have seen a surge in adoption to alleviate the vRES weather-dependance, but the technology is still expensive and concerns about the best usage method and durability remain a current subject of research. To effectively integrate LiBESS in power production applications, it is necessary to know its behavior in the short and long term given the financial commitment they imply for power plant investors. This is commonly done through battery models revolving mainly around the State-of-Charge (SoC), the State-of-Health (SoH) or the thermal behavior. In this thesis, the question of how to generate a LiBESS model that simultaneously incorporates SoC, SoH and thermal estimation, while also being proficient and adapted for vRES power applications is addressed. To tackle this question, the followed process focused at first on the on-line development of SoC, SoH and temperature models for high-capacity LiBESS used in industrial hybrid photovoltaic (PV) power plants operating under a capacity firming framework. The resulting LiBESS model for each parameter was then used in a unified model than simultaneously estimates the three values, of which investigations and error analysis were done to validate the accuracy. At last, the resulting unified model was used in optimal scheduling for hybrid systems. The financial impact the temperature and degradation have on both, optimal operation and scheduling, were evaluated for the industrial use case of PV capacity firming. The applicability of this model was also extended and evaluated for a micro-grid scenario with multiple LiBESS, this to observe the cost evolution due to the battery model.

KEYWORDS

Smart Grids Intelligent Energy Management Renewable Energies Battery modelling Optimal scheduling Capacity firming Hybrid PV-battery plant Photovoltaics Energy storage